

**THE ROLE OF PHOTODYNAMIC THERAPY IN
WOUND HEALING AND SCARRING IN HUMAN
SKIN**

A Thesis submitted to the University of Manchester for the degree of
Doctor of Philosophy in the Faculty of Engineering and Physical
Sciences

2015

Jenifer Guadalupe Mendoza Garcia

SCHOOL OF MECHANICAL, AEROSPACE AND CIVIL ENGINEERING

TABLE OF CONTENTS

LIST OF FIGURES	8
LIST OF TABLES	13
ABBREVIATIONS	14
NOMENCLATURE	19
ABSTRACT	20
DECLARATION	21
COPYRIGHT	21
ACKNOWLEDGEMENTS	22
DEDICATIONS	23
CHAPTER ONE: INTRODUCTION	24
1.1 Overview	24
1.2 Background	26
1.3 Aim and general methodology of the research	27
CHAPTER TWO: ADULT HUMAN SKIN, WOUND HEALING AND SCARS FORMATION	31
2.1 Introduction	31
2.2 Physiology and anatomy of adult human skin	32
2.2.1 Anatomical layers of the skin and accessories	34
2.2.1.1 The epidermis	35
2.2.1.2 The basement membrane	39
2.2.1.3 The dermis	40
2.2.1.4 The hypodermis	41
2.2.1.5 Skin accessories	42

2.3 Cellular and molecular biology of adult human skin	41
2.3.1 Keratinocytes	43
2.3.2 Fibroblasts	45
2.3.3 Extracellular matrix	47
2.3.3.1 Collagens	49
2.4 The wound healing process	51
2.4.1 The inflammatory stage	52
2.4.2 The proliferative stage	55
2.4.3 The remodelling stage	58
2.5 Skin scars formation	60
2.5.1 Definition and phenotypic characteristics	60
2.5.2 Molecular mechanisms of scarring	63
2.5.3 Scar treatments	66
CHAPTER THREE: PHOTODYNAMIC THERAPY IN DERMATOLOGY AND TISSUE MODELS	68
3.1 Introduction	68
3.2 Photodynamic therapy concept	70
3.3 Molecular mechanism of photodynamic therapy	72
3.4 Photosensitisers	77
3.4.1 5-aminolevulinic acid	78
3.4.2 Methyl-ester aminolevulinate	80
3.5 Light sources	81
3.6 Photodynamic therapy treatment in wound healing and scars	82
3.7 Tissue models	84
3.7.1 In vitro models	85
3.7.2 In vivo models	87

3.7.3 Ex vivo models	87
3.7.4 In virtuo models	91
CHAPTER FOUR: PHOTODYNAMIC THERAPY AND KELOID	
FIBROBLASTS	
4.1 Introduction	93
4.2 Experimental set up	94
4.3 Materials and methods	96
4.3.1 Cell culture	96
4.3.2 Drugs	98
4.3.3 PDT apparatus and treatment	99
4.3.4 Fluorescence measurement of Protoporphyrin IX accumulation	99
4.3.5 Cell proliferation analysis	100
4.3.6 Phototoxic analysis	100
4.3.7 Cytotoxic analysis	100
4.3.8 Apoptosis, necrosis and senescence analysis	101
4.3.9 Reactive oxygen species generation analysis	101
4.3.10 mRNA isolation, cDNA synthesis and qRT-PCR	102
4.3.11 Statistical Analysis	103
4.4 Results	103
4.4.1 Protoporphyrin IX accumulation and MALA/5ALA cytotoxicity in keloid fibroblasts	103
4.4.2 Phototoxicity of a LED arrangement of red light (635 nm)	112
4.4.3 Cytotoxic analysis after MALA/5ALA-PDT	113
4.4.4 Cell proliferation after MALA/5ALA-PDT	115
4.4.5 Cell death (Apoptosis/necrosis) analysis after MALA/5ALA-PDT	116

4.4.6 Senescence analysis after MALA/5ALA-PDT	117
4.4.7 Reactive oxygen species generation analysis after MALA/5ALA-PDT	119
4.4.8 Gene expression analysis of markers of apoptosis and keloid pathogenesis	120
4.5 Discussion	124
CHAPTER FIVE: PHOTODYNAMIC THERAPY AND EX VIVO WOUND HEALING	
	130
5.1 Introduction	130
5.2 Experimental set up	131
5.3 Materials and methods	133
5.3.1 Skin explants	133
5.3.2 Wounding procedure	134
5.3.3 Tissue support systems and growth media	135
5.3.4 Photodynamic therapy treatment	136
5.3.5 Histology	137
5.3.6 Immunohistochemistry/immunofluorescence	137
5.3.7 mRNA isolation, cDNA synthesis and qRT-PCR	139
5.3.8 Statistical analysis	140
5.4 Results	141
5.4.1 Optimization of a wound healing model ex vivo	141
5.4.2 Analysis of normal skin compared to wound healing organ culture	145
5.4.3 Photodynamic therapy effects in a wound healing organ culture	150
5.4.4 Apoptosis and proliferation analysis in WHOCs post-PDT	152
5.4.5 Extracellular matrix analysis, oxidative stress and MMPs expression post-PDT	156
5.5 Discussion	164

CHAPTER SIX: PHOTODYNAMIC THERAPY AND SKIN SCARRING	171
6.1 Introduction	171
6.2 Experimental set up	172
6.3 Material and methods	173
6.3.1 Study subject selection and recruitment	173
6.3.2 Skin explant preparation	174
6.3.3 Photodynamic therapy treatment	175
6.3.4 Histology	177
6.3.5 Immunofluorescence/Immunohistochemistry	177
6.3.6 mRNA isolation, cDNA synthesis and qRT-PCR	178
6.3.7 Statistical analysis	179
6.4 Results	180
6.4.1 Histological evaluation post-5ALA/MALA-PDT	180
6.4.2 Epidermal apoptosis and proliferation analysis after 5ALA/MALA-PDT	182
6.4.3 Extracellular matrix analysis after 5ALA/MALA-PDT	186
6.5 Discussion	192
CHAPTER SEVEN: CONCLUSIONS AND SUGGESTIONS FOR FUTURE WORK	196
7.1 Conclusions	196
7.1.1 Conclusions for the effect of PDT in keloid fibroblasts	196
7.1.2 Conclusions for the effect of PDT in an optimized ex vivo adult human wound healing model	197
7.1.3 Conclusions for the effect of PDT in skin scarring	198
7.2 Suggestions for future work	199
7.2.1 Role of PDT in keloid disease	199

7.2.2 Role of PDT in wound healing using ex vivo models	200
7.2.3 Role of PDT in skin scars and striae distensae using ex vivo models	200
PUBLICATIONS	201
REFERENCES	203
ANNEX 1	222

Word count: 41, 851

LIST OF FIGURES

Figure 2.1 Anatomical layers of the adult human skin	35
Figure 2.2 The epidermis	36
Figure 2.3 The dermis	41
Figure 2.4 The hypodermal tissue	42
Figure 2.5 A dermal fibroblast	45
Figure 2.6 Epidermal-dermal paracrine communication	47
Figure 2.7 Collagen and elastic fibre arrangement in adult human skin	50
Figure 2.8 Stages of adult human wound healing process	51
Figure 2.9 Suggested molecular mechanisms of the inflammatory stage of wound healing	54
Figure 2.10 Suggested molecular mechanisms of the proliferative stage of wound healing	59
Figure 2.11 Suggested molecular mechanisms of the remodelling stage of wound healing	57
Figure 2.12 Skin scars	63
Figure 3.1 PDT associated photochemical reactions	72
Figure 3.2 Effects of PDT on cancer cells	73
Figure 3.3 PDT related photophysical and photochemical mechanisms involved in of ROS generation	75
Figure 3.4 Immunity related phenomena induced by PDT	77
Figure 3.5 Protoporphyrin IX synthesis pathway post-5ALA or MALA	79
Figure 3.6 Tissue models for investigating skin and treatments	85
Figure 4.1 Cross section of a typical keloid scar showing different site-specific lesional sites	95

Figure 4.2 Site-specific keloid fibroblasts	95
Figure 4.3 Flow chart of the methodology used in chapter four	98
Figure 4.4 Kinetics of PpIX accumulation in normal skin post-incubation with MALA	104
Figure 4.5 Kinetics of PpIX accumulation in keloid fibroblasts from the margin of the scar post-incubation with MALA	105
Figure 4.6 Kinetics of PpIX accumulation in keloid fibroblasts from the middle with MALA	105
Figure 4.7 Kinetics of PpIX accumulation in keloid fibroblasts from the top with MALA	106
Figure 4.8 Kinetics of PpIX accumulation in normal skin post-incubation with 5ALA	107
Figure 4.9 Kinetics of PpIX accumulation in keloid fibroblasts from the margin of the scar post-incubation with 5ALA	107
Figure 4.10 Kinetics of PpIX accumulation in keloid fibroblasts from top with 5ALA	108
Figure 4.11 Kinetics of PpIX accumulation in keloid fibroblasts from the middle with 5ALA	108
Figure 4.12 Fluorescence intensity of PpIX accumulated in normal skin and keloid fibroblasts after 3 hours of incubation with 4 mM of M-ALA or 5ALA	109
Figure 4.13 Cytoproliferation of normal skin fibroblasts post 3 and 6 hours of incubation with varying concentrations of MALA or 5ALA	110
Figure 4.14 Cytoproliferation of keloid fibroblasts from margin of the scar after 3 and 6 hours with varying concentrations of MALA or 5ALA	110
Figure 4.15 Cytoproliferation of keloid fibroblasts from top of the scar after 3 and 6 hours with varying concentrations of MALA or 5ALA	111
Figure 4.16 Cytoproliferation of keloid fibroblasts from middle of the scar after 3 and 6 hours with varying concentrations of MALA or 5ALA	111

Figure 4.17 Percentage of phototoxicity in site-specific keloid fibroblasts compared to normal skin fibroblasts at increasing fluence rates (without treatment)	112
Figure 4.18 Percentage of cytotoxicity immediately after PDT in site-specific keloid fibroblasts compared to normal skin fibroblasts	113
Figure 4.19 Percentage of cytotoxicity 24 hours post-PDT in site-specific keloid fibroblasts compared to normal skin fibroblasts	114
Figure 4.20 Percentage of cytotoxicity 72 hours post-PDT in site-specific keloid fibroblasts compared to normal skin fibroblasts	115
Figure 4.21 Percentage of cell proliferation in site-specific keloid fibroblasts compared to normal skin fibroblasts at increasing fluence rates with precursors of photosensitiser	115
Figure 4.22 Hoechst 33258/PI staining in normal skin compared to site-specific keloid fibroblasts 24 hours after MALA-PDT treatment	116
Figure 4.23 Hoechst 33258/PI staining in normal skin compared to site-specific keloid fibroblasts 24 hours after 5ALA-PDT treatment	117
Figure 4.24 β -galactosidase staining at pH 6 in normal skin compared to site-specific keloid fibroblasts after MALA and 5ALA PDT treatment	118
Figure 4.25 Positive senescence induction on site-specific keloid and normal skin fibroblasts	118
Figure 4.26 ROS generation post MALA/5ALA-PDT treatment in normal skin compared to site-specific keloid fibroblasts	119
Figure 4.27 COLI relative gene expression levels in normal skin and keloid fibroblasts post-PDT	120
Figure 4.28 COLIII relative gene expression levels in normal skin and keloid fibroblasts post-PDT	121
Figure 4.29 HIF-1 relative gene expression levels in normal skin and keloid fibroblasts post-PDT	121
Figure 4.30 HSP90 relative gene expression levels in normal skin and keloid fibroblasts post-PDT	122

Figure 4.31 HSP70 relative gene expression levels in normal skin and keloid fibroblasts post-PDT	122
Figure 4.32 CASP3 relative gene expression levels in normal skin and keloid fibroblasts post-PDT	123
Figure 4.33 CASP9 relative gene expression levels in normal skin and keloid fibroblasts post-PDT	123
Figure 4.34 BCL-2 relative gene expression levels in normal skin and keloid fibroblasts post-PDT	124
Figure 4.35 Proposed mechanism of cell death/cell survival of keloid fibroblasts post-PDT	129
Figure 5.1 Flow chart of the methodology used in chapter five	132
Figure 5.2 Wound healing organ culture (WHOC) models	136
Figure 5.3 Epidermal thickness of WHOCs maintained in different media and supported with collagen embedded matrix or well chamber inserts	143
Figure 5.4 Morphological analysis by Weigert's differential staining in the healthy peripheral skin adjacent to the wound	144
Figure 5.5 Partial-thickness dermal WHOCs	146
Figure 5.6 Full-thickness dermal WHOCs	147
Figure 5.7 Analysis of normal skin compared to WHOCs after 14 days ex vivo	149
Figure 5.8 H&E images of WHOC models with 2 mm wound centre, untreated and post-PDT	150
Figure 5.9 Analysis of full-thickness WHOCs post-PDT	151
Figure 5.10 Apoptotic analysis of full-thickness WHOCs post-PDT	153
Figure 5.11 Proliferation analysis post-PDT	154
Figure 5.12 Analysis of CK14 expression post-PDT	155
Figure 5.13 Herovici's differential staining analysis post-PDT	157
Figure 5.14 Representative images of Weigert's elastic stain post-PDT	158
Figure 5.15 MMP3 and MMP19 analysis post-PDT	159

Figure 5.16 p16 analysis post-PDT	161
Figure 5.17 Representative images of α -SMA IHC post-PDT	162
Figure 5.18 CD31 endothelial marker analysis post-PDT	163
Figure 5.19 Schematic representation of optimal WHOC model	165
Figure 5.20 Schematic representation of the effect of PDT in WHOCS on day 7	170
Figure 6.1 Flow chart of the methodology used to investigate the effect of PDT in skin scars ex vivo	166
Figure 6.2 Schematic representation of normal skin, striae distensae and skin scar explants	176
Figure 6.3 Morphological analysis by H&E staining	181
Figure 6.4 Epidermal apoptosis analysis	183
Figure 6.5 Epidermal proliferation analysis	185
Figure 6.6 Elastic fibre arrangement analysis	187
Figure 6.7 Tropoelastin analysis	188
Figure 6.8 Collagen type I and collagen type III analysis	190
Figure 6.9 MMP3 analysis	191
Figure 6.10 Schematic representation of the effects of PDT in phenotypically different skin scars	193

LIST OF TABLES

Table 2.1 Growth factors expressed by keratinocytes in normal homeostasis	44
Table 2.2 Molecules expressed in the epidermal layers related to cell adhesion and shape	44
Table 2.3 Biomolecules normally expressed by fibroblasts	46
Table 2.4 MMPs and TIMPs localized in the ECM	48
Table 2.5 Collagen types found in normal human skin	49
Table 2.6 Keratinocytes expression factors at the proliferative stage of wound healing	56
Table 2.7 Skin scar classification	62
Table 3.1 Dermatologic conditions treated with photodynamic therapy (5ALA or MALA)	61
Table 3.2 Commercial features of MALA and 5ALA	81
Table 3.3 Full-thickness ex vivo models used to study human scars	89
Table 3.4 Ex vivo models to study human wound healing	91
Table 4.1 Clinical demographic data of subjects used in the study	96
Table 4.2 List of Primers	102
Table 5.1 Demographic data and source of skin explants	133
Table 5.2 List of antibodies	139
Table 5.3 Gene and primer sequences for qRT-PCR	140
Table 6.1 Clinical data and source of scar/skin explants	174
Table 6.2 List of antibodies	178
Table 6.3 Gene and primer sequences for qRT-PCR	178

ABBREVIATIONS

3D	Tridimensional
5ALA	Aminolevolinic acid
ADAMs	Disintegrin-metalloproteinases
AGES	Advanced glycation end products
ALEs	Advanced lipid peroxidation en products
ANOVA	Analysis of variance
Aret	Advancing re-epithelialization tongue
bFGF	Basic fibroblast growth factor
BCL-2	B-cell CLL/lymphoma 2
BM	Basement membrane
CASP3	Caspase-3
CASP9	Caspase-9
CD31	Platelet/endothelial cell adhesion molecule 1
CK14	Cytokeratin 14
CK	Cytokeratin
COLI	Collagen type I
COLIII	Collagen type III
CTGF	Connective tissue growth factor
DAMPs	Damage-associated molecular patterns
DMEM	Dulbecco's modified Eagle's medium
DNA	Deoxyribonucleic acid
cDNA	Complementary DNA
ECM	Extracellular matrix
EDGS	EpiLife Define Growth Supplement
EGF	Ephitelial growth factor

ET-1	Endothelin 1
Epi	Epidermis
FLS	Fine line scar
FBS	Foetal bovine serum
GAGs	Glycosaminoglycans
GABA	γ -Aminobutyric acid
GCSF	Granulocyte-colony stimulating factor
GM-CSF	granulocytemacrophage colony-stimulating factor
H&E	Haematoxylin and eosin stain
HB-EGF	Heparin-binding EGF-like growth factor
HIF-1 α	Hypoxia inducible factor 1 α
HGF	Hepatocyte growth factor
HS	Hypertrophic scar
HSP47	Heat shock 47 kDa
HSP70	Heat shock 70kDa protein 4
HSP90	Heat shock protein 90kDa alpha (cytosolic)
HSPs	Heat shock proteins
HV	Herovici's differential staining
IHC	Immunohistochemical staining
IL-1 α	Interleukin-1 alpha
IL-8	Interleukin- 8
rhIL-10	recombinant human interleukin-10
INF	Interferon
INF γ	Interferon gamma
KD	Keloid disease
KF	Keloid fibroblasts

KGF	Keratynocyte growth factor
LAMA5	Laminin 5
LED	Light emitting diodes
LDH	Lactate dehydrogenase
MALA	Methyl-ester aminolevulanate
MED3	Medium three
MCSF	Macrophage colony-stimulating factor
MMP1	Matrix metalloproteinase 1
MMP2	Matrix metalloproteinase 2
MMP3	Matrix metalloproteinase 3
MMP8	Matrix metalloproteinase 8
MMP9	Matrix metalloproteinase 9
MMP19	Matrix metalloproteinase 19
MMP28	Matrix metalloproteinase 28
MMPs	Matrix metalloproteinases
mTOR	Mammalian target of rapamycin
Neo	Neo-epidermos
NF	Normal fibroblasts
NS	Normal skin
NT	Untreated
OC	Organ culture
CO ₂	Carbon dioxide
p16	Cyclin-dependent kinase inhibitor 2A
PAMPs	Pathogen-associated molecular patterns
PCNA	Proliferating cell nuclear antigen
PD	Papillary dermis

PDT	Photodynamic therapy
PDGF	Platelet-derived growth factor
pO ₂	partial pressure of oxygen
PpIx	Protoporphyrin IX
Ps	Peripheral skin
qRT-PCR	Quantitative real time polymerase chain reaction
RCCs	reactive carbonyl compounds
RD	Reticular dermis
mRNA	Ribonucleic acid
ROS	Reactive oxygen species
RPL32	Ribosomal protein L32
SD	Striae distensae
STAT3	Signal transducer and activator of transcription 3
SPARC	secreted protein acidic and rich in cysteine
TGFα	Transforming growth factor alpha
TGFβ	Transforming growth factor beta
TGFβ3	Transforming growth factor beta 3
TIMPs	Tissue inhibitor of metalloproteinases
TNFα	Tumor necrosis factor alpha
UVB	Ultraviolet B
UK	United Kingdom
VEGF	Vascular endothelial growth factor
WE	Williams medium E
WELA	Weigert's elastic differential staining
WHOC	Wound healing organ culture
WHOCs	Wound healing organ culture models

WST-1

Water-soluble Tetrazolium salts 1

α -SMA

α -Smooth muscle actin

NOMENCLATURE

%	Percentage
a.u.	Arbitrary units
°C	Degree Celsius
hrs	Hours
J/cm ²	Fluence; Joule per centimetre square
µg/ml	Microgram per milliliter
ng/ml	Nanogram per milliliter
IU/ml	International Units Per Millilitre
mins	Minutes
mm	Millimetres
mg/cm ²	Miligrams per centimetre square
nm	Nanometres
µm	Micrometers

ABSTRACT

The skin acts as a protective barrier, is crucial for thermoregulation and also forms part of the sensory, immunological and endocrine system. Therefore skin preservation is paramount to preserving life. The loss of skin homeostasis, through injury, initiates the wound healing process where the final outcome is the formation of a scar. Scar treatment remains a challenge, despite a plethora of treatments, resulting in a poor outcome and sub-optimal response to existing therapies. Photodynamic therapy (PDT) has been used to treat oncologic conditions affecting the skin. Its action depends on a photosensitiser and a specific light source. Aminolevulinic acid (5ALA) and its methyl ester (MALA) are commonly used prodrugs of the photosensitiser protoporphyrin IX (PpIX), which in combination with red light produces reactive oxygen species (ROS). ROS will cause different responses such as cell death and tissue destruction. There is limited clinical evidence emerging for the use of PDT in treating wound healing and pathological skin scarring. For this reason, further investigations are required to better understand the role of PDT in adult human skin wound healing and skin scarring. The aim of this investigation was to evaluate the accumulation of PpIX after exposure to 5ALA or MALA, phototoxicity of red light arrangement, cytotoxicity, cell death induction, ROS generation and a gene related analysis post-PDT in keloid fibroblasts compared to normal skin fibroblasts. Optimization of a wound healing organ culture (WHOC) model and evaluation of re-epithelialization, cell death, proliferation, extracellular matrix rearrangement (ECM) and a related gene analysis after 5ALA-PDT ex vivo. General histology, cell death, proliferation, ECM rearrangement and a gene related analysis after PDT in skin scarring ex vivo.

This investigation found PpIX accumulation higher with MALA compared to 5ALA. Phototoxicity and cytotoxicity was site specific within the lesion and increased proportionately to fluence rates. ROS generation leads to the decrease of cytoproliferation and increased apoptosis and necrotic cell death, COLI, COLIII and HSP70 were found down-regulated. Ex vivo wound geometry, system of support and growth media were optimized in a human wound healing organ culture (WHOC). WHOCs treated with 5ALA-PDT (20 J/cm^2), showed an advancing re-epithelialization tongue 3.5 folds longer, which were highly proliferative, showing increased CK14 and p16 levels. The neo-epidermis was fully differentiated and neo-collagen was present. PCNA, p16, COLI, COLIII, MMP3, MMP19 and α -SMA were significantly more expressed in the dermis. MALA/5ALA-PDT (40 J/cm^2) applied to striae alba, fine line, hypertrophic and keloid scars ex vivo caused an increased of apoptosis while proliferation decreased, matrix components were found to be re-organised, both according to the severity of the scar. COLI and COLIII genetic expression decreased while MMP3 and tropoelastin increased significantly. However, no statistically significant difference was observed between 5ALA and MALA-PDT treatments.

In conclusion, this thesis shows that cytotoxicity post-PDT in KD fibroblasts is dependent on the lesional site within the scar, a precursor of intracellular photosensitiser and fluence. PDT in wound healing ex vivo shows increased re-epithelialization and ECM reconstruction and remodelling. Finally, in dermal fibrosis morphological and cellular effects of the application of PDT correlate with the degree and severity of dermal fibrosis. In view of this, PDT may be ideal for treating abnormal skin scarring and improving human cutaneous wound healing.

DECLARATION

No portion of the work referred to in the thesis has been submitted in support of an application for another degree or qualification of this or any other university or other institute of learning.

COPYRIGHT

The author of this thesis (including any appendices and/or schedules to this thesis) owns any copyright or related rights in it (the “Copyright”) and she has given The University of Manchester rights to use such Copyright for any administrative, promotional, educational and/or teaching purposes.

Copies of this Thesis, either in full or in extracts and whether in hard or electronic copy, may be made only in accordance with the Copyright, Designs and Patents Act 1988 (as amended) and regulations issued under it or, where appropriate, in accordance with licensing agreements which the University has from time to time. This page must form part of any such copies made..

The ownership of certain Copyright, patents, designs, trademarks and other intellectual property (the “Intellectual Property”) and any reproductions of copyright works in the Thesis, for example graphs and tables (“Reproductions”), which may be described in this Thesis, may not be owned by the author and may be owned by third parties. Such Intellectual Property and Reproductions cannot and must not be made available for use without the prior written permission of the owner(s) of the relevant Intellectual Property and/or Reproductions.

Further information on the condition under which disclosure, publication and commercialisation of this Thesis, the Copyright and any Intellectual Property and/or Reproductions described in it may take place is available in the University IP Policy, in any relevant Thesis restriction declarations deposited in the University Library, The University Library’s regulations and in The University’s policy on Presentation of Theses.

ACKNOWLEDGMENTS

I would like to give my sincerest gratitude to my supervisors, Prof Teresa Alonso-Rasgado and Dr Ardesir Bayat. Thanks for all the support and guidance.

In addition, I wish to gratefully acknowledge the PhD Scholarship from The National Council on Science and Technology of Mexico (CONACyT).

I would also like to thank to Dr Anil Sebastian, post doctoral research associate working in Dr Bayat's laboratory for all his support in the laboratory. Finally, I would like to thank to all my fellows of the Bioengineering group at MACE school and the PRSR group based at the MIB, for all their support.

DEDICATIONS

First I want to thank to Lord God Almighty and its blessed Holy Trinity. “Before the sun raised, because you loved me, before the light shine, because you loved me, Thank you Lord for your love” (schola catorum) and our merciful mother Our Lady of Guadalupe, who granted us her love, compassion, help and protection. Many thanks for all the blessings received in order to pursue this doctoral degree.

I would like to thank to my mom Eugenia, who uncodinitonal love and support through my life, allow me to follow all my objectives. I also want to thanks to all my family for all their support in all matters. Many thanks to my family Alberta and Leonardo, Olga and Jesus, Carmen and Erasto, Mary and Marcos, Herminia, and Juanita and Gil, my cousins Adelina, Israel, Norma, Maribel, Eduardo, Anahi, Gabriela, Sergio, Gonzalo, Victor, MarcoTulio, Marisol, Julieta, Tono, Jose Manuel and my new family Gema, Gemita, Arturo Sr, Perla, Erica, Oscar, Ana and Alfredo.

I want to dedicate this work to my lovely husband, friend and colleague, Arturo, for all his support and advice no matter what difficult appears.

I want to especially dedicate this work to my daughter, Esmeralda, with my entire hearth and my blessings. God bless you my sunshine.

Finally, I dedicated this work to the memory of my aunt Manuela and uncle Paciano and my grandmother and grandfather Eulalia and Julio.

CHAPTER ONE: INTRODUCTION

1.1 Overview

The skin is the most outer and largest organ of the human body; it has various functions in order to preserve body homeostasis, which aim to preserve life (Tobin, 2006). The loss of skin homeostasis, through injury, initiates the wound healing process that is destined to restore skin integrity and functions as quickly as possible. The final outcome of the wound healing process is the inevitable formation of a permanent scar (Schreml, et al., 2010). However, from unknown causes injuries can lead to the formation of pathological scars such as those present in keloid disease (Bayat, et al., 2003; Shih, et al., 2010).

Management of keloid scars is a clinical challenge as existing treatment modalities result in limited response coupled with a high recurrence rate (Butler, et al., 2008). Importantly treatments that have shown promising results *in vitro*, may then subsequently fail when translated into clinical practice (Agren et al., 2014). Therefore, the validity of the ideal scar model to evaluate candidate scar treatments is currently being questioned. Current *in vitro* models of scars and wound healing suffer from lack of a proper 3D environment and in appropriate animal models as animal skin and mode of healing as well as scarring process are different to what is observed in human skin. Monolayer and organotypic cultures provide valuable information about one or a few components of the skin at a time, but they lack 3D complexity of human skin. Additionally, animal models can present major structural

and biological differences notwithstanding the potential cost, ethical, and moral issues associated with their use (Lebonvallet, et al., 2010; Groeber, et al., 2012).

Therefore, some of the existing wound models fall short of the ideal scenario observed in human skin. Therefore, short of trials needed to be conducted in vivo in human skin, the in vitro model coupled with the ex vivo model may provide valuable tools for understanding the physiopathology of the human skin and the evaluation of novel treatments (Moll, et al., 1998; Lebonvallet, et al., 2010; van Kilsdonk, et al., 2013; Mathes, et al., 2014).

Photodynamic therapy (PDT) is a protocol widely used in treating skin oncology. PDT depends on the combined use of a photosensitiser, along with energy from illumination with a specific wavelength, and the presence of oxygen, resulting in the generation of reactive oxygen species (ROS; Robertson, et al., 2009). ROS triggers different responses depending upon the site of generation and amount (Wyld, et al., 2001; Castano, et al., 2004). Responses include proliferation, senescence, autophagy, apoptosis and necrosis at the cellular level (Castano, et al., 2005). Additionally, collagen degradation, damage-associated molecular patterns release and paracrine stimulation of metalloproteinases and immunological cells have also been observed (Garg, et al., 2010).

A limited number of studies had shown evidence of improved human wound healing after PDT (Statius, et al., 1997; Reddy, et al., 2010; Mills, et al., 2014). Similarly, a few reports on hypertrophic and keloid scars treated with PDT have shown a reduction of volume, erythema and improvement of scar colour (Campbell, et al.,

2010; Nie, et al., 2010; Ud-Din, et al., 2013). These findings suggest that PDT may have an important role in improving the human wound healing process and extracellular matrix remodelling of scars. Therefore, better understanding of the mechanisms and effects of PDT in adult human skin wound healing and scars are clearly required.

1.2 Background

Keloid organotypic co-cultures treated with PDT have been shown to induce rearrangement of collagen fibres (Ud-Din, et al., 2013), while some clinical reports on hypertrophic and keloid scars have demonstrated an effective reduction in the volume and improvement of the physical appearance of scar tissue (Nie, et al., 2010;).

In addition, anti-ageing studies in human skin have shown an increase in the expression of MMP9 and elastogenesis (Alameida-Issa, et al., 2009; Sanclement, et al., 2012). Moreover, human wound healing exposed to PDT showed an increase of MMP1, 2 and 9 suggesting that PDT may have an important role in the treatment of wounds, however more precise mechanisms remain unknown (Mills, et al., 2014; Almeida-Issa, et al., 2009; Calzavara-Pinton, et al., 2013).

Although a number of candidate therapies for enhancing skin repair have been evaluated using wound healing organ culture (WHOC) models (Companjen, et al. 2001; Tomic-Canic, et al. 2007; Kilsdonk, et al. 2013; Balaji, et al. 2014), there had not been any previous reports on the role of PDT in cutaneous wound healing using

the WHOC model. Despite the number of such WHOCs previously reported for the study of cutaneous wound healing processes, there has been a lack of standardization and conformity in testing of WHOCs.

The variations in these methodologies include the use of the following; a partial or full thickness wound, different culture conditions, and a range of support and growth mediums. Thus in the absence of a standardized protocol the most optimal set-up in relation to growth media, physical support systems such as collagen embedding or well-chamber inserts and the type of wound were optimized in order to study the wound healing process and functional testing of photodynamic therapy.

In view of the above findings, the current work evaluated the cytotoxic effects of PDT in vitro using keloid fibroblasts and compared them to normal skin fibroblasts. Then, a WHOC model of human adult skin was developed and optimized to evaluate the PDT effects on human wound healing. Finally, the effects of PDT in phenotypically different scars and striae distensae ex vivo were assessed and compared to normal skin and untreated controls.

1.3 Aim and general methodology of the research

This research project investigated the effect of PDT in cutaneous wound healing and skin scarring. The first approach was to investigate the cytotoxic effects of MALA-PDT compared to 5ALA-PDT in site-specific keloid fibroblasts compared to normal skin fibroblasts. First, the accumulation of protoporphyrin IX (PpIX) in keloid fibroblast compare to normal skin fibroblasts was evaluated by fluorescence

emission after various concentrations and incubation times with MALA or 5ALA only. Phototoxicity of the LED arrangement was also evaluated in a fluence range from 0-100 J/cm². According to PpIX accumulation and phototoxicity, a selection of suitable parameters for PDT treatment was selected for further analysis. These parameters were incubation for 3 hrs with MALA/5ALA and a fluence of 10, 20, 40 J/cm². Subsequent analyses included cytotoxicity, cytoproliferation, ROS generation, cell death (apoptosis/necrosis induction), senescence induction and a related differential genetic expression analysis of keloid pathogenesis and apoptosis.

Following the establishment of the cytotoxic effects of PDT in fibroblasts, the next aim was to optimize a wound healing organ culture (WHOC) model of human adult skin, in order to evaluate the effects of PDT. In accordance with the previous study, WHOCs were PDT treated with 5ALA as the pro-photosensitiser and illuminated with 20 J/cm² of red light. Hematoxylin and eosin stain (H&E), Weigert's elastic stain and Herovic's differential stain assessed general morphology. Tunel assay assessed cell death. Proliferating cell nuclear antigen (PCNA), Cytokeratin 14 (CK14), Platelet endothelial cell adhesion molecule (CD31) and alpha smooth muscle actin (α -SMA) assessed cellular activity while metalloproteinase 3 and 19 (MMP3 & 19) assessed extracellular matrix (ECM) remodelling and oxidative stress was assessed through cyclin-dependent kinase inhibitor 2A, multiple tumor suppressor 1 (p16). Additionally a gene related expression measured the effect of PDT on the optimized WHOC.

Finally scars and striae were evaluated ex vivo post-PDT. Scars and striae distensae organ cultures were compared with skin and non-treated controls. PDT was applied

to striae alba, fine line, hypertrophic and keloid scars. 5ALA-PDT was compared to MALA-PDT, both using a fluence of 40 J/cm^2 of red light. The general morphology was assessed by H&E, Herovici's and Weigert's differential staining. Apoptosis, proliferation, metalloproteinase 3 and tropoelastin expression was quantified immunohistochemically and differential gene expressions of PCNA, COLI, COLIII, MMP3 and ELN were assessed by qRT-PCR.

This thesis has the following structure:

Chapter 2 describes the human skin, the adult skin wound healing process and skin scar classification and formation. A description of the physiology and anatomy of human skin is included along with a brief description of the cellular and molecular biology of adult human skin. The wound healing process is described following the molecular biology of its various overlapping stages. Scar definitions, classification, bimolecular mechanisms involved in its formation and treatments are also described.

Chapter 3 describes the PDT concept and dermatological application. This chapter also includes PDT mechanisms of cellular and tissue destruction and a description of the most common pro-photosensitisers and light sources in dermatology. Furthermore, a literature review of PDT in the treatment of adult human wound healing and skin scarring also is included. Additionally, a brief description of tissue engineering methods, used to study the skin, is given in the final part of this chapter.

Chapter 4 presents the cytotoxic investigation at cellular level using a monolayer culture of site-especific keloid fibroblasts compare to normal skin. PpIX

accumulation kinetics after incubation with MALA or 5ALA only and red light phototoxicity were assessed in order to establish PDT parameters for further experiments.

Chapter 5 presents the optimization of an ex vivo wound healing organ culture (WHOC) model of adult human skin, considering wound geometry, physical support of the organ culture and three different growth media. Optimized WHOC was functionally evaluated with 5ALA-PDT.

Chapter 6 presents an evaluation of PDT in fine line, hypertrophic and keloid scars compared to striae distensae and normal skin ex vivo. Skin, striae and scar organ cultures were treated with 5ALA-PDT and compared to MALA-PDT. Then, organ cultures were compared to normal skin and untreated controls.

Chapter 7 presents the conclusion of the investigation of the effect of PDT on keloid fibroblasts compared to normal skin fibroblasts, the effect of PDT on adult human wound healing evaluated ex vivo and the effect of PDT on skin scarring evaluated in phenotypically different scar, striae and normal skin organ cultures. This chapter also includes suggestions for future work.

CHAPTER TWO: ADULT HUMAN SKIN, WOUND HEALING AND SCARS FORMATION

2.1 Introduction

The skin is a heterogeneous tissue formed by three layers, the epidermis, the dermis and the hypodermis (McLafferty, et al., 2012; Venus, et al., 2011). The principal components of the epidermis are the keratinocytes in different stages of differentiation. In the dermis the principal components are fibroblasts and collagens, whilst the hypodermis is composed of adipose tissue (Alberts, et al., 2002). These all work together in a network with each other, communicating through biomolecules and several other components, in order to preserve skin homeostasis and body function. Therefore skin preservation is paramount to preserving life function (Menon, et al., 20090).

The loss of skin homeostasis, through injury, initiates the wound healing process. The wound healing process of adult skin *in vivo* is an accumulative process divided into three stages, 1) the inflammatory stage, 2) the proliferative stage and 3) the remodelling stage, which all aim to restore skin integrity and body function. The final outcome of the wound healing process is visualized as a scar (Amar, et al., 2014; Schreml, et al., 2010).

Scars can cause disability, psychosocial and emotional distress, therefore affecting quality of life (Brown, et al., 2010). Even though skin scarring involves new skin generation, it is of a lower quality than the uninjured intact skin, as scarred skin lacks skin appendages, often has varied pigmentation and possesses reduced mechanical properties (Gurtner, et al., 2011). It may also develop into an abnormal pathological scar such as in keloid disease, which can be physically and psychosocially disturbing which can be damaging to quality of life (Junker, et al., 2014). Despite a plethora of scar treatments, results often fail when translated into clinical practice. Consequently, the identification of novel treatments is still required (Bayat, et al., 2003).

This chapter describes the physiology, anatomy, cellular and molecular biology of the human skin. A brief description of the adult human wound healing process is also included along with the definition and classification of skin scarring and its suggested mechanism of formation, which form the biological basis of this investigation.

2.2 Physiology and anatomy of adult human skin

The human skin is the largest organ in the body which presents with a highly organized gathering of fibres, cells, biomolecules and fluids (McLafferty, et al., 2012). Human skin varies according to anatomical location, for instance the scalp area contains the highest amount of hair follicles while the palmoplantar skin lacks hair follicles (Jablonski, 2004; Rinn, et al., 2008).

Regardless of anatomical site, the skin has several functions, providing a barrier of protection, thermoregulatory system, sensory system and it is part of the neuroendocrine and the immunological systems (Menon, et al., 2009; Venus, et al., 2011). However, skin quality and quantity changes with ageing causing detrimental effects on its functions (Ryan, 2004).

The main functions of the skin are:

1. Protective barrier

The skin is the first barrier against environmental insults, providing protection to internal organs from mechanical injuries, UV radiation, water loss and microbial hostility (Venus, et al., 2011).

2. Thermoregulation.

The skin helps to maintain the body internal conditions, including temperature and fluid balance through two processes; sweating and blood flow. These processes allow the body to work effectively by dissipating or accumulating heat and water. The skin has different permeability properties according to body location; the most permeable areas are the face, forehead and dorsum of the hand, while the palms are the least permeable (Jablonski, 2004; Venus, et al., 2011).

3. Sensory system.

The skin is the largest feedback sensory and mechanoresponsive system in the body, which relies on cutaneous innervations, cells and ECM fibres. Sensations

are received at the skin and transmitted to the brain through different corpuscles and receptors attached to Schwann cells. Meissner's corpuscles transmit variations in touch and vibration. Merkel cells sense touch and pressure, Pacinian corpuscles sense vibration and pressure, Ruffini receptors sense tensegrity, whilst nerve endings have a multimodal sense for nociception, temperature and xenobiotics and D-hair mechanoreceptors sense mechanical load (McKee, 1999; Venus, et al., 2011; Wong, et al., 2011).

4. Part of the endocrine system.

The skin is the place where keratinocytes synthesize pre-vitamin D. The ultraviolet B spectrum of sunlight transforms 7-dehydrocholesterol (pro-vitamin D₃) into cholecalciferol (pre-vitamin D₃), which actively participates as a precursor of several dietary sterols (Holick, 1998).

5. Socio-psychological behaviour.

The skin contributes to the social behaviour of a person since their aesthetic look determines gender, race and health, all of which influences the way that a person is accepted into society (Baker, 1989).

2.2.1 Anatomical layers of the skin and accessories

The skin is a heterogeneous tissue formed by three layers, the epidermis, the dermis and the hypodermis. Additionally the epidermis and dermis are separated by the basement membrane (Figure 2.1; Tortora, et al., 2005). The skin also has several

appendages, such as sweat glands, hair follicles and nails (McLafferty, et al., 2012).

The quantity of cells, fibres and appendages in the skin depends on their anatomical location and gender, while the quality depends on age, nutrition and hormone production (Hussain, et al., 2013).

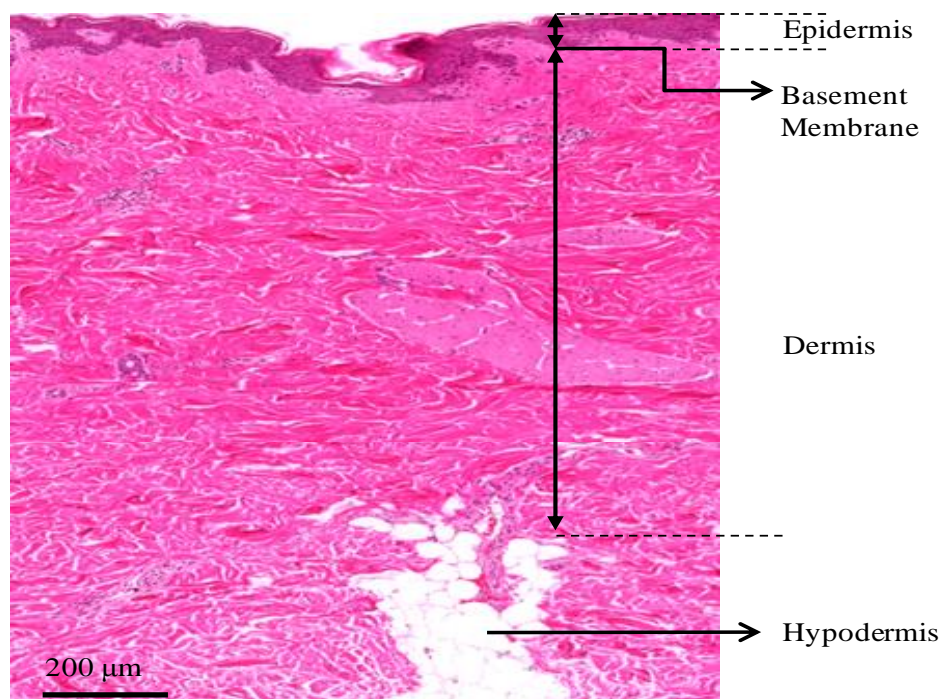


Figure 2.1 Anatomical layers of the adult human skin. Haematoxylin and eosin (H&E) staining of normal adult human skin (Original magnification 50x).

2.2.1.1 The epidermis

The epidermis is the most outer layer of the skin, which can measure from 0.06 to 1.00 mm. The eyelids have the thinner layer while the soles of the feet have the thicker layer (Brooker, 1998). It has an embryonic ectoderm origin. Thick epidermis is localized in and thin epidermis in the epidermis is avascular and in this sense is dependent on the dermis to survive (Schulz, et al., 2000; Venus, et al., 2011).

The epidermis is formed by four types of cells; keratinocytes (90-95%), melanocytes (8%), Langerhans cells (3%) and Merkel cells, however transient T-cells can also be found (Nestle, et al., 2009; Toebak, et al., 2009;).

Keratinocyte differentiation takes approximately 14 days, they change shape and size according to the differentiation layer, and these changes are driven by a change in adhesion structures and its cytoskeletal connection known as cytokeratins (Hwa, et al., 2011; Seltmann, et al., 2013).

Keratinocytes form four or five strata in the epidermis; each stratum represents one phase of keratinocyte differentiation. The number of layers depends on the body site—palmoplantar skin has five strata while the rest of the body has four. These strata are called 1) stratum basale, 2) stratum spinosum, 3) stratum granulosum, 4) stratum corneum as shown in figure 2.2, and 5) stratum lucidum below the stratum corneum (only in palmoplantar skin; Baker, 1989; Tortora, et al., 2013).

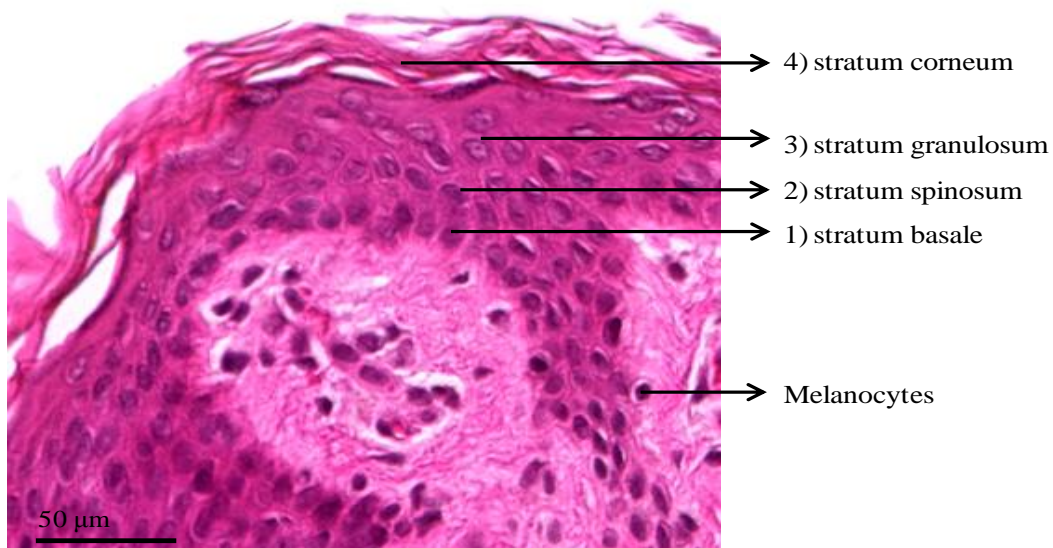


Figure 2.2 The epidermis. H&E staining in normal adult human epidermis (Original magnification 40X).

1. The stratum basale, stratum germinativum or basal layer is the deepest layer in the epidermis and it is attached to the basement membrane. Here the keratinocytes are generated by mitosis and the melanocytes can also be found (Tortora, et al., 2013).

The Melanocytes have a neuronal crest origin and a dendritic nature. The melanocytes produce melanin (Lin, et al., 2007). The melanin granules are transferred to the keratinocytes in the suprabasal layers through tentacles-like projections. Melanin is a pigment which protects from ultraviolet radiation. Melanin colour varies from brown to black and in addition to other components such as carotenes, haemoglobin and UVR exposure, contributes to the skin colour (Baker, 1989; Jablonski, 2004; Tortora, et al., 2013).

Keratinocytes in the basal layer are cuboidal cells with large nuclei with many ribosomes, small Golgi complexes, few mitochondria, and some rough endoplasmic reticulum and have tonofilaments as part of the cytoskeleton (Alberts, et al., 2002). The keratinocytes in the basal layer are attached by desmosomal junctions between each other, and hemidesmosomal junctions between them and the basal lamina of the basement membrane. Both attachments give the proliferative potential of the stem cells and decide the fate of the cell. The loss of basement membrane attachment initiates keratinocytes differentiation, with concomitant migration into the next strata (Alberts, et al., 2002; Hwa, et al., 2011).

2. The stratum spinosum, is where the keratinocytes begin to mature and produce intermediate filaments, as cytokeratins and laminins. Here, the keratinocytes are polyhedral cells, joined by desmosomes, which contribute to the strength and flexibility of the skin. This layer is 1 to 12 cells thick. In this stratum, Langerhans cells can be found. Langerhans cells function as antigen presenting cells and can release Immunoglobulin isotype A (IgA) as part of the immunological system (McLafferty, et al., 2012).
3. The stratum granulosum or the granular cells layer marks the end of cell differentiation. The layer is made of 3 to 5 layers of cells. Here, Keratinocytes become flattened and elongated, contain mainly keratohyalin and lamellar granules and are no longer able to perform any metabolic activity (Alberts, et al., 2002; McLafferty, et al., 2012).
4. The stratum corneum, or the corneal cell layer, is the last layer which has around 25-30 layer of dead cells. It has been divided into stratum compactum and disjunctum. The fingers, palms, and soles have one layer more called stratum lucidum and a thick stratum corneum. At the stratum corneum, dead keratinocytes are planar polyhedral shapes without nuclei and totally packed with keratin and lamellar granules, which are waterproof particles. Although the stratum corneum is a dead layer, it acts as a thin, sealant and flexible membrane and skin barrier that can be predicted upon its integrity (Alberts, et al., 2002; Hwa, et al., 2011; McLafferty, et al., 2012; Tortora, et al., 2013).

Keratinocytes at the stratum corneum, have few desmosomal attachments compared with basal cells and no hemidesmosomal attachment. Their attachment is made by lipid membrane interactions (Alberts, et al., 2002). This interaction also provides protection against radiation, heat, microbial attack and xenobiotics. Finally keratinocytes are desquamated, or shed, from the epidermis (Hwa, et al., 2011; McLafferty, et al., 2012; Tortora, et al., 2013).

2.2.1.2 The basement membrane

The basement membrane (BM) is about 50-100 nm thick and joins the epidermis and dermis. It functions as a reservoir for biomolecules, a barrier to control the interchange of cells and biomolecules between epidermis-dermis, and provides support for cell organization, migration, proliferation and differentiation (LeBleu, et al., 2007). BM is composed of two layers, the basal lamina and the reticular lamina (Figure 3.2; Alberts, et al., 2002).

The basal lamina layer contains collagen IV and VII, laminin, nidogen, glycoproteins and proteoglycans mainly perlecan. The basal lamina provides a scaffold after epidermal injury for tissue repair and regeneration and promotes cell metabolism, organization, proliferation, survival and migration (LeBleu, et al., 2007). The reticular lamina is made of fibrous proteins that restrict the passage of large molecules. Both layers are synthesized by epidermal keratinocytes and dermal fibroblasts. (Alberts, et al., 2002; Tortora, et al., 2013).

2.2.1.3 The dermis

The second layer of the skin is the dermis. It has a mesodermal origin and its thickness varies according to anatomical location from 1 to 4 mm. The dermis includes fibrillar, cellular and interstitial components. Fibrillar components include collagen, glycosaminoglycans, hyaluronic acid, chondroitin, dermatan, heparin and elastin. Cellular components of the dermis include immune cells, sensory cells, capillaries of blood and lymphatic vessels, nerve cells and fibroblasts. The interstitial components include bioactive molecules, polysaccharides, proteoglycan, proteins, salts and water. Fibrillar and extrafibrillar components are commonly known as extracellular matrix (ECM) and together give the skin strength, elasticity, sensory features and also provide a template for repair and regeneration of the epidermis (Schulz, et al., 2000).

The dermis can be divided in two, the papillary dermis (~300 µm thick) and reticular dermis (~700 µm thick). The papillary region contains, capillary loops, Meissner corpuscles and nerve endings. The reticular region contains few adipose cells, Valer-Pacinian corpuscles, glands and epidermal appendages. Both contain collagen and elastin fibres, however in different amounts and structure as shows in Figure 2.3 (Sorrell, et al., 2004; Tortora, et al., 2013).

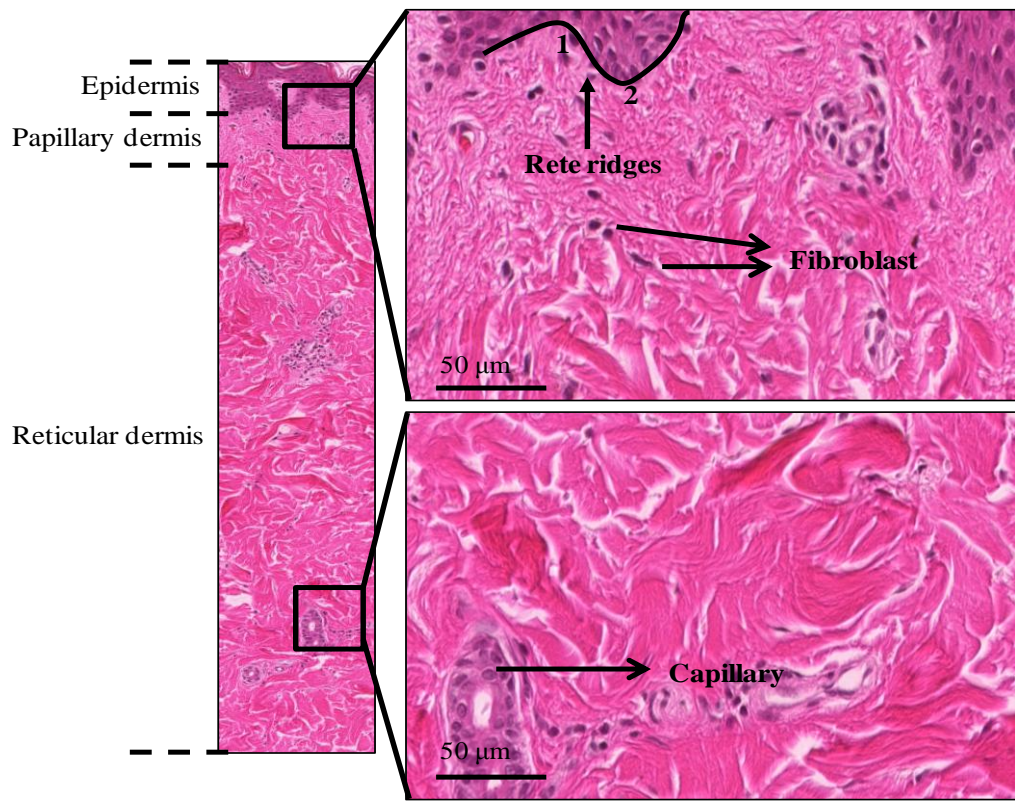


Figure 2.3 The dermis. 1 denotes valleys and 2 denote peaks of rete ridges. The dermis joins the epidermis and the basement membrane forming rete ridges, which provide mechanical protection and a spatial organization for stem cells (Original magnification 40x; Ghazizadeh, et al., 2005; Venus, et al., 2011).

The reticular dermis has a network of blood vessels which can be divided in deep plexus and superficial plexus. They are responsible for the supply of nutrients, oxygen to the dermis and epidermis. Blood vessel density varies according physical location and is related to temperature and pressure, the highest vessel density is found in skin covering the head, nipples, palms and soles (McLafferty, et al., 2012).

2.2.1.4 The hypodermis

The hypodermis is composed of adipose tissue, macrophages, stromal vascular cells and stem cells. Its main function is the management and storage of energy as fat and is part of the thermoregulation system (Choi, et al., 2008). However, the hypodermis

also works as a production-house for hormones, cytokines, growth factors and stem cells and has a major neurovascular bundles and lymphatics vessel to supply nutrients and drain waste (Figure 2.4; Klein, et al., 2007; Sundberg, et al., 2012).

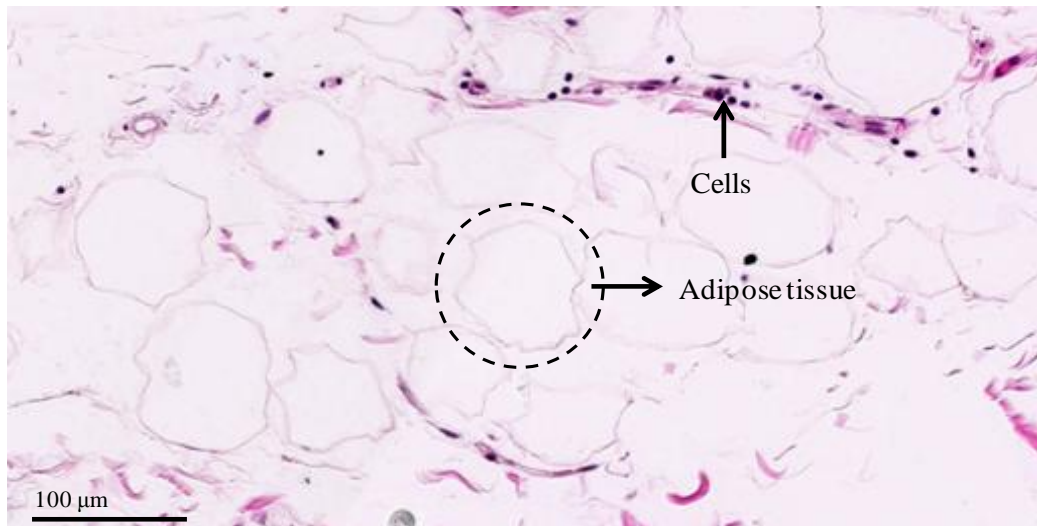


Figure 2.4 The hypodermal tissue. Adipose tissue stained with Haematoxylin and eosin, original magnification 20x.

2.2.1.5 Skin accessories

The dermis has ectodermal derivatives called epidermal appendages; these include hair follicles, sweat glands, sebaceous glands, ceruminous glands, mammary glands, and nails (McLafferty, et al., 2012). The hair also works as protection and is part of the sensory, thermoregulatory and social communication systems (Inoue, et al., 2009). The hair follicles are composed by a hair shaft, an epithelial root sheath and a dermal papilla covered with a matrix of transient amplifying cells. The epithelial root sheath is divided in outer and inner sheath. The outer root sheath has a reservoir of stem cells known as the “bulge” region and the outer root sheath is connected to an arrector pili muscle, sebaceous and sweat glands. The dermal papilla is connected to blood vessels and sensory nerves (Yu , et al., 2008; Blanpain, et al., 2009; Buffoli, et al., 2014).

2.3 Cellular and molecular biology of adult human skin

Keratinocytes and fibroblast can be studied in order to assess the effects of external stimuli, in order to provide further insight and elucidate mechanisms for observed responses. However, the ECM has been found to actively participate in all skin functions. For this reason, the most comprehensive evaluations should consider the 3D features of the ECM and its molecular components.

2.3.1 Keratinocytes

The keratinocytes form a dynamic homeostatic structure of new and differentiated cells in order to provide the first defence barrier in the human skin. They secrete abundant molecules as part of their autocrine and paracrine communication. Their main function is to stimulate surrounding cells to grow, migrate, proliferate, differentiate, and survive (Alberts, et al., 2002).

The keratinocytes, in normal homeostasis, secrete several biomolecules as growth factors and cytokines, some of which are produced without external stimulus. Some biomolecules as MMPs are only produced after paracrine stimulation, as part of a 3D structure or in the wound healing process (Alberts, et al., 2002; O'Toole, 2001).

Table 2.1 Growth factors expressed by keratinocytes in normal homeostasis

Growth factors
Amphiregulin (AREG)
Betacellulin (BTC)
Epiregulin (EREG)
Epidermal growth factors (EGF)
Heparin-binding EGF-like growth factor (HB-EGF)
Normal epidermal growth factor (EPGN)
Keratinocyte growth factor (KGF)
Transforming growth factor (TGF) α and β
Trypsinogen
Enteropetidase

(Grone, 2002; Kajiya et al., 1997; Nakanishi et al., 2010; Stoll et al., 2010)

Adhesion structures include integrins and cadherins and are mainly present in the basal layer. Cytokeratins vary according to the epidermal layer as shown in table 2.2. These changes have been related to the regulation of proliferation, differentiation and morphogenesis (Hwa, et al., 2011; Seltmann, et al., 2013). Cytokeratins are part of the cytoskeleton, which preserve keratinocyte tensegrity, and vary according to the mechanical load and thus are related to mechanotransduction signalling (Wong, et al., 2011).

Table 2.2 Molecules expressed in the epidermal layers related to cell adhesion and shape

Epidermal layer	Molecule
Basal layer	Cytokeratin 5 (CK-5) and 14 (CK-14)
Spirillum layer	Cytokeratin 1 (CK-1) and 10 (CK-10)
Granulosum layer	Cytokeratin 1 (CK-1) and 10 (CK-10) Filaggrin Loricrin Involucrin Epidermal transglutaminase

(Seltmann, et al., 2013; Suter, et al., 2009)

2.3.2 Fibroblasts

Fibroblasts, the main cellular components of the dermis, are specialized cells of the connective-tissue family (Figure 2.5). Fibroblasts are elongated and spindle-shaped in 2D culture but can easily adapt themselves to the shape of the underlying substrate in 3D environments (Tschumperlin, 2013).

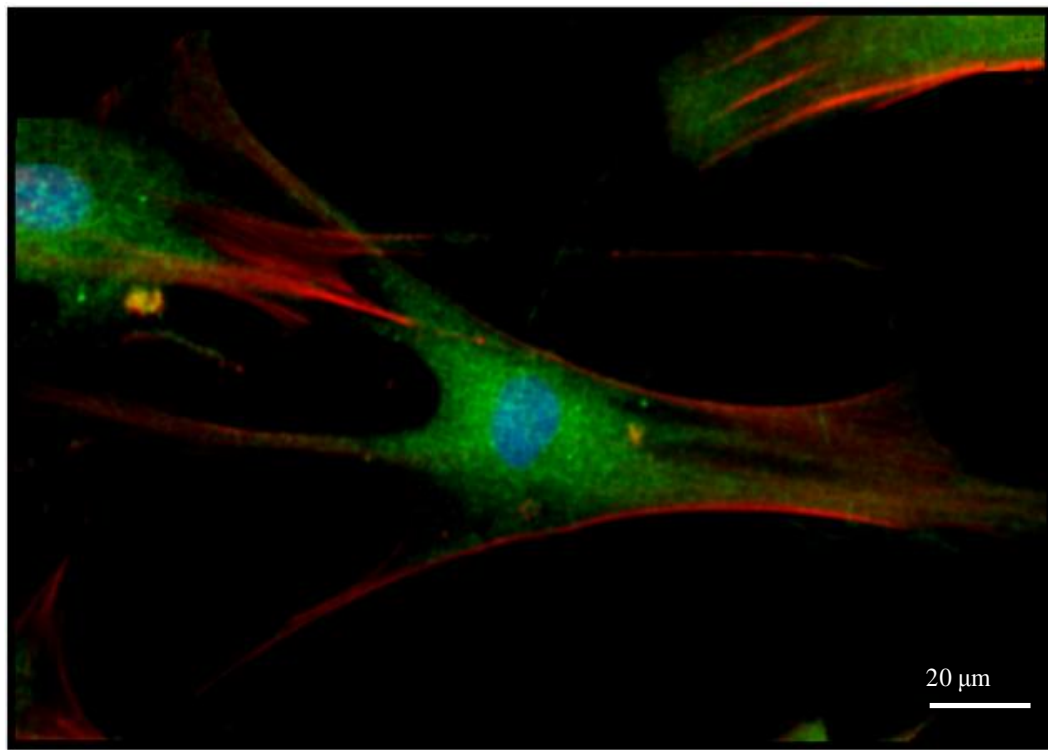


Figure 2.5 A dermal Fibroblast. Picture shows a fibroblast in monolayer culture, where nucleus is stained in blue (DAPI), focal adhesions in green (anti-Vinculin) and F-actin fibres of the cytoskeleton in red (Phalloidin-Alexa Fluor 488; Original magnification 100X).

Fibroblasts synthesize and store ECM proteins, growth factors, cytokines, prostaglandins and leukotrienes, some of the most studied molecules are shown in Table 2.3. These molecules can function as communication signals, deciding the fate of the neighbouring cells. For instance fibroblast can induce keratinocyte

proliferation and migration (Figure 2.6), as well as recruit immunological cells in case of injury (Alberts, et al., 2002). However fibroblast morphology is similar in all dermal layers, their genetic expression varies according to physical origin and dermal layer localization, which influences specific quantity of ECM synthesis, paracrine communication and cell fate, but in culture exhibit different characteristics (Rinn, et al., 2008).

Fibroblast isolated from the papillary dermis growth a faster and achieve a higher cell density compare to fibroblast for the reticular layer. Papillary fibroblast produces low levels of versican and high levels of collagen XVI, decorin, ration granulocytomacrophage colony-stimulating factor (GM-CSF)/keratynocyte growth factor (KGF), while reticular fibroblast produces high levels of versican and low levels of collagen XVI, decorin and GM-CSF/KGF ratio (Sorrell, et al., 2004; Tschumperlin, 2013).

Table 2.3 Biomolecules normally expressed by fibroblasts.

ECM proteins	Growth factors	Cytokines	MMPs
Collagens	TGF β family	interleukin-1 α and -6 (IL-1 α ; IL-6).	MMP1
Fibronectin	Fibroblast growth factors 1 and 2 (FGF -1, -2)		MMP2
Proteoglycan	Platelet derived growth factor (PDGF) family		
Elastin			
Glycoproteins			

(Alberts, et al., 2002; Rinn, et al., 2008; Shariati, et al., 2009; Sorrell, et al., 2004)

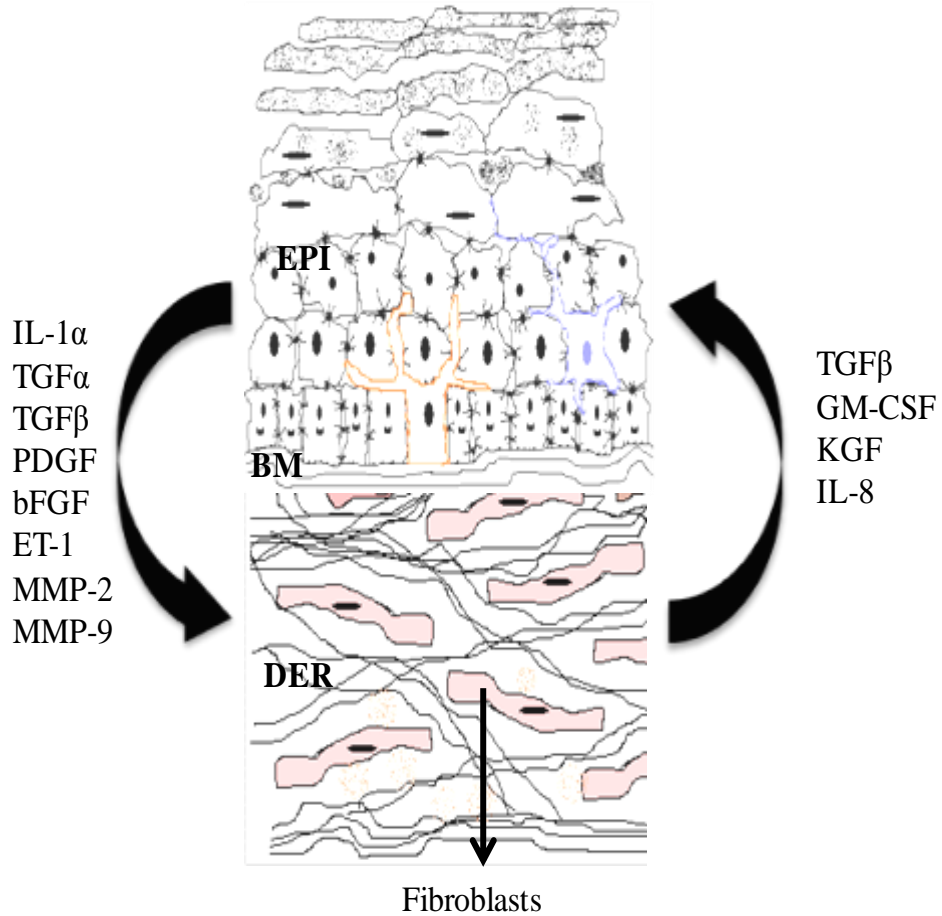


Figure 2.6 Epidermal-dermal paracrine communication. Schematic representation of epidermal-dermal communication driven by keratinocyte-fibroblast signal factors. EPI denotes epidermis, BM denotes basement membrane and DER denotes dermis.

2.3.3 Extracellular matrix

The extracellular matrix (ECM) determines the biochemical and biomechanical properties of the skin and in this sense influences cell behaviour (Wong, et al., 2011). Since ECM arrangement can regulate biochemically and mechanically the cellular behaviour, disturbance on them can contribute to development of certain skin disorders (Silver, et al., 2003).

ECM structure has three essential functions 1) provides a mechanical support, which allows cell adhesion, growth, proliferation, differentiation, 2) a reservoir of biomolecules, such as growth factors, cytokines, matrix metalloproteinases (MMPs) and tissue inhibitor of MMPs (TIMPs; Table 2.4 and 3) allows the flow of nutrients, metabolites, signal biomolecules and proteins between the capillaries and the skin (Chakraborti, et al., 2003; Martins, et al., 2013; Stamenkovic, 2003).

The tridimensional (3D) structure of the ECM is pivotal to maintain the normal homeostasis of the skin for instance some biomolecules as MMPs, which in normal homeostasis are expressed in very low quantities, change their expression upon disruption of the 3D structure of the ECM. An exacerbate and long lasting change in the 3D structure may leads to the dysregulation of proteins, starting pathological process as well (Chakraborti, et al., 2003; Gattazzo, et al., 2014; Martins, et al., 2013; Stamenkovic, 2003).

Table 2.4 MMPs and TIMPs localized in the ECM

MMPs	TIMPs
Collagenases MMP1,8 and 13	TIMP1
Gelatinases MMP2 and 9	TIMP 2
Stromelysins MMP3, 10 and 11	TIMP 3
Matrilysins MMP7 and 26	TIMP 4
Others MMP14-17, 19-20, 23 and 24	

(Chakraborti, et al., 2003)

2.3.3.1 Collagens

Collagens have long, rigid, triple-stranded helical structures. They can be classified depending on their amino-acid sequences (Table 2.5). Collagens can be found in many different arrangements depending on their location; therefore its network configuration ultimately results in the Langer's lines, which are lines of skin tension parallel to muscles fibres (Carmichael, 2014; Silver, et al., 2003).

The papillary dermis has poorly organized collagen bundles while the reticular dermis has thick bundles, however both are formed by collagen (COL) I and III (Figure 2.6). The collagen has an interwoven arrangement in order to support tensile stress. Collagen represents 75% of dry weight and 30% of the volume in the dermis, from which 75 % is collagen I and 15% is collagen III (Silver, et al., 2003).

Table 2.5 Collagen types in normal human skin

Type of collagen	Localization
I	Reticular dermis
III	Papillary dermis
IV	Basal lamina
V	Interstitial tissue
VI	Papillary dermis and blood vessels
VII	Anchoring fibrils
VIII	Endothelium
XII	Hemidesmosomes
XIII	Hemidesmosomes
XVII	Hemidesmosomes

Glycosaminoglycans (GAGs) are polysaccharide chains found as proteoglycans in the ECM but in different amounts according to dermis layers (Alberts, et al., 2002). The GAGs usually work to form a gel-like scaffold, regulating the trafficking of molecules, proteins and cells, enhancing or inhibiting paracrine communication, regulating enzymatic activity, and as co-receptors (Hussain, et al., 2013).

Elastin represents around 4% of the dry weight of skin. It is the main component of the elastic fibres. It has a great range of extensibility which allows collagen bundles to return to their original shape upon removal of a strain (Figure 2.6). Elastic fibres give the skin, its property to stretch and shrink, however they do not contribute to tensile strength of the skin (Alberts, et al., 2002; Hussain, et al., 2013).

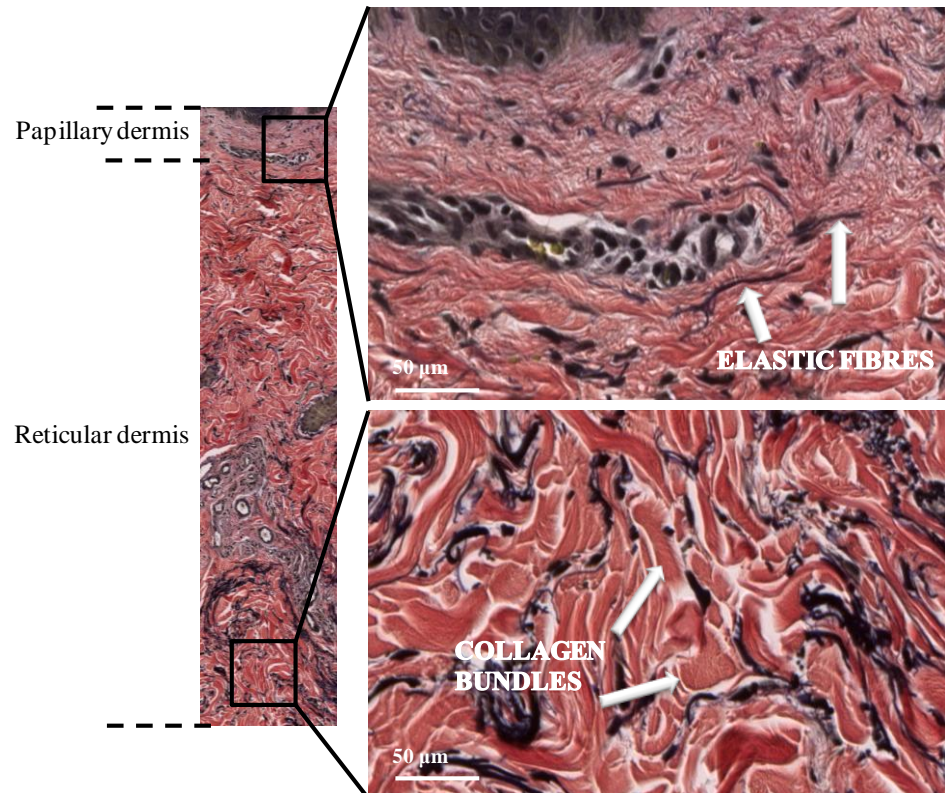


Figure 2.7 Collagen and elastic fibre arrangement in adult human skin. Pictures shows elastic (black) and collagen (pink) fibre arrangement, stained with Weigert's differential elastic stain.

2.4 The wound healing process

The wound healing process of adult skin *in vivo* is a complex process that repairs the skin after an injury. It is usually divided into three stages, which can be overlapped in time and space — 1) the inflammatory stage, 2) the proliferative stage and 3) the remodelling stage (Schreml, et al., 2010).

From a histological point of view, the wound healing process is divided into granulation tissue formation, wound contraction and scar formation. These stages overlap, until they reach a final result known as a scar. Alterations in the wound healing process may cause chronic wounds or pathological scarring. Both could cause functional problems upon size and localization (Amar, et al., 2014).

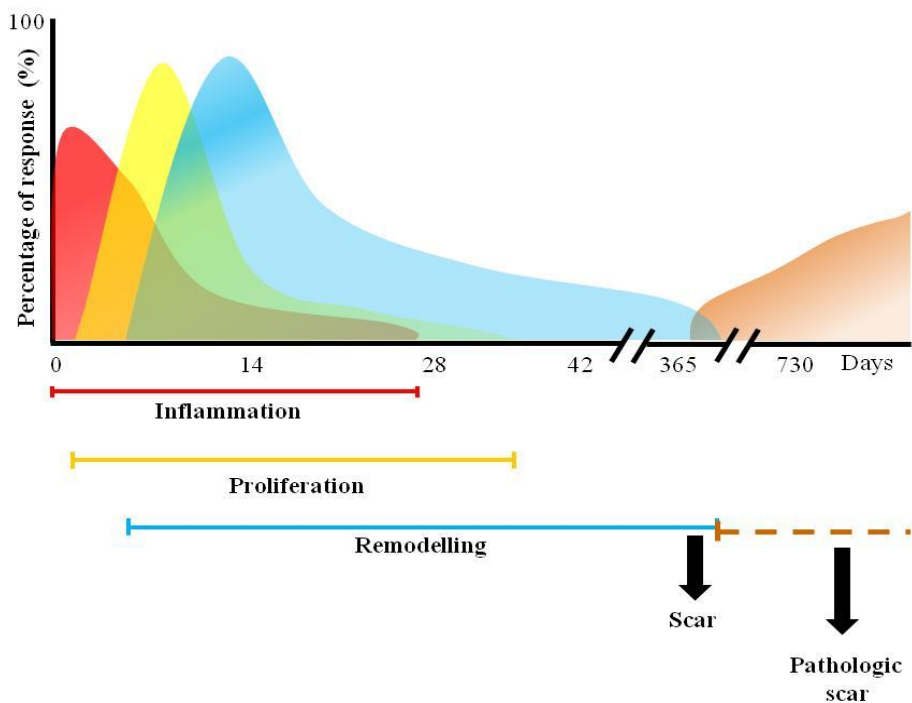


Figure 2.8 Stages of adult human wound healing process.

2.4.1 The inflammatory stage

The inflammatory stage includes the formation of a blood clot to stop bleeding and the recruitment of immunological cells to clean the wound bed. The clotting cascade includes a combination of fibrin (95%), platelets, fibronectin, SPARC/osteonectin, thrombospondin and vitronectin. The platelets are phagocytosed later and replaced with collagen (Schreml, et al., 2010).

If the injury damages a blood vessel, vasoconstriction occurs followed by vasodilatation. The damage caused by the injury also causes damage and pathogen-associated molecular patterns (DAMPs, PAMPs) and ECM protein domains as matrikines and elastokins among cytokines, growth factors, and proinflammatory factors that all together initiate signals that initiate a highly active immunological response (Maquart, et al., 2014). These attract cells such as polymorphonuclear neutrophils, macrophages, dendritic cells, leukocyte, an arsenal of chemotactic factors, MMPs, disintegrin-metalloproteinases (ADAMs) and ultimately keratinocytes and fibroblasts (Schreml, et al., 2010).

The inflammatory stage has been related to the generation of a scar, mainly through the inflammatory factors present at the wound site and their paracrine effect. The main inflammatory signals, besides cytokines, are reactive ROS, heat shock proteins (HSPs), DAMPs, PAMPs, matrikines and elastokins (Bryan, et al., 2012; Bainchi, 2007).

However ROS generation has a ubiquitous function, it can delay wound healing process, especially peroxiredoxin-6, which reduces hydrogen peroxide, which functions as one product of protection in keratinocytes and endothelial cells. On the other hand it can induce cell proliferation through overexpression of HIF-1 α , which is also related with improvement of angiogenesis and wound healing (Schreml, et al., 2010;).

Oxidative stress also causes protein and lipid peroxidation, forming reactive carbonyl compounds (RCCs), advanced glycation end products (AGEs), advanced lipid peroxidation end products (ALEs), malondialdehyde, 4-hydroxy-2-nonenal (HNE) and oxysterol. The interaction and cross-links of these products with cells and tissue proteins, produces tissue damage which may progress to pathologies as atherosclerosis, neurodegenerative diseases and cancer (Negre-Salvayre, et al., 2008; Thanan, et al., 2014).

The HSP family are highly conserved proteins, which contribute to the wound healing process in this stage. Fibroblasts can release HSP upon stimulus of stress and death risk, especially HSP 70 and 90 (Schreml, et al., 2010; Tschumperlin, 2013).

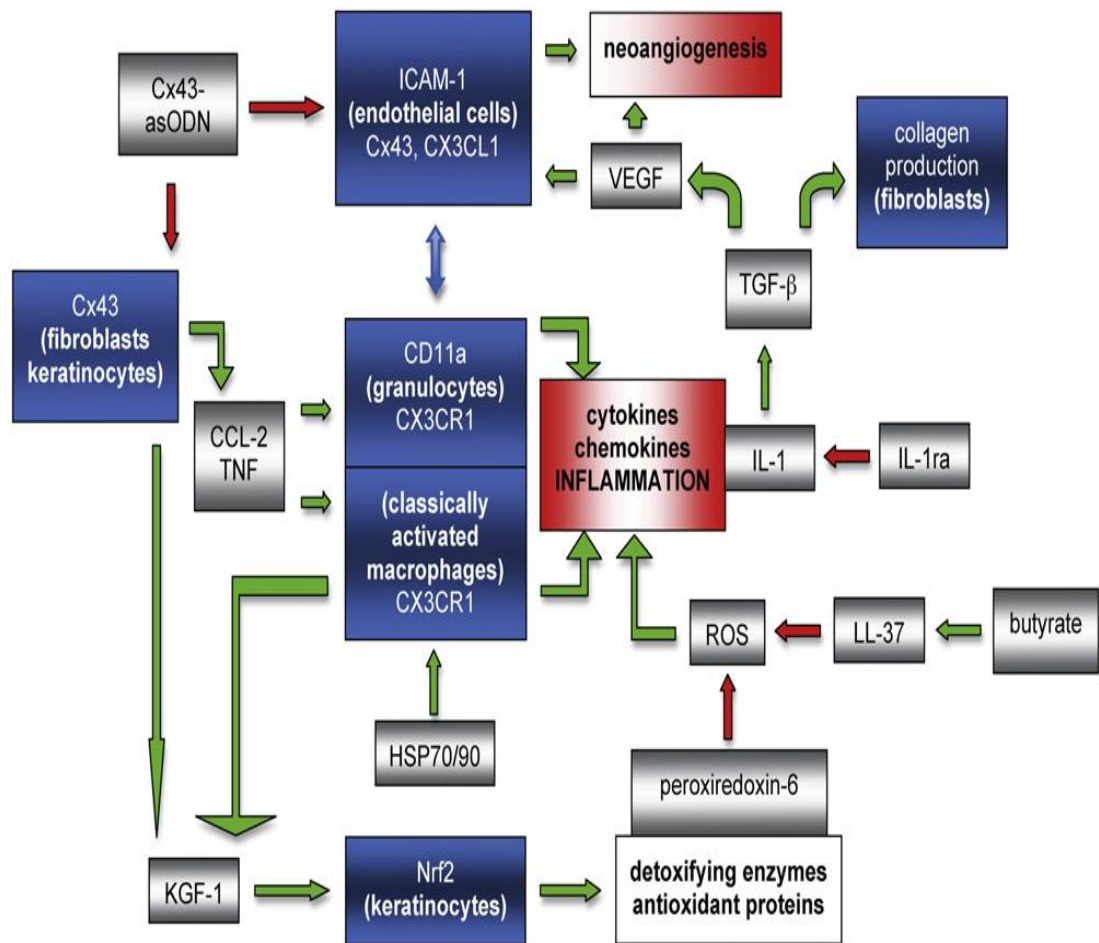


Figure 2.9 Suggested molecular mechanisms of the inflammatory stage of wound healing. Cell communicate through different messengers as CCL-2, TNF, IL-1 initiating the inflammatory phase, while TGF β and KGF-1 induces the proliferative phase while ROS, HSP are produced to induce both stages. “Green arrows, positive regulation: activation; red arrows, negative regulation: inhibition” (Schreml et al., 2010).

Matrikines and elastokines are ECM domains that have been generated upon proteolytic degradation of ECM after injury, while DAMPs are released following injury and PAMPs by the damage to the skin microbiota. All of the above can stimulate wound healing induction through the activation of immune cells, chemotaxis, keratinocyte migration, fibroblast proliferation, vasodilatation, angiogenesis and ECM remodelling (Bainchi, 2007; Maquart, et al., 2014).

2.4.2 The proliferative stage

The proliferative stage includes granulation tissue formation, re-epithelialization, neoangiogenesis, and regeneration of the ECM and wound contraction. Granulation tissue consists of laminin and fibronectin scaffolds that allow the re-epithelialization of the wound by keratinocytes (Amar, et al., 2014). In this stage, keratinocytes change from a cubical or round shape to a flat and elongated morphology with extensions called lamellipodia, in order to migrate from the edges of the wound and from dermal appendages. This process, known as the keratinocyte activation cycle, also involves many genes and protein expression changes. Once the keratinocyte, or epithelial tongue, is formed keratinocyte proliferation also begins in the epithelial tongue (O'Toole, 2001; Suter, et al., 2009).

Keratinocytes upon injury release several factors for autocrine and paracrine communication some as shown in Table 2.6 (Grone, 2002). Their effects include an autocrine effect of migration, proliferation, differentiation, paracrine effect on neighbouring fibroblasts, stimulating migration of immune cells and myofibroblasts to the wound site (O'Toole, 2001). The overall effect is to promote wound closure and ECM remodelling. The Figure 2.9 shows a suggested molecular mechanism of this stage (Amar, et al., 2014; Suter, et al., 2009; Tomic-Canic, et al., 1998).

Table 2.6 Keratinocytes expression factors at the proliferative stage of wound healing

Growth factors and cytokines	Keratin expression	ECM proteins
TGF α ,	CK-6, CK-14	MMP 1,2,3,7,17,19
GCSF	CK-16 and CK-17	
GM-CSF		
IL-1, 3, 6, 8, 10, 12, 15, 18 and 20		Cathepsin S
Interferon (IFN) α , β and γ		
MCSF		
Tumor necrosis factor α (TNF α)		
(Amar, et al., 2014; Blumenberg, 2006; Grone, 2002; O'Toole, 2001; Suter, et al., 2009; Tomic-Canic, et al., 1998)		

The hair follicles have two reservoirs of stem cells known as the “bulge” region and the upper isthmus. Both populations of stem cells are capable of migrate and differentiating into keratinocytes, sebocytes, hair in the wound healing response. However its action ends as soon as the injury is healed and its action has found diminish with age (Teng , et al., 2014; Blanpain, et al., 2009; Buffoli, et al., 2014).

At this stage transforming growth factor β_1 (TGF- β_1) and the mechanical microenvironment trigger a transdifferentiation of fibroblasts into myofibroblasts. Myofibroblasts express α -smooth muscle actin, which allow them to have a increased motility and produce strong contractile forces (Heng, 2011). They enhance skin repair synthesizing a higher amount of ECM proteins, for instance deposition of collagen III and fibronectin. Myofibroblasts also express several growth factors and chemotactic factors in order to attract immune cells as well as more myofibroblasts.

As result repair, remodel the ECM and wound contraction (Hinz, 2007; Schreml, et al., 2010).

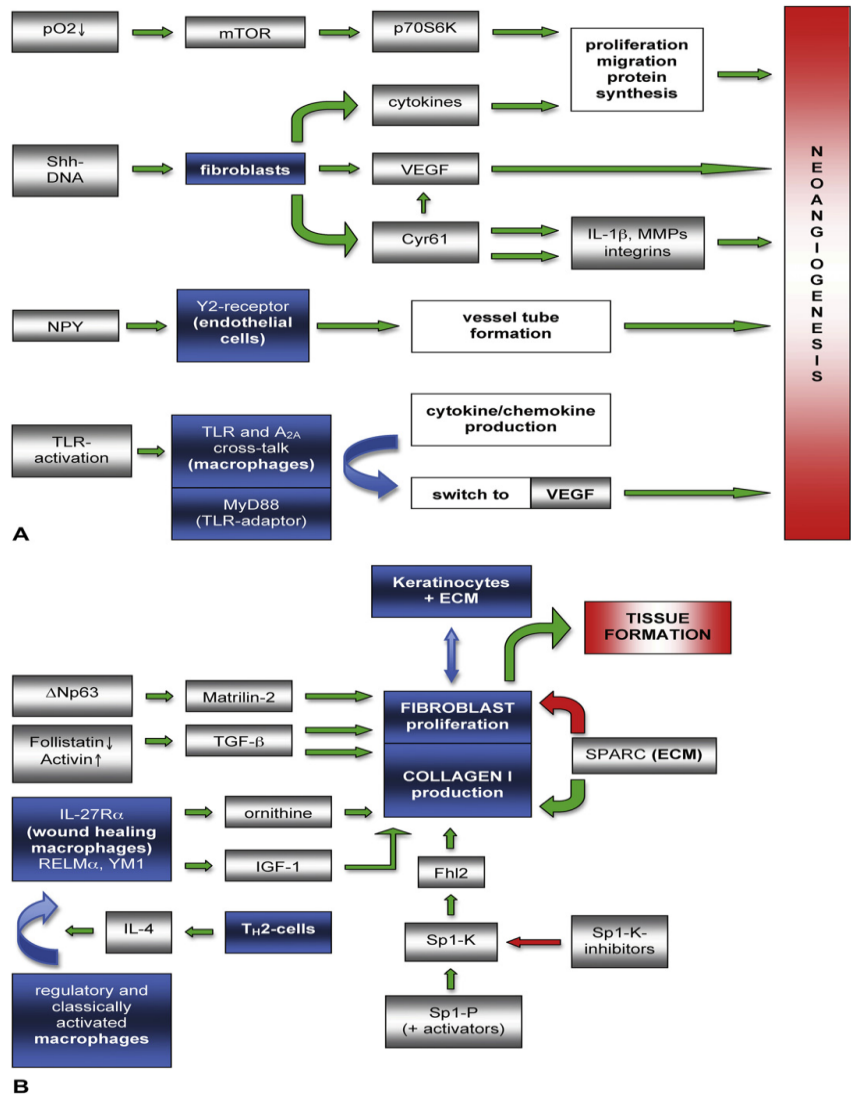


Figure 2.10 Suggested molecular mechanisms of the proliferative stage of wound healing. Proposed mechanisms for (A) neoangiogenesis and (B) tissue formation. “Green arrows, positive regulation: activation; red arrows, negative regulation: inhibition” (Schreml et al., 2010).

Neoangiogenesis is also caused by the activity of fibroblasts and endothelial cells, at the same time fibroblasts migrate to the wound site, proliferate and produce collagen and other ECM proteins until new tissue fills up the whole wound space. Here, hypoxia causes a delay in the healing of chronic cutaneous wounds, inducing the

activation of proliferation and angiogenesis by several suggested molecular mechanism as show figure 2.9. In this stage other restrictive factors include the availability of nutrients and oxygen which regulate the cross talking between fibroblast and keratinocytes. This talk is also regulated by chemotactic factors such as TGF β and MMPs (Schreml, et al., 2010).

2.4.3 The remodelling stage

The remodelling stage can last from several months up to two years depending on wound size. At the beginning of the remodelling phase, fibroblasts synthesize different fibres and send chemical signals to produce the ECM components and initiate angiogenesis. The formation of the new ECM will be directed by cell signalling in a paracrine manner through HGF, TGF β s, EGF, CTGF and FGF family and in an autocrine manner by HSP90 (Alfaro, et al., 2013; Beanes, et al., 2003; Hance et al., 2014; Ramirez, et al., 2014).

Further on, the maturation of the scar will involve changes in the ECM composition as collagen III is replaced by collagen I and aligned with the tension lines of the scar. This stage is regulated by MMP family and their inhibitors, TIMPs, both are major effectors of scar formation and ECM remodelling, which in turn determines scar quality (Figure 2.10; Chaudhuri, et al., 2006; Eckes, et al., 2010).

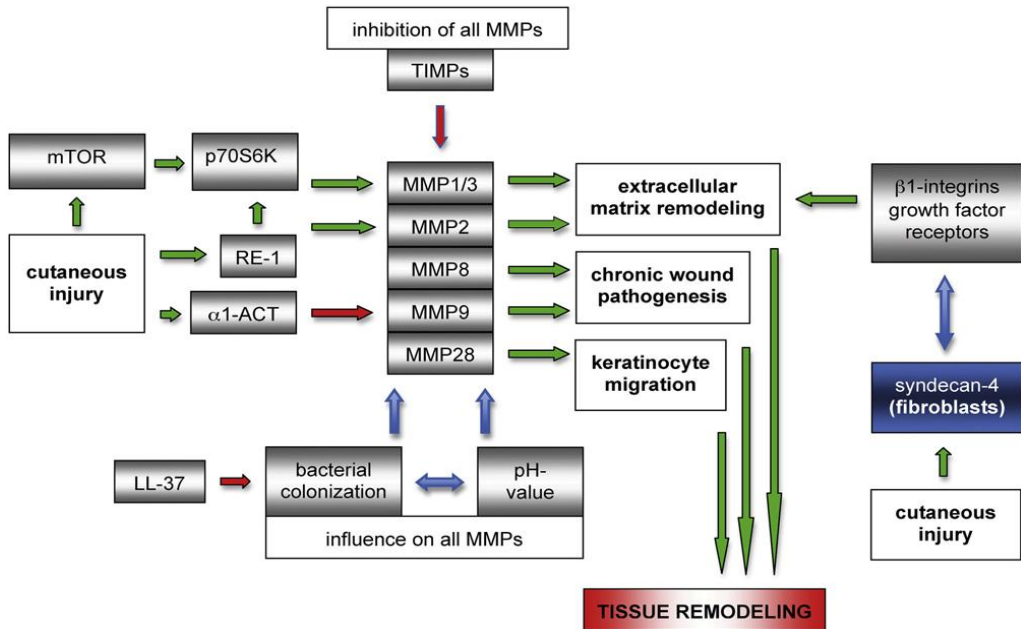


Figure 2.11 Suggested molecular mechanisms of the remodelling stage of wound healing. “Green arrows, positive regulation: activation; red arrows, negative regulation: inhibition” (Schreml, et al., 2010).

Migration of keratinocytes and fibroblasts requires the action of MMPs especially MMP1, MMP2 and MMP9, which modify the ECM in a feedback fashion. In particular, keratinocyte migration is closely related to mechanical stress, size of injury and epidermal-dermal communication. MMP1 and MMP3 are regulated by mTOR after DNA damage caused by UVB exposure, so can be considered as markers of wound healing that is caused mainly by photodamage (Eckes, et al., 2010; Maquart, et al., 2014).

MMP3 is closely related with proliferative cells, while MMP1 is localized in the advancing tongue. MMP3 regulates the organization of actins in dermal fibroblasts, activates other pro-MMPs and increases the bioavailability of HB-EGF and bFGF (Martins, et al., 2013; Schreml, et al., 2010; Stamenkovic, 2003).

The overall result in this stage is the contraction of the collagen which reduces the scar surface area. However with time, fibroblasts become senescent. Senescent cells

also have a decrease ability to remodel the ECM (Schafer, 2008; Enoch, 2010). Senescence is a state where cells stop dividing themselves, however remain metabolically active and release a pro-inflammatory secretome. Those characteristic, also known as senescence associated secretory phenotype (SASP), which may trigger beneficial or harmful process, upon the physiological context. However when a person become older senescent cells accumulate, contributing to ageing, Nevertheless a define percentage of senescent fibroblast in human skin still unknown due to many factors contributing to aging as disease, habits and genetic charge (Campisi, et al., 2014).

Finally the end solution of the wound healing phases induce a variety of responses visualized as the spectrum of scars, however for unknown reason also a scar may progress to a pathological process as keloid disease (Bayat, et al., 2005) .

2.5 Skin scars formation

2.5.1 Definition and phenotypic characteristics

Skin scars are defined as the inevitable conclusion of the wound healing process with the aim to restore skin homeostasis and maintain functions (Bayat, et al., 2003). However, scars do not fully achieve this and have a lower quality compared to the original Skin (Gurtner, et al., 2011). Scars can cause psychosocial and emotional distress, even if they are positioned in non-visible areas (Brown, et al., 2010). Additionally, the cause of scarring and its size may also result in disability with negative impact on self-image, therefore affecting life quality (Bayat, et al., 2003; Junker, et al., 2014; Lee, 2011; Satish, et al., 2010).

Multiple intrinsic and extrinsic factors influence scar quality, which in turn define its phenotype. Intrinsic factors related to scar outcome include skin mechanical properties; related to its location, depth and tension, underlying conditions and genetic factors (Dunkin, et al., 2007; Huang, et al., 2012; Yang, et al., 2012). Although these factors have been related to the final outcome, their complete molecular mechanisms remain unknown.

Lesions that do not perturb the basement membrane (BM) usually do not cause a scar but dermal lesions with a perturbed BM usually produce a fibrotic scar (Dunkin et al., 2007). In cases where dermal damage is above 33% a hypertrophic, or keloid scar, is more likely to form (Wong, et al., 2011). Hypertrophic scars rarely occur in people older than 65 years and in palms, soles, scalp, and eyelid (Ramos, et al., 2008;). Additionally small lesions that perturb the ECM tend to reduce their size due to skin elasticity while larger lesions increase their size due to greater disruptions beyond the elastic limit, where the deformation of the skin is irreversibly (Bush, et al., 2005; Wong, et al., 2011).

Extrinsic factors involve microbial infection, oxygen tension and the physical cause of the wound such as burns, surgery and lacerations (Coolen, et al., 2010; Dunkin, et al., 2007; Satish, et al., 2010). Similar to intrinsic factor, these factors are implicated in the final outcome, however their biology is still unknown.

Skin scars have been characterized clinically based on their phenotypic features, such as colour, texture, margins, size and quantity as shown in Table 2.7 and figure 2.12 (Fearmonti, et al., 2010; Junker, et al., 2014; Lee, 2011).

Table 2.7 Skin scar classification

Type of scar	Phenotype	Histology	Example
“Normal” fine line	Thin line	No rete ridges	First intention healing
Stretch	Flat, pale, soft, not elevations, thickening or nodularity.	Thin epidermis, fine collagen bundles arranged in straight parallel lines	Striae rubra Striae alba
Contracted	Shortening and dystrophy of the affected area.		Usually appear at joints or concavities
Atrophic	Flat and depressed below the surrounding skin.		Post-dermatoses as acne and herpes
Raised			
Hypertrophic	Coloured red, inflamed, itchy and sometimes painful, also exhibit an elevation following the shape of the original injury which regresses spontaneously between a period of months to one year.	Increased fibroblast density and distorted collagen bundles.	
Keloid	Spread beyond the original lesion invading healthy tissue. Subject to genetic influences. Likely appear on sites with high tension given its characteristic crab's claw and dumbbell shape.	Increased fibroblast density and proliferation rates. At the nodule predominates collagen I and III with abnormal pattern.	
Burns	Very sensitive		
Intermediate	The ones that not fit in any other category.		

(Bayat, et al., 2003; Kowal-Vern, 2005; Lee, 2011; Perry, et al., 2010; Gold, et al., 2014).

Scar pathology remains largely unknown, with limited effective treatments and prognosis, especially when excessive or pathological scarring appears as seen with raised scars such as hypertrophic and keloid scars (Fearnonti, et al., 2010; Junker, et al., 2014).

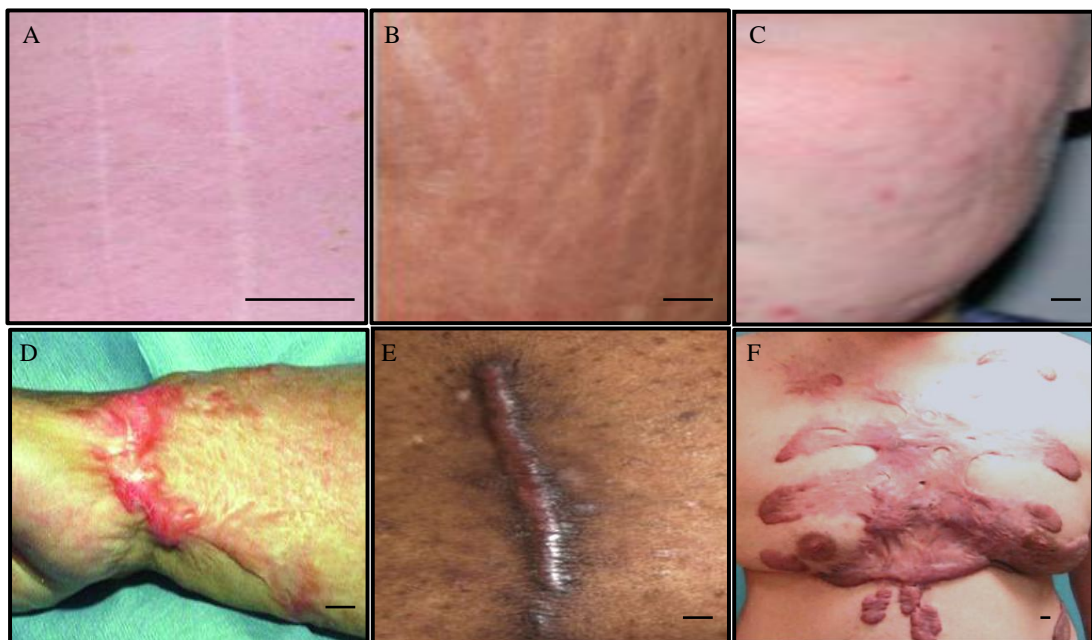


Figure 2.12 Skin scars. (A) Fine line, (B) Stretch, (C) Atrophic, (D) Contracted, (E) hypertrophic and (F) keloid (Al-Himdani, et al., 2014; Bayat, et al., 2003; Goodman, et al., 2006; Ogawa, et al., 2012; Ud-Din, et al., 2014). — Bar represents 1 cm approximately.

2.5.2 Molecular mechanisms of scarring

Molecular mechanisms of human adult skin scarring are not well understood yet. However alterations in gene and cell signalling, dysregulated metabolic pathways, variations of skin mechanical properties and alteration of the 3D environment have been related to excessive or pathologic scarring.

Altered paracrine factors implicated in abnormal scarring are TGF β s, α -SMA, HSP47, Interleukins (IL) 1, 6, 8 and 10, TNF α , PDGF, CTGF and their interaction with the MMPs family and its inhibitors TIMPs, alter ECM deposition and remodelling (Ghahary, et al., 2007; Lopes, et al., 2009; Muehlich, et al., 2007; Shih, et al., 2010; Stamenkovic, 2003; Tandara, et al., 2011; Vincent, et al., 2008).

TGF β s have been associated with excessive fibroplasia, and are considered as the main regulators of scarring. Interleukins have also been found up-regulated in several types of scars, therefore altering and perpetuating the inflammatory environment leading to pathologic scarring (Ramirez, et al., 2014).

MMPs can interact with almost every fibre of the ECM and therefore influence cell shape, movement, adhesion, growth, differentiation and death. They also have an impact on collagen orientation, density and maturity (Schafer, et al., 2008; Stamenkovic, 2003).

MMPs high expression may cause non-healing ulcers and low expression may lead to raised scar formation. For instance MMP28, which is related to basal membrane restructuring, has been found in hypertrophic scars but not in normal scars (Renò, et al., 2005; Martins, et al., 2013; McCarty, et al., 2012).

Dysregulation of gene and cell signalling pathways has also been related to excessive scarring. For instance, genetic dysregulation of STAT3 and its cell signalling

pathways involving apoptosis, proliferation, senescence, α -SMA, Wnt/ β -catenin, calcium, interleukins and mTOR have been implicated in formation of keloids and hypertrophic scars (Akasaka, et al., 2000; Blazić, et al., 2006; Phan, et al., 2005).

Variation in the mechanical behaviour of the skin shows dysregulation of nociceptors, neuropeptides, TGF β /Smad, integrins, mitogen activated protein kinase G, TNF α /nuclear factor- κ B, Wnt/ β -catenin and protease-activated receptor-2 (PAR-2; Arany, et al., 2006; Ferreira, et al., 2009; Materazzi, et al., 2007). Integrins have been related with mechanotransduction during scar development, involving, $\alpha 2\beta 1$ -integrin bound to type I collagen promoting MMP1. Overexpression of MMP1 has been related to hypertrophic scars (Antony, et al., 2010; Ogawa, et al., 2012; Salgado, et al., 2012; Tandara, et al., 2011).

Alterations in the 3D structure of the ECM has also been shown to influence scar formation. Therefore the collagen arrangement may influence scar formation and evolution. Collagen in keloid tissue greatly differs from normal scars and healthy skin in amount and arrangement (collagen I/III ratio in keloids is ~17:1; normal scars ~6:1; Sidgwick, et al., 2012). Intact collagen decreases MMPs expression but denatured collagen increases its expression. Chondroitin-4-sulfate has been found covering the collagen nodules in hypertrophic scars, this reduces the action of MMPs. Elastin, hyaluronan and fibronectin arrangement has also been altered in hypertrophic and keloid scars (Ramos, et al., 2008; Sternlicht, et al., 2001; Tandara, et al., 2011; Volk, et al., 2011).

2.5.3 Scar treatments

Skin scars are treated with either a single therapy or combination, both of which can be invasive or non-invasive. Common treatments include occlusion with silicone and non-silicone gel, topical application of imiquimod 5% cream, 5-fluorouracil, hyaluronic acid and bleomycin, or radiotherapy, laser therapy and brachytherapy (Agren, et al., 2014; Namazi, et al., 2011; Wolfram, et al., 2009).

However, most of the treatments show promising results *in vitro* but fail to recreate these results at the clinical application. For instance, IFN γ treatment caused a decrease in collagen in a murine model of fibrosis, but with controversial results in the clinic (Lopes, et al., 2009). A similar trend follows rhIL-10 and TGF- β 3, which showed promising results in the treatment of mucosal-buccal scars in mice models. In other investigations, injections of recombinant-TGF- β 3 was shown to reduce scar formation in lacerations of 1 cm, however the discomfort and immunological reactions made it difficult to be applied to large scars at the clinical level (Namazi, et al., 2011; Agren, et al., 2014; Wolfram, et al., 2009; Gold, et al., 2014).

Controversy has also arisen about the optimal time to apply treatments and the amount required to produce a significant improvement without secondary effects (Gurtner, et al., 2011; Lopes, et al., 2009; Occlleston, et al., 2008; Ohno, et al., 2011).

The majority of the current treatments for scars are largely ineffective, for instance therapy with X-Ray radiation (Sakamoto, et al., 2012) and beam lasers (Bouzari, et

al., 2007) show relieve of the symptoms cause by a keloid scar, but can have dangerous secondary effects and the disease still regret. Conversely photodynamic therapy (PDT) has shown to improve the wound healing response and decrease keloid scar volume, without dangerous secondary effects (Mills, et al., 2014; Nie, et al., 2010).

Chiu et al. (2005) investigated the possibility of applying PDT to an organotypic co-culture of keloid scars, but found that for this purpose it is necessary to design a better system; however they found a rearrangement of collagen fibres. Anti-ageing and oncological investigations has found that PDT induces metalloproteinases which leads to the rearrangement of collagen fibres of the ECM (Almeida-Issa, et al., 2009), reduces local Langerhans cells, inhibits keratinocyte proliferation, kills keratinocytes with viral infections and damages sebaceous glands (Robertson, et al., 2009; Steinbauer, et al., 2010). Consequently a better understand of the effects of photodynamic therapy on scars would lead to improvement treatment and the eradication of the condition.

CHAPTER THREE: PHOTODYNAMIC THERAPY IN DERMATOLOGY AND TISSUE MODELS

3.1 Introduction

Photodynamic therapy (PDT) is commonly used to treat skin cancer; and its use in dermatology has increased over the last few decades. PDT in dermatology has been used to treat malignant lesions, microbial infections and aesthetic conditions (Morton, et al., 2002; Rhodes, et al., 2007).

PDT uses a photosensitiser, a light with a specific wavelength and intensity and oxygen (Robertson, et al., 2009). The overall reactions cause reactive oxygen species generation, which are the cytotoxic cellular effectors. Effects investigated in cancer vary from proliferation, apoptosis, senescence, autophagy and necrosis on a cellular level, while at the tissue level photothermolysis, hypoperfusion and hypoxia, all of them upon cell type, amount and photosensitiser localization (Garg, et al., 2010; Ji, et al., 2010; Lam, M, 2001; Steinbauer, et al., 2010; Wyld, et al., 2001).

A limited number of studies have shown evidence of improved human wound healing using PDT after excisional surgery (Reddy et al., 2010; Sakamoto et al., 2012). Similarly, some reports of hypertrophic and keloid scars treated with PDT have been published, which showed a reduction of volume, erythema and improvement of scar colour (Campbell, et al., 2010; Nie, et al., 2010; Ud-Din, et al.,

2013;). However, more precise insight into the mechanism is required as the effects of PDT in adult human skin wound healing and scars remain unknown.

Tissue engineering techniques allow for investigating healing processes in living tissue, such as the use of wound healing and scar models (Lebonvallet, et al., 2010).

Cell-based models, which involve isolation of a single type of cell, either keratinocytes or fibroblasts can be correlated with the *in vivo* response to some extent. However, in order to have a wider vision in the absence of accurate animal models, *ex vivo* cutaneous studies provide a more complete system. *Ex vivo* models preserve the actual 3D structure of the skin, some of its functions and most of its cellular components. For these reasons and especially in the case of keloid scars, which only occur in humans, organ culture becomes the most accurate model to study the biology and development of novel treatments (Broek, et al. 2014; Groeber, et al., 2012; Lebonvallet, et al., 2010).

This chapter describes the photodynamic concept, molecular mechanisms, the most common pro-photosensitiser, aminolevulinic acid (5ALA) and its methyl-ester (MALA), used in dermatologic practice, and the light sources used with them. It also provides a review of photodynamic therapy in wound healing and skin scarring. Additionally, a brief insight into tissue engineering techniques used to study skin biology and development of novel treatments are included, which are of special interest for this investigation.

3.2 Photodynamic therapy concept

PDT has been used in skin oncology; however its use has been increased in recent years in dermatology. It is an approved method to treat actinic keratoses in United States and in the European community, however also has been used off-label in other conditions as acne and in aesthetic problems as ageing (Wan, et al., 2014).

The essential components of PDT treatment are a photosensitiser, light and oxygen. Its combined action produces ROS specifically at the site of application. For this reason; topical PDT is a localized treatment, with no systemic secondary effects; however other secondary effects are mentioned elsewhere (Morton, et al., 2002).

The most common pro-drugs applied topically to induce photosensitivity in dermatology are aminolevulinic acid (5ALA) and methyl aminolevulinate (MALA). 5ALA and MALA accumulate significantly higher in tumorigenic cells than in normal cells. As a result the tumour is affected to a greater extent than the surrounding healthy skin. Hence PDT is also considered to be a selective treatment. PDT in dermatology has been used to treat a variety of lesions as malignancies, microbial infections and aesthetic conditions as shown in Table 3.1 (Morton, et al., 2002; Plaetzer, et al., 2009; Wan, et al., 2014).

Table 3.1. Dermatologic conditions treated with photodynamic therapy (5ALA or MALA).

Disease	Light	Fluence	Photosensitiser	Incubation time	Number of treatments
Malignancies					
Actinic keratoses	Blue or red	50 J/cm ²	5ALA MALA	1-4hrs	>1
Squamous cell carcinoma (in situ)	Red	75 J/cm ²	5ALA MALA	3 hrs	2
Basal cell carcinoma	Halogen light	150-230mW/cm ²	5ALA		
	Red	60-125 J/cm ²	5ALA 75 J/cm ² MALA	6 hrs 3 hrs	2 1
Nodular basal cell carcinoma	Red	75 J/cm ²	5ALA MALA	3hrs	>2
Bowen's disease	Red	75 J/cm ²	5ALA MALA	3 hrs	>1
Infections					
Mycosis fungoide	Red	37 J/cm ²	5ALA	3 hrs	3
Warts	Red	37 J/cm ²	MALA	3 hrs	3
Aesthetic conditions					
Acne	Blue and red	34-37 J/cm ²	5ALA MALA	< 3 hrs	>2
Rejuvenation	Red	37 J/cm ²	MALA	3 hrs	2
Others					
Necrobiosis lipoidica	Red	37-75 J/cm ²	MALA	3 hrs	>3

(Almeida-Issa, et al., 2009; Berking, et al., 2009; Morton, et al., 2002; Morton, et al., 2008; Peng, et al., 1997; Rhodes, et al., 2007; Szeimies, et al., 2012; Wan, et al., 2014)

PDT contraindications include history of porphyria, systemic lupus erythematosus, photosensitive dermatoses and allergy to the photosensitiser. Secondary effects include erythema, edema, pruritis, pain, epidermal exfoliation, pustules and hyperpigmentation. However the photosensitiser usually does not accumulate in cell nuclei. For this reason it is considered to have low carcinogenic potential, it does not have cumulative toxicity and there is no known maximum cumulative dose (Macdonald, et al., 2001; Wan, et al., 2014).

3.3 Molecular mechanism of photodynamic therapy

PDT action is based on three factors 1) a photosensitiser, 2) an appropriate source of light with similar wavelength to the absorption properties of the photosensitiser and 3) oxygen, which can be cellular or interstitial (Robertson, et al., 2009). PDT action follows the describe mechanism as follow. Upon illumination, the photosensitiser becomes activated passing from a ground state to an active state, as it returns to ground state, energy is release in the form of ROS. This activation causes the generation an increases the amount of ROS, which irreversibly oxidize essential tissue components upon place of generation and accumulation in the cell and tissue. (Garg, et al., 2010; Ji, et al., 2010; Lam, et al., 2001; Steinbauer, et al., 2010; Wyld, et al., 2001).

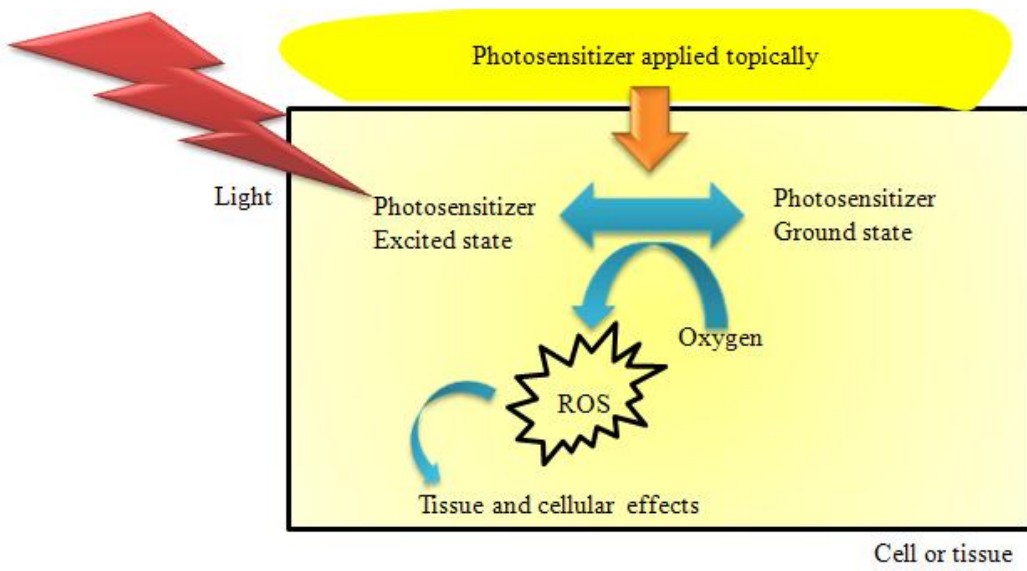


Figure 3.1 PDT associated photochemical reactions. Photosensitiser is applied topically and uptake by the cell o tissue, subsequent illumination triggers the generation of ROS, which in turn become the tissue o cellular effectors.

ROS effects have been studied in cancerous cells and animal models. These investigations show that PDT effects depend on photosensitiser, cell type, energy

delivered and sub-cellular/tissue accumulation (Lam, et al., 2001; Wyld, et al., 2001; Blázquez-Castro, et al., 2012). Therefore PDT stimulates several biochemical pathways that can decide the fate of the cell leading to protection, proliferation, apoptosis, senescence, autophagy and necrosis on a cellular level, while at the tissue level photothermolysis, hypoperfusion and hypoxia have been observed (Figure 3.1; Allison, et al., 2010). Oncologic studies also had found inflammation trigger by the faster action of immune cells, which later develop anti-tumour immunity (Garg, et al., 2010). Anti-ageing studies have shown that PDT can affect elastic and collagen fibres as well as an overall effect inducing ECM remodelling. These responses in turn trigger other processes related to wound healing, immunological responses and immunity as well (Almeida-Issa, et al., 2009; Ji, et al., 2010; Steinbauer, et al., 2010;).

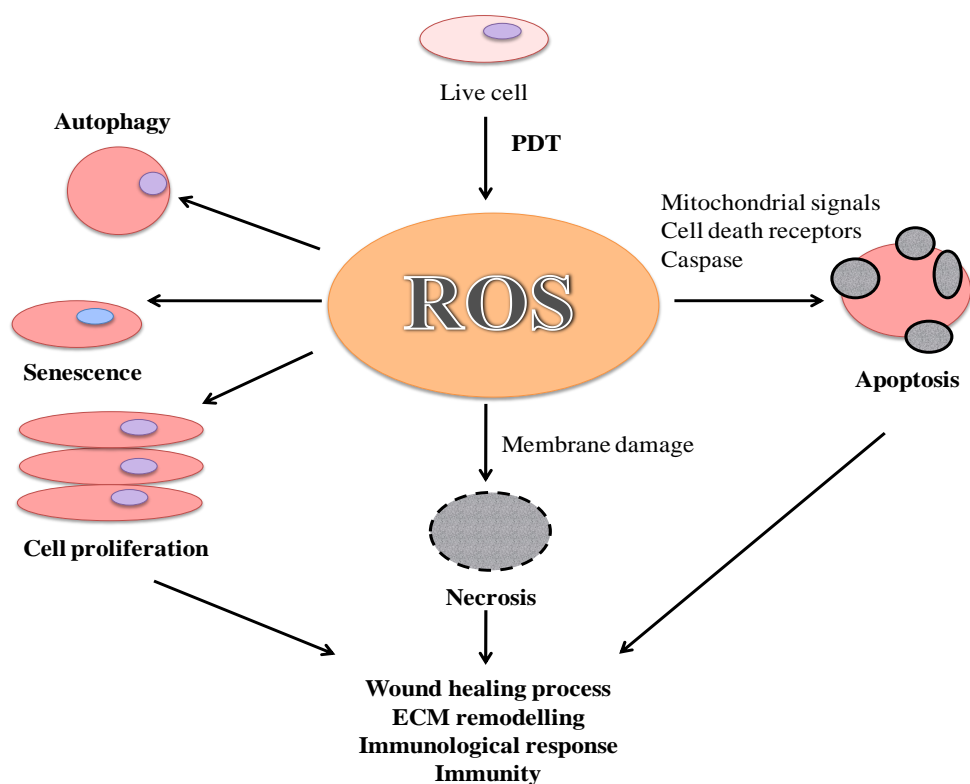


Figure 3.2 Effects of PDT on cancer cells.

The main target for PDT is the mitochondria, where PDT is likely to induce apoptosis through the cascade of caspase activation and Bcl-2 family. However, when it accumulates in other organelles it usually induces necrosis. Membrane structures are notably vulnerable and the effects of PDT can be observed within minutes after light exposure as swelling, bleb formation and shedding of vesicles containing plasma. Damage to the cytosol and lysosomes causes a reduction of active transport, depolarization of the plasma membrane, inhibition of the activities of plasma membrane enzymes such as Na⁺K⁺-adenosine triphosphatase (ATPase) and Mg²⁺-ATPase, a rise in Ca²⁺, up- and down-regulation of surface antigens, lipid peroxidation and damage to multidrug transporters (Lam, et al., 2001). However depending on the concentration these may lead to apoptosis, autophagy and necrosis (Castano, et al., 2004; Robertson, et al., 2009).

After PDT, depletion in the levels of oxygen has been observed, to be caused by vascular damage and the consumption of oxygen to produce ROS. ROS are composed by singlet oxygen (¹O₂), superoxide anion (•O₂⁻), hydrogen peroxide (H₂O₂), singlet oxygen, hydroxyl radical (HO[•]), peroxy radical (ROO[•]), hypochlorous acid (HOCL), nitric oxide (NO) and peroxynitrite anion (ONOO; Allison, et al., 2010). The singlet oxygens produced in a type II redox reaction, where the radical has a short lifetime of approximately <0.04 microseconds and radius of action of <0.02 μm. However they can immediately react with cysteine, methionine, tyrosine, histidine and tryptophan, leading to the above described process. Hydroxyl radical and superoxide ions produced in a type I reaction are less toxic than singlet oxygen(Peng, et al., 1997; Kwitniewski, et al., 2009). However they can react with

themselves producing hydrogen peroxide, which has a beneficial effect, although upon increased concentration may also cause considerable damage (Figure 3.2; Castano, et al., 2005).

The depletion in oxygen levels caused by ROS generation induces cell and tissue hypoxia. This has been associated with the induction of hypoxia-inducible factors (HIFs), which are important in the initiation of the wound healing response and have been linked to several processes including proliferation, apoptosis, necrosis and autophagy (Allison, et al., 2010; Dewaele, et al., 2011; Peng, et al., 1997).

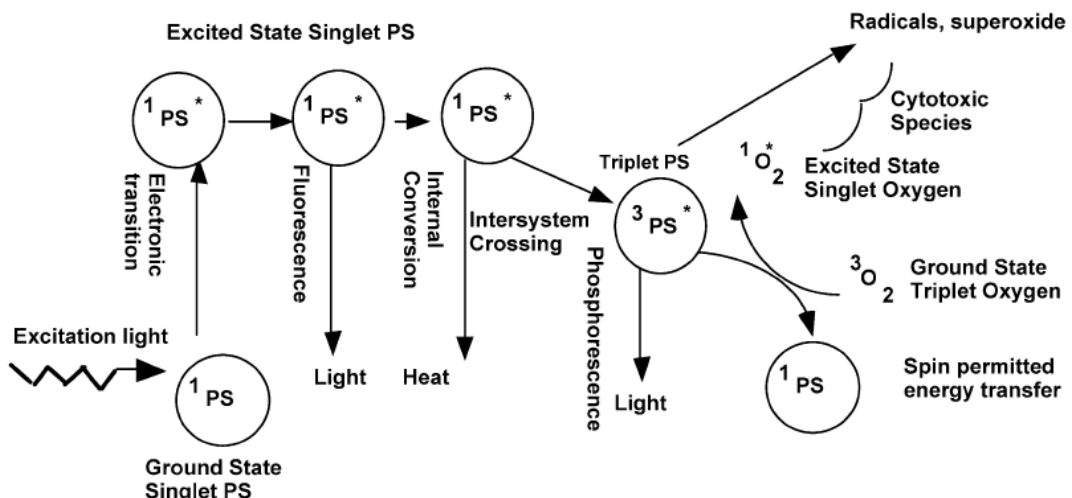


Figure 3.3 PDT related photophysical and photochemical mechanism involved in ROS generation. (Castano, et al., 2004)

ROS generation causes the production of several molecules including cytokines (TNF- α , IL-1, -1 α , -2, -6, -8, -10) and other molecules such as MMP9 which have been found to be up-regulated. (Almeida-Issa, et al., 2009; Peng, et al., 1997).

Tissue effects such as phototermolysis can trigger the wound healing process, resulting in faster wound healing as has been observed in laser treatment, since some studies have shown improved healing after PDT (Peplow, et al., 2012).

The most studied mechanism of cell death after PDT includes apoptosis and necrosis; however PDT also can cause autophagy. Autophagy is promoted during nutrient starvation, pathogen infection, ageing, neurodegenerative process and after massive organelles damage. PDT has been found to induce massive cell organelle damage.

that causes induction of autophagy. This autophagy has been related to mitochondrial dysfunction after loss of mitochondrial membrane potential and reduction of cellular ATP. This dysfunction leads to activation of activated protein kinases (AMPK). AMPK regulates cell energy after depletion of (adenosine triphosphate) ATP or (adenosine monophosphate) AMP and hypoxic and oxidative stress. AMP as response inhibits cellular anabolism, which also induces anti-apoptotic effects, resulting in autophagic cell death (Ji, et al., 2010).

Immune effects of PDT are triggered by apoptotic, necrotic and autophagy cell death. These types of death cause the release and exposure of several molecules that can function as antigens. These molecules can be damage-associated molecular patterns (DAMPs). Especially necrosis causes the release of an important number of cellular and tissue debris. Other tissue responses such as hypoxia can reduce blood flow and cause chemotactic signals. The overall result is recruitment of immune cells.

Immune cells that have been found near the lesion after PDT include macropahges and dendritic cells. Both can function as antigen-presenting cells. This may induce adaptive immunity and trigger anti-tumour immunity (Garg, et al., 2010).

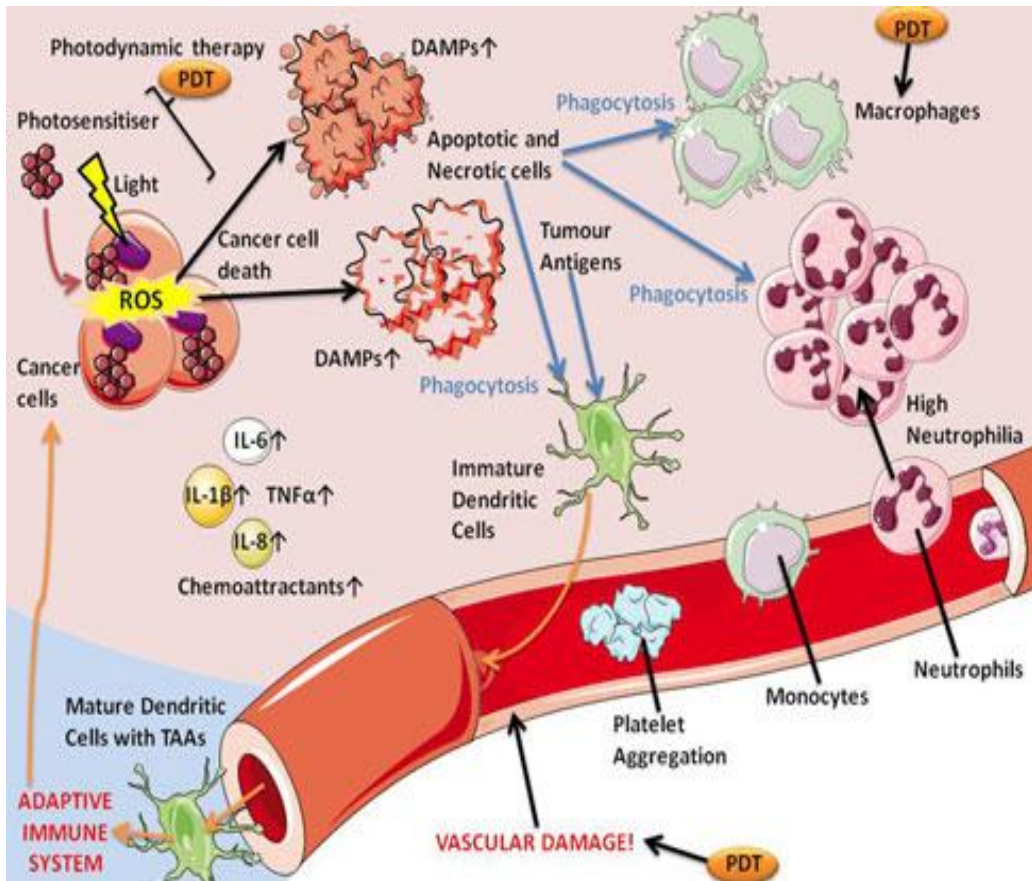


Figure 3.4 Immunity related phenomena induced by PDT. (Garg, et al., 2010)

3.4 Photosensitisers

In 1960 Lipson and Schwartz observed that hematoporphyrin gives a special fluorescence to neoplastic lesions during surgery, leading to the production of pro-drug 5-aminolevulinic acid, the most widely used pro-photosensitiser and its other derivate methyl-ester aminolevulinate, both precursors of the photosensitiser

protoporphyrin IX (PpIX) and other photosensitive porphyrins (Bjerring, et al., 2011). PpIX synthesis has been found to be significantly higher in cancerous cells when compared to healthy cells due to an increased selectivity effect in tumours (Robertson, et al., 2009; Steinbauer, et al., 2010; Uehlinger, et al., 2000).

3.4.1 5-aminolevulinic acid

5-Aminolevulinic acid also known as 5ALA, 5-ALA or ALA is formed at the beginning of the haeme synthesis from glycine and succinyl-CoA in the matrix side of the mitochondria and upon enzymatic biosyntheses of the haeme pathway becomes protoporphyrin IX, which is the actual photosensitiser (Steinbauer, et al., 2010).

5ALA can be metabolized for several cells of the human body for instance porphyrins accumulation can be found in hypodermal tissue, sebaceous glands and in the epidermis. 5ALA applied topically can penetrate the epidermis, however the stratum corneum is especially difficult to penetrate, although topical application is especially susceptible to photobleaching, for this reason, it has to be applied under dark conditions. Some other factors such as temperature can affect 5ALA absorption, which increases in higher temperatures (Wan, et al., 2014; Fritsch, 1995).

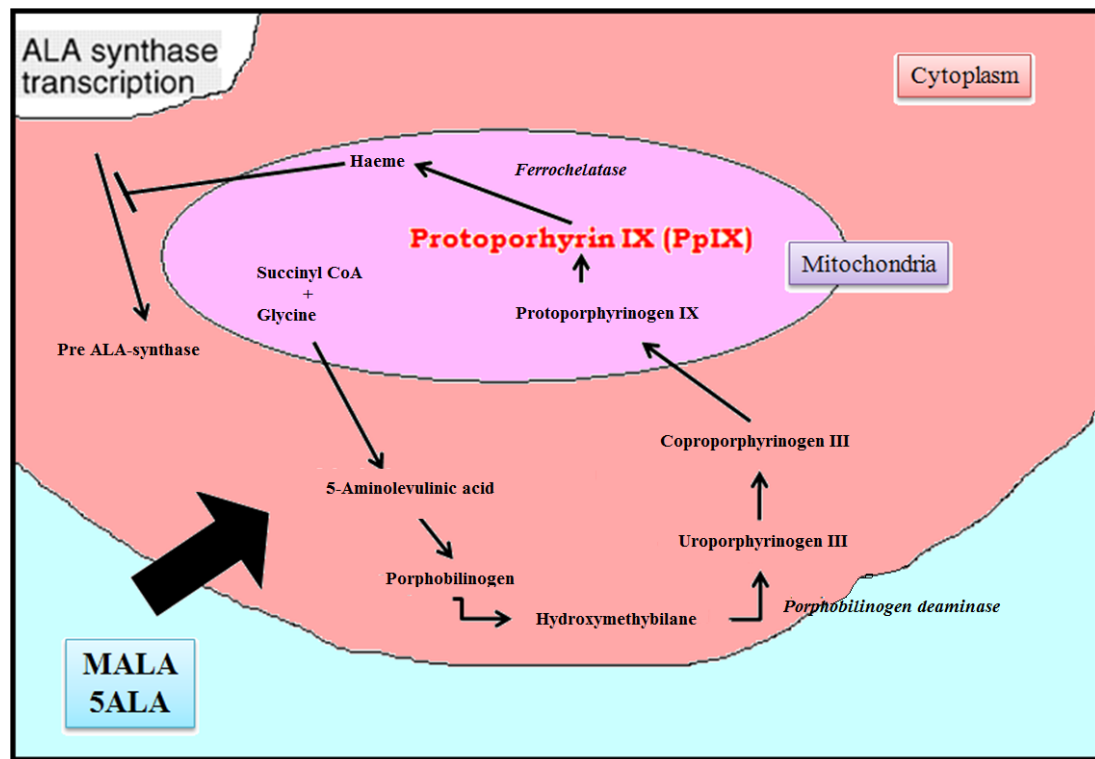


Figure 3.5 Protoporphyrin IX synthesis pathway post-5ALA or MALA.

5-aminolevulonic acid can be produced as a hydrophilic drug, since aqueous solution becomes unstable. It has low lipid solubility and does not cross the membranes easily, especially in keratinocytes. However synthetic 5ALA is taken up by the cells and transformed in to PpIX, similar to the native metabolic pathway. This process takes place in the mitochondria through the action of the enzyme ferrochelatase, which incorporates iron into protoporphyrin IX to become porphyrin IX, both with photosensitive properties. 5ALA can be applied systemically, orally or topically and can also be used for diagnostic purposes, either alone or in combination with other agents (Uehlinger, et al., 2000; Wan, et al., 2014).

The concentration of 5ALA usually depends on the mode of treatment but the range is between 2-40% systematically a 30-50 mg/cm² topically. It is usually applied for less than 4 hours and it has a peak of accumulation between 3 and 8 hrs (Castano, et al., 2004).

As a drug ALA has non-toxic interactions. ALA-PDT has been used to treat skin, bladder and prostate cancer, non-cancerous tumours and skin diseases such as actinic keratosis and cosmetic conditions as skin rejuvenation. There are a wide variety of concentrations used depending on the disease and the light source (Morton, et al., 2008).

3.4.2 Methyl-ester aminolevulinate

Methyl aminolevulinate, also known as MALA, M-ALA or MAL, is an esterified derivative of 5ALA, with higher lipophilicity permitting it to reach deeper into skin layers and allowing a homogeneous concentration within the cell compared to 5ALA. Studies showed that 5ALA can penetrate 1 mm and MALA up to 2 mm in pig skin depth (Wan, et al., 2014). MALA uptake also differs to that of 5ALA. MALA penetrates into the cell by different mechanisms which include the facilitation by active transporters of non-polar amino acids or by diffusion, while 5ALA is taken up by β -amino acids and γ -aminobutyric acid (GABA; Washbrook, et al., 1997). Upon cell internalization MALA is hydrolysed to 5ALA in the cytosol, suggesting an increased amount of PpIX in cells with high metabolism such as cancerous cells but previous studies have found less fluorescence with MALA and

higher levels of PpIX synthesis with 5ALA. Even so the treatment is less painful with MALA compared to 5ALA (Allison, et al., 2010; Christensen, et al., 2010).

Table 3.2 Commercial features of MALA and 5ALA

Brand name	Formulations	Company
5-aminolevulonic acid	20% ALA hydrochloride	Mandeville Medicines, UK
Levulan Kerastick®	20% ALA hydrochloride	DUSA, USA
BF-200ALA®	ALA nanoemulsion	Biofrontera AG, Leverkusen Germany
PD P 506 A Alacare®	ALA in tape base	Biofrontera AG, Leverkusen Germany
Metvix® or	16% ALA methyl ester	Galderma, Dusseldorf, Germany
Metvixia®	16% ALA methyl ester	Galderma SA, Lausanne Switzerland
ALAcare®	gel	Spirig Pharma AG, Egerkingen Switzerland
Ameluz®	Nanoemulsion	Spirit Healthcare Ltd, Oadby UK

(Steinbauer, et al., 2010; Wan, et al., 2014)

3.5 Light sources

The light source used in PDT may have a coherent or incoherent origin, depending on the material used in the lamp. Coherent sources are either lasers with a range from 60-250 J/cm² or non- laser sources but with a defined wavelength of 30-540 J/cm²,

including light-emitting diode arrays, fluorescent tubes and flash lamps. Incoherent sources include incandescent and halogen lamps (Allison, et al., 2010).

Usually the light source is fitted with IR filters to avoid heating but some authors suggest that this may be beneficial in the treatment of certain pathologies such as keloids (Allison, et al., 2010).

The most commonly used wavelengths are 405 nm (UV to blue light), 505 nm (blue light), 540 nm (green light), 580 nm (yellow light) and 635 nm (red light), the last one having a penetration depth of 3–5mm. Even 700 nm can penetrate to twice the depth as it is near to the IR spectrum, which may have toxic effects (Peng, et al., 1997; Steinbauer, et al., 2010).

However, PpIX has two photosensitive wavelength peaks, the first in the blue region of light between 404-420 nm and the second in the red region of light at 635 nm, both in the visible spectrum. Therefore PDT treatment usually uses blue or red light (Stapleton, et al., 2003; Wan, et al., 2014).

3.6 Photodynamic therapy treatment in wound healing and scars

A limited number of animal studies and clinical cases have shown evidence of improvement in wound healing after PDT. Concerning human studies, Statis et al, (1997) showed that ECM deposited in culture dishes by endothelial cells (EC) and later treated with PDT caused an inactivation of TGF β as result it was observed an

increased of EC proliferation. Later Reddy et al., (2010) in a single case reported the use of MALA-PDT as an adjuvant treatment after Mohs micrographic surgery (Technique to excise skin tumours basis on the study of fresh-fixed-IHC stain horizontal sections of it, section are used to define the tumour margins the same day of the surgery) on a large multifocal basal cell carcinoma. Reddy et al., found faster re-epithelialization and improvement of the resulting scar after treatment. Recently Mills et al. showed that MALA-PDT with 3 hours of incubation and illumination with red light (34 J/cm^2) increases TGF- $\beta 3$, MMP1 and MMP9 leading to an improvement of ECM in human wound healing *in vivo* (Jayasree et al., 2001; Medrado, et al., 2008; Mills, et al., 2014; Peplow, et al., 2012; Reddy, et al., 2010).

On the subject of skin scarring, few reports have been published with respect to PDT. Chiu et al., (2005) reported an *in vitro* investigation on keloid organotypic culture showing that 5ALA-PDT with 3 hrs of incubation and illumination of a diode laser of red light (635 nm) using 20 J/cm^2 reduced collagen synthesis and preserved cell viability. Later Mendoza et al., (2013) showed that PDT had dose-dependant cytotoxicity on keloid fibroblasts while Li et al., (2014) found a similar trend using 5ALA-PDT in fibroblasts isolated from hypertrophic scars.

Two more recent reports on PDT in hypertrophic scars (n=3) have found an improvement in their clinical characteristics. Similarly, there was a single case of a non-responsive keloid that was successfully treated with MALA-PDT (3 hrs incubation and illumination with red light 37 J/cm^2), visualized as reduction of volume, reduction in erythema and improvement of scar colour (Nie, et al., 2010). Sakamoto et al., (2012) reported (n=21) that MALA/5ALA-PDT used as adjuvant

therapy for nonmelanoma skin cancer, showed a statistically significant improvement in scar appearance.

A recent report of Ud-Din et al.,(2013; n=20) has also found an improvement in keloid scar appearance and reduced keloid scar formation. However to understand the mechanisms involved in the use of PDT in adult human skin wound healing and scars further investigations are required (Basdew, et al., 2013; Bruscino, et al., 2011; Cai, et al., 2011; Campbell, et al., 2010).

3.7 Tissue models

Tissue engineering techniques are the best potential options in order to perform investigation on living tissues (Figure 3.6). These techniques permit the study of the biology of skin, the effects of a specific drug or treatment, (at different hierarchical levels such as molecular, cellular and organ level), without the use of the whole organism or in the absence of an animal model. Systematic experimental studies of wound healing and scarring are very challenging. Firstly because many processes are happening at the same time and usually overlap one to another, secondly because there is a lack of robust models. However, four different experimental approaches had been used 1) *in vitro*, 2) *in vivo*, 3) *ex vivo* and 4) *in virtuo* (Groeber, et al., 2012; Lebonvallet, et al., 2010; Tomic-Canic, et al., 1998).

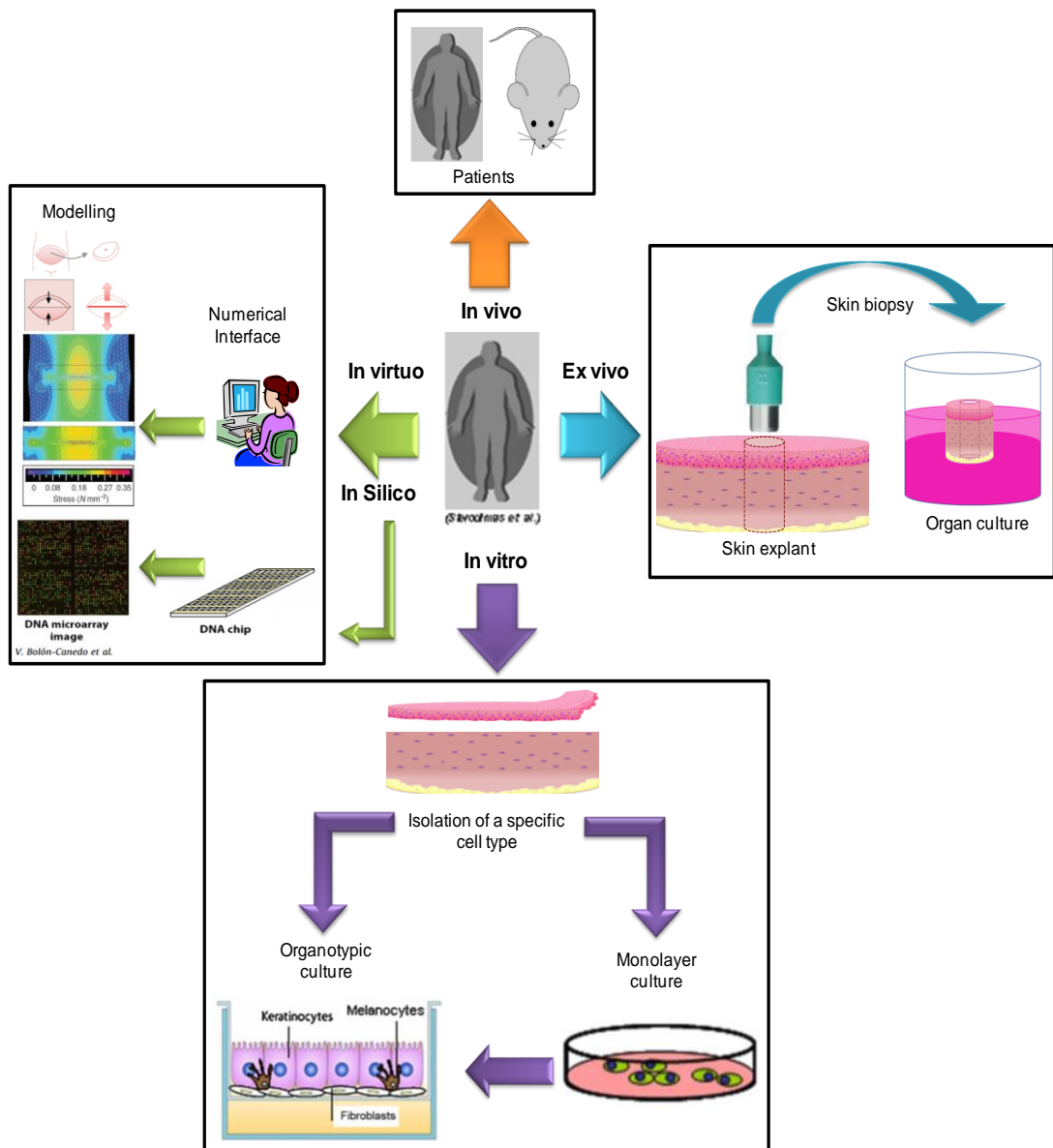


Figure 3.6 Tissue models for investigating skin and treatments. (Blumenberg, 2006; Böttcher-Haberzeth et al., 2010; Wong, et al., 2011).

3.7.1 In vitro models

In vitro models allow systematic analysis of one component to be performed. In the simplest hierarchy, protein expression, protein knock down, signalling pathways, etc can be evaluated in silico in a micro-environment within a population or a single cell (Lebonvallet, et al., 2010).

In vitro research has two branches; and both include cell-based models, which involve isolation of a single type of cells from the original tissue. The first uses a monolayer culture of primary or established cell cultures. The second involves the creation of more complex environments known as artificial tissues or organotypic cultures or skin equivalents (Lebonvallet, et al., 2010). The translation of findings in such models have been successful in some situations but their lack of complexity also carries several limitations (Brohem, et al., 2010; Groeber, et al., 2012; Tomic-Canic, et al., 1998).

Skin engineering models provide a valuable customized tool in a controlled complex three-dimensional environment and reduce animal experimentation. The advantage of such models is that they can be customized by adding or removing cellular components, fibres and chemotactic factors. However, they present several biological and technical limitations (Andreadis, 2007; Brohem, et al., 2010; Lebonvallet, et al., 2010).

Biological limitations include the lack of skin appendages, vascularisation, basement membrane, different cellular organization and fibre arrangement, and different mechanical and physical properties of the scaffold. Some technical limitations include the long time taken for its production, several steps to achieve the final result, lack of reproducibility and consistence and expense (Brohem, et al., 2010; Hadjipanayi, et al., 2009; Lebonvallet, et al., 2010; MacNeil, 2007; Ramos, et al., 2008).

3.7.2 In vivo models

In vivo models should ideally have the same genotypic and phenotypic characteristics as the healthy and diseases human skin. Animal models are limited due to ethical considerations. However some clinical trials have been useful as commercial scarification has been used to study the relation between the depth of the wound and the formation of the scar (Lebonvallet, et al., 2010; Ramos, et al., 2008).

Rats, sheep, pigs and mice are animal models commonly used to study wound healing and scars. Murine models also offer a set of options as nude mice, transgenic, knock-out, humanized and with scar xenografts. However structural difference and ethical considerations limit the creation and use of animal models (Lebonvallet, et al., 2010; Sullivan, et al., 2001).

Translating the findings in animal models to human biology, can cause a lack of understanding. Sullivan et al show that results from pig models translate into humans with up to a 78 % accuracy. Findings in small mammals can be correlated with a 53% and in vitro studies with a 57% of accuracy (Lebonvallet, et al., 2010; Ramos, et al., 2008; Sternlicht, et al., 2001; Sullivan, et al., 2001).

3.7.3 Ex vivo models

Ex vivo culture, also called organ culture, involves just a part of the whole organ maintained in artificial conditions. Ex vivo cutaneous studies provide a more

complete system than cell-based models but the lack of vascularisation decreases their lifespan (Between 14-21 days; Lebonvallet, et al., 2010).

Skin organ culture is especially challenging due to differences in skin depending on body site and other factors including wound depth, skin pliability, firmness, thickness, surface area, texture, pigmentation and vascularity. These factors can be related to age, sex, surrounding environment, habits, and so on, but requires robust inexhaustible and ethnically diverse source, which brings several practical limitations (Lebonvallet, et al., 2010).

Despite these limitations, organ culture aids the study of tissue morphology and structure more than alternatives through the conservation of the actual 3D structure, some functions and most of cellular components. For this reason functional investigations of new treatments using skin organ culture have significantly increased in last few years, especially since the ban of animal models in the European community. However in some cases such as human scars, organ culture becomes the most accurate model to study its biology and novel treatments. Some studies related to this topic are shown in Table 2.8 (ALTEX, 2013; Lebonvallet, et al., 2010).

Skin organ culture can be studied using full or partial thickness skin. Partial thickness refers to the use of partial dermis and full epidermis, or its possible combinations, while full thickness includes at least full epidermis and dermis.

Skin organ culture preserves the 3D structure and most of its cellular components; however they depend on the culture conditions, physical support and growth media. In this sense a lack of agreement persists. The same situation occurs in the study of wound healing, since there is lack of agreement about shape, size and the way to produce the initial injury. Table 2.9 shows some of the most representative studies related to human wound healing. It also shows physical support, wound size and growth media used to maintain the organ culture.

Table 3.3 Full-thickness ex vivo models to study human scars.

Study	Conditions	Growth media
Collagenase expression on hypertrophic scar.	Rocking organ culture	CMRL-1066 medium + 5% FBS
Long-term organ culture of Keloid scar.	Air-liquid, collagen embedded organ culture	WE serum free
Long-term organ culture of keloid scar.	Air-liquid, collagen embedded organ culture	DMEM/HAM F12 – serum free
Comparative study of foetal, adult and hypertrophic scar tissue.	Air-liquid interface	
Effects of an anti-fibrotic compound in a keloid organ culture.	Air-liquid, collagen embedded organ culture	WE serum free
Activation of peroxisome proliferator-activated receptor- γ in hypertrophic scar.	Submerge in liquid	DMEM + 20% FBS
Aldosterone effects in normal skin, stretch-marked skin, dermal scars, and keloids.	Submerge in liquid	culture medium + 5% FBS

(Bagabir, et al., 2012; Coolen, et al., 2010; Duong, et al., 2005; Ehrlich, et al., 1984; Katnitakis, 2002; Mitts, et al., 2010; Zhang, 2009)

Beside the preservation of human skin characteristics organ culture aims to preserve the processes of keratinocyte differentiation. To achieve this, a common technique called “Air-liquid interface” has been used. This allows complete keratinocyte differentiation, maintained by the air exposure, while feeding the epidermal layer is carried out by the liquid phase (Lebonvallet et al., 2010).

Other factors, such as temperature, CO₂/O₂ tension, humidity and pH have been decided based on previous knowledge of cell culture and the human body conditions. However, Companjen et al. showed that specific diseases need specific requirements in order to preserve their characteristics in ex vivo culture. Several investigations have been developed in order to preserve scars ex vivo, while less attention has been given to studying wound healing ex vivo. In this case the efforts have been directed towards improving the process through novel therapies rather than understanding the process itself happening ex vivo (Lebonvallet, et al., 2010).

Wound healing studies have also found that growth media supplements, such as foetal bovine serum (FBS), play a paramount role in sustaining the process. In this specific case 10% of FBS induces wound healing, visualized as a full re-epithelialization of the wound area while lower amounts only maintain viability and may arrest the wound healing process (Companjen, et al., 2001; Kratz, 1998; Lebonvallet, et al., 2010).

Table 3.4 Ex vivo models to study human wound healing

Study	Wound geometry	Physical support	Growth media
Wound healing of incisional and burn wounds.	Donut-like model 3mm/6mm.	Submerge in liquid.	DMEM + 10% FBS
IL-10 homologous for dermal wound healing.	Donut-like model 3mm/6mm.	Epidermal left in air-liquid interface and dermal layer embedded in rat tail collagen I gel.	DMEM without FBS
Wound healing.	Complete epidermis Partial-dermis.	Stitched in a transwell plate.	DMEM +10% FBS
Wound healing for functional testing.	Enzymatic peel of the epidermis (6mm).	Fixed into a steel chamber.	DMEM +10% FBS
Wound healing: acceleration by transplanted keratinocytes.	Donut model (3mm/6mm).	Partially submerge.	DMEM + 5% FBS
Wound healing.	Linear excisional wound (2mm).	Submerge in liquid.	DMEM + 10% FBS
Wound healing.	Skin outgrowth (2mm).	Well plate chamber.	DMEM/Ham's F12 + 20% FBS

(Balaji, et al., 2014; Harris, et al., 2009; Kratz, 1998; Rizzo, et al., 2012; Steinstraesser, et al., 2009; Xu, et al., 2012)

3.7.4 In virtuo models

In virtuo investigations may include in silico investigations. In virtuo models, unlike in silico, provide a 3D environment as highly interactive as numerical modelling. They are able to simulate the actual system through the use of specialized software and hardware. In silico includes all microarrays of genes and cytokines. Numerical models or computational modelling has been used to study the mechanical stress of

scars and wound healing outcomes. Microarrays have been used to compare genetic expression on scarless and scarred healing (Akaishi, et al., 2008; Schneider, et al., 2008).

Another quasi in virtuo model is the creation of organs on a chip which nowadays most often resembles a small plastic disk filled with cells and nutrients, where the great promise is that they may become more consistent and very useful when an animal model is not possible (Baker, 2011; Broek, et al., 2014; Menke, et al., 2010; Menon, et al., 2012; Vermolen, et al., 2010).

CHAPTER FOUR: PHOTODYNAMIC THERAPY AND KELOID FIBROBLASTS

4.1 INTRODUCTION

Keloid disease (KD) is a relatively common fibroproliferative disorder of unknown aetio-pathogenesis. Keloids are defined as benign tumours that grow beyond their border, thereby invading healthy tissue. They are characterized by excessive disorganized production of extracellular matrix (ECM; Seifert, et al., 2009; Shih, et al., 2010), where apoptosis is down-regulated compared to normal scars (Seifert, et al., 2009; Luo, et al., 2001; Sayah, et al., 1999). Keloids also exhibit regions with different genotypic and phenotypic features (Bagadir, et al., 2011; Hollywood, et al., 2010; Syed, et al., 2011; Tucci-Viegas, et al., 2010).

Photodynamic therapy (PDT) is an accepted therapeutic modality for treatment of non-melanoma skin cancer and other skin conditions. PDT action is based on a photosensitiser and a light with a specific wavelength (Allison, et al., 2010; Robertson, et al., 2009). According to the literature, the most common photosensitiser used is aminolevulinic acid (5ALA) and its methyl ester (MALA) from which protoporphyrin IX (PpIX) is synthesized within the cell (Casas, et al., 2001; Lee, et al., 2008; Rodriguez, et al., 2006). PpIX upon illumination with red light generates ROS, which are the cytotoxic cellular effectors, resulting in cell death and tissue destruction (Allison, et al., 2010;; Robertson, et al., 2009).

In view of the above findings, this chapter describes the cytotoxic effects of MALA-PDT compared to 5ALA-PDT in keloid fibroblasts isolated from different anatomical sections within the keloid tissue compared to normal skin fibroblasts. In order to achieve this, the kinetics of PpIX accumulation was determined following incubation with different concentrations of MALA or 5ALA and followed by cytoproliferation analysis. These results led to 3hrs of incubation of 4 mM of MALA/5ALA. Similarly, phototoxicity was determined following illumination with red light (635 nm) with fluence from 0 to 100 J/cm² only. This result shows that phototoxicity increases proportionally with fluence. Consequently 10, 20, 40 J/cm² of fluence were used in subsequent experiments, since a further increase of fluence resulted in cytolysis. Consequently, cytotoxicity, cytoproliferation, cell death, senescence, reactive oxygen species generation and relative gene expression (keloid pathogenesis and apoptosis) were assessed post-PDT.

4.2 Experimental set up

Keloid disease tissue was divided into the following sections (a) top, which included epidermis and papillary dermis; (b) middle, which was comprised of reticular dermis only; and (c) margin, otherwise known as the peripheral active margin of the scar (Figure 4.1).

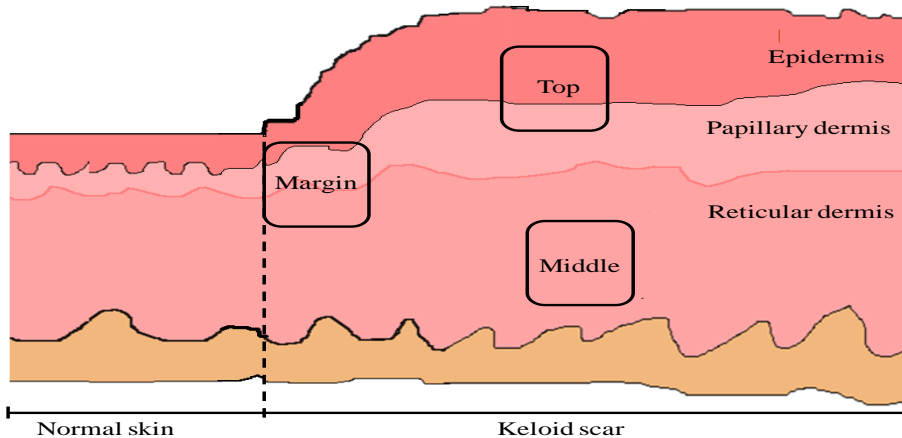


Figure 4.1 Cross section of a typical keloid scar showing different site-specific lesional sites. Top denotes the upper part of the keloid scar (includes epidermis and papillary dermis); middle denotes the centre part of the keloid scar (reticular dermis only). Both top and middle are intralesional samples. Margin denotes the perilesional or peripheral margin of the keloid scar. Samples have an approximately mesure of a punch biopsy of 8 mm.

Keloid fibroblasts were isolated from the biopsies of the described sections and maintained in a monolayer cell culture (Figure 4.2). PDT consisted in applications of light energies from 10 J/cm^2 to 40 J/cm^2 after incubation with different concentrations of MALA/5ALA on the cultures. PpIX was quantified in the different cell types and examined the cytotoxicity mechanisms in the absence of pro-drugs with light only. Subsequently, PDT was applied and ROS generation cytoproliferation, apoptosis, necrosis and senescence were investigated.

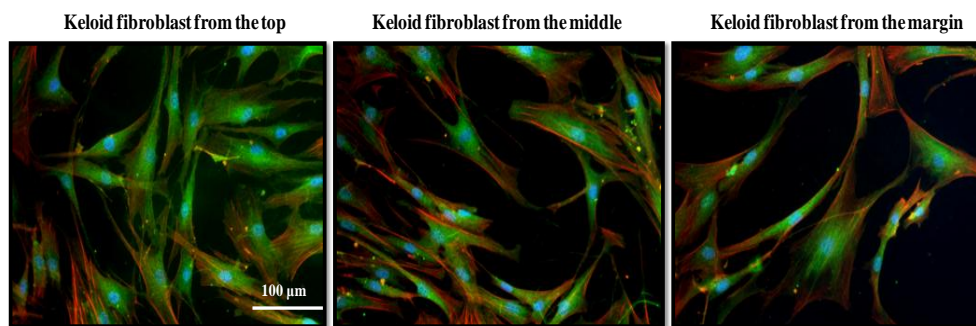


Figure 4.2 Site-specific keloid fibroblasts. Pictures show keloid fibroblasts in monolayer culture, where nucleus is stained in blue (DAPI), focal adhesions in green (anti-Vinculin) and F-actin fibres of the cytoskeleton in red (Phalloidin-Alexa Fluor 488; Original magnification 100x).

4.3 Materials and methods

4.3.1 Cell culture

Keloid biopsies were obtained from patients after surgical removal of the keloid scar following written consent (Table 4.1). Ethical approval was granted by North West (England, UK) Research Ethics Committee (Ethics Code - 11/NW/0683). Normal skin biopsies were obtained from healthy skin of non-keloid patients. Patients with keloid scars, where the scar was differentiated from hypertrophic scars by its typical phenotypic characteristics and histologically features to ensure accurate diagnosis, were recruited in this study regardless age, sex or habits.

Table 4.1 Clinical demographic data of subjects used in the study

Sample	Sex	Age (years)	Biopsy site	Age of scar (years)	Ethnicity	Treatment
Ks1	M	36	Scalp	5	Black	Recurrence post surgery
Ks2	F	35	Sternum	13	Black	None
Ks3	F	26	Earlobe	7	Black	Recurrence post surgery
Ks4	F	54	Sternum	12	Black	Recurrence post surgery
Ks5	F	66	Ear	23	White	None
Ks6	F	28	Chest	7	Black	Recurrence post surgery
Ks7	M	26	Chest	15	Black	Recurrence post surgery
Ks8	M	26	Sternum	13	White	Recurrence post surgery
Ns1	F	39	Abdomen	-	White	-
Ns2	F	25	Breast	-	White	-
Ns3	F	47	Abdomen	-	White	-

Ks denotes keloid scar, the size of keloid lesions range between 3 to 5 cm in width and 0.5 cm to 1 cm in height; Ns denotes normal skin

Keloid and normal tissues were washed with phosphate-buffer saline solution (PBS; PAA Laboratories) three times, followed by enzymatic digestion with Dispase II, 10

mg/ml (Roche, Burges Hill, UK) for 3 hrs at 37°C. Epidermis and fat were removed and the dermis was mince a followed by enzymatic digestion with Collagenase type I, 0.5mg/ml (Roche) for 3 hrs at 37°C. The resulting tissue was passed through a 100 µm strainer (BD Biosciences, Oxford, UK) and wash one time with DMEM (PAA Laboratories) supplemented with 2 mmol/L, L-glutamine, 100 U/mL, penicillin and 100 U/mL and streptomycin, 10% heat-inactivated FCS (PAA Laboratories). The cellular pellet, after wash was transfer into a T25 CellBind flask (Nunc, Life Technologies LTd, Wiesbaden, Germany) and manteine at 37°C with 5% CO₂ in a humidified atmosphere until 80-90% confluency (Syed, et al., 2011).

Then 1 x 10⁴ cells/well were transferred in 96-well plates or 1.5 x 10⁵ cells were seeded in 8 cm² culture dishes (35 mm diameter, Corning, Sigma-Aldrich, UK) and incubated at 37°C with 5% CO₂ / 16% O₂ in humidified atmosphere, before being harvested (6 days) with trypsin and passaged. Cell passages used in the experiments were restricted between 2 and 4 in order to preserve all keloid characteristics, as describe Syed, et al., (2011), this work studied the expression of collagen in keloid fibroblasts, he found that older passages of keloid fibroblasts change the collagen expression for such a reason suggest that older passages may not preserve keloid fibroblast characteristics. The outline of the experimental methodology is depicted on Figure 4.3.

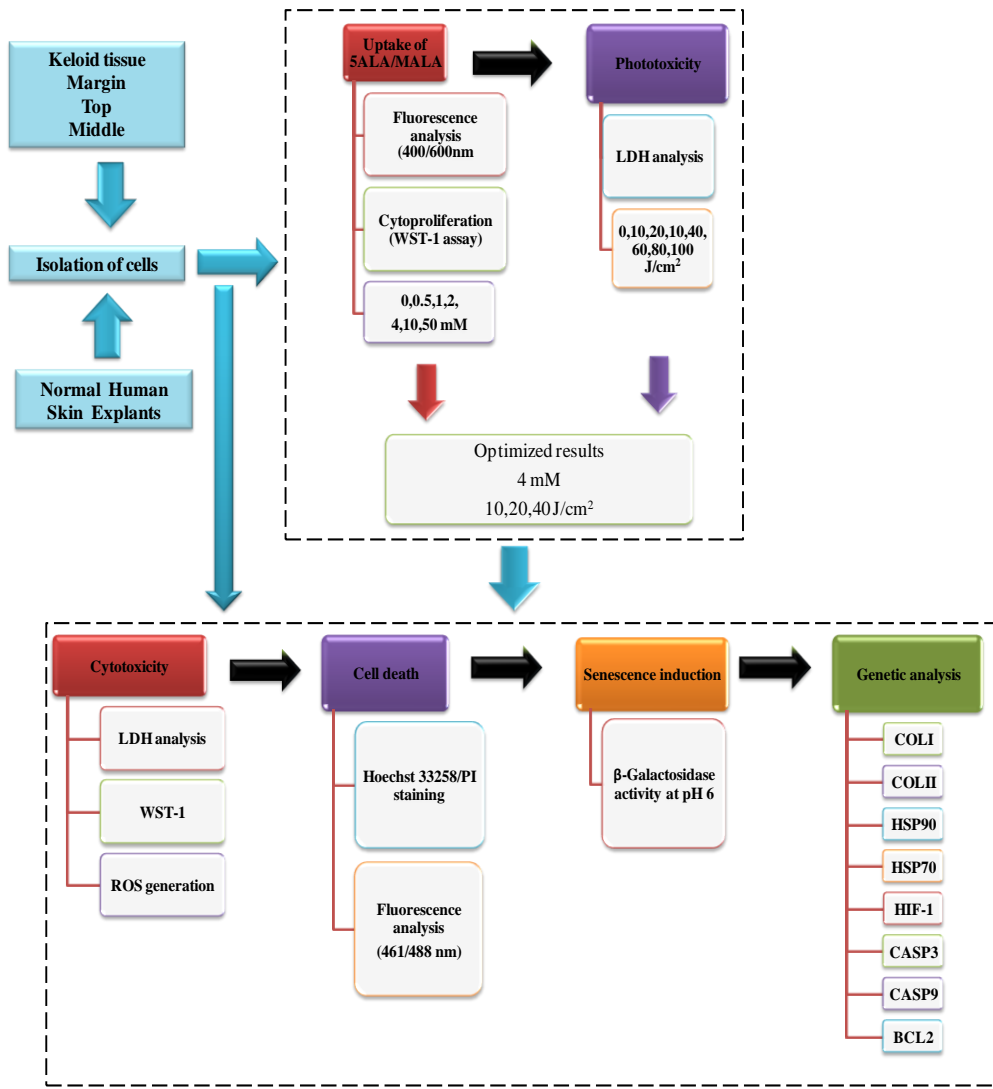


Figure 4.3 Flow chart of the methodology used in chapter four.

4.3.2 Drugs

5-aminolevulinic acid (5ALA; Mandeville Medicines, UK) and methyl aminolevulinic acid (MALA; Galderma, UK) were dissolved in serum-free DMEM medium at different concentrations of 0.5 mM, 1 mM, 2 mM, 4 mM, 10 mM, and 50.0 mM. Similar concentrations of these drugs had been used in clinical practice (Wan and Lin, 2014).

4.3.3 PDT apparatus and treatment

This study used PDT machine (Omnilux PDTTM, Photo Therapeutics, PA, USA) with a light-emitting diode (LED) and air-cooling system, which emitted red light of wavelength $633\text{ nm} \pm 3\text{ nm}$. It was adjusted to 35 mW/cm^2 of power intensity, which was configured and calibrated with an IL1700 radiometer (International Light Technologies Inc, MA, USA).

Photodynamic therapy treatment consisted in photosensitization of cells with the precursor of PpIX, 5ALA or MALA followed by illumination with the PDT machine. Monolayer cultures seeded in culture dishes were washed twice with PBS and incubate with the precursor. After incubation cell culture dishes were washed twice with PBS and a small amount of serum-free DMEM medium was replaced only to prevent desiccation. The lid of the culture dish was taken off during illumination and all experiments were carried out in a clean room for cell culture and complete darkness.

4.3.4 Fluorescence measurement of Protoporphyrin IX accumulation

In order to determine the time taken for intracellular accumulation of PpIX, the fluorescence intensity of PpIX was measured at 400/620 nm in a fluorometric microplate reader (Fluostar optima, BMG Labtech, UK). The different cell types were incubated for different time periods (0, 1, 2, 3, 4, 6, 8, and 10 hrs) after MALA or 5ALA treatment at different concentrations (0, 0.5, 1, 2, 4, 10 and 50 mM) and the values were normalised with cells without any treatment.

4.3.5 Cell proliferation analysis

Cell proliferation was determined by WST-1 assay (WST-1 cell proliferation kit, Roche-Diagnostics, Mannheim, Germany). WST-1 reagent was added to cells cultured in 96-well plates and treated according to the manufacturer's instructions. The end point absorbance was measured at 450 nm and 650 nm with a microplate reader (Fluostar optima, BMG Labtech, UK).

4.3.6 Phototoxic analysis

In order to study the phototoxic effect of the light alone, keloid and normal skin fibroblasts were grown in 8 cm² cell culture dishes. Here, cells were not incubated with photosensitising precursors. However, cells were exposed to light energies from 5, 10, 20, 40, 60, 80, and 100 J/cm² at a power intensity of 35 mW/cm². Subsequent after light exposure, lactate dehydrogenase (LDH) release into the medium (LDH Cytotoxicity Detection kit, Roche Diagnostics, Roche Mannheim, Germany) was measured at 490 nm and 600 nm with a microplate reader.

4.3.7 Cytotoxic analysis

After incubation with MALA or 5ALA, the cells were treated with 10, 20, and 40 J/cm² of light energy. The serum-free cell medium was replaced with complete DMEM medium for further incubation at 37°C and 5% CO₂ post light exposure.

Cytoproliferation (WST-1 assay) was analysed immediately after treatment while cytotoxicity (LDH assay) was assessed at 0, 24 and 72 hrs after treatment. WST-1 analysis consisted in the spectrophotometric quantification of formazan which is produced by proliferative cells after the enzymatic cleaved of tretrazolium salts (Vietti, et al., 2013).

4.3.8 Apoptosis, necrosis, and senescence analysis

Apoptosis and necrosis were analysed by fluorescence microscopy with Hoechst 33258 (Invitrogen Ltd, USA) and propidium iodide (PI; Sigma-Aldrich company Ltd, UK) respectively. They were analysed 24 hrs post treatment. Senescence was assessed by measuring the intracellular activity of β -galactosidase at pH 6 according to the manufacturer's instructions (Senescence β -galactosidase Staining Kit, Cell Biolabs, Cambridge, UK).

4.3.9 Reactive oxygen species generation analysis

ROS generation was measured by the intracellular accumulation of the fluorescent probe 2',7'-Dichlorodihydrofluorescin (DCF; OxiSelect ROS Assay kit, Cell Biolabs, CA, USA), which mainly detected hydroxyl, peroxy, hydrogen peroxide, peroxynitrite anion, and Peroxynitrite anion inside the cells. The assay was performed according to manufacturer's instructions and fluorescence was measured at 480 nm/530 nm.

4.3.10 mRNA isolation, cDNA synthesis and qRT-PCR

Cells were incubated with 4 mM MALA/5ALA and exposed to 10 and 40 J/cm². The cell lysates were collected in TRIzol reagent (Invitrogen, Abingdon, UK) and were processed for mRNA isolation, cDNA synthesis and qRT-PCR as described previously (Syed et al., 2013). The gene expression levels were normalized with an internal reference gene, RPL32. The primers used in the study are detailed in the Table 4.2.

Table 4.2 List of Primers

Primers	Gene ID	Sequence 5'-3'	Primer position	Amplicon size (bp)
RPL32-L	NM_000994.3	gaagttcctggtccacaacg	319-338	77
RPL32-R	NM_000994.3	gagcgatctcggcacagta	377-395	77
Collagen I-L	NM_000088.3	gggattccctggacctaag	1866-1885	63
Collagen I-R	NM_000088.3	ggaacacctcgctctcca	1911-1928	63
Collagen III -L	NM_000090.3	ctggaccccagggtcttc	3101-3118	75
Collagen III-R	NM_000090.3	catctgatccagggttcca	3156-3175	75
HIF-1-L	NM_001530.3	cgcgaacgacaagaaaaag	422-440	121
HIF-1-R	NM_001530.3	aagtggcaactgtatggcaa	523-542	121
Caspase-3-L	NM_004346.3	tggaattgtatgcgtatgtt	553-572	73
Caspase-3-R	NM_004646.3	tggctcagaaggcacacaaac	606-625	73
Caspase-9-L	NM_001229.3	agtggaggccacacctaaac	1075-1094	75
Caspase-9-R	NM_001229.3	agtggaggccacacctaaac	1131-1149	75
BCL-2-L	NM_001191.2	gaggccggctgagttacc	126-143	60
BCL-2-R	NM_001191.2	tttgtatcacaggtcgggaga	165-185	60
HSP90-L	NM_0010117963.2	gggcaacacctctacaagga	661-680	76
HSP90-R	NM_0010117963.2	cttgggtctgggttcctc	718-736	76
HSP70-L	NM_002154.3	cagcagacaccagcagaaaa	1887-1906	65
HSP70-R	NM_002154.3	cttggatccagcttgagagg	1933-1952	65

RPL32, ribosomal protein L32; HIF-1, hypoxia inducible factor 1; BCL-2, B-cell CLL/lymphoma 2; HSP90, heat shock protein 90kDa alpha; HSP70, heat shock 70kDa protein 4.

4.3.11 Statistical Analysis

The results are presented as the mean values \pm standard deviation. Statistical significance was calculated with non-parametric ANOVA and Bonferroni post-test and graphics were generated with GrahPad Prism 5 (GraphPad Software, La Jolla, CA, USA). Differences between different data sets were compared with the control (cells without any treatment) or within each set (Normal skin vs. keloid scar fibroblasts) and were considered significant if $p<0.05$.

4.4 Results

4.4.1 Protoporphyrin IX accumulation and MALA/5ALA cytotoxicity in keloid fibroblasts

The rate of intracellular accumulation of PpIX with MALA in keloid fibroblasts varies compared to 5ALA

The intracellular accumulation of PpIX followed two patterns a bell-shaped pattern and similar to growth curve pattern as it reached its maximum, however depending in the concentration and type of cells. The star shows where the cells significant increases the synthesis of PpIX with respect to cells not exposed to its precursor MALA/5ALA. However it was not possible to go further than 10 hour in the kinetics of uptake due to the detachment of the cells from the culture dish (Figure 4.4-7).

Normal cells post incubation with MALA or 5ALA followed a growth curve pattern. Showing two peaks of PpIX, the first was found between 2 and 3 hrs and the second at 10 hrs (Figure 4.3). Keloid fibroblast from the margin and top followed a bell-shape pattern while keloid from the middle followed a growth curve when incubate to MALA. Normal fibroblasts and keloid fibroblasts from the margin and middle forms a a plateau after incubation with 5ALA while to top show a bell-shape form. Keloid fibroblasts from the margin and middle (Figure 4.5&6) reach the maximum concentration of PpIX at 3 and 6 hrs while keloid fibroblast from the top at 6 hrs (Figure 4.7).

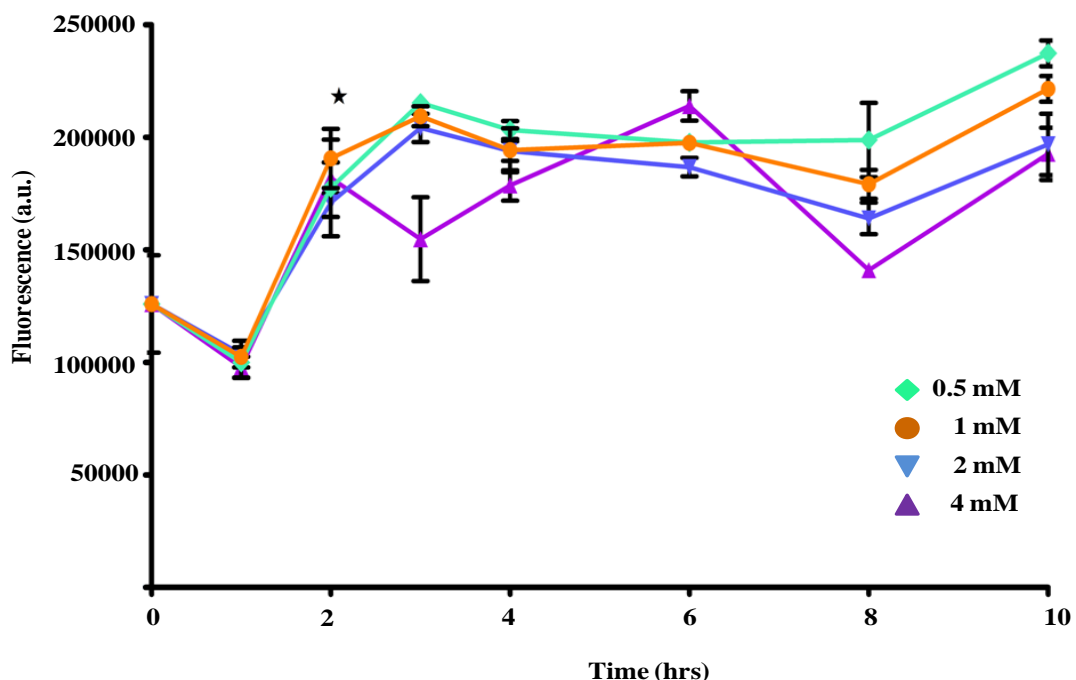


Figure 4.4 Kinetics of PpIX accumulation in normal dermal fibroblasts post-incubation with MALA. ★ Denotes significant difference in comparison with cells not exposed to MALA at time zero ($p<0.05$; $n=8$). Graph represents mean and standard deviation.

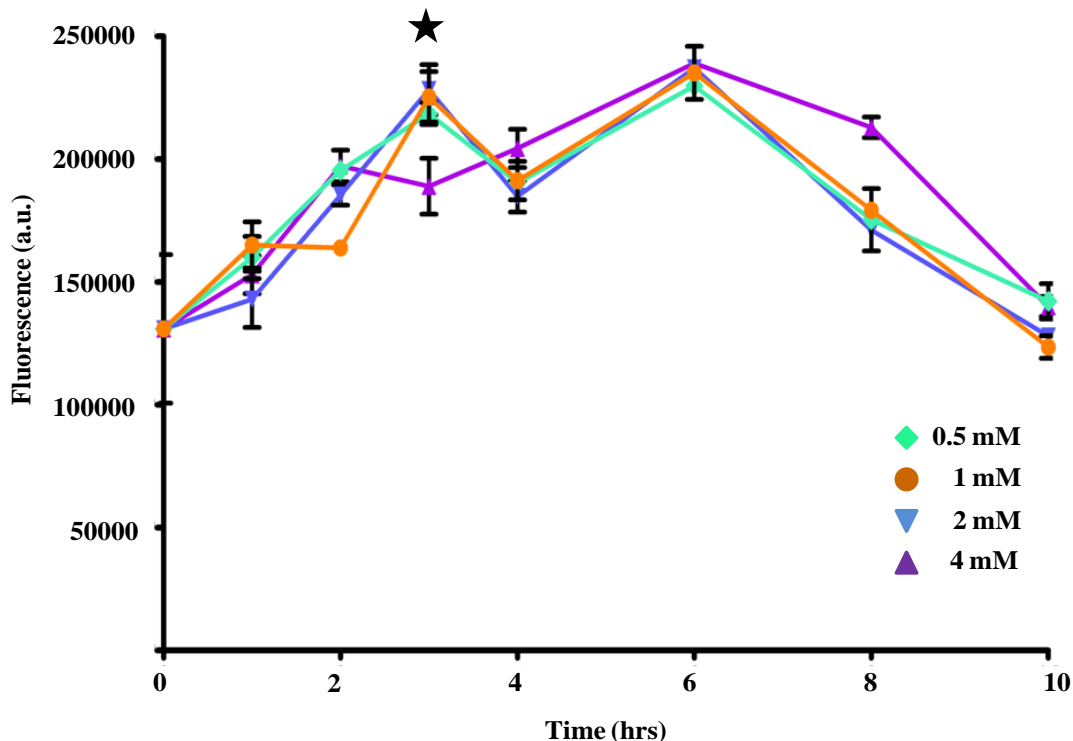


Figure 4.5 Kinetics of PpIX accumulation in keloid fibroblasts from the margin of the scar post-incubation with MALA. ★ Denotes significant difference in comparison with cells not exposed to MALA at time zero ($p<0.05$; $n=8$). Graph follows a bellshape curve with two points at three and six hours. Graph represents mean and standard deviation.

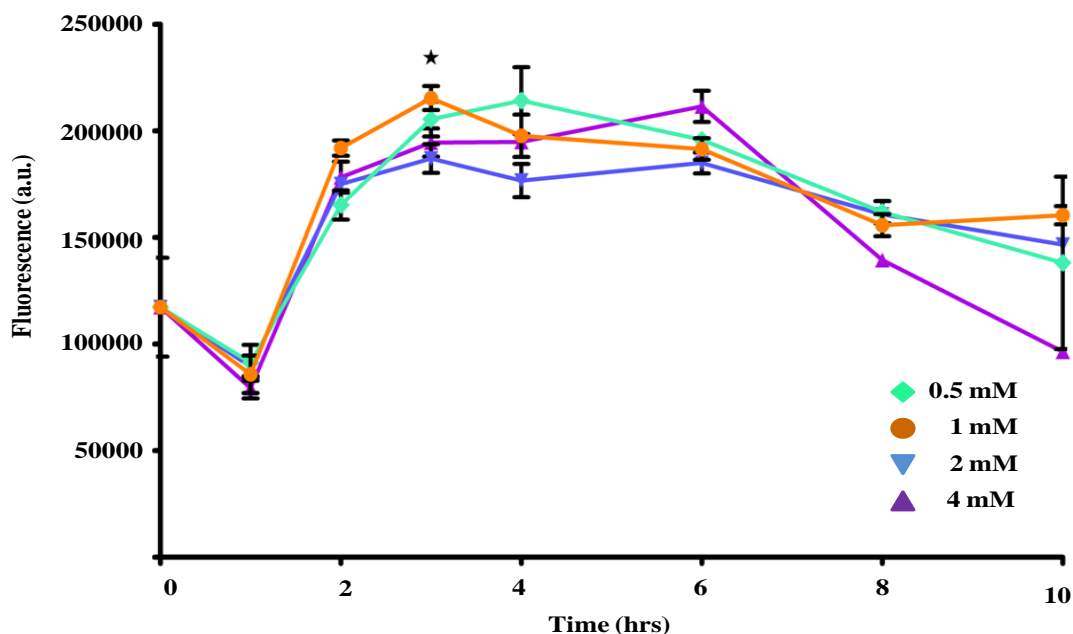


Figure 4.6 Kinetics of PpIX accumulation in keloid fibroblasts from the middle with MALA. ★Denotes significant difference in comparison with cells not exposed to MALA at time zero ($p<0.05$; $n=8$). Graph follows a similar bellshape curve with a peak at three. Graph represents mean and standard deviation.

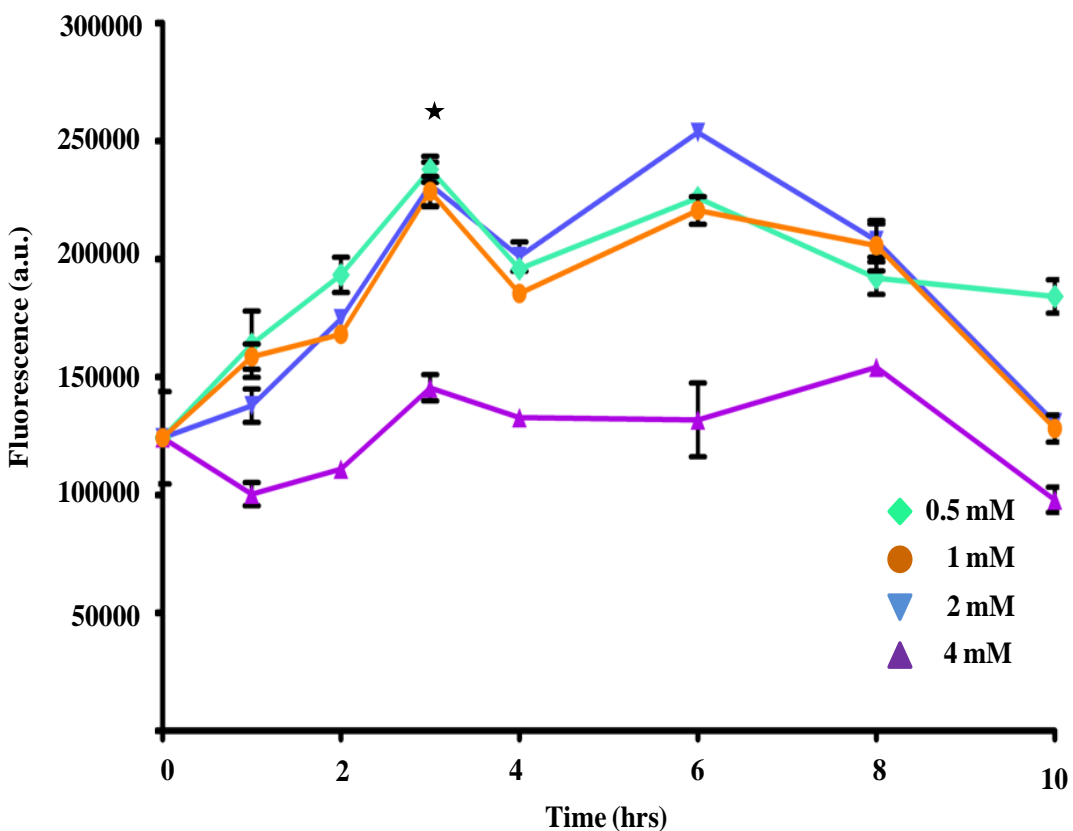


Figure 4.7 Kinetics of PpIX accumulation in keloid fibroblasts from the top with MALA. ★Denotes significant difference in comparison with cells not exposed to MALA at time zero ($p<0.05$; $n=8$). Graph follows a similar bellshape curve with a peak at three hrs. Graph represents mean and standard deviation.

5ALA followed a different “growth curve” pattern compared to MALA (Figure 4.8-11). Normal cells post incubation with 5ALA showed two peaks of PpIX, the first at 2 hrs and the second at 10 hrs (Figure 4.8) while keloid fibroblast showed a continued accumulation of PpIX after 2 hrs. All concentration of 5ALA followed a similar trend except, 4 mM in keloid margin. This shows an increased level of 5ALA compared to MALA in fibroblasts upon incubation time (Figure 4.9 and 4.10).

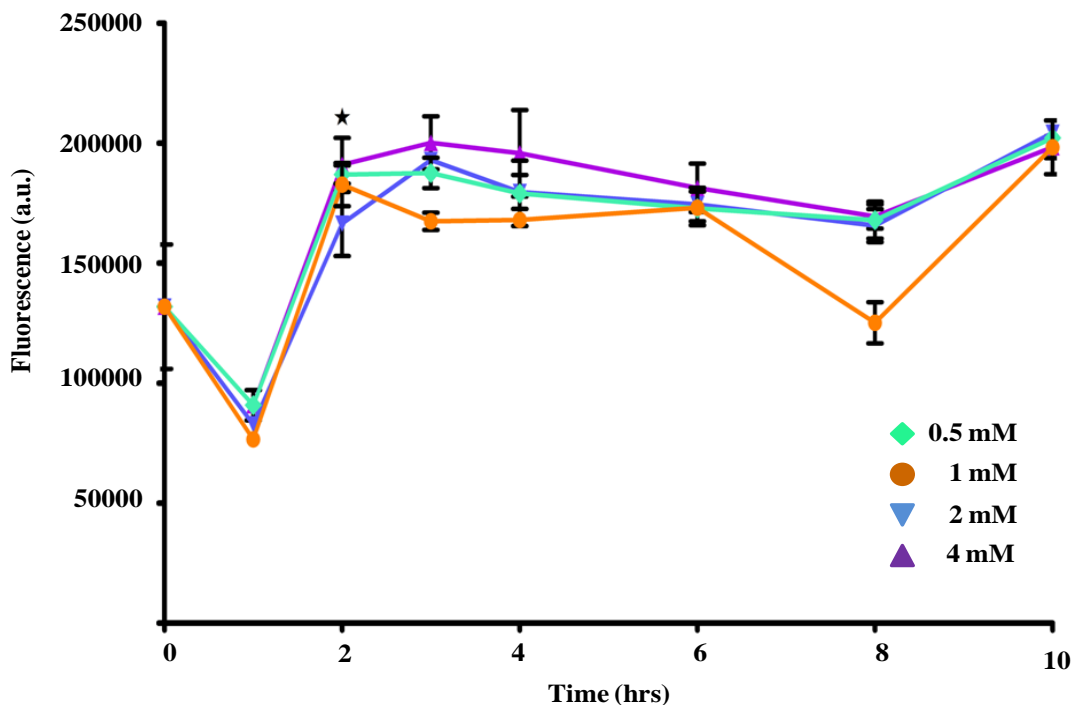


Figure 4.8 Kinetics of PpIX accumulation in normal dermal fibroblasts post-incubation with 5ALA. ★ Denotes significant difference in comparison with cells not exposed to 5ALA at time zero ($p<0.05$; $n=8$). Graph follows a growth curve with a plateau from two to eight hrs. Graph represents mean and standard deviation.

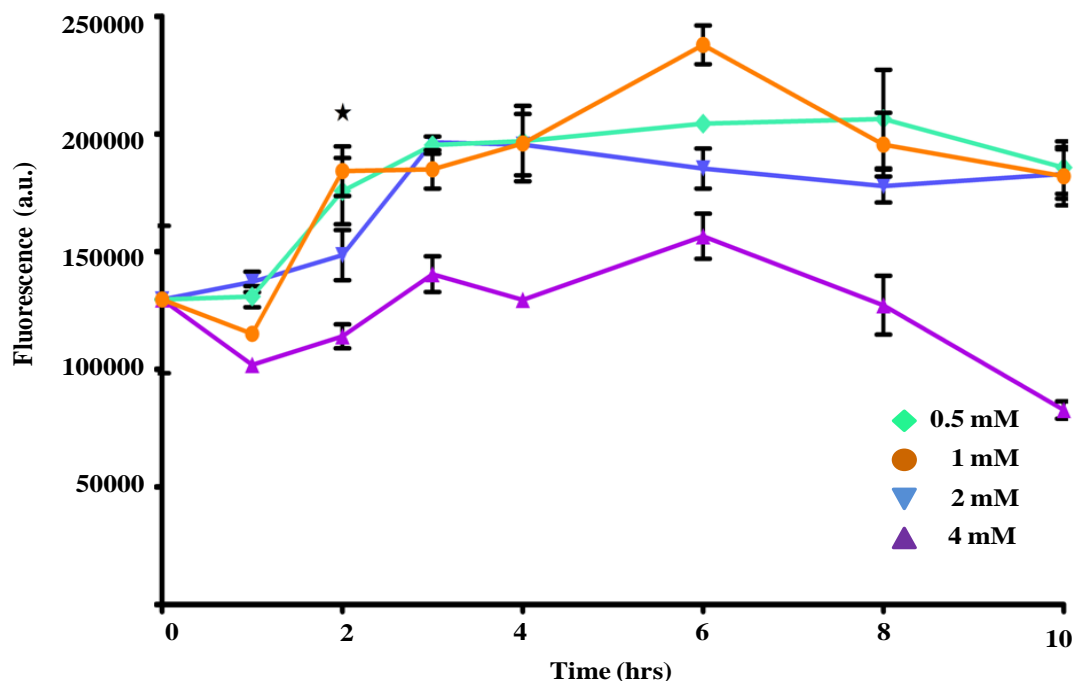


Figure 4.9 Kinetics of PpIX accumulation in keloid fibroblasts from the margin of the scar post-incubation with 5ALA. ★ Denotes significant difference in comparison with cells not exposed to exogenous 5ALA at time zero ($p<0.05$; $n=8$). Graph represents mean and standard deviation.

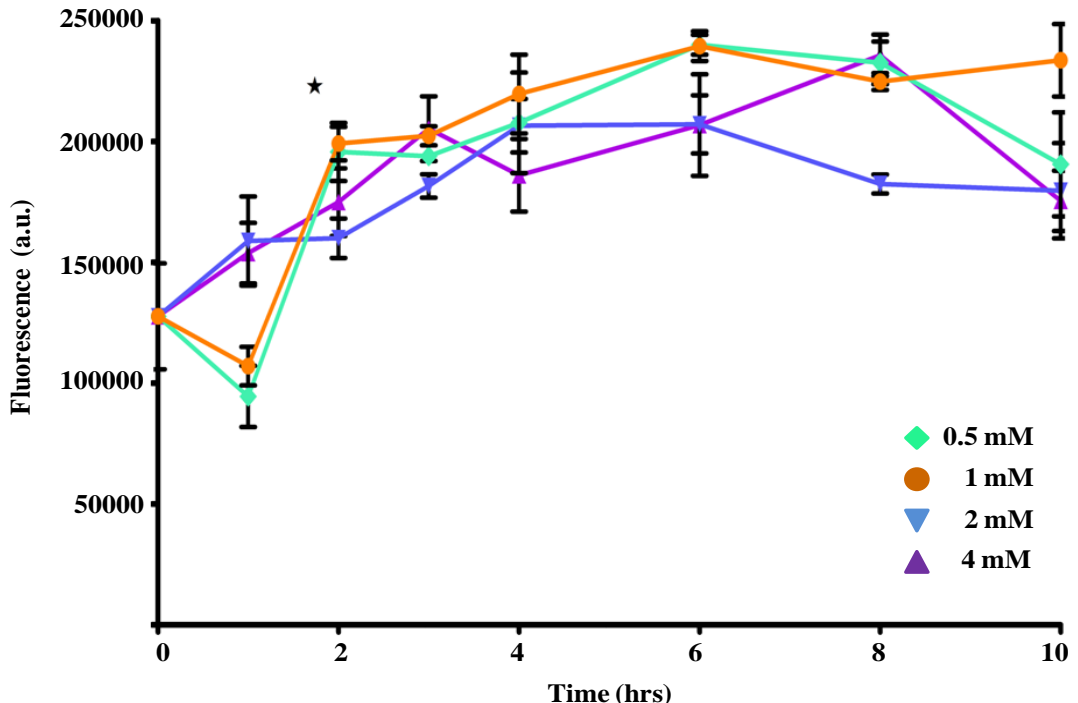


Figure 4.10 Kinetics of PpIX accumulation in keloid fibroblasts from top with 5ALA.
★Denotes significant difference in comparison with cells not exposed to 5ALA at time zero ($p<0.05$; $n=8$). Graph follows a growth curve, with significant accumulation after two hrs which tend to increase up to eight hrs. Graph represents mean and standard deviation.

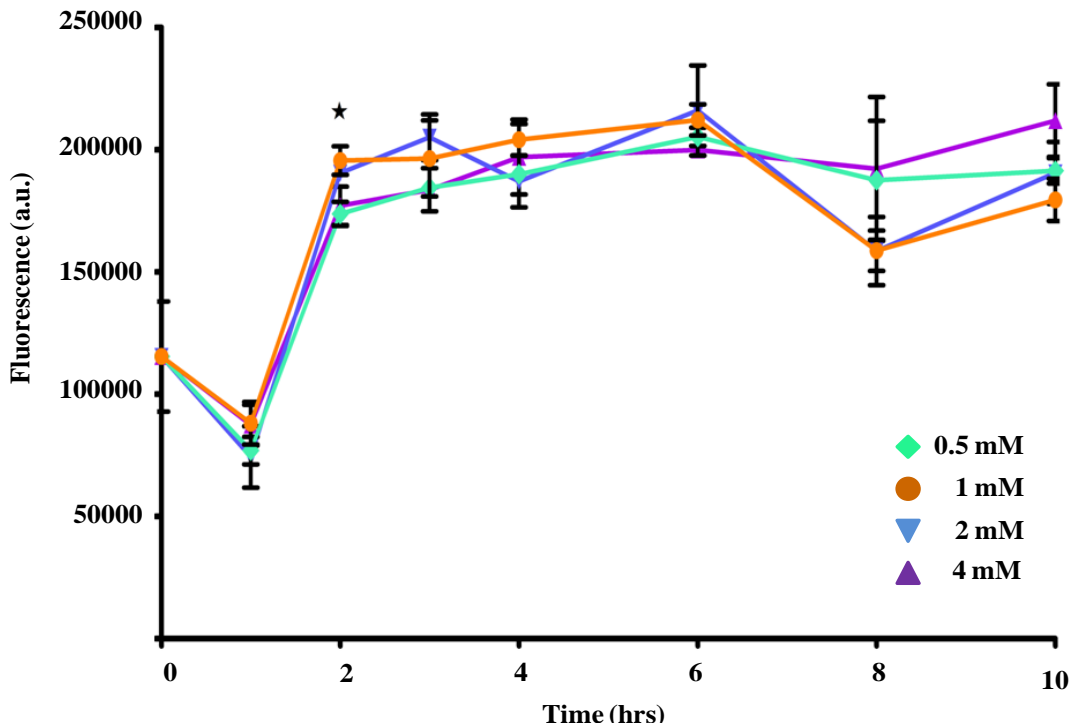


Figure 4.11 Kinetics of PpIX accumulation in keloid fibroblasts from the middle with 5ALA.
★Denotes significant difference in comparison with cells not exposed to 5ALA at time zero ($p<0.05$; $n=8$). Graph follows a growth curve with a plateau from two to six hrs. Graph represents mean and standard deviation.

The difference between PpIX accumulation in KF and NF were highest at 4 mM compared to other precursor concentrations. Moreover, solutions with 4 mM of MALA or 5ALA had better uptake of drugs by keloid fibroblasts without affecting their viability, when compared to other precursor concentrations. However, there was no significant difference in PpIX generation between different keloid cell types after MALA/5ALA treatment. The control bar represents the fluorescence of the three keloid cell type (Figure 4.12).

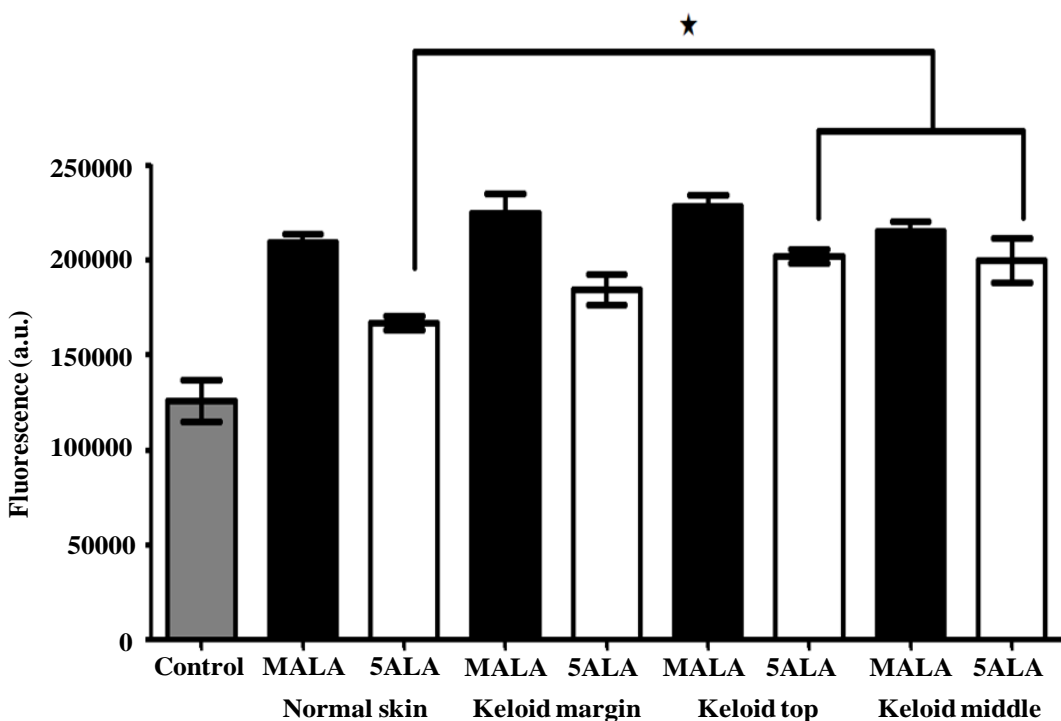


Figure 4.12 Fluorescence intensity of PpIX accumulated in normal skin and keloid fibroblasts after 3 hrs of incubation with 4 mM of MALA or 5ALA. 5ALA showed significant increase in PpIX accumulation in keloid top and middle fibroblasts compared to normal skin fibroblasts. ★ Denotes statistical significance ($p<0.05$; $n=8$).

WST-1 assays measure viability state of the cells; moreover this can be related with the cytoproliferative potential of them. Cytoproliferation was not affected by MALA/5ALA in any primary culture of normal skin and keloid fibroblasts, although exposure to 10 mM and 50 mM of MALA/5ALA increased cytotoxicity significantly (Figure 4.13-16).

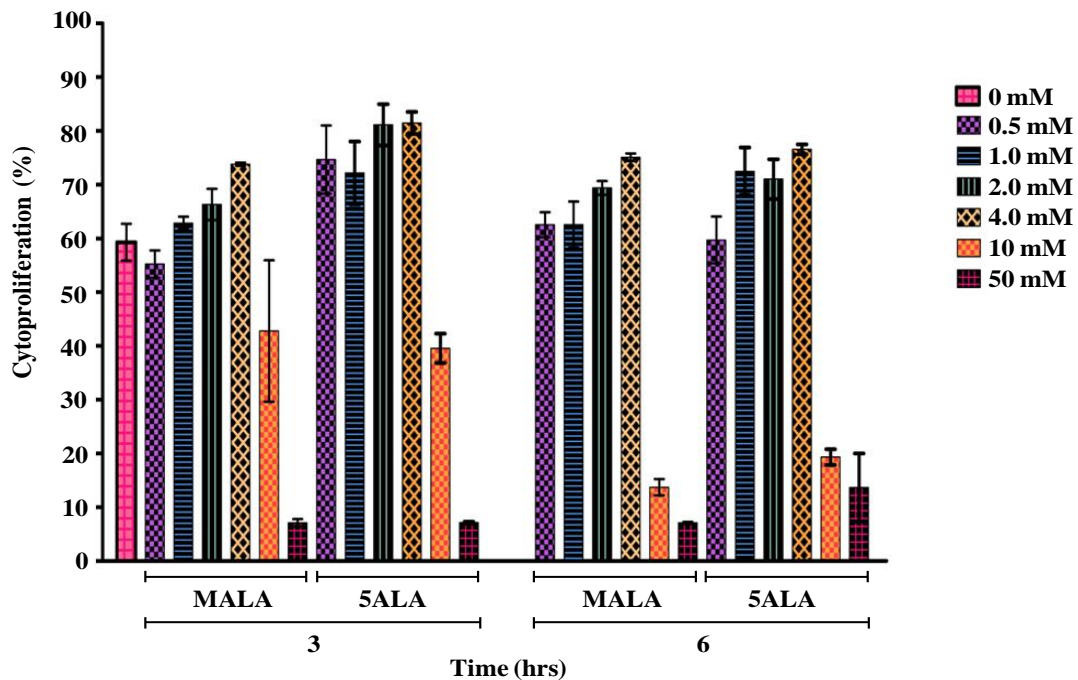


Figure 4.13 Cytoproliferation of normal skin fibroblasts post 3 and 6 hours of incubation with varying concentrations of MALA or 5ALA. ($n=8$).

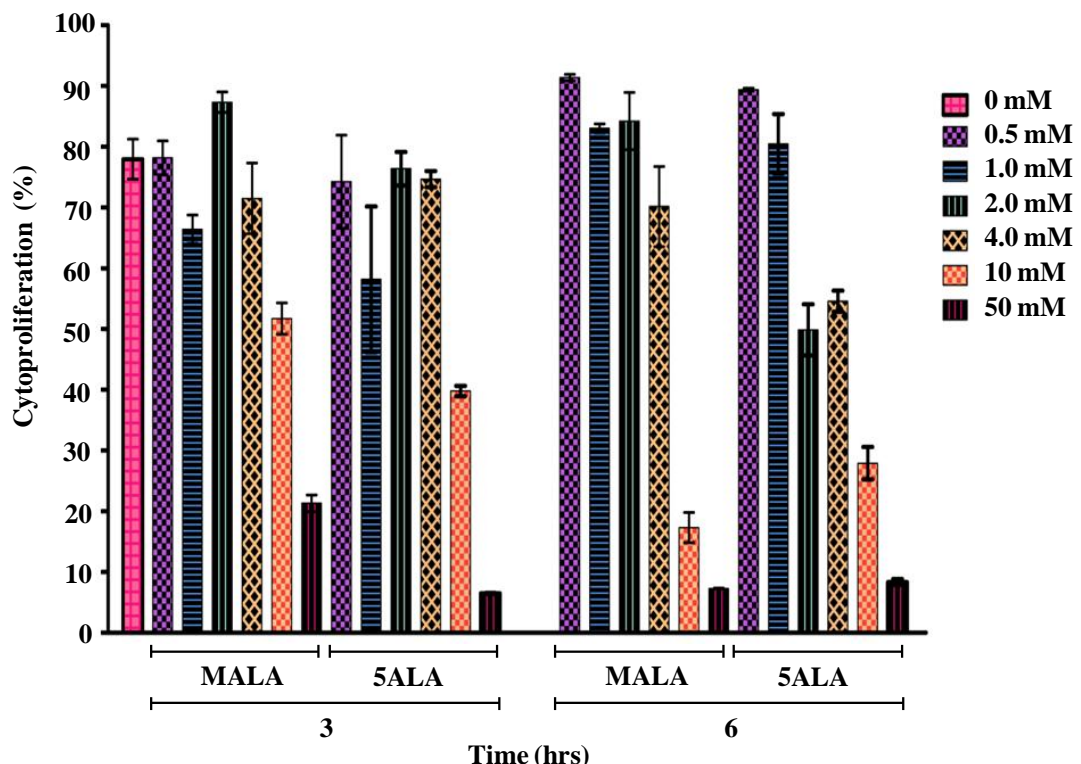


Figure 4.14 Cytoproliferation of keloid fibroblasts from margin of the scar after 3 and 6 hours with varying concentrations of MALA or 5ALA. ($n=8$).

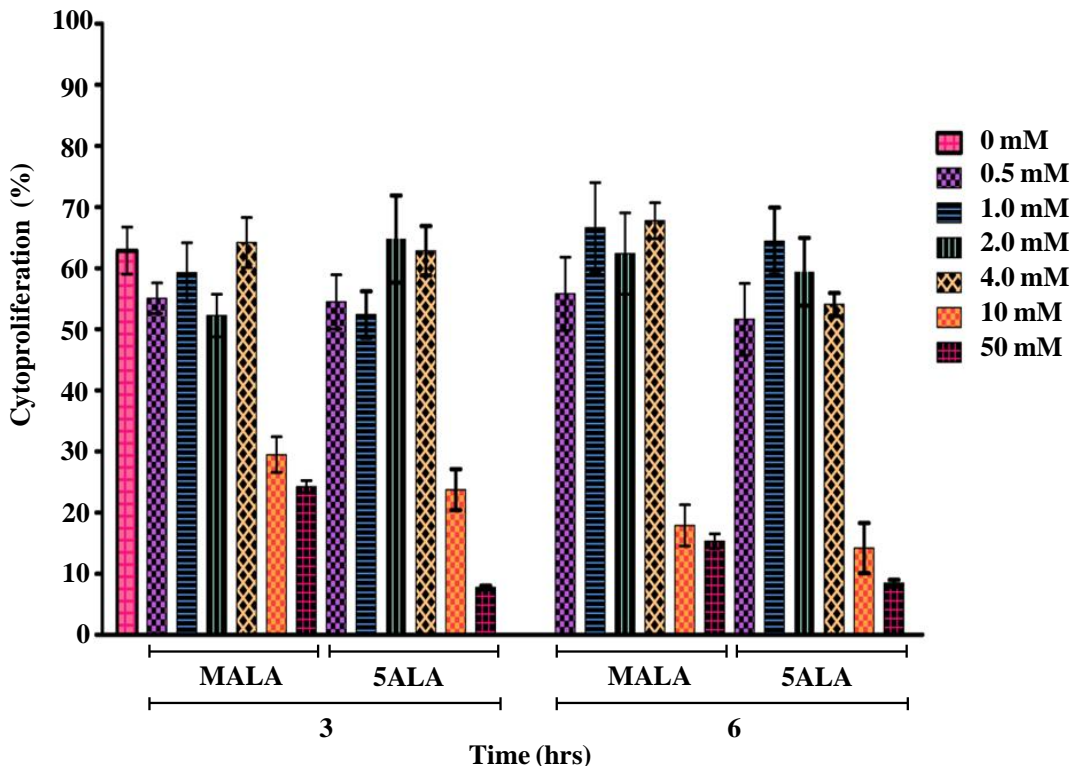


Figure 4.15 Cytoproliferation of keloid fibroblasts from top of the scar after 3 and 6 hours with varying concentrations of MALA or 5ALA. ($n=8$).

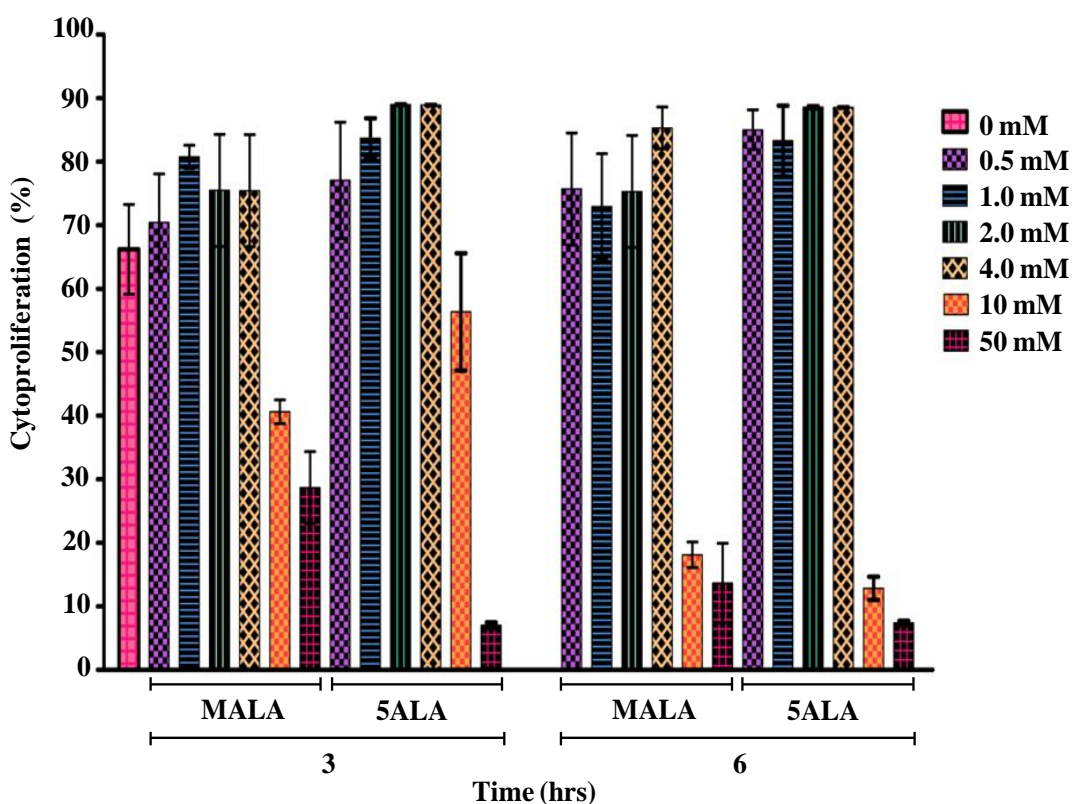


Figure 4.16 Cytoproliferation of keloid fibroblasts from middle of the scar after 3 and 6 hours with varying concentrations of MALA or 5ALA. ($n=8$).

4.4. 2 Phototoxicity of a LED arrangement of red light (635 nm)

Phototoxicity in keloid fibroblasts increased proportionately with fluence

Phototoxicity of KF was significantly higher after light treatment alone compared to NF (Figure 4.17). Cell death was higher for fibroblasts from the top and middle of the keloid at fluence $<20 \text{ J/cm}^2$, whilst fibroblasts from the top and margin were more cytotoxic at 100 J/cm^2 . However cell death was less than 12%, even at 100 J/cm^2 .

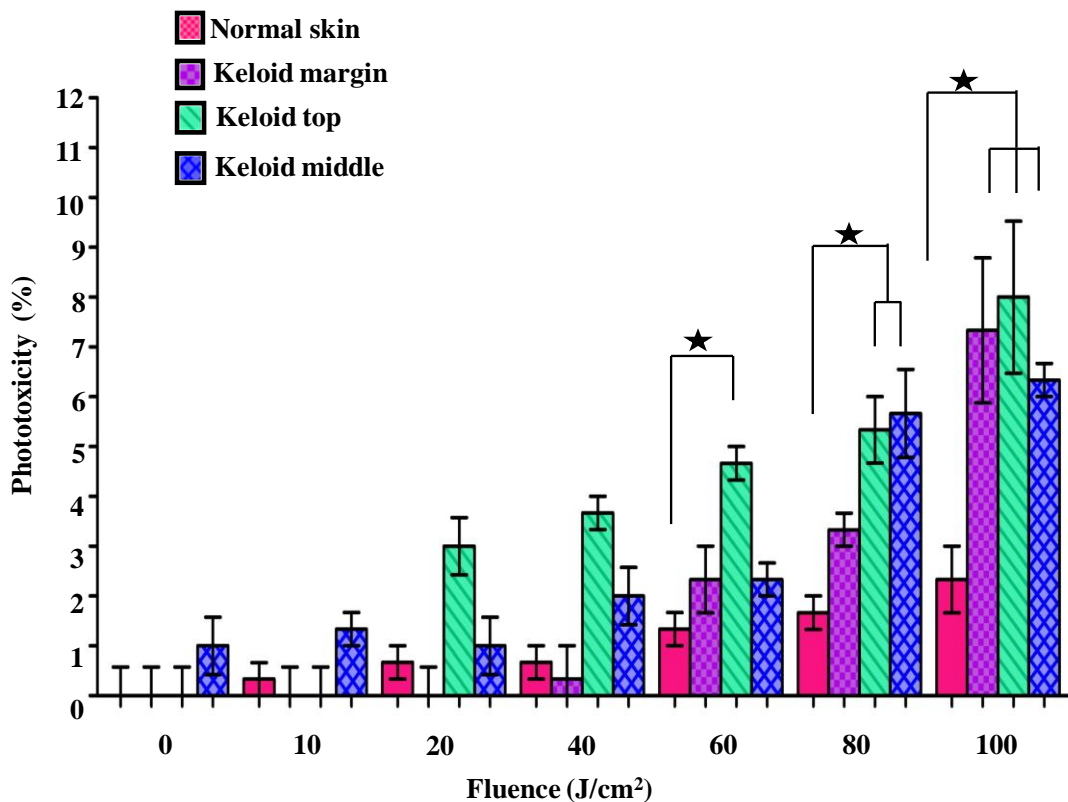


Figure 4.17 Percentage of phototoxicity in site-specific keloid fibroblasts compared to normal skin fibroblasts at increasing fluence rates (without treatment). Phototoxicity analysis was measured upon fluence rate from a light-emitting diode (LED) arrangement ($633 \pm 3 \text{ nm}$ of wavelength and at 35 mW/cm^2 power intensity) by LDH assay. Phototoxicity was found dose-dependant. ★ Denotes statistical significance ($p<0.05$; $n=8$). Graph represents mean and standard deviation.

4.4.3 Cytotoxic analysis after MALA/5ALA-PDT

Cytotoxicity post-PDT followed fluence in a dose-dependent manner

LDH cytotoxicity increased with higher light energies and this increase was proportionate to the fluence (Figure 4.18-20). There was significant increase in cytotoxicity after 72 hrs compared to 24 hrs after PDT. 20 J/cm^2 had better cytotoxic differentiation between KF and NF than any other energy level at 72 hrs.

Cytotoxicity post treatment with MALA and 5ALA was higher for middle-specific keloid fibroblasts compared to cells derived from other keloid lesional sites ($p<0.05$ and $p>0.05$ respectively).

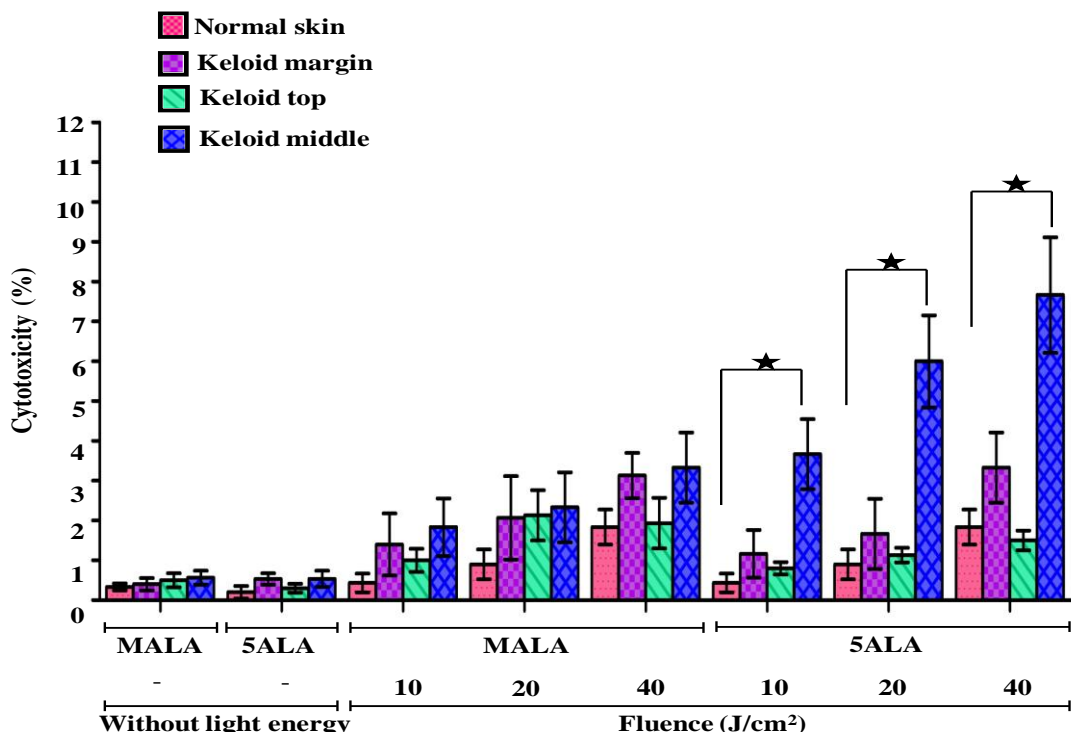


Figure 4.18 Percentage of cytotoxicity immediately after PDT in site-specific keloid fibroblasts compared to normal skin fibroblasts. LDH assay was measure after increasing fluence rates with precursors of photosensitiser MALA/5ALA. However using 5ALA the difference was significant, between normal fibroblasts compared to fibroblast from the middle of the keloid. ★ Denotes statistical significance ($p<0.05$; $n=8$). Graph represents mean and standard deviation.

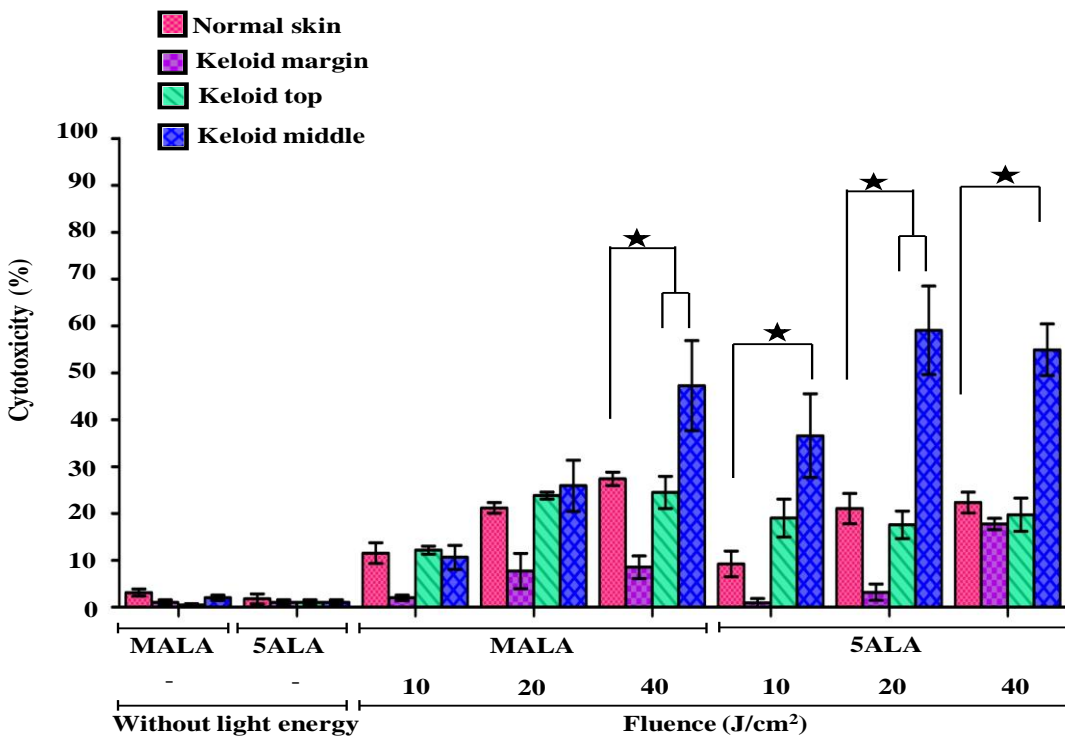


Figure 4.19 Percentage of cytotoxicity 24 hours post-PDT in site-specific keloid fibroblasts compared to normal skin fibroblasts. LDH assay was measure after increasing fluence rates with precursors of photosensitiser MALA/5ALA. ★ Denotes statistical significance ($p<0.05$; $n=8$). Graph represents mean and standard deviation.

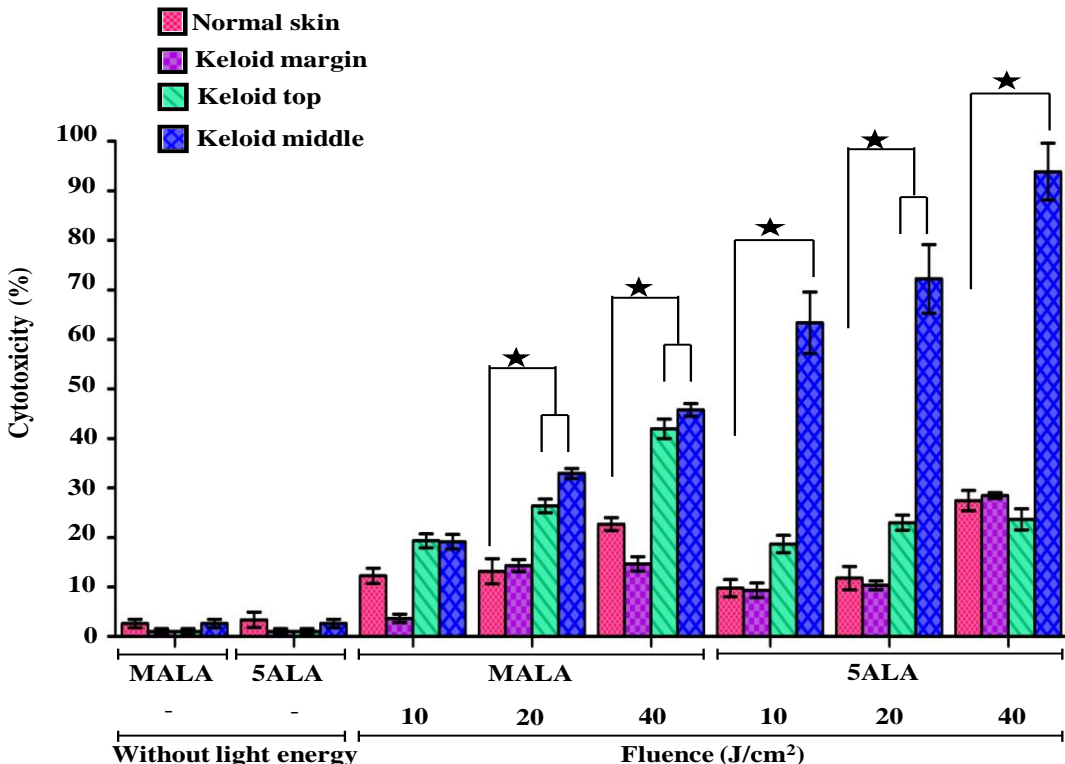


Figure 4.20 Percentage of cytotoxicity 72 hours post-PDT in site-specific keloid fibroblasts compared to normal skin fibroblasts. LDH assay was measure after increasing fluence rates with precursors of photosensitiser MALA/5ALA. ★ Denotes statistical significance ($p<0.05$; $n=8$). Graph represents mean and standard deviation.

4.4.4 Cell proliferation after MALA/5ALA-PDT

Cytoproliferation decreased with PDT in an energy-dependent manner

Cytoproliferation of keloid and normal skin fibroblasts decreased significantly after PDT in an energy-dependent manner (Figure 4.21). Cytoproliferation decreased by 8-fold in KF post MALA/5ALA treatment at 40 J/cm² and NF decreased by 6-fold compared to cells without any treatment. However, there was only significant difference between cells derived from middle of the keloid compared to normal skin cells post 5ALA treatment at energies ≤ 20 J/cm².

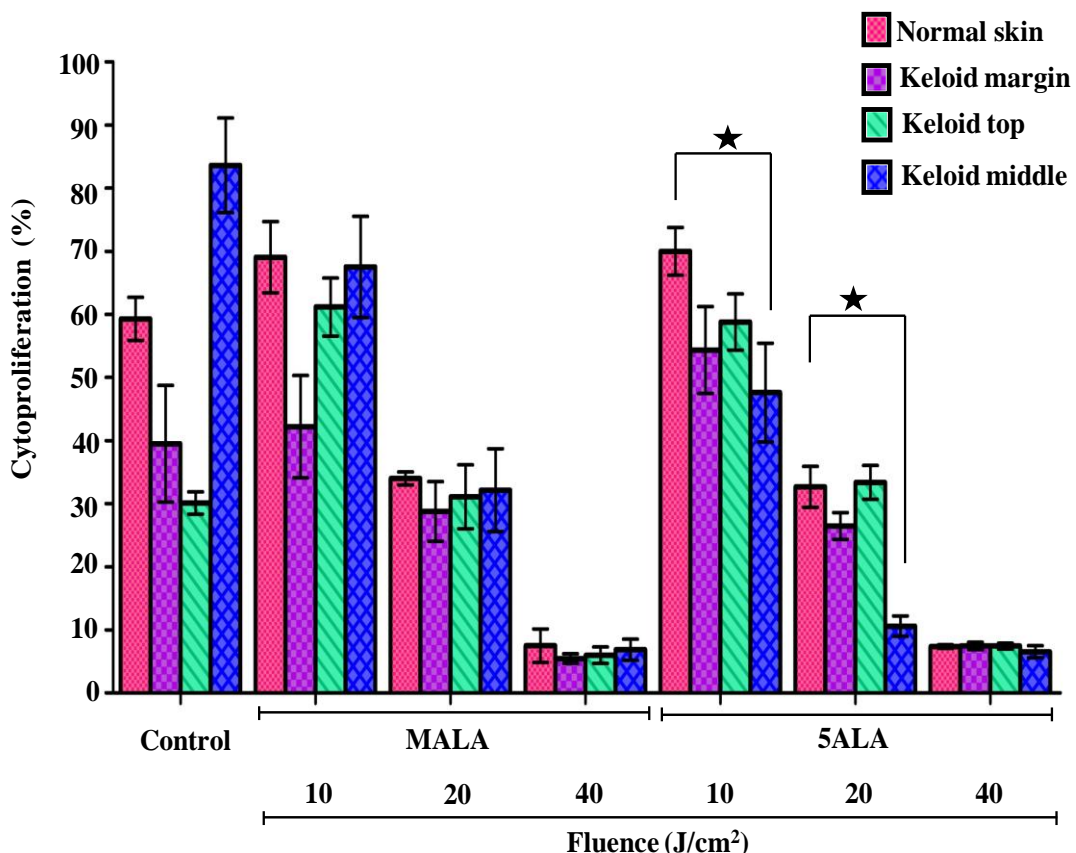


Figure 4.21 Percentage of cell proliferation in site-specific keloid fibroblasts compared to normal skin fibroblasts at increasing fluence rates with precursors of photosensitiser. Cytoproliferation of normal skin and keloid fibroblasts significantly decreased after PDT in an energy-dependent manner as measured by mitochondrial WST-1 enzyme assay. ★ Denotes statistical significance ($p<0.05$; $n=8$). Graph represents mean and standard deviation.

4.4.5 Cell death (Apoptosis/necrosis) analysis after MALA/5ALA-PDT

Apoptosis and necrosis were dependent on keloid lesional site and fluence

Cytotoxicity post PDT in KF was lesional site-specific with more cells prone to necrosis with higher fluence. From Hoechst 33258/PI fluorescence analysis for apoptosis/necrosis, margin-specific keloid fibroblasts were more prone to cell death post MALA treatment at low fluence ($\leq 10 \text{ J/cm}^2$; Figure 4.22) whilst the same was found with middle-specific keloid fibroblasts post 5ALA treatment at low fluence ($\leq 10 \text{ J/cm}^2$; Figure 4.23). Interestingly, higher number of normal skin fibroblasts (~ 55%) were prone to apoptosis following 5ALA treatment at 20 J/cm^2 whilst, they were better prone to necrosis post MALA treatment at 20 J/cm^2 (~ 65%). MALA instigated higher KF cytotoxicity at lower fluence ($\leq 20 \text{ J/cm}^2$) while 5ALA instigated higher KF cytotoxicity at higher fluence, with the exception of middle-specific keloid cells.

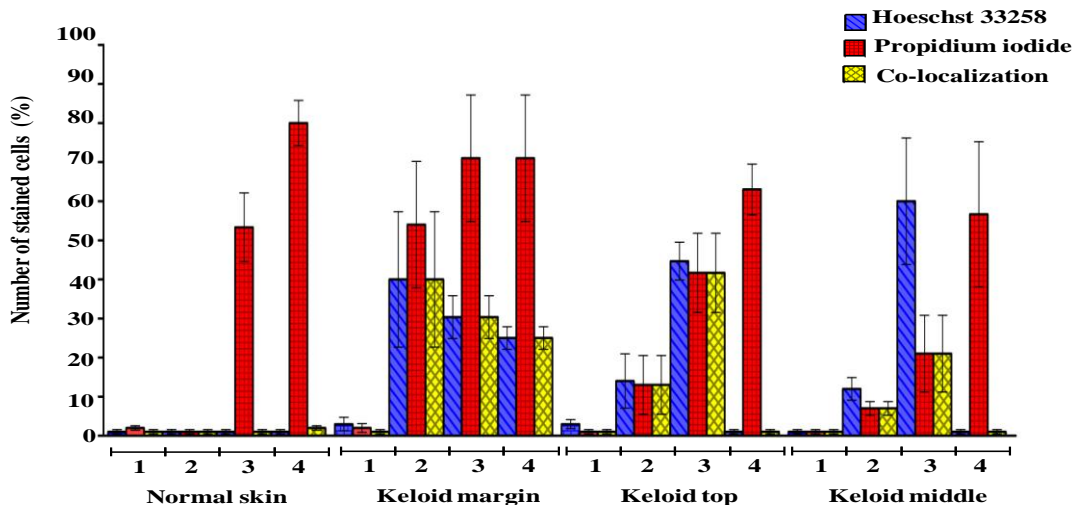


Figure 4.22 Hoechst 33258/PI staining in normal dermal fibroblasts compared to site-specific keloid fibroblasts 24 hours after MALA-PDT treatment. (1) Control, (2) Treatment with 10 J/cm^2 , (3) Treatment with 20 J/cm^2 , and (4) Treatment with 40 J/cm^2 . ($n=8$). Graph represents mean and standard deviation. Necrosis was evident after MALA-PDT and increases with light doses.

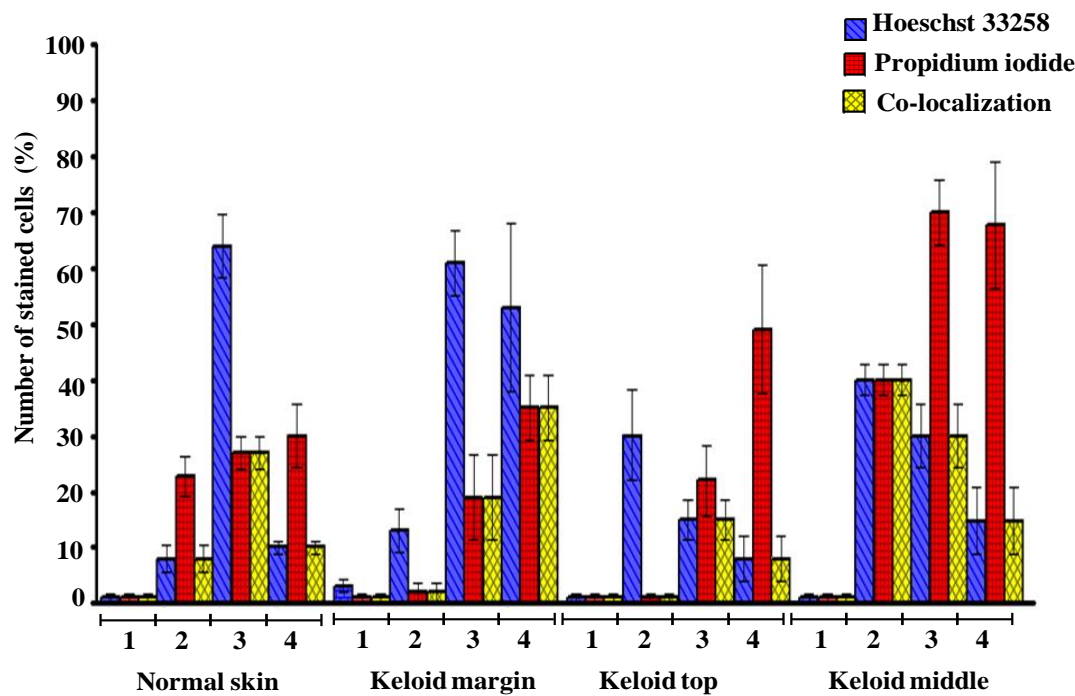


Figure 4.23 Hoechst 33258/PI staining in normal dermal fibroblasts compared to site-specific keloid fibroblasts 24 hours after 5ALA-PDT treatment. (1) Control, (2) Treatment with 10 J/cm^2 , (3) Treatment with 20 J/cm^2 , and (4) Treatment with 40 J/cm^2 . ($n=8$). Graph represents mean and standard deviation. 5ALA-PDT induces apoptosis in keloid margin but necrosis in top and middle, in three cell-type necrosis increases accordingly with the increase of fluence.

4.4.6 Senescence analysis after MALA/5ALA-PDT

Senescence increased up to 10 J/cm^2 and completely disappeared at higher energies

β -galactosidase activity increased in KF and NF after exposure to lower light energies (Figure 4.24). At 10 J/cm^2 , MALA induced least activity of β -galactosidase in middle-specific keloid fibroblasts while 5ALA had the maximum for middle-specific cells. Senescence was not present at higher energies. Therefore induction of senescence was precursor of PS and lesional site-specific. Quantitative data for senescence positive cells are shown figure 4.25.

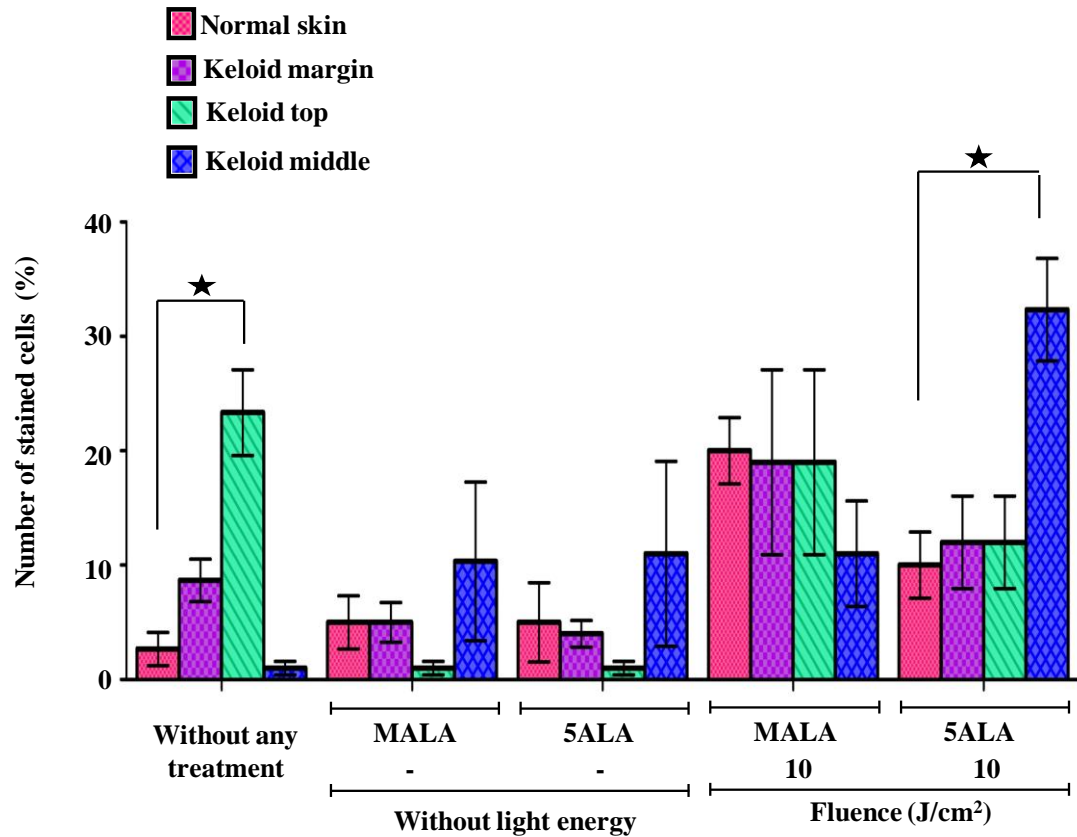


Figure 4. 24 β -galactosidase staining at pH 6 in normal skin compared to site-specific keloid fibroblasts after MALA and 5ALA PDT treatment. Senescence was not observed at higher energies either due to cell death or incapability of the cell to break down the chromogenic substrate X-gal. ★ Denotes statistical significance ($p < 0.05$; $n=8$).

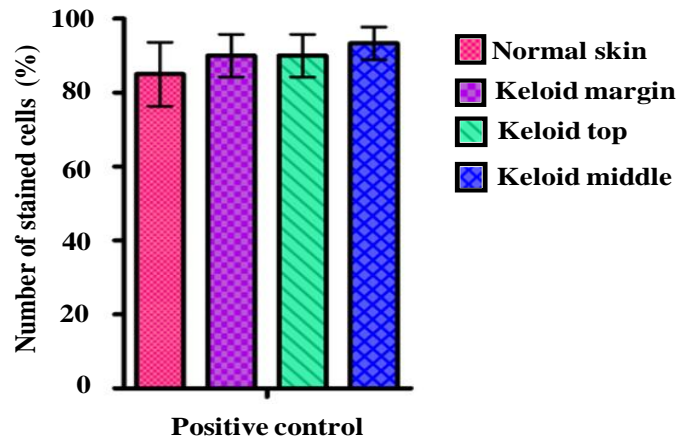


Figure 4.25 Positive senescence induction on site-specific keloid and normal skin fibroblasts. Senescence was induced by maintaining in PBS for 24-48 hours at room temperature. Cytotoxicity tests were shown to be <5% positive on the senescence-induced cells. ($n=3$).

4.4.7 Reactive oxygen species generation analysis after MALA/5ALA-PDT

ROS generation increased with the amount of energy delivered

ROS generation could be correlated to necrosis in any of the cell types and was precursor of PS and lesional site-specific (Figure 4.26). ROS generation increased with every site-specific keloid cell following fluence. However, KF from the middle of the keloid scar generated higher amount of ROS after MALA/5ALA treatment (at any fluence) compared to any other cell types ($p<0.05$ and $p>0.05$ respectively).

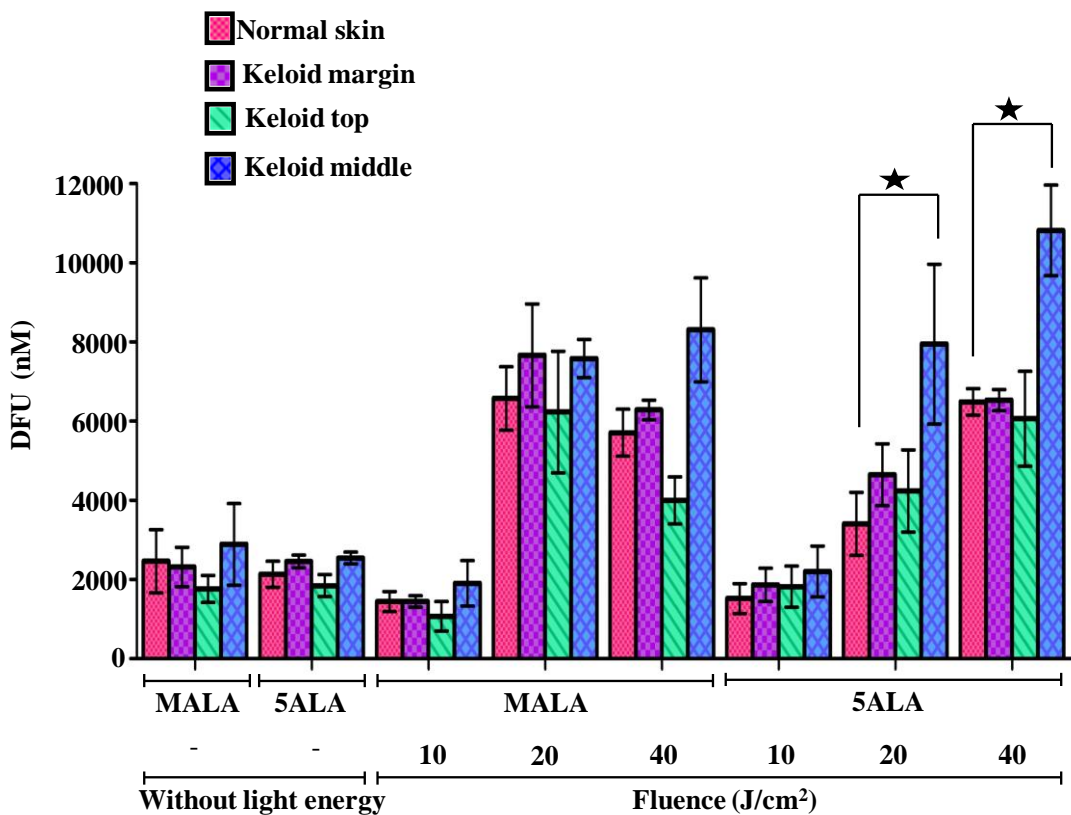


Figure 4.26 ROS generation post MALA/5ALA-PDT treatment in normal skin compared to site-specific keloid fibroblasts. Keloid fibroblasts from the middle of the scar generated more ROS after either M-ALA or 5-ALA PDT compared to all other cell types. ★ Denotes statistical significance ($p<0.05$; $n=8$).

4.4.8 Gene expression analysis of markers of apoptosis and keloid pathogenesis

Keloid and apoptosis related genes were down-regulated post-PDT

Figures 4.27-34 shows the selected genes for qRT-PCR studies were markers for apoptosis, keloid pathogenesis and tumour growth. Collagen I, HIF-1, HSP70, Caspase(CASP) -3 and 9, BCL-2 and Collagen III were down-regulated after PDT. There was a higher down-regulation of cell survival gene B-cell lymphoma 2 (BCL-2) in KF by 5ALA compared to MALA while hypoxia-inducible factor (HIF-1) was down-regulated by 5ALA compared to MALA in both KF and NF. The levels of CASP3 & 9 were up regulated post 5ALA compared to MALA treatment.

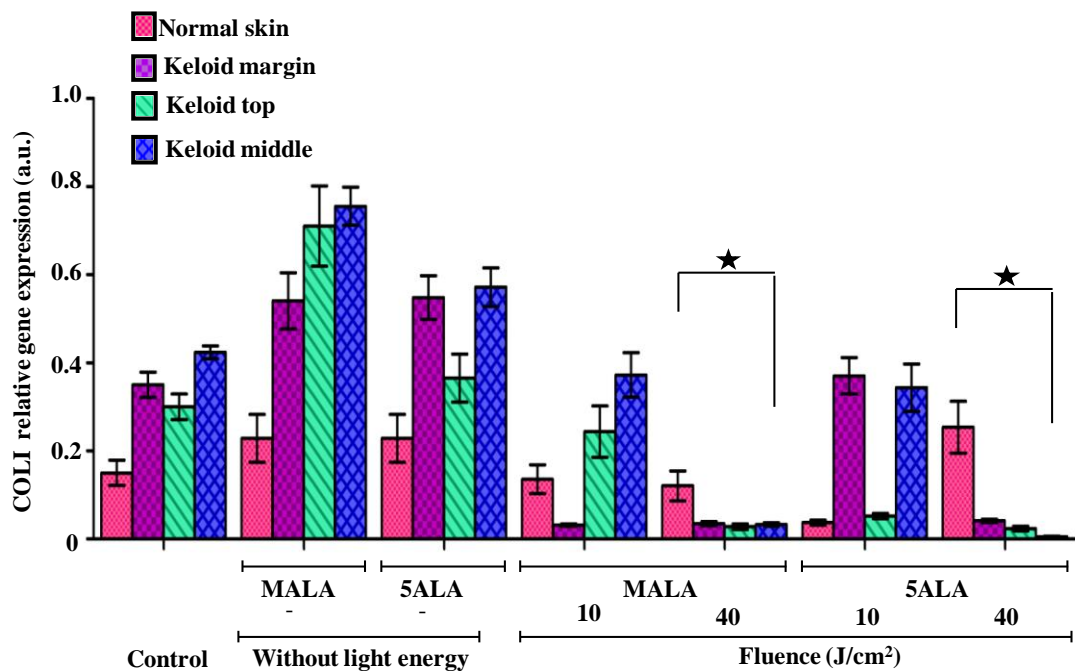


Figure 4.27 COLI relative gene expression levels in normal skin and keloid fibroblasts post-PDT. In the graphs, comparisons are made between PDT-treated NF and PDT-treated KF. ★ Denotes statistical significance ($p<0.05$; $n=8$). COLI expression increases after incubation with the precursor only, however after treatment dramatically decreases.

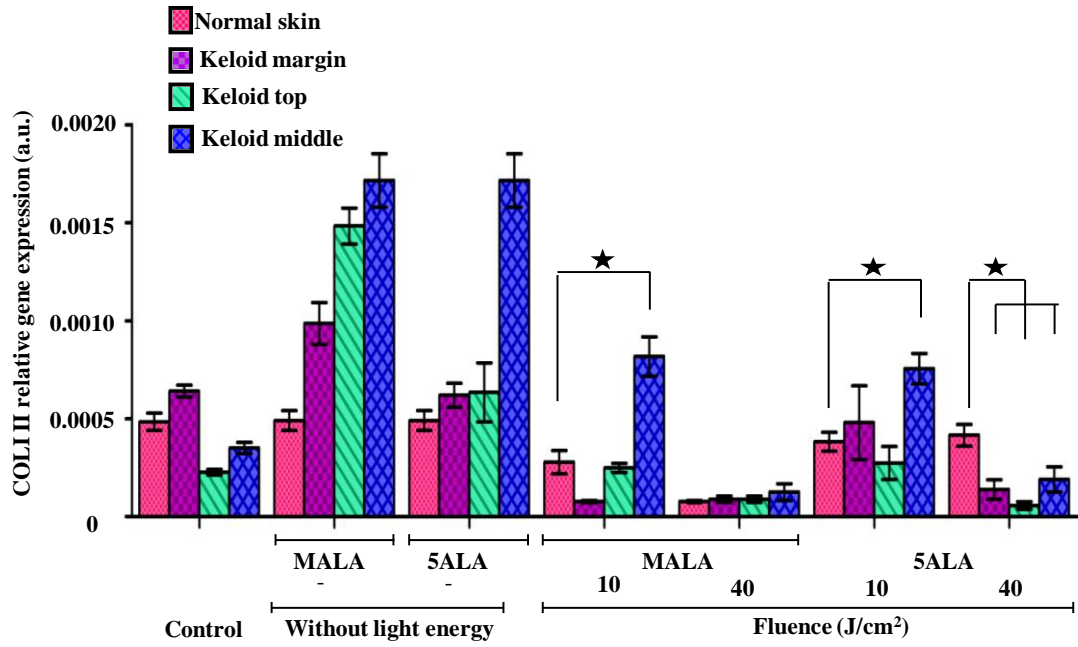


Figure 4.28 COLIII relative gene expression levels in normal skin and keloid fibroblasts post-PDT. In the graphs, comparisons are made between PDT-treated NF and PDT-treated KF. ★ Denotes statistical significance ($p<0.05$; $n=8$).

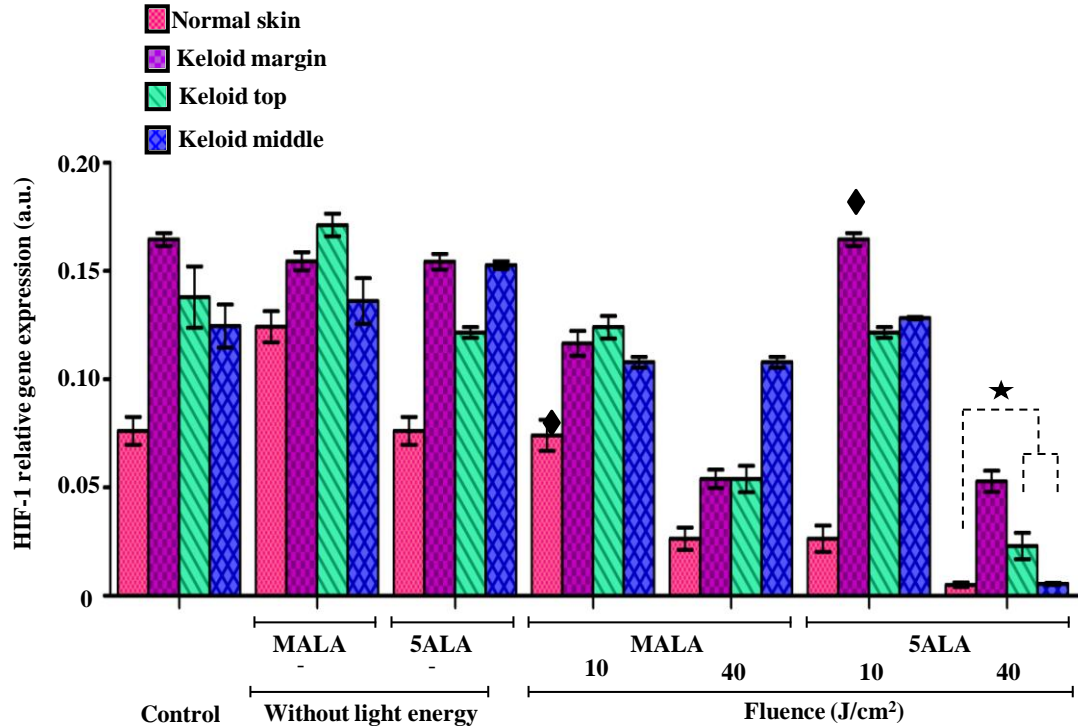


Figure 4.29 HIF-1 relative gene expression levels in normal skin and keloid fibroblasts post-PDT. In the graphs, comparisons are made between PDT-treated NF and PDT-treated KF. ★ Denotes statistical significance ($p<0.05$; $n=8$). ◆ Denotes no-significant compared to cells without any treatment ($p>0.05$).

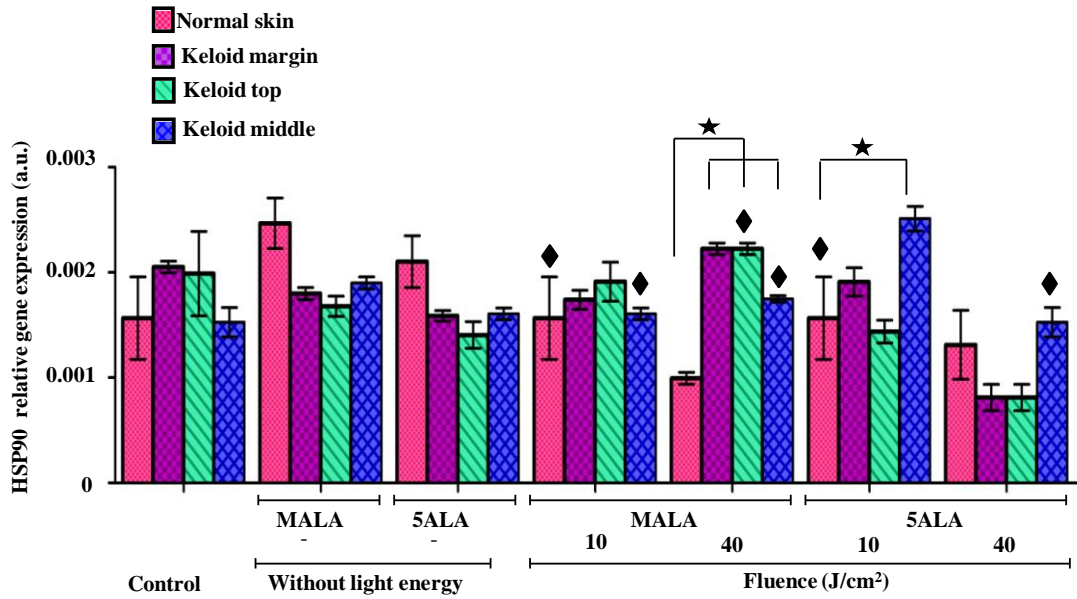


Figure 4.30 HSP90 relative gene expression levels in normal skin and keloid fibroblasts post-PDT. In the graphs, comparisons are made between PDT-treated NF and PDT-treated KF. ★ Denotes statistical significance ($p<0.05$; $n=8$; ♦ Denotes no-significant compared to cells without any treatment $p>0.05$).

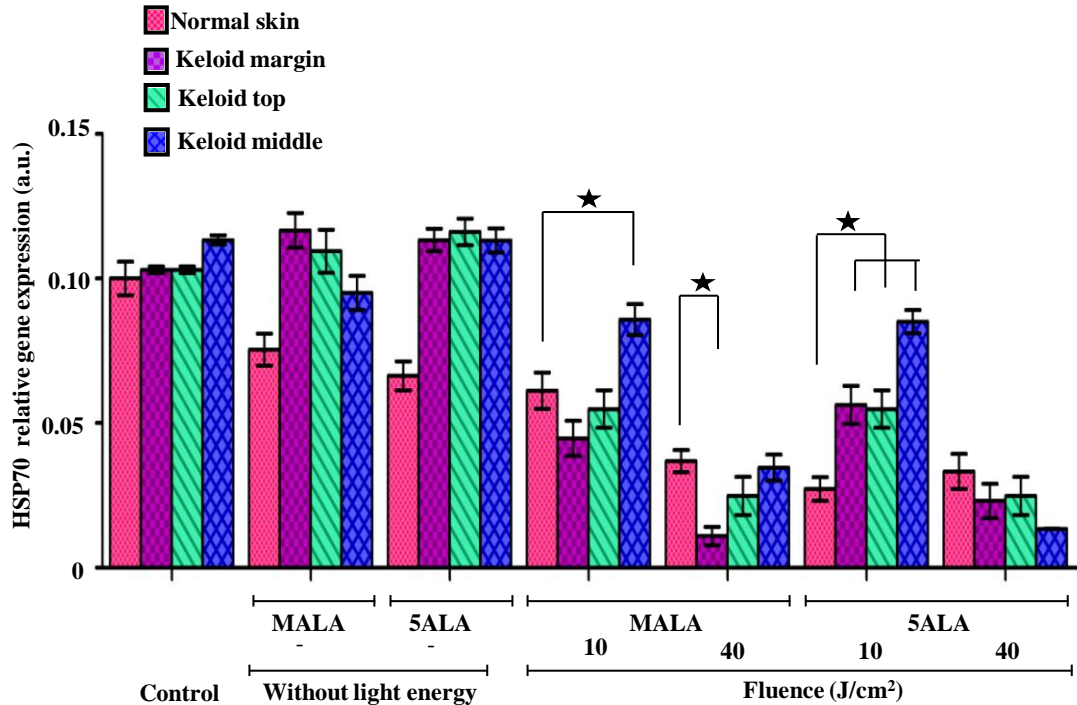


Figure 4.31 HSP70 relative gene expression levels in normal skin and keloid fibroblasts post-PDT. In the graphs, comparisons are made between PDT-treated NF and PDT-treated KF. ★ Denotes statistical significance ($p<0.05$; $n=8$).

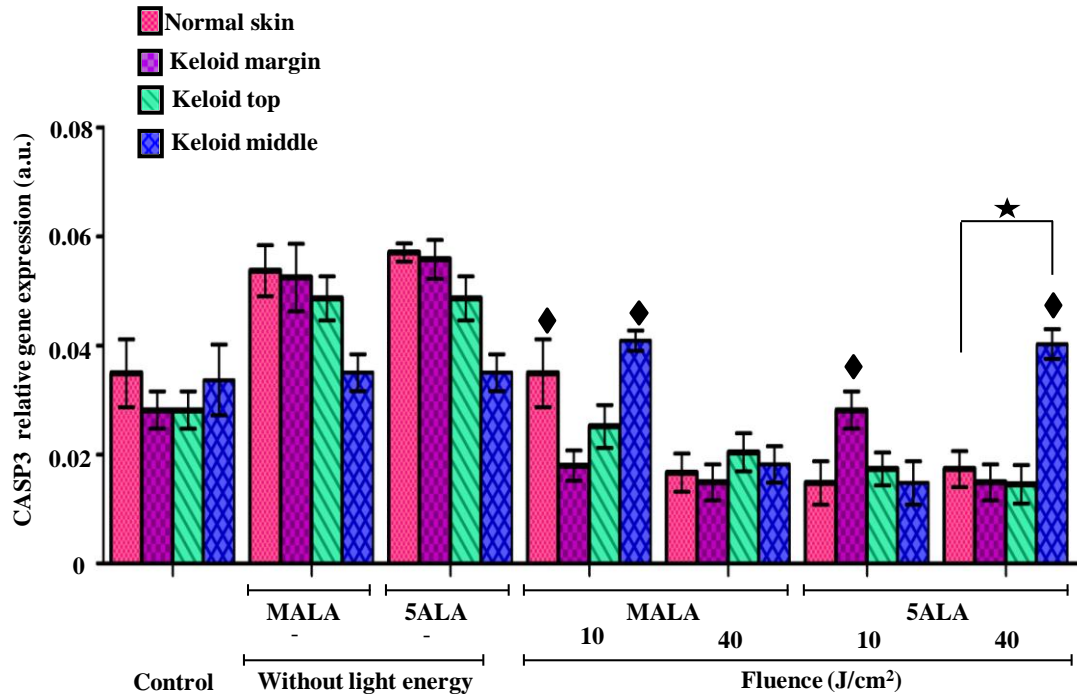


Figure 4.32 CASP3 relative gene expression levels in normal skin and keloid fibroblasts post-PDT. In the graphs, comparisons are made between PDT-treated NF and PDT-treated KF. ★ Denotes statistical significance ($P<0.05$; $n=8$). ♦ Denotes no-significant compared to cells without any treatment ($p>0.05$).

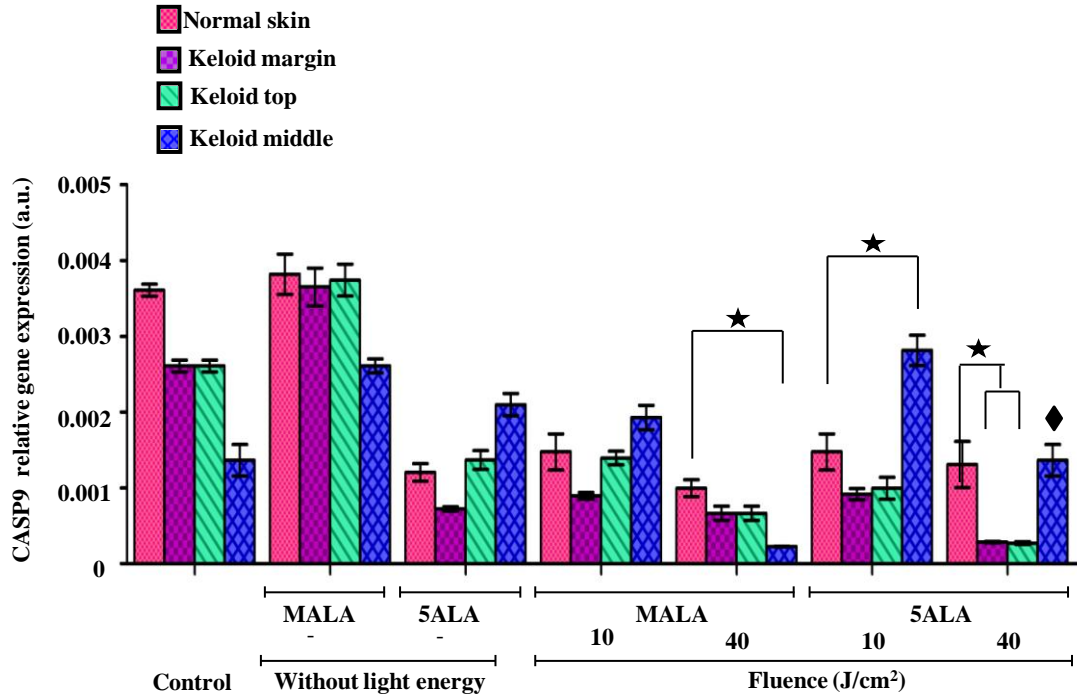


Figure 4.33 CASP9 relative gene expression levels in normal skin and keloid fibroblasts post-PDT. In the graphs, comparisons are made between PDT-treated NF and PDT-treated KF. ★ Denotes statistical significance ($P<0.05$; $n=8$). ♦ Denotes no-significant compared to cells without any treatment ($p>0.05$).

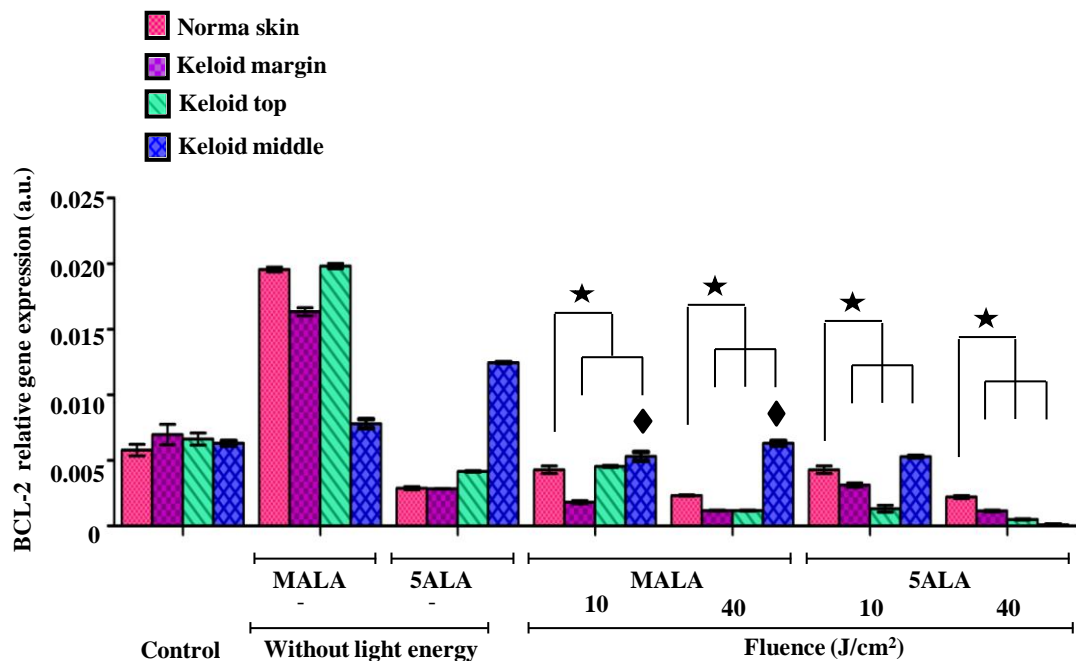


Figure 4.34 BCL-2 relative gene expression levels in normal skin and keloid fibroblasts post-PDT. In the graphs, comparisons are made between PDT-treated NF and PDT-treated KF. ★ Denotes statistical significance ($P<0.05$; $n=8$). ♦ Denotes no-significant compared to cells without any treatment ($p>0.05$).

4.5 Discussion

This study has demonstrated the cytotoxicity levels of normal skin and keloid site-specific fibroblasts following the application of PDT. We compared two precursors of photosensitiser, investigated the intracellular accumulated and degraded profile of photosensitiser, and measured cytoproliferation, apoptosis and necrosis rate, and senescence, in correlation to PpIX accumulation and ROS generation. Our results show that ROS generation and intracellular PpIX localisation are more critical in determining cytotoxicity than intracellular PpIX accumulation. In addition, ROS generation, cytotoxicity, cytoproliferation and senescence had fluence dependent profiles. Fluorescence analysis revealed that MALA instigated higher KF

cytotoxicity at lower fluence ($\leq 20 \text{ J/cm}^2$) while 5ALA instigated higher KF cytotoxicity at higher fluence, except in middle-specific keloid cells. Middle specific keloid cells were more prone to cell death post 5ALA treatment while inconsistencies were observed with other site-specific keloid cells and MALA.

5ALA is an endogenous amino acid and has been promoted as a precursor for the photosensitising agent (PpIX) in PDT (Luo, et al., 2001; Noodt, et al., 1996; Stapleton, et al., 2003). In ALA-based PDT, intracellular PpIX accumulation has proved to be higher in tumour cells and could be detected through the typical red fluorescence under illumination with blue light (Ji, et al., 2006; Rodriguez, et al., 2006). Our results coincided with Sebastian et al. (2011), illustrating the higher accumulation of PpIX in KF compared to NF. However, there was no significant difference in PpIX accumulation in different lesional sites in the keloid scar itself. Higher degree of PpIX generation in KF was observed after incubation with MALA compared to 5ALA ($P>0.05$). This is because MALA penetrates into the cell by different mechanisms which include the facilitation by active transporters of non-polar amino acids or by diffusion, while 5ALA is taken up by β -amino acids and γ -aminobutyric acid (GABA; Aalders, et al., 2001; Rodriguez, et al., 2006; Robertson, et al., 2009).

Phototoxicity of cells increased in a dose-dependent manner with the amount of light energy delivered. Phototoxicity of NF was only 2% when compared to 10% of KF even at the highest energy delivered (100 J/cm^2). However, the reduced innate apoptotic activity of KF compared to normal scar fibroblasts was shown by Sebastian et al., (2011). It is possible that external stimuli may accelerate the

cytotoxic mechanism in KF more than NF (Chiu, et al., 2005). Interestingly, following 72 hours of PDT treatment, cytotoxicity of KF reached 90% at 40 J/cm², whilst NF was only at 30% under the same conditions.

It has been reported that top and middle regions in keloid scars are generally quiescent while the margin is highly proliferative (Syed, et al., 2011); This is in agreement with our results showing higher cell death in keloid middle-specific cells whilst least proliferative compared to fibroblasts from other sites. However, selective cell death mechanisms through apoptosis, autophagy and necrosis post PDT are suggested to be based on the cell type, the quantity of PpIX and intracellular PpIX localisation (Angel-Petersen, et al., 2006; Cai, et al., 2011; Garg, et al., 2010; Lee, 2008; Noodt, et al., 1996; Panzarini, et al., 2011).

Intracellular localisation of PpIX occurs in lysosomes, mitochondria, plasma membrane, Golgi apparatus and endoplasmic reticulum, however the precise cellular localisation of PpIX in keloid fibroblasts have not been studied to date. Additionally, it has already been shown that PpIX accumulation in mitochondria results in higher cell death (Kessel, et al., 1997), which may explain our findings with the middle-specific keloid cells. Indeed, this was verified with higher generation of Caspases-3 & 9 seen in middle-specific keloid cells compared to cells in other sites (Castano, et al., 2004).

Furthermore, middle-specific keloid cells treated with 5ALA showed higher senescence, higher cytotoxicity and least proliferation compared to MALA treatment. There was a difference in cytotoxic mechanism induction post PpIX

accumulation and ROS generation after incubation with 5ALA/MALA as indicated previously by Castano et al. (2004). Moreover, faster elimination of MALA than 5ALA was observed in cultured epithelial cells, which could further generate PpIX, post irradiation (Washbrook, 1997).

Apoptosis is more preferable to necrosis in clinical situations as it leads to reduced tissue reactions. However, higher concentration of PpIX and light dosage will direct apoptosis towards necrosis as the principal cell death mechanism (Uehlinger, et al., 2000). We observed the same result beyond 20 J/cm² where the major cellular apoptotic pathway was switched to necrosis.

In the present study, we observed that the generation of ROS was mostly in accordance with fluence but not with PpIX accumulation. Even though PpIX formation was higher in human epidermoid carcinoma cells, any blockade in cellular mechanism inhibited the generation of ROS and subsequent cell death (Lam, 2001). This was in agreement with PpIX accumulation and ROS generation where middle-specific keloid cells generated more ROS in spite of lower PpIX accumulation compared to other cell sites. The pattern of ROS generation could be correlated with apoptosis/necrosis mechanisms, with the ratio of necrosis increasing with ROS generation (>10 J/cm²). This also demonstrated ROS as the principal effectors of cell damage post PDT that is demonstrated in figure 4.32. Here, the subcellular target in PDT was mainly affected by ROS, which could potentially lead to lipid peroxidation, cytoskeleton, biological membrane and DNA damage as has been suggested also by 22 Kim, et al., (2011).

ROS generation in mitochondria can lead to apoptosis/necrosis through Caspase-dependant pathway, which was evident from the differential expression of Caspases-3 & 9 post-PDT. Generally, cytochrome c is released from the mitochondria as a pro-signal for apoptosis leading to a reduction in mitochondrial membrane potential, which is followed by the activation of Caspase-3-like proteases (He, et al., 1998; Kim, et al., 2011; Zhao, et al., 2011). This could be an early indication of apoptosis, post-PDT. However, the dependence of apoptosis/necrosis on Caspases-3 & 9 activation has not been verified in this study. The decreased expression of BCL-2 (marker for mitochondrial cell viability) with increased light energy also supports decreased cell viability.

HSP70 has been shown to be expressed at lower levels in normal skin compared to keloid fibroblasts and is up-regulated during wound healing process and keloid formation (Totan, et al., 2011; Shi, et al., 2010b). The mRNA levels were observed down-regulated in post-PDT, which is another indication of increased cell death. HSP90, which acts as a molecular chaperone to prevent protein unfolding and aggregation, was expressed to similar levels in keloid and normal skin fibroblasts. Our results indicate the minor role of HSP90 in cell death post-PDT. A consistent up-regulation of HIF-1 α was observed in keloids compared to normal skin (Zhang, et al., 2003). However, HIF-1 α was down-regulated in both KF and NF at higher fluence. This could be another indication of the cytotoxic conditions prevailing after PDT as indicated in figure 4.35. Further decrease of HIF-1 α in middle-specific keloid cells following 5ALA incubation and 40 J/cm² indicate higher cell death, compared to other treatments.

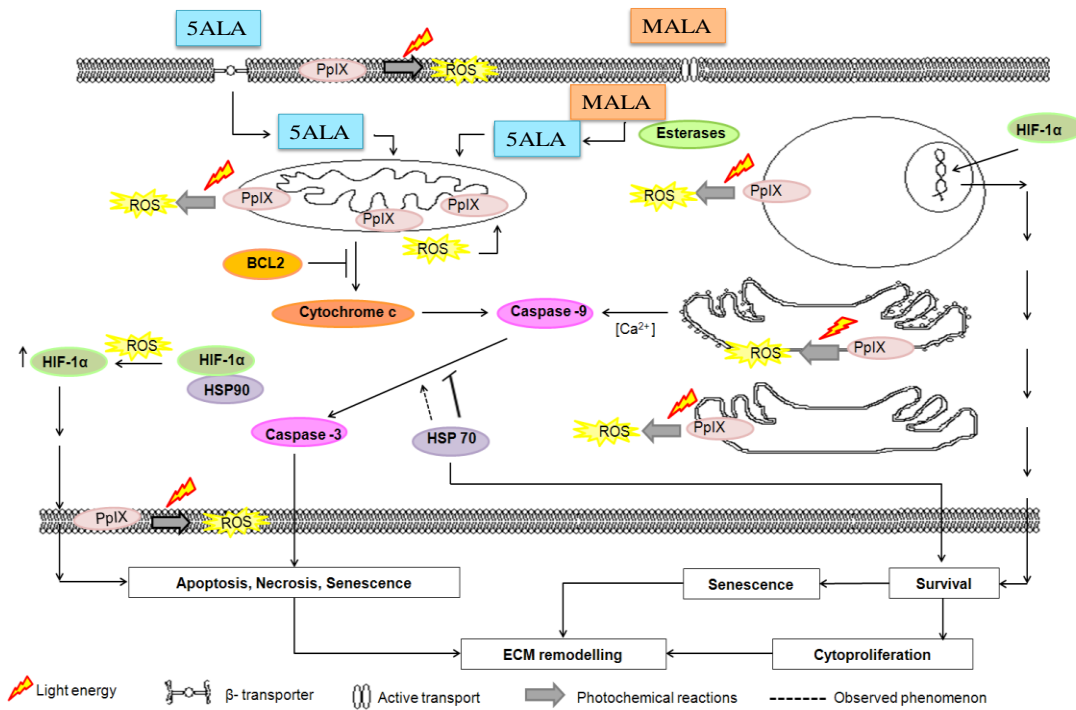


Figure 4.35 Proposed mechanism of cell death/cell survival of keloid fibroblasts post-PDT. MALA penetrates into the cell by different mechanisms, which include the facilitation by active transporters of non-polar amino acids or by diffusion, while 5ALA is taken up by β -amino acids and γ -aminobutyric acid (GABA). Esterases cut MALA into 5ALA, which is converted into PpIX in the inner membrane of the mitochondria (Rodriguez, et al., 2006). The photosensitive properties of PpIX generate intracellular ROS after photochemical reactions. ROS leads to organelle damage, which initiates several mechanisms which are pro-apoptosis or pro-survival (Castano, et al., 2005). Caspase-9 and subsequently Caspase-3 are activated by Cytochrome c released from mitochondria, which leads to apoptosis. HIF-1 binds to nuclear DNA, thereby translating proteins, which can enhance cell survival. HSP70 has been observed to be up-regulated during wound healing process and also in keloid tissue (Zhang, et al., 2003). The combined activity of HSP70 and Caspase-9 may enhance Caspase-3 activity, which may further guide keloid fibroblasts to a preferred cell death mechanism.

CHAPTER FIVE: PHOTODYNAMIC THERAPY AND EX VIVO WOUND HEALING

5.1 Introduction

An ideal wound healing model of adult human skin should not only resemble and incorporate all adult human skin components, processes and functions needed for cutaneous repair but also allow functional testing of therapies ex vivo, when the whole human organism or an animal model is not possible. However, in vitro and animal models fall short of this ideal scenario. Human skin wound healing organ cultures (WHOCs) are comprised of all skin components and importantly include the complex interactions between these components, which are maintained ex vivo. (Lebonvallet et al., 2010; Mathes et al., 2014; Vermolen, 2010).

A number of such WHOCs have been previously reported as being relevant in studying cutaneous wound healing processes and possible new therapies, although there has not been any previous report of the role of Photodynamic Therapy (PDT) in cutaneous wound healing using the WHOC model (Reddy et al., 2010; Mills et al., 2014; Peplow et al., 2012).

Despite these previously reported approaches, there is a lack of standardization and conformity in testing of WHOCs. Thus, in the absence of a standardized protocol,

the most optimal set-up in relation to growth media, physical support systems such as collagen embedding or well-chamber inserts and type of wound, in order to study the wound healing process and functional testing of products remains unclear (Balaji et al., 2014; Companjen, et al., 2001; Kilsdonk, et al., 2013; Kratz, 1998; Peramo, et al., 2010; Tomic-Canic, et al., 2007; Xu, et al., 2012; Moll, et al., 1998).

Thus, this chapter describes the optimization of a WHOC model of human adult skin and PDT effects on wound healing ex vivo compared to WHOCs without treatment. The optimization took into consideration two types of wound, partial and full thickness, two types of physical support of the WHOC (collagen embedded or well chamber insert) and three different growth media. WHOCs were evaluated and compared to normal skin and skin ex vivo. Subsequently optimized WHOCs were exposed to PDT with 5ALA and 20 J/cm². Pro-photosensitiser 5ALA and fluence were selected according to the results described in the previous chapter. 5ALA shows less cytotoxic effects compared to MALA. 20 J/cm² of red light (635 nm) was the maximum amount of light without statistically significant cytotoxic effect on the fibroblasts isolated from normal skin. Apoptosis, proliferation, ECM remodelling, oxidative stress and related gene expression measured the effect of PDT in wound repair.

5.2 Experimental set up

WHOCs with a full thickness wound or a partial thickness wound were cultured after optimized conditions of physical support and growth media. Afterwards a unique

WHOC model was functionally evaluated with PDT using 5ALA and 20 J/cm² of red light (635 nm). Histological, immunohistochemical and differential gene expression analyses were performed post-PDT. Followed methodology is depicted in figure 5.1

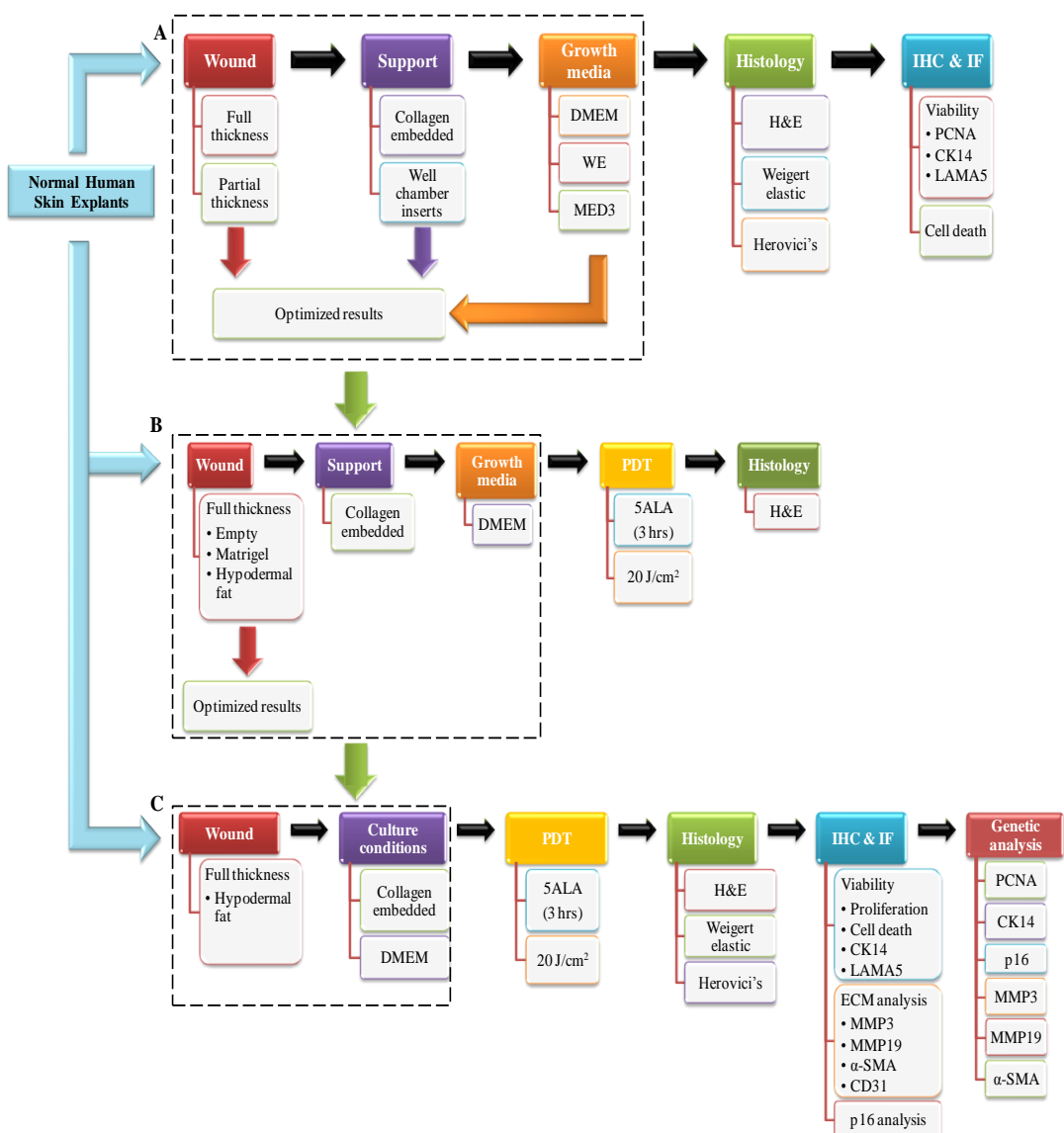


Figure 5.1 Flow chart of the methodology used in chapter five. Green arrows show the sequential step of this investigation. Dotted squares show the procedure followed. First, after an optimization of WHOCs (A), two different scaffolds were also analyzed post-PDT (B), finally WHOCs where functionally evaluated post-PDT (C).

5.3 Materials and methods

5.3.1 Skin explants

Skin explants were obtained from 11 healthy patients undergoing routine elective cosmetic surgery, which were not exposed to any tanning procedure. Abdominoplasty and reduction mammoplasty were the preferred surgery for skin resection due to the amount of skin available, but regardless of age and sex (Table 5.1). Ethical approval for this work was granted by the North West (England, UK) Research Ethics Committee (Ethics Code - 11/NW/0683). Tissue samples were collected following informed consent.

Table 5.1 Demographic data and source of skin explants

Patient number	Gender	Age (years)	Anatomical source of skin explants
1	Male	71	Abdomen
2	Female	42	Abdomen
3	Female	38	Abdomen
4	Male	28	Abdomen
5	Female	42	Abdomen
6	Male	42	Breast
7	Female	60	Breast
8	Female	61	Breast
9	Female	51	Breast
10	Female	37	Breast
11	Female	31	Breast

Explants were washed several times in phosphate buffer solution (PBS, Sigma-Aldrich, Dorset, UK) and soaked in Dulbecco's modified Eagle's medium (DMEM; Sigma-Aldrich, Dorset, UK) supplemented with Primocin (InvivoGen, Nottingham, UK) for 30 mins. Skin explants were cut with a full thickness punch biopsy of 8 mm. Two different wounds were then created within the punch biopsy (either partial or full thickness wound). The punch biopsies were placed in two different support systems and maintained with three different commercial media. WHOCs were maintained at 37°C and 5% CO₂/16% O₂ in a humidified atmosphere in a cell culture incubator (Figure 5.1).

5.3.2 Wounding procedure

Wound healing organ cultures (WHOC) were made with 2 different wounds. I) A partial thickness incisional wound, comprising the epidermis and upper part of the dermis, was made with 2 parallel cuts using a scalpel. The width of each cut was either 1 mm, 2 mm or 3 mm (Figure 5.2A). II) A full thickness excisional wound (donut-shaped model) comprising the epidermis and dermis was made using a punch biopsy kit with a 1 mm, 2 mm or 3 mm punch in the centre of the 8 mm diameter full thickness biopsy (Figure 5.2B).

The inner wound was filled in with either subcutaneous fat (excised from the harvested tissue) or BD Matrigel™ (BD Biosciences, Oxford, UK) inside the wound as a fill-in scaffold. The autologous hypodermal fat used to make a scaffold was washed several times with PBS and vortex for 5 mins at room temperature. The suspension was put in a centrifuge at 1800 x for 5 mins. The upper oil-layer was

discarded. The viscous suspension was rinsed 3 times with PBS and placed into the wound (Bagabir, et al., 2012).

5.3.3 Tissue support systems and growth media

Two different systems of tissue biopsy support were used: I) the WHOCs dermal part was embedded in rat tail collagen type one gel (2 mg/ml; BD Biosciences, Oxford, UK; Bagabir et al., 2012) and the epidermis was left exposed to the air-liquid interface. Collagen gels were made with the same growth media used in the liquid-air interface (Figure 5.2C&E); II) the WHOCs were placed in the middle of a well chamber insert (5 µm; Millipore, Darmstadt, Germany), with a 6 mm diameter perforation. The dermal part was submerged in the liquid medium and the epidermis was left exposed to air-liquid interface (Companjen, et al., 2001; Figure 5. 2D&F).

WHOC models were maintained with 3 different media, I) DMEM, II) William's E medium (WE) and III) a mixture of DMEM/Ham's F12/EpiLife (MED3;1:1:3). DMEM and WE were supplemented with 100 IU/ml penicillin, 10 µ/ml streptomycin, 10% Foetal Bovine Serum (FBS), 10 µg/ml of insulin, 10 ng/ml of hydrocortisone and 2 mM of L-glutamine. MED3 was supplemented with EpiLife Define Growth Supplement (EDGS). The media was changed every other day. All reagents were from Sigma-Aldrich (Dorset, UK), except EpiLife medium (Cascade Biologics, Portland, USA). WHOCs were harvested on the 14th day and histologically processed under standard protocols.

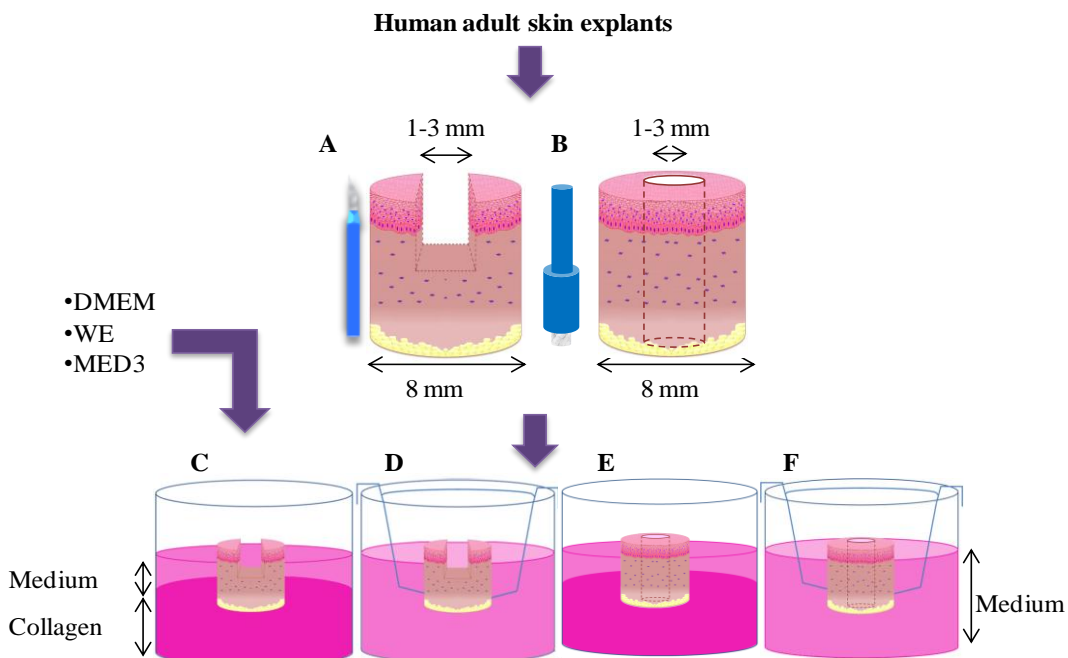


Figure 5.2 Wound healing organ culture (WHOC) models. Partial (A) or full thickness (B) wounds of 1, 2 or 3 mm in the centre of an 8 mm punch biopsy. WHOCs were supported in collagen embedded matrix (C&E) or introduced in well chamber inserts (D&F) and maintained with different supplemented growth media such as DMEM, WE or MED3. All WHOC models were exposed to air-liquid interface and collected on day 14.

5.3.4 Photodynamic therapy treatment

WHOCs with a 1.5 mm full thickness excisional biopsy wound filled with either fat or Matrigel™ scaffold inside the wound were exposed to PDT. 20% 5-aminolevulonic acid (5-ALA; Mandeville Medicines, UK) was consistently applied onto the WHOCs surface and incubated for 3 hrs.

This was subsequently illuminated with a PDT machine (Omnilux PDT™, Photo Therapeutics, Pennsylvania, USA), with an arrangement of red light-emitting diodes (LEDs) of 633 ± 3 nm wavelength. The power intensity of the PDT machine was adjusted to 20 J/cm^2 and calibrated with an IL1700 radiometer (International Light Technologies Inc, Massachusetts, USA; Mendoza et al., 2012). PDT treatment was

given once on the 3rd day after collection. The WHOCs were collected on the 7th and 14th day post-PDT application. WHOCs were washed twice with PBS before illumination. After illumination, WHOCs were re-embedded in collagen. All procedures were undertaken under darkness and sterile conditions. The WHOCs were fixed, paraffin embedded, sectioned and de-paraffinized using standard procedures (Bagabir, et al., 2012).

5.3.5 Histology

Representative sections of 5 µm, cut nearest to the centre of the biopsies were stained. Tissue morphology was examined using haematoxylin and eosin (H&E, Sigma-Aldrich), Herovici's (HV) and Weigert's elastic differential staining (WELA; Sigma-Aldrich). H&E and WELA staining were done according to the manufacturer's instructions. HV staining was carried out as described by Bagabir, et al. (2012). Stained sections were scanned in a Hamamatsu NanoZoomer 2.0-HT and analysed with NDP view2 image software (Hamamatsu, Hertfordshire, UK). Analyses were done by three blind independent evaluators.

5.3.6 Immunohistochemistry/immunofluorescence

Cell death and proliferation were assessed by the 3'-OH DNA end-labelling method (Tunel; FragEL™, Calbiochem-Merck, Darmstadt,GER) and with Proliferating Nuclear Antigen (PCNA) immunohistochemical staining (IHC) respectively. Additionally selected markers for epidermal differentiation- cytokeratin 14 (CK-14),

extracellular matrix remodelling- metalloproteinase 3 (MMP3) and metalloproteinase 19 (MMP19), senescence oxidative stress-induction- cyclin-dependent kinase inhibitor 2A (p16), a wound contraction marker α -smooth muscle actin (α -SMA) and vessels marker- platelet endothelial cell adhesion molecule marker CD31 were immunostained with panel of antibodies as shown in table 5.2 (Abcam®, Cambridge, UK). IHC were detected with Novocastra Peroxidase Detection Systems (Leica, Milton Keynes, UK).

IHC and peroxidase detection were performed according to the manufacturer's instructions. Stained sections were scanned in a Hamamatsu NanoZoomer 2.0-HT and analysed with NDP.view2 image software (Hamamatsu, Hertfordshire, UK). Objective quantification of cellular markers was performed using Definiens Tissue Studio 3.5 Software (Definiens, Munich, Germany; Samaroo, et al., 2012).

Six patients were analysed in the standarization of the WHOC and six patientes were used in the functional evaluation of PDT in WHOC, one patient was the same in both analyses. At least three tissue sections of 5 μ m, from the nearest point to the center of the organ culture were analysed. Briefly, the scanned tissues were load into the workspace of the analysis software. Using the "Analysis Builder window" it was configured the analysis settings. The general settings were two regions of interest (ROI), the basal layer of the epidermis and the dermis. It was load a defined solution for a prefixed marker area (nuclei, cytoplasm or vessels; Definiens®, 2012). It was set a nuclei average size of 6 μ m for the basal layer of the epidermis and 2 μ m for the dermis. Positive staining was considered if the intensity has a level within a value of 0.4-0.7 arbitrary units (since no staining means negative and staining means

positive). Once runned the analysis the results were review and exported to GraphPad Prims 5 (GraphPad Software, La Jolla, CA, US). The graphs generated include mean values \pm standard deviation between patients.

Table 5.2 List of antibodies

Primary antibody	Dilution	Incubation time
Anti-PCNA antibody (ab18197); Rabbit polyclonal; IgG.	1:200	1 hr
Anti-Cytokeratin 14 antibody [EPR1612] (ab108417); Rabbit monoclonal; IgG.	1:400	30 min
Anti-CDKN2A/p16INKa [2D9A12] antibody (ab54210); Mouse monoclonal; IgG2b.	1:1000	30 min
Anti-MMP3 antibody [EP1186Y] (ab52915); Rabbit monoclonal; IgG.	1:1000	1 hr
Anti-MMP19 antibody (ab53146); Rabbit polyclonal; IgG.	1:1000	1 hr
Anti-alpha smooth muscle actin antibody (ab5694); Rabbit polyclonal; IgG.	1:400	1 hr
Anti-CD31 antibody (ab32457); Rabbit polyclonal; IgG.	1:200	30 min

PCNA, proliferating cell nuclear antigen; MMP3, metalloproteinase 3; CDKN2A/p16INK, cyclin-dependent kinase inhibitor 2A; CD31, platelet endothelial cell adhesion molecule marker.

5.3.7 mRNA isolation, cDNA synthesis and qRT-PCR

Complete WHOCs were collected in TRIzol reagent (Invitrogen, Abingdon, UK) and processed for mRNA isolation, cDNA synthesis and qRT-PCR (Qiagen, Manchester, UK) according to the manufacturer's instructions. The gene expression levels were normalized with an internal reference gene, RPL32. The primers used in the study are detailed in table 5.3.

Table 5.3 Gene and primer sequences for qRT-PCR

Primers	Gene ID	Sequence 5'-3'	Primer position	size (bp)
RPL32-L	NM_000994.3	gaagttcctggccacaacg	319-338	77
RPL32-R	NM_000994.3	gagcgatctcgccacagta	377-395	77
PCNA -L	NM_002592.2	tggagaactggaaatggaaa	755-775	95
PCNA-R	NM_002592.2	gaactgggtcattcatctatgg	826-849	95
Keratin 14 -L	NM_000526.4	ccattgaggacacctgaggaac	564-583	69
Keratin 14-R	NM_000526.4	caatctgcagaaggacattgg	612-632	69
p16 -L	NM_000077.4	gtggacacctggctgaggag	649-666	132
p16 -R	NM_000077.4	cttcaatcgggatgtctg	761-780	132
Collagen I-L	NM_000088.3	gggattccctggacctaag	1866-1885	63
Collagen I-R	NM_000088.3	ggaacacacctcgctctcca	1911-1928	63
Collagen III-L	NM_000090.3	ctggaccccagggtcttc	3101-3118	75
Collagen III-R	NM_000090.3	catctgatccagggtttcca	3156-3175	75
MMP3 -L	NM_002422.3	caaaacatattctttgtagaggacaa	1259-1285	91
MMP3 -R	NM_002422.3	ttcagctatttgcttggaaa	1329-1349	91
MMP19-L	NM_002429.5	atgccagacccttgcatgt	1006-1025	76
MMP19-R	NM_002429.5	cccccttgaagcataggtc	1062-1081	76
α -SMA-L	NM_001141945.1	ctgtccagccatccttcat	1262 - 1281	70
α -SMA-R	NM_001141945.1	tcatgtgcttgttaggttgt	1310 - 1331	70

RPL32, 60S ribosomal protein L32; PCNA, proliferating cell nuclear antigen; p16, cyclin-dependent kinase inhibitor 2A; MMP3, metalloproteinase 3; α -SMA, α -smooth muscle actin

5.3.8 Statistical analysis

Results are presented as the mean values \pm standard deviation. Statistical significance was calculated with One-way ANOVA and Bonferroni comparison test. Graphics and statistics were generated with GraphPad Prims 5 (GraphPad Software, La Jolla, CA, USA). The differences were considered statistically significant if $p < 0.05$.

5.4 Results

5.4.1 Optimization of a wound healing model ex vivo

Ex vivo WHOCs embedded in collagen and supplemented DMEM preserved epidermal and dermal architecture and characteristics

In order to understand the optimal ex vivo conditions for long-term maintenance of WHOC models, we evaluated the growth medium, the physical WHOC support system in relation to wound size and shape. From H&E analysis, neither epidermolysis nor necrosis was observed after 14 days (D14) ex vivo, indicating the maintenance of intact functional skin. In order to perform the above described analyses, WHOCs were divided in two sections, the peripheral skin (PS) to the wound and the neo-epidermis formed was replacing the open wound (Neo). A diagrammatic depiction is shown in figure 5.3A.

1. Epidermal analysis (D14)

WHOCs embedded in collagen and well chamber inserts, maintained in DMEM and WE preserved epidermal stratification with presence of melanocytes in the basal layer, intact dermal-epidermal junctions and rete ridges with peaks and valleys (Figure 5.3C-H).

Additionally, WHOCs fed with only DMEM maintained cuboidal basal keratinocytes as observed on day 0. WHOCs maintained in MED3 showed loss of stratification in both support systems (Figure 5.3G-H). Epidermal thickness of WHOCs maintained in both support systems was not significantly different from

each other. However, epidermal thickness was more dependent on growth media rather than on support systems. Better maintenance of rete ridges was observed in tissues maintained in collagen matrix and cultured in DMEM when compared to all other growth conditions. As assessed with the height of peaks and valleys of rete ridges, WHOCs cultured in collagen matrix and maintained in DMEM and WE were significantly thicker and closer to normal skin than those cultured in MED3 (Figure 5.3I). Collectively, the epidermal morphology of WHOCs on day 14 was better when collagen embedding and DMEM medium were used.

2. Dermal analysis (D14)

ECM components, capillaries and cellular components in the dermis of WHOC models embedded in collagen and well chamber inserts maintained in DMEM and WE were morphologically similar to day 0 biopsies. However, those cultured in MED3 appeared to be degraded. WHOCs maintained in well chamber inserts showed an increase in cellularity and fibroblasts exhibited an altered phenotypic morphology with slight elongation. However, the appearance of swollen tissue and degradation of interstitial and extrafibrillar components in the dermis were distinct from WHOCs maintained in collagen matrix. WHOCs fed with MED3 showed nuclear dissolution, epidermal-dermal junction degradation and dislocation as well as inconsistencies in epidermal thickness when compared to those cultured in DMEM and WE (Figure 5.3B-H).

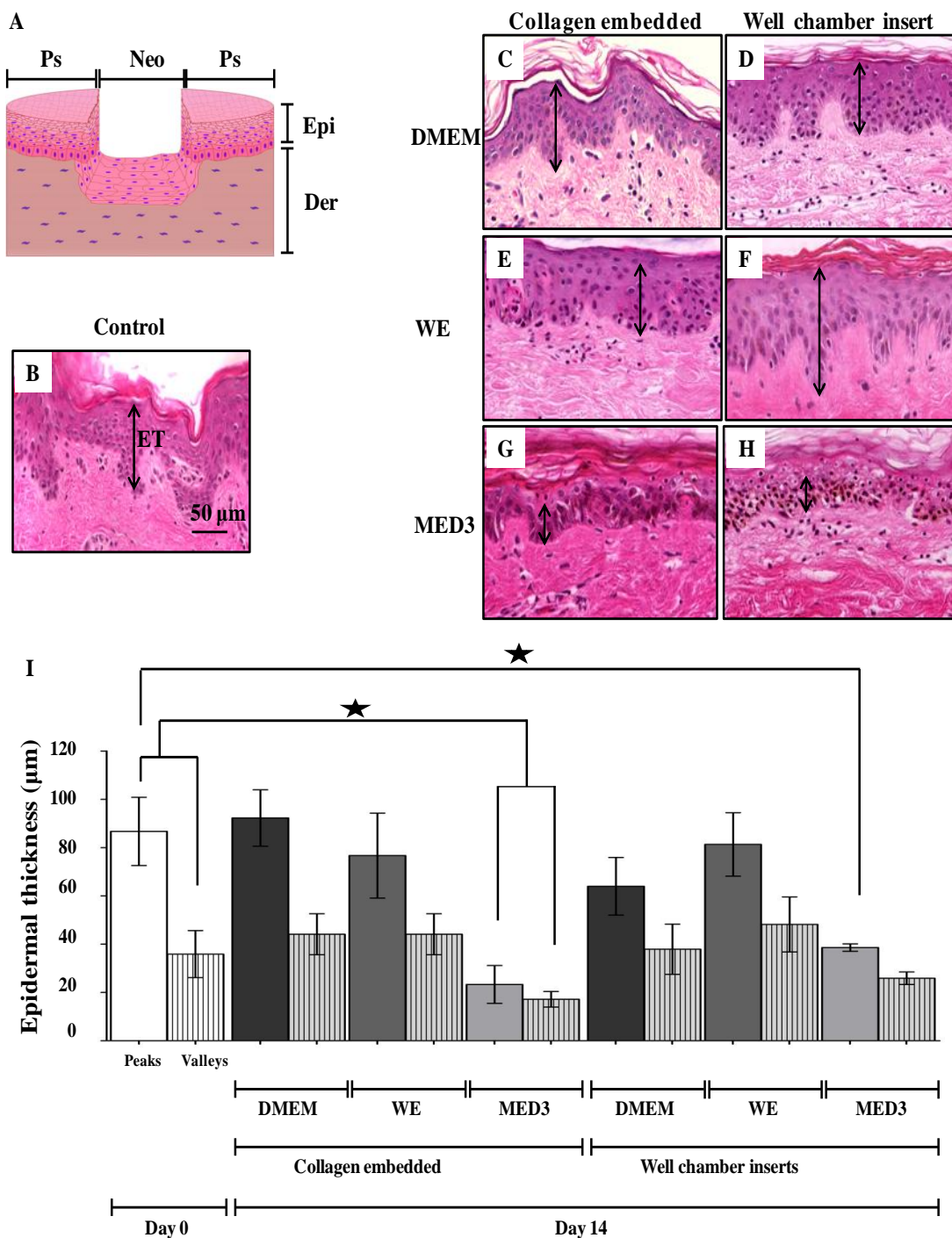


Figure 5.3 Epidermal thickness of WHOCS maintained in different media and supported with collagen embedded matrix or well chamber inserts. Diagram of studied sections (A). Sections of WHOCS were stained with H&E (B-H) and peripheral skin (PS) to the wound was compared to human normal skin processed on 0 day (B). Graph I shows epidermal thickness of rete ridges were □ denotes peaks and ▨ denotes valleys in the epidermis of skin biopsies on day 0, ■ denotes peaks and ▨■ denotes valleys in the epidermis of skin biopsies on day 14. Mean and standard deviation between patients are represented. ★ Denotes significant difference ($p < 0.05$; $n = 6$).

Furthermore, the morphology of elastic fibres was evaluated with Weigert's staining. On day 0, elastic fibres in the papillary dermis were thin and elongated, while those in the reticular dermis were aggregated into thick compartments (Figure 5.4A). WHOCs maintained for 14 days in collagen matrix were similar to day 0 tissues. However, those cultured in well chambers appeared loose and degraded. Therefore, better preservation of elastic fibres was achieved with collagen matrix compared to using a well chamber support system (Figure 5.4 B-G).

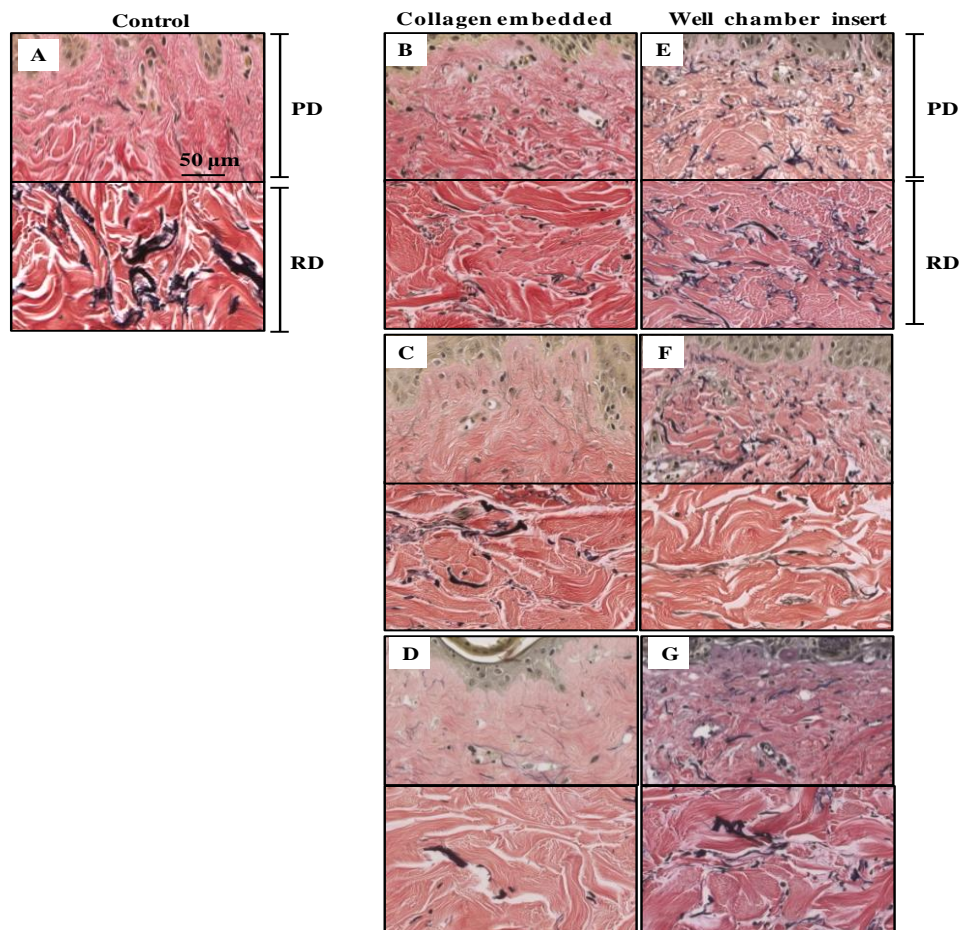


Figure 5.4 Morphological analysis by Weigert's differential staining in the healthy peripheral skin adjacent to the wound. WHOC models were maintained in three different media such as DMEM, WE and MED3, and supported in collagen embedded or in well chamber inserts. Human normal skin processed on day 0 stained with H&E (A) or WHOC models processed on day 14 (B-G; Original magnification 40X; $n = 6$). Elastin fibres were stained black and collagen fibres pink at the papillary dermis (PD) or reticular dermis (RD).

5.4.2 Analysis of normal skin compared to wound healing organ cultures

1. Ex vivo wounds re-epithelialization varied according to wound type and tissue support system

In order to identify the optimal wound dimensions that heal ex vivo, we performed partial and full thickness wounds with the following dimensions- 1, 2 and 3 mm wide. Partial thickness wounds were re-epithelialized by day 14 (Figure 5.5) compared to full thickness wounds (Figure 5.6), however, depending on the support system. Keratinocytes in the neo-epidermis of all healed WHOCs appeared to be flat with spindle-shape nuclei, with the absence of any rete ridges in the epidermis (Figure 5.5A-F).

Re-epithelialization was observed only in all partial wound and full thickness wounds of 1 mm thickness. Well chamber inserts had a higher rate of re-epithelialization compared to collagen matrix embedding. However, on day 14, degradation of ECM fibres and liquid retention was more noticeable in well chamber inserts compared to collagen embedded WHOCs.

DMEM supported re-epithelialization in WHOCs cultured in both collagen matrix and well chamber inserts. MED3 growth media did not support healing in partial and full thickness (Figure 5.5G& 5.6G). Morphology of the healed wounds in DMEM or WE were found to be better compared to those cultured in MED3 media.

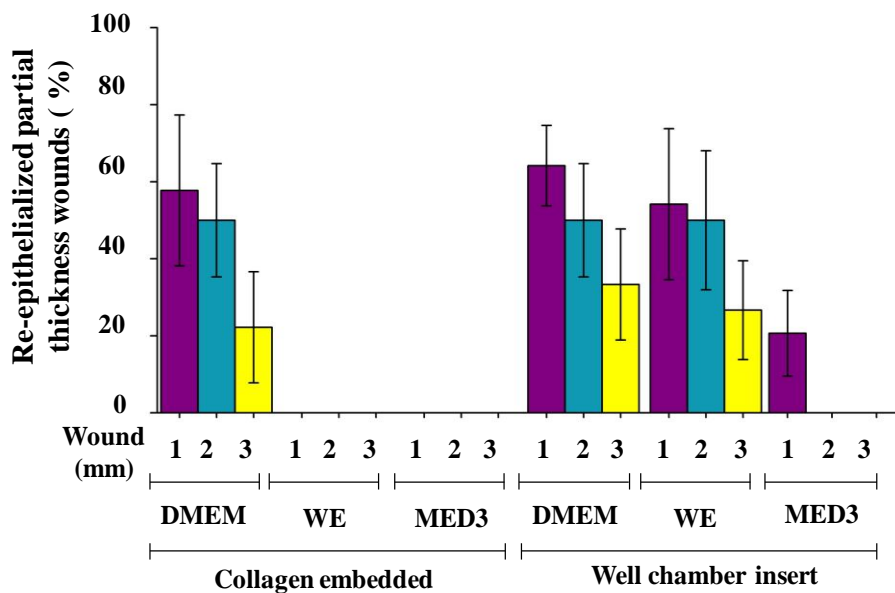
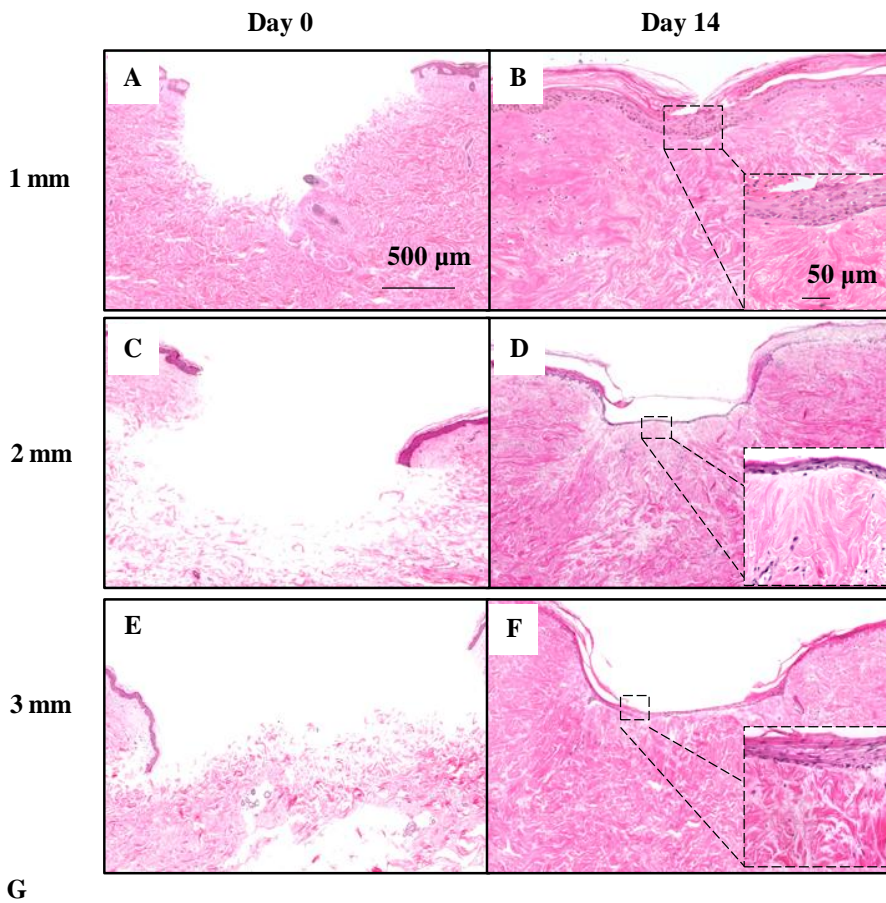


Figure 5.5 Partial-thickness WHOCS. WHOCS with partial thickness wound (A-F) cultured ex vivo in collagen embedded matrix. These WHOCS were maintained in DMEM and stained with H&E (original magnification 2.5X & 40X respectively). The wounds measure 1 mm (A-B), 2 mm (C-D) and 3 mm (E-F). Dotted square shows detail of the re-epithelialized area. Graph represents statistical analysis of re-epithelialized WHOCS (G) according to the system of support, growth medium and wound size. Mean and standard deviation between patients are represented ($n = 6$).

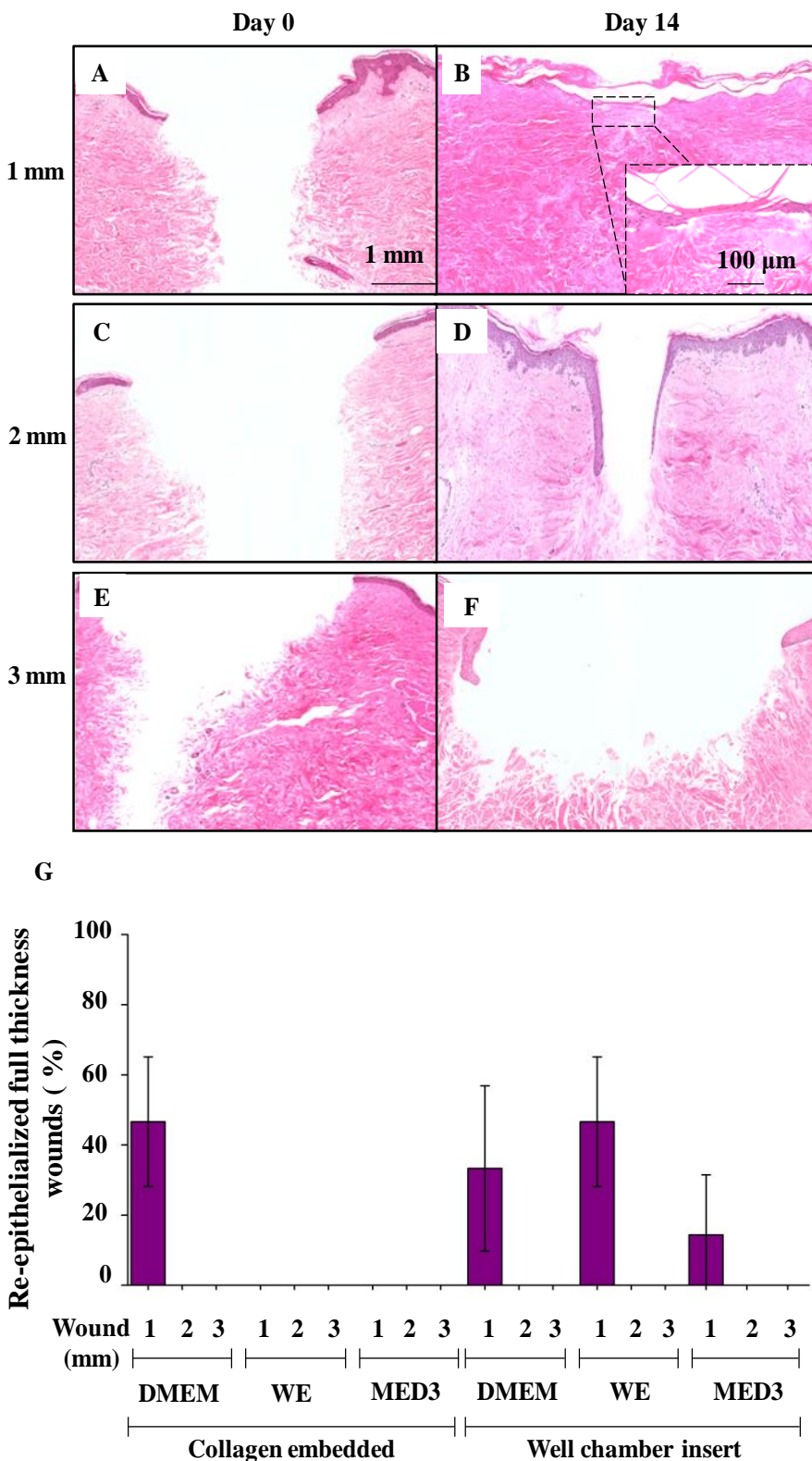


Figure 5.6 Full-thickness dermal WHOCS. WHOCS with full thickness wounds (A-F) cultured ex vivo in collagen embedded matrix. These WHOCS were maintained in DMEM and stained with H&E (original magnification 2.5X & 40X respectively). The wounds measure 1 mm (A-B), 2 mm (C-D) and 3 mm (E-F). Dotted square shows detail of the re-epithelialized area. Graph represents statistical analysis of re-epithelialized WHOCS according to the system of support, growth medium and wound size of full thickness wounds (G). Mean and standard deviation between patients are represented ($n = 6$).

2. Wound closure characteristics of re-epithelialization and dermal reconstruction

Analysis of ex vivo healing was performed on 2 mm partial thickness wounds cultured in DMEM and support in collagen embedding. Here, cell death was observed with 3'-OH DNA end-labelling method (Tunel), which increased to 20% in peripheral skin and 32% in the neo-epidermis on day 14, compared to normal skin on day 0. The upper epidermal layers in the peripheral skin appeared to have more apoptotic cells compared to the rest of the epidermal layers. Also, apoptotic cells were mostly observed in the upper layers of the reforming neo-epidermis (Figure 5.7B- E). Proliferation was decreased in peripheral skin (12%) and in the neo-epidermis (10%), compared to normal skin on day 0 (15%; Figure 5.7F-I).

Cytokeratin 14 (CK-14) is a marker for undifferentiated keratinocytes and disappears at the onset of differentiation (Seltmann et al., 2013). CK-14 staining was altered in normal skin on day 14 compared to day 0. CK-14 was expressed in several layers of the (basal and suprabasal layers) epidermis compared to the basal layer expression on day 0 (Figure 5.7J-M). Laminin 5 (LAMA5), which is a marker of epidermal-dermal junction integrity, was significantly increased in the basement membrane of the re-epithelialized wounds when compared to normal skin on days 0 and 14 (Figure 5.7N-Q). Additionally, Herovici's polychrome staining, showed a significant increase in COLIII synthesis near to the re-epithelialized wound compared to normal skin on days 0 and 14 (Figure 5.7R-T).

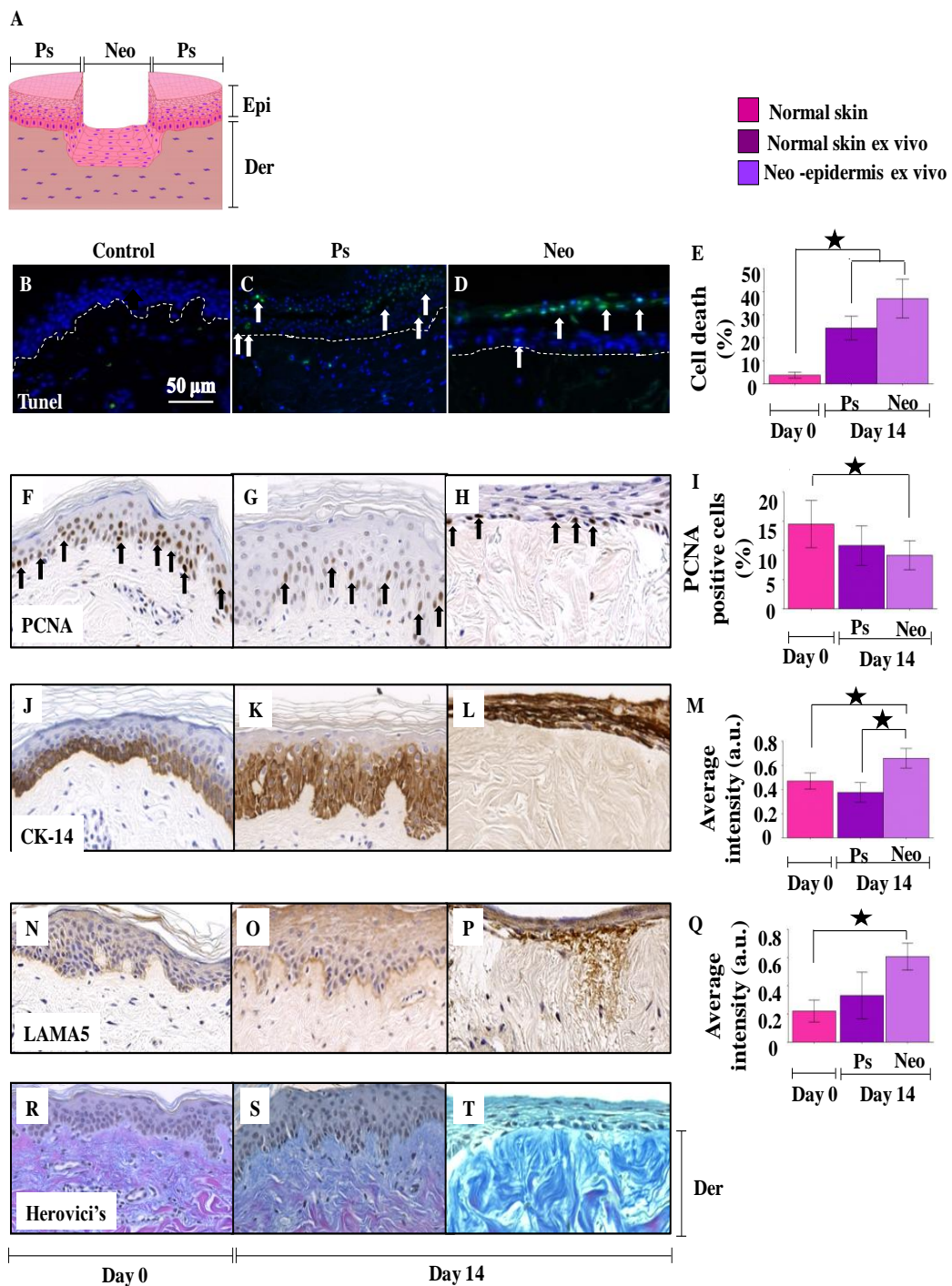


Figure 5.7 Analysis of normal skin compared to WHOCs after 14 days ex vivo. Schematic representation of analysed biopsy areas (A). Epi denotes epidermis and Der denotes dermis. WHOC model with 2 mm partial thickness wound re-epithelialization, which was cultured in DMEM in collagen embedding (original magnification 40X). Representative pictures are cell death by TUNEL analysis (B-D), PCNA (F-H), CK-14 (J-L), LAMA5 (N-P) and Herovici´s differential staining for COL I/COLIII (R-T). Arrows indicate dead cells (B-D) or proliferative cells (F-H). Graphs represent quantitative analysis of cell death (E), PCNA positive cells quantification (I), average intensity of CK-14 (M) and LAMA5 (Q). Mean and standar deviation between patients are represented. ★ Denotes significant difference ($p < 0.05$; $n = 6$).

5.4.3 Photodynamic therapy effects in a wound healing organ culture

WHOC models exposed to PDT showed higher rate of wound closure

Next, we investigated whether the rate of wound healing closure in 1.5 mm full thickness WHOCs would be affected by PDT treatment. Here, the re-epithelialization tongue was 3-fold longer compared with the untreated WHOCs. In order to provide a dermal template for the keratinocytes tongue during wound healing, we introduced either fat or MatrigelTM into the wound centre. The re-epithelialization tongue in WHOCs with MatrigelTM was separated from the scaffold while those with fat exhibited firm attachment to the scaffold (Figure 5.8C-G). Therefore, better re-epithelialization was observed with the fat scaffold.

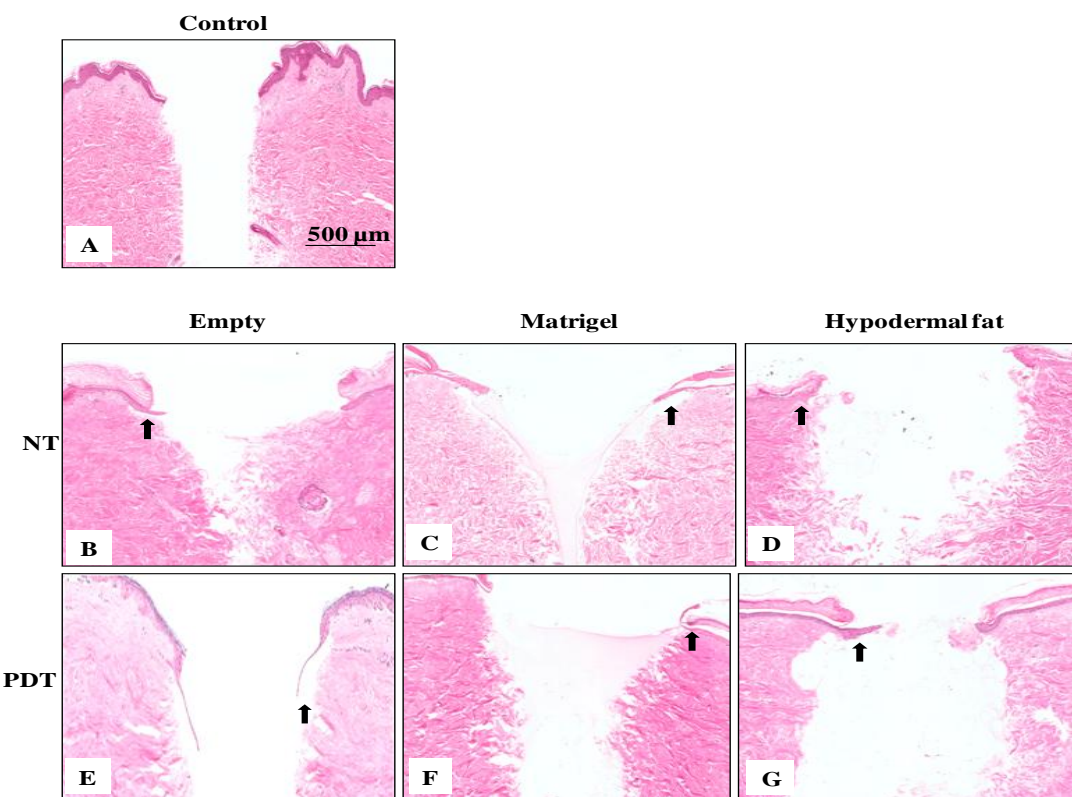


Figure 5.8. H&E images of WHOC models with 2 mm wound centre, untreated and post-PDT. The initial day is represented in A. WHOC models with empty wound centre (B&E), filled with MatrigelTM (C&F) and autologous hypodermal fat (D&G) on the 7 day. Arrows show the advancing re-epithelialization tongue. ($n = 3$).

Post-PDT, re-epithelialization tongue on day 7 was 35% longer compared to the untreated controls (Figure 5.9A-B). Additionally, in WHOCs post-PDT, re-epithelialization tongue was 33% longer, compared to untreated controls on day 14 (Figure 5.9C-F). Cellular quantification of neo-epidermis showed a 2.6 fold increase in cell numbers compared to untreated WHOCs (Figure 5.9G). However, small areas of epidermal detachment were observed in the peripheral skin to the neo-epidermis on day 14 in WHOCs treated with PDT compared to untreated controls.

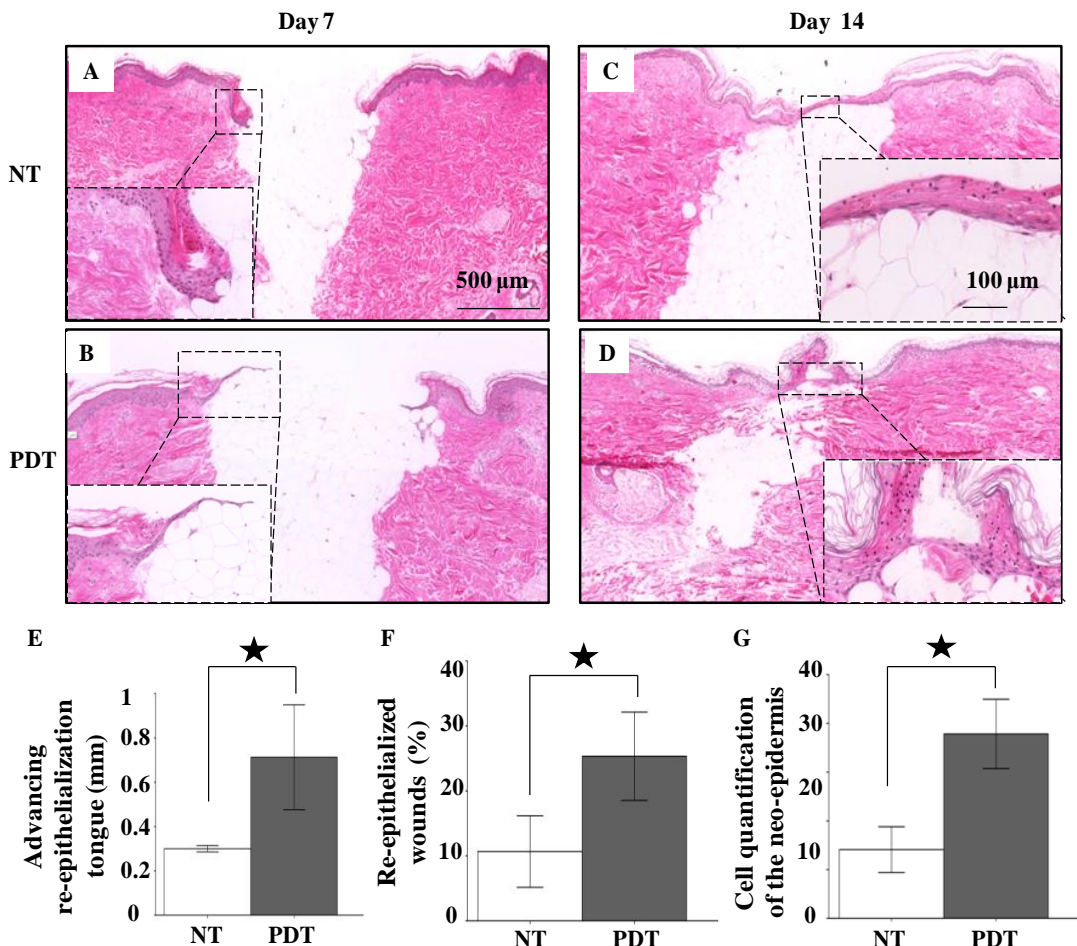


Figure 5.9 Analysis of full-thickness WHOCs post-PDT. Representative images of ex vivo maintained WHOCs which were untreated (NT) or post-PDT (PDT) after 7 (A&B) and 14 days (D&E) maintained ex vivo (original magnification 5X & 20X respectively). Dotted square shows detail of the advancing epithelial tongue or re-epithelialized area. Graphs represent advancing re-epithelialization tongue on 7 day (C), re-epithelialized WHOCs on 14 day (F) and cell quantification in the neo-epidermis (G). □ Denotes untreated WHOCs and ■ denotes WHOCs post-PDT. ★ Denotes significant difference ($p < 0.05$; $n=6$). Mean and standar deviation between patients are represented.

5.4.4 Apoptosis and proliferation analysis in WHOCs post-PDT

PDT increased apoptosis plus proliferation and maintained the rate of differentiation in WHOCs

Apoptotic and proliferative effect of PDT in WHOCs, were evaluated using TUNEL and PCNA-IHC respectively. TUNEL assay on day 7 showed no significant difference in apoptosis between PDT-treated and non-treated WHOCs, both in the peripheral skin and in the advancing tongue (5%). However, on day 14, there was a significant increase in cell death in both peripheral skin (40%) and neo-epidermis (59%) post-PDT. This increase in apoptosis was 1.9-fold post-PDT treatment in the neo-epidermis and 1.6-fold in the peripheral skin, compared to the untreated controls (Figure 5.10).

PCNA-stained cells were distributed haphazardly in the re-epithelialization tongue of PDT-treated WHOCs. Additionally, there was increase in proliferation in the dermis of PDT-treated WHOCs compared to untreated WHOCs. Although, proliferation decreased significantly on Day 14 in PDT-treated WHOCs compared to the untreated controls in the epidermis, a higher cellular proliferation in dermis was sustained until day 14 in PDT-treated WHOCs (Figure 5.11A-J). Proliferation assay showed that post-PDT, the re-epithelialization tongues on day 7 had significant up-regulation of PCNA compared to the untreated WHOCs (1.8 fold; Figure 5.11D-E&J). There was a significant increase of PCNA gene expression post-PDT compared to untreated controls (Figure 5.11K).

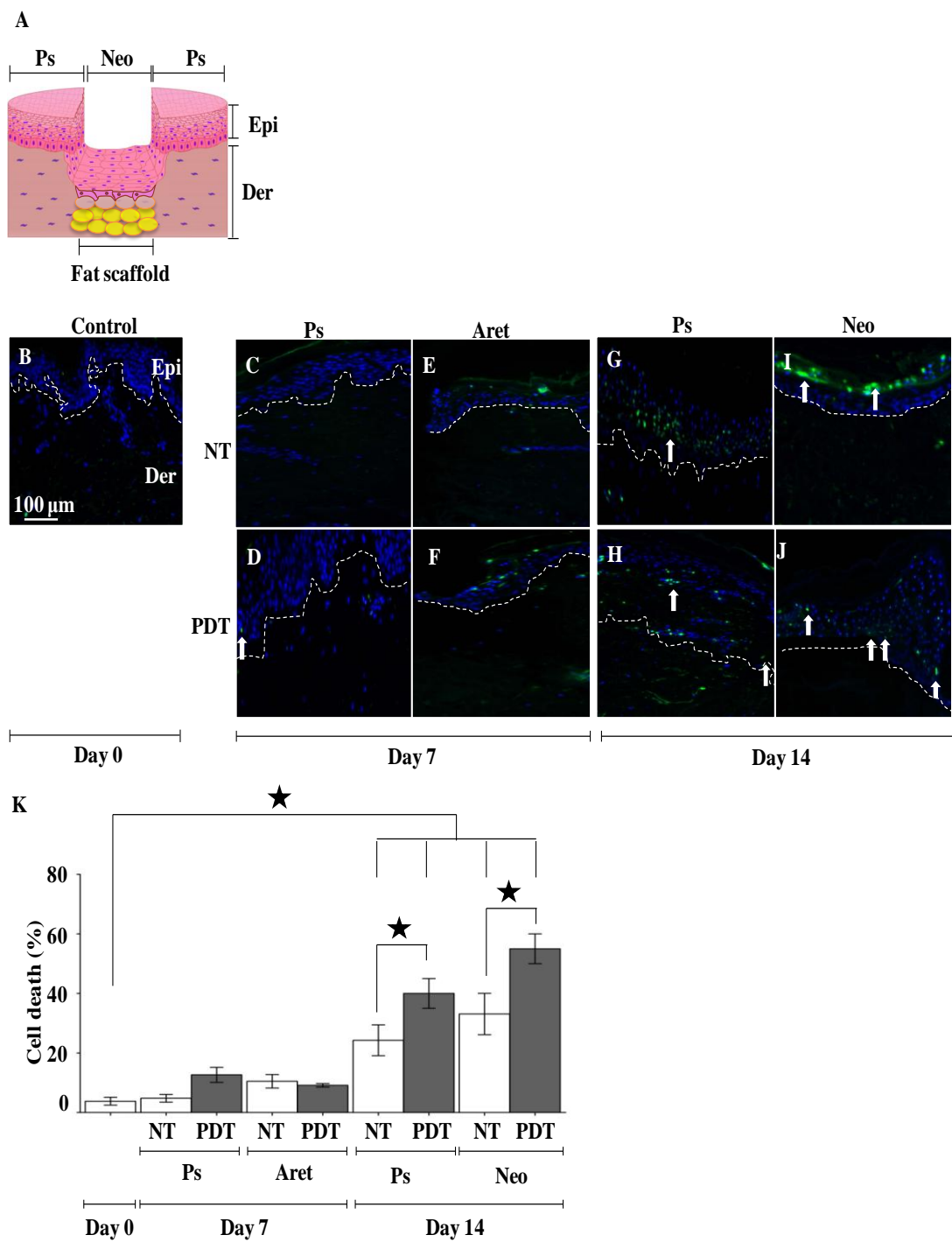


Figure 5.10 Apoptotic analysis of full-thickness WHOCS post-PDT. Schematic representation of analysed biopsy areas (A). Epi denotes the epidermis, Der denotes the dermis. Normal human skin processed on day 0 (B) was compared to peripheral skin (Ps) and advancing re-epithelialization tongue (Aret) on day 7 and Ps and neo-epidermis (Neo) on 14 day (original magnification 40X). WHOCS were untreated (NT; C,E,G&I) or exposed to PDT (D,F,H&J). Arrows indicate apoptotic cells. Graph represents quantitative analysis of apoptotic cell death (K). □ Denotes control WHOCS and ■ denotes WHOCS post-PDT treatment. ★ Denotes significant difference ($p < 0.05$). Mean and standard deviation between patients are represented ($n = 6$).

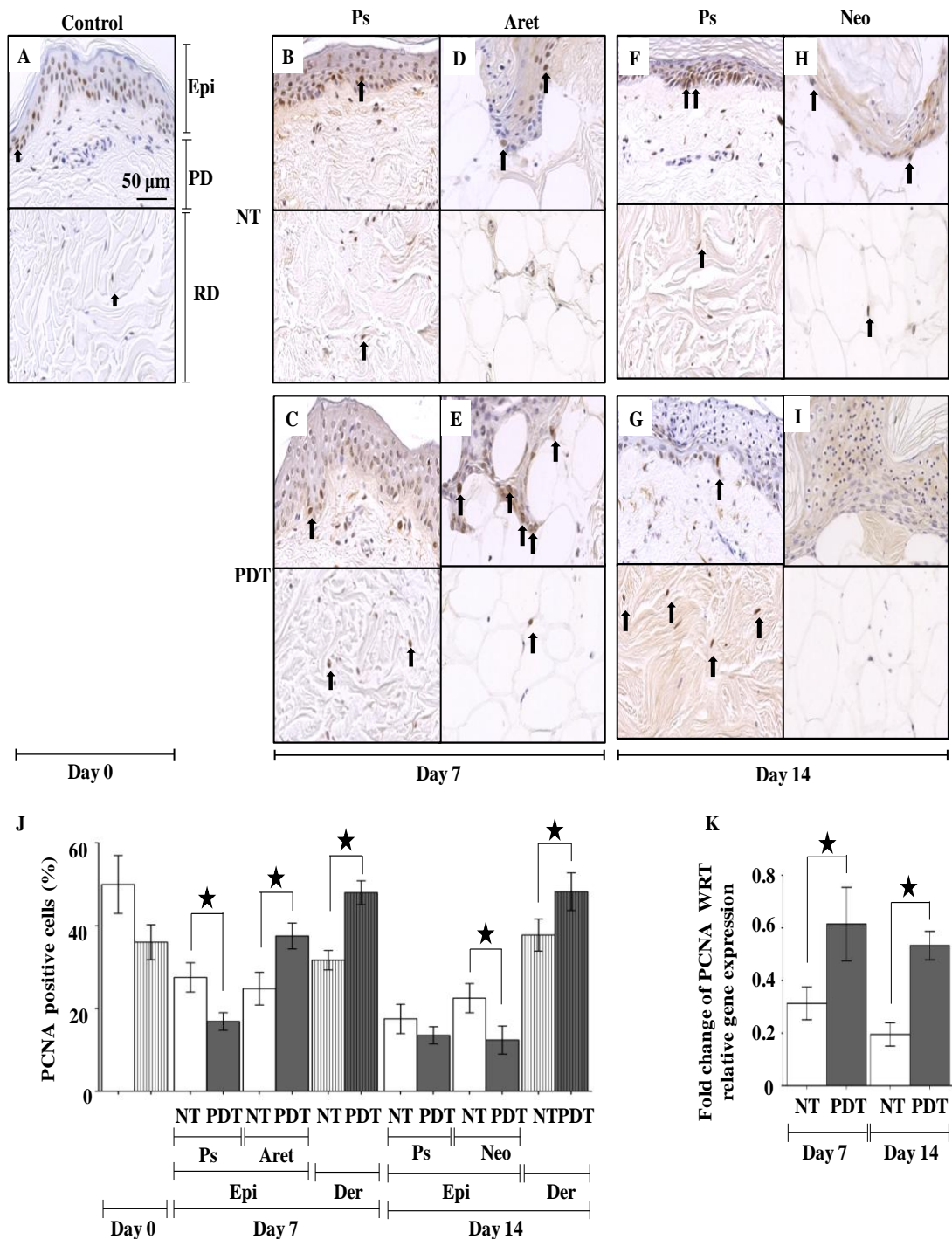


Figure 5.11 Proliferation analysis post-PDT. Normal human skin processed on day 0 (A) was compared to peripheral skin (Ps) and advancing re-epithelialization tongue (Aret) on day 7 and Ps and neo-epidermis (Neo) on day 14 (original magnification 40X). WHOCS were untreated (NT; B,D,F&H) or expose to PDT (PDT; C,E,G&I). Arrows indicate PCNA positive cells in the epidermis (Epi), papillary dermis (PD) and reticular dermis (RT). Graphs represent quantitative analysis of PCNA positive cells (N) and genetic expression analysis (O). □ Denotes epidermis and ▨ denoted dermis of WHOCS on day 0 or untreated WHOCS in day 14. ■ Denotes epidermis or ■ denoted dermis of WHOCS post-PDT. ★ Denotes significant difference ($p < 0.05$). Mean and standar deviation between patients are represented ($n = 6$).

Post-PDT, CK14 increased in both PDT-treated and non-treated controls on day 7 (Figure 5.12A-E&J). However, in addition to its presence in the basal layer, CK14 was also distributed in stratum spinosum and stratum granulosum of the epidermis. However, on day 14, CK14 was decreased and was mainly confined to the basal layer of peripheral skin in PDT-treated samples while the spatial pattern of CK14 staining in non-treated samples was similar to that on 7 day (Figure 5.12F-I). PCNA genetic expression was found similar on day 7 in controls and treated WHOCs, although decreases on day 14 in treated WHOCs (Figure 5.12K).

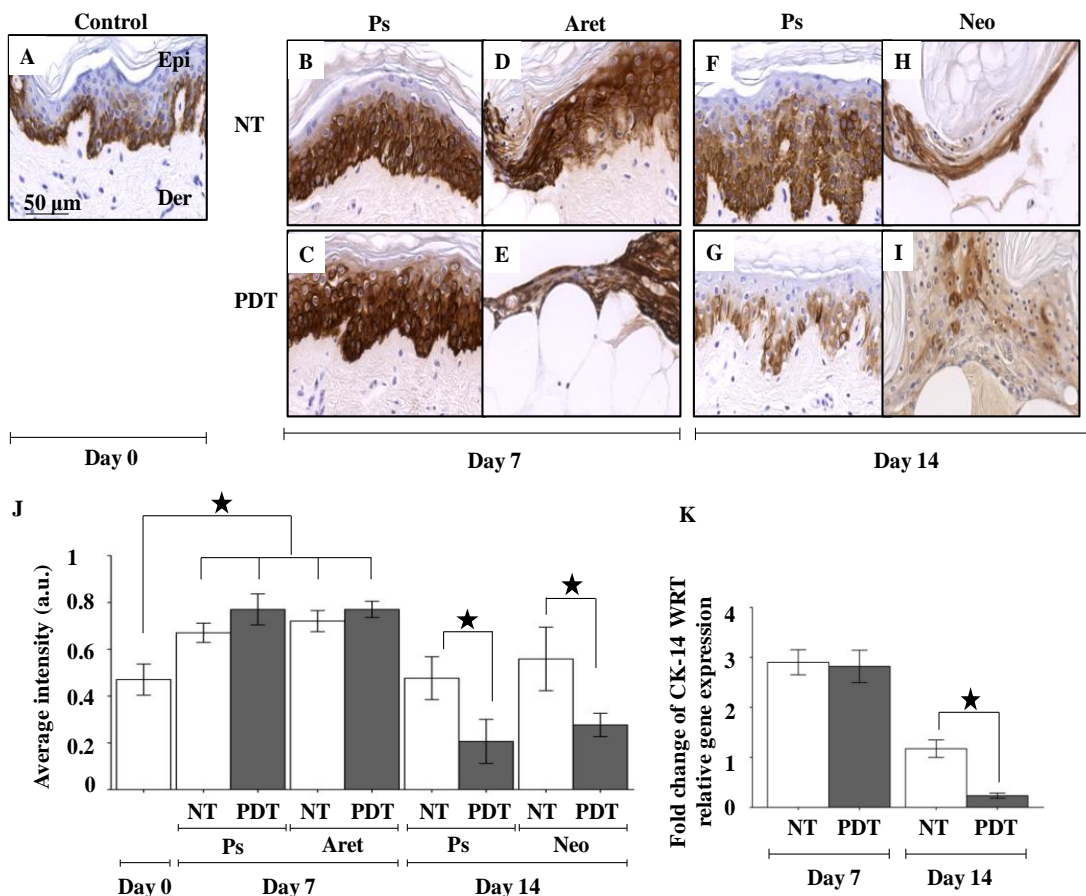


Figure 5.12 Analysis of CK14 expression post-PDT. Normal human skin (day 0 control; A) was compared to untreated (NT; B,D,F&H) controls and post-PDT (C,E,G&I). CK14 expression is shown in the peripheral skin (Ps), advancing re-epithelialization tongue (Aret) on 7 day and Ps and Neo-epidermis (Neo) on 14 day (original magnification 40X). Graph represents average intensity of CK-14 IHC (J), and genetic expression analysis (K). □ Denotes untreated WHOCs, ■ denotes WHOCs post-PDT. ★ Denotes significant difference ($p<0.05$). Mean and standar deviation between patients are represented ($n = 6$).

5.4.5 Extracellular matrix analysis, oxidative stress and MMPs expression post-PDT

PDT increased ECM remodelling plus p16, MMP3, and MMP19 expression, but decreased capillaries staining

1. Collagen I and III synthesis increased after PDT treatment

Herovici's polychrome staining showed COLI and COLIII synthesis to be higher in PDT-treated WHOCs compared to untreated samples. PDT treatment enhanced COLI and III levels in the dermis on days 7 and 14 (x5 and 7-fold change respectively on days 7 and 14 for COLI, x10 and 13.5-fold change respectively on days 7 and 14 for COLIII; Figure 5.13A-J). Small areas of neo-collagen were observed substituting the fat scaffold, only in WHOCs post-PDT.

Figure 5.13 shows normal human skin processed on day 0 (A) was compared to peripheral skin (Ps) and advancing re-epithelialization tongue (Aret) on day 7 and Ps and neo-epidermis (Neo) on day 14 (original magnification 40X). Pictures show papillary dermis (PD) and reticular dermis (RD) of WHOCs untreated (NT; B,D,F&H) and post-PDT (C,E,G&I). Mature collagen (COLI) was red stain and immature collagen (COLIII) was blue stain, overlapping COLI and COLIII results in a purple stain, as showed other authors (Syed, et al., 2011; Levame, et al., 1986).

On day 14, degradation of elastic fibres was observed to be increased in PDT-treated WHOCs compared to day 0 and untreated WHOCs on day 14. A number of

shortened bundles of elastic fibres were also observed in the ECM post-PDT samples (Figure 5.14).

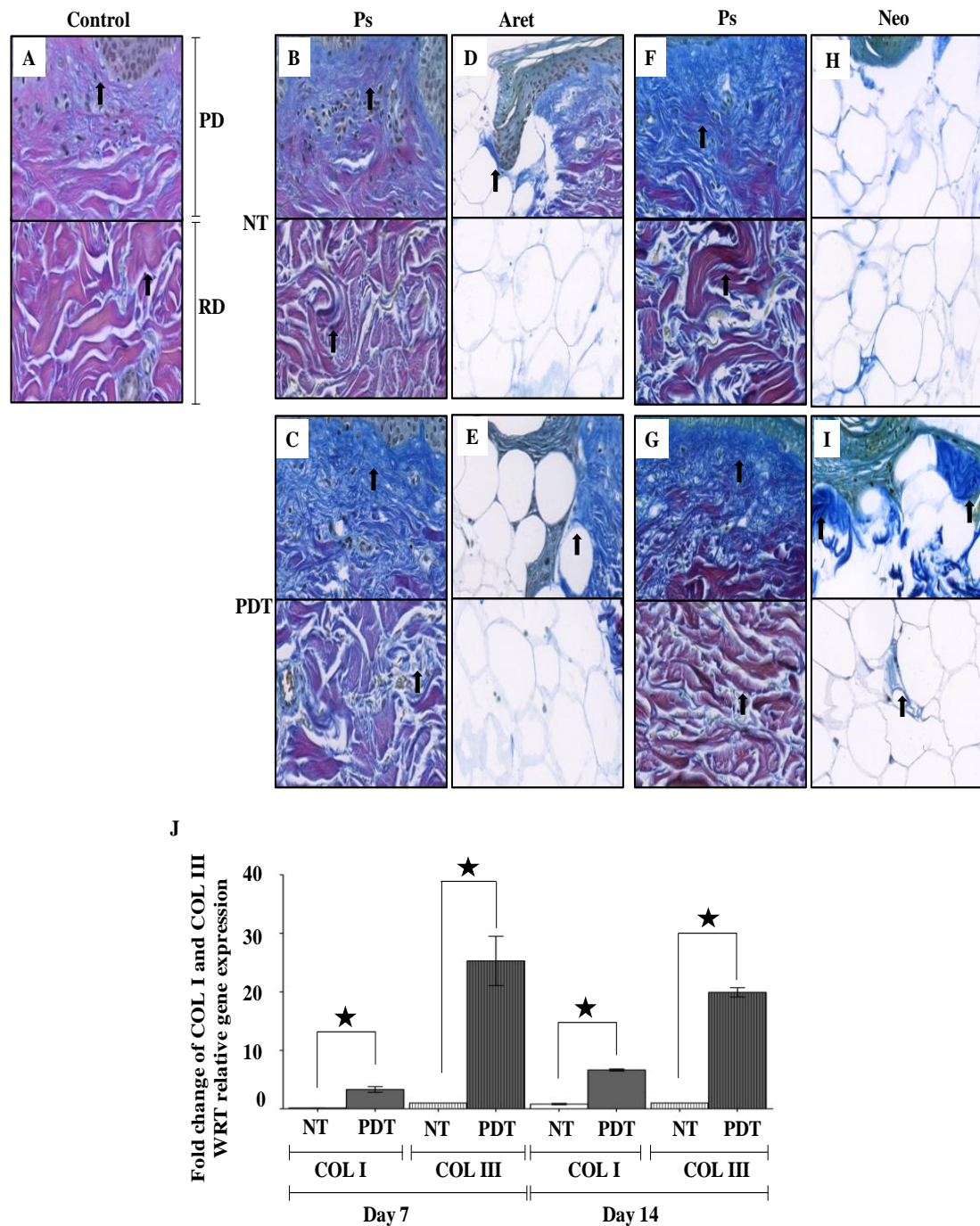


Figure 5.13 Herovici's differential staining analysis post-PDT. Graph represents COLI and COLIII genetic expression analysis (J). □ Denotes COLI and ■ denotes COLIII expression in untreated WHOCs, ■ denotes COLI and ■■ COLIII in WHOCs post-PDT. ★ Denotes significant difference ($p<0.05$). Mean and standard deviation between patients are represented ($n=6$).

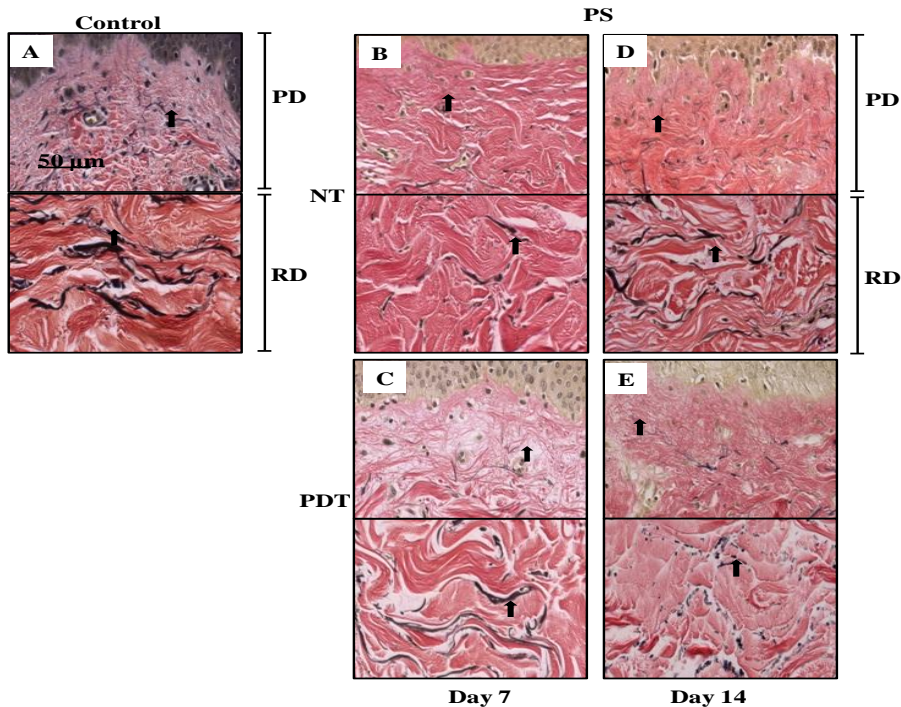


Figure 5.14 Representative images of Weigert's elastic stain post-PDT. Pictures show schematic representation of analysed areas (A) in papillary dermis (PD) and reticular dermis (RD). WHOC untreated (NT C&E) and post-PDT (D&F; original magnification 40X). Arrows show elastic fibres which were stained black. ($n=6$).

2. Enhanced MMP3 and MMP19 in PDT-treated WHOCs

Histochemical expression of MMP3 was found to be higher in WHOCs post-PDT compared to untreated and unwounded controls (Figure 5.15A-F). MMP3 gene expression was also found to be 7.5 fold higher until day 14 day (Figure 5.15G). In addition, histochemical expression of MMP19 was found to be higher post-PDT, however by day 14, it was similar to untreated controls, but higher than unwounded controls (Figure 5.15H-M). Similarly, MMP19 gene expression was found to be higher on day 7 (statistically significant) but similar to untreated controls on day 14, however higher than unwounded controls (Figure 5.15N).

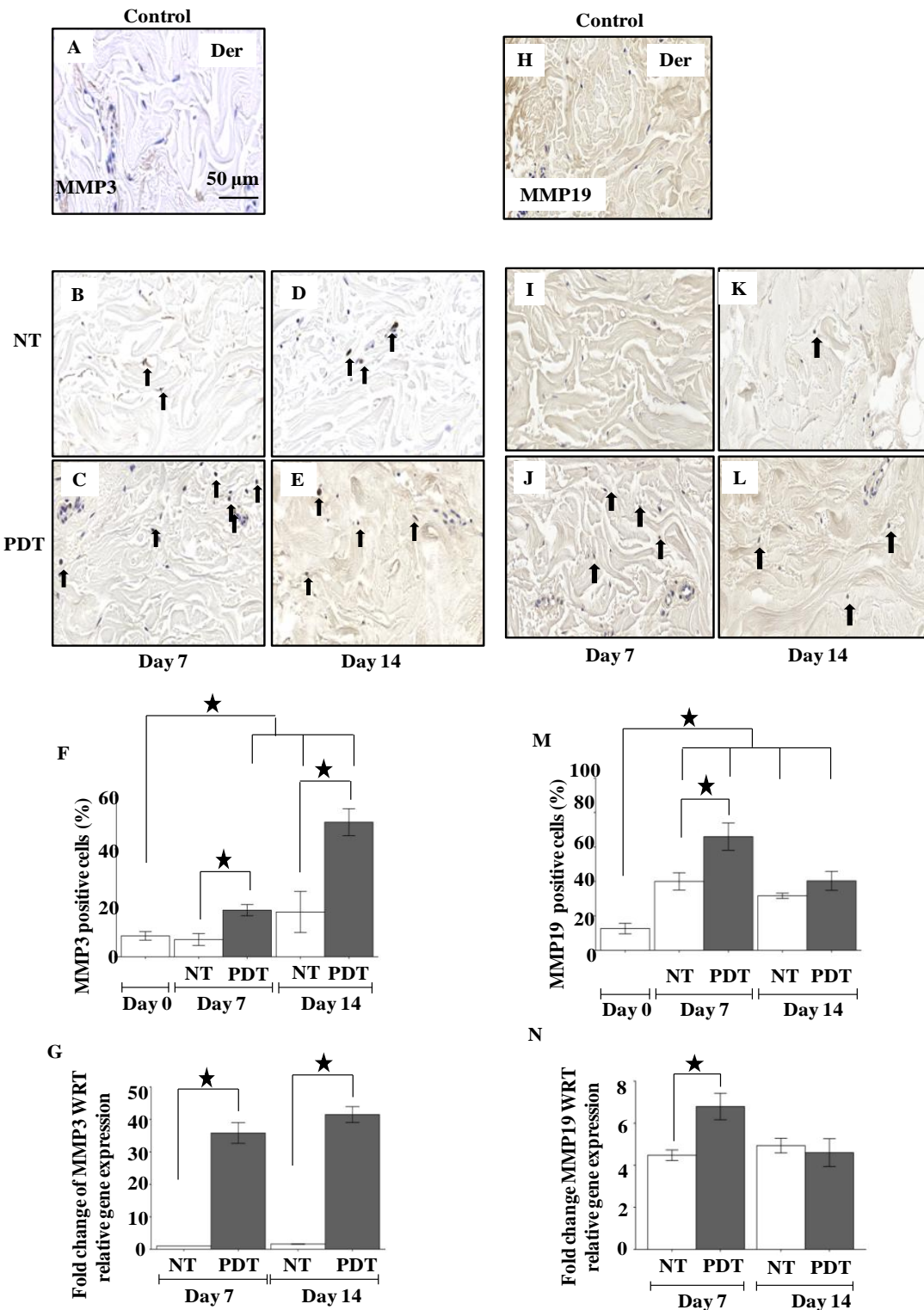


Figure 5.15 MMP3 and MMP19 analysis post-PDT. Dermis of normal human skin processed on day 0 (A) was compared to dermis post-PDT on day 14 after MMP3-IHC (A-E) and MMP19-IHC (H-L; Original magnification 40X). MMP3 or MMP19 positive cells quantification (F&M) and genetic expression respectively (G&N), □ denotes untreated WHOCs and ■ WHOCs post-PDT. ★ Denotes significant difference ($p<0.05$). Mean and standard deviation between patients are represented ($n=6$).

3. Enhanced expression of p16 post-PDT treatment

p16 has been correlated to cellular oxidative stress level (Tavakkol et al., 1999). p16 histological expression was found to be significantly higher at the advancing tongue (30%) compared to day 0, peripheral skin and untreated control (Figure 5.16A-I). p16 was also found to be increasing overtime in the untreated compared to PDT-treated WHOCs. Although, p16 was found to be significantly higher in the epidermal layer of WHOCs post-PDT, the expression in the dermis was similar in both the untreated and PDT-treated WHOCs on day 14 (Figure 5.16J). p16 gene expression was up-regulated by 8 fold on day 14 compared to untreated control on day 0 and was significantly higher compared to the untreated control on day 14 (Figure 5.16K). Therefore, post-PDT, there was an increase in p16 levels when compared to day 14 controls, which indicated the ability of PDT to activate stress-related oxidative mechanisms in wound healing.

4. Increased α -SMA gene expression post-PDT treatment

Histochemical expression of α -SMA was increased minimally but not significantly (Figure 5.17A-F). However, α -SMA gene expression was found to be up-regulated by 1.5 times higher than the untreated WHOCs (Figure 5.17G).

5. CD31 intensity decreased post-PDT treatment

On day 14, CD31 staining was significantly decreased in PDT-treated WHOCs compared to the non-treated WHOCs (Figure 5.18A-F). This correlates with the increase in MMP3 activation post-PDT (Sternlicht, 2001).

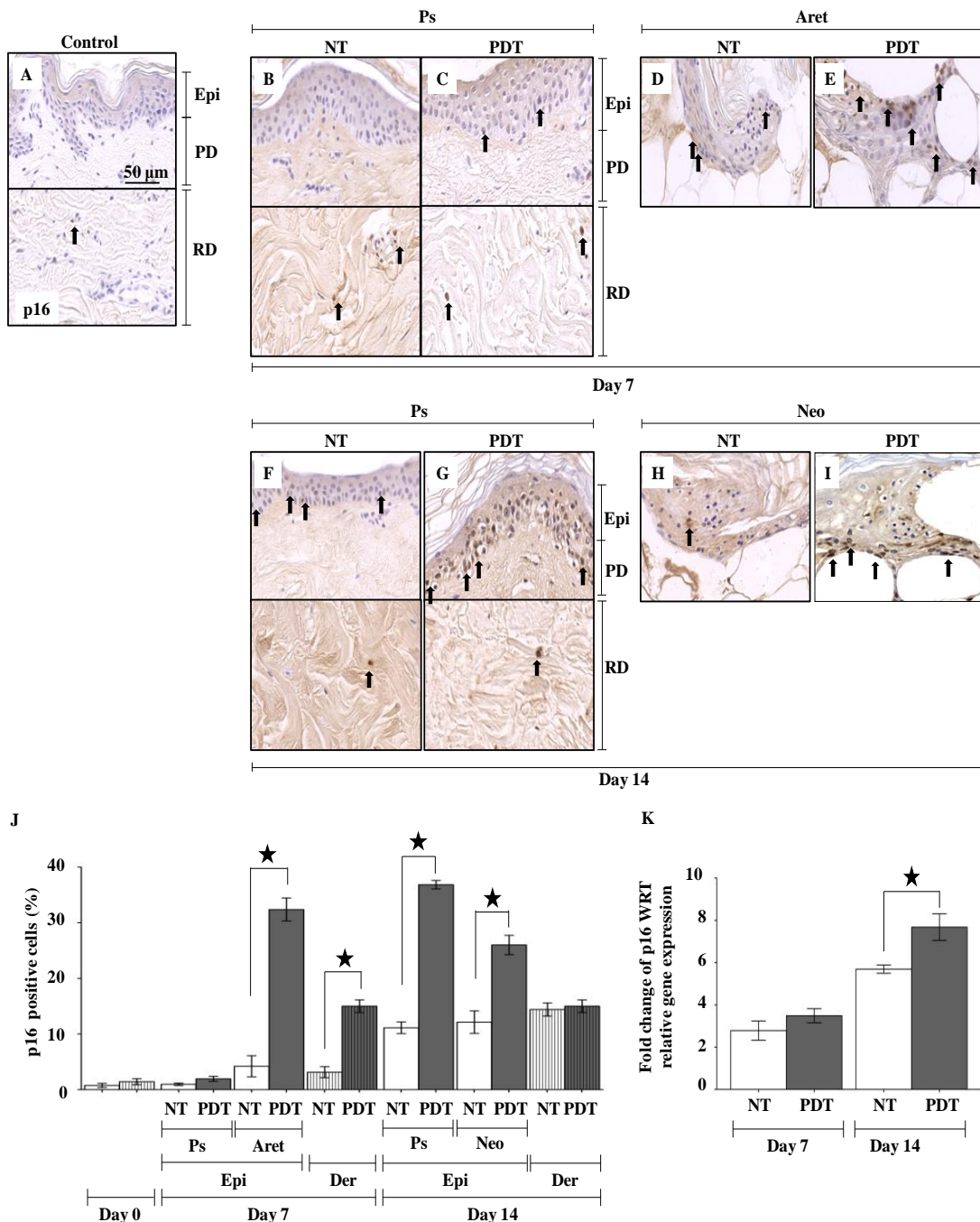


Figure 5.16 p16 analysis post-PDT. Representative images of p16-IHC (B-I) where papillary dermis (PD) and reticular dermis (RD) of normal human skin processed on day 0 (A) and WHOCS untreated (NT) and post-PDT (Original magnification 40X). Arrows show p16-positive cells in the peripheral skin (PS) advancing re-epithelialization tongue (Aret) and neo-epidermis (Neo). Graph represents quantification of p16 positive cells (J), p16 genetic expression (K), □ Denotes positive cells in the epidermis of untreated WHOCS or average intensity of untreated WHOCS and ■ Denotes positive cells in the dermis in untreated WHOCS. ■ Denotes positive cells or average intensity of WHOCS post-PDT. ★ Denotes significant difference ($p<0.05$). Mean and standard deviation between patients are represented ($n=6$).

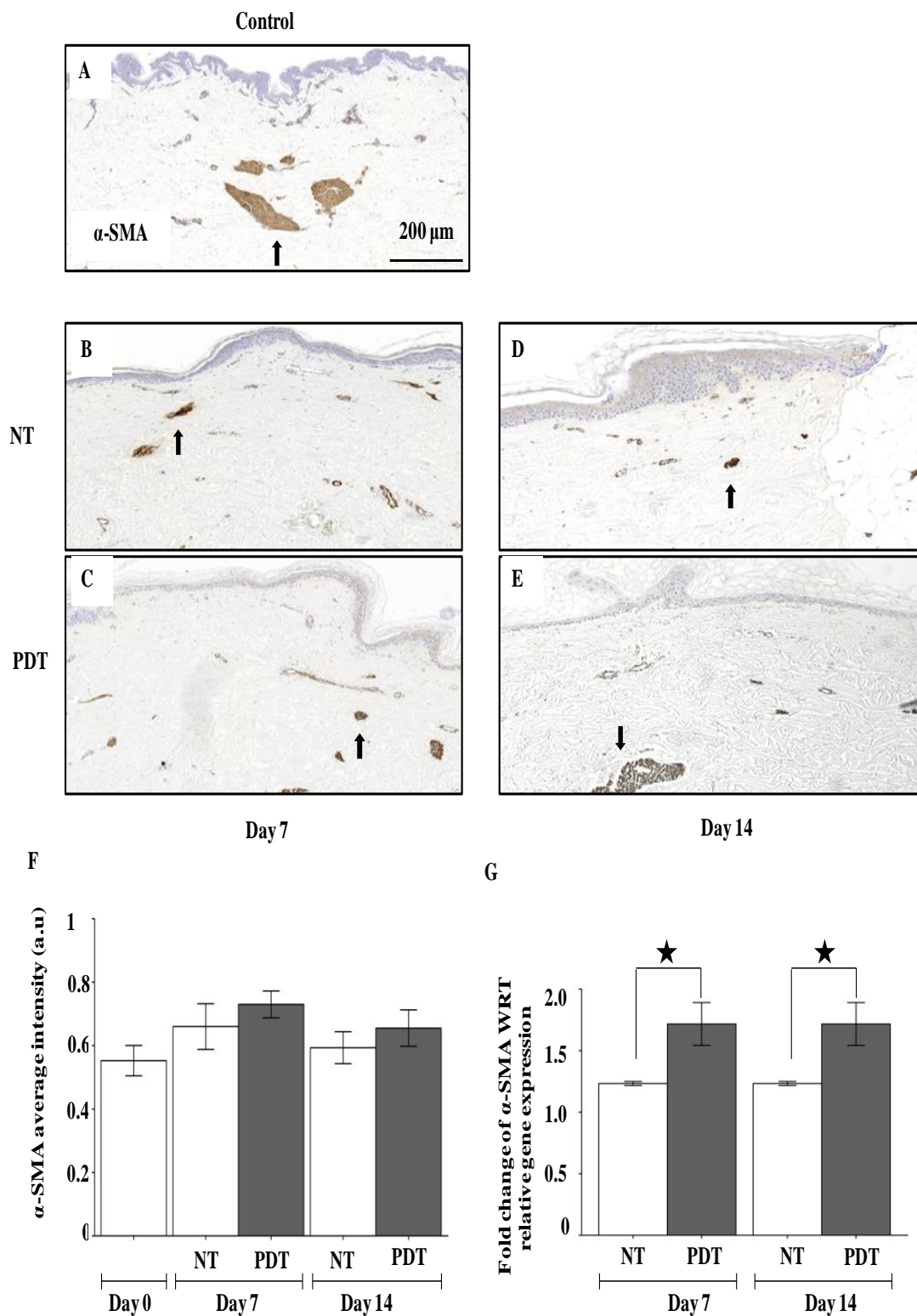


Figure 5.17 Representative images of α -SMA IHC post-PDT. Normal human skin processed on day 0 (A) was compared to WHOCS untreated (NT) and post-PDT treated and post-PDT (B-E; Original magnification 5X). Graph represents average intensity α -SMA expression in WHOCS (F) and α -SMA genetic expression (G). □ Denotes average intensity of untreated WHOCS ■ Denotes average intensity of WHOCS post-PDT. ★ Denotes significant difference ($p<0.05$). Mean and standar deviation between patients are represented ($n=6$).

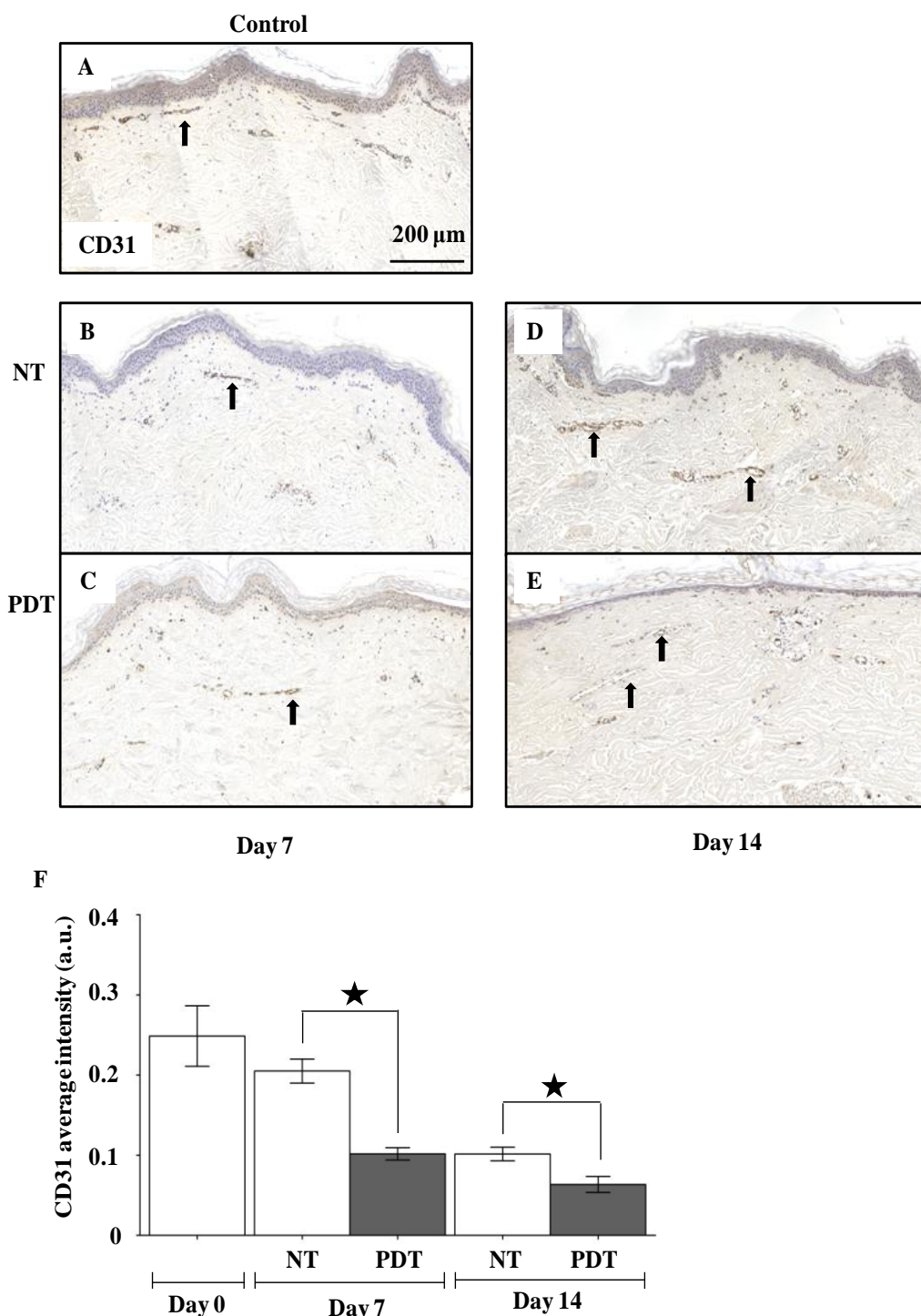


Figure 5.18 CD31 endothelial marker analysis post-PDT. Normal human skin processed on day 0 (A). WHOCs on day 0 were compared to untreated (NT) and post-PDT treated WHOCs on days 7 and 14 (B-E; Original magnification 5X). Graph represents average intensity of capillaries (F). □ Denotes average intensity of untreated WHOCs ■ Denotes average intensity of WHOCs post-PDT. ★ Denotes significant difference ($p<0.05$). Mean and standar deviation between patients are represented ($n=6$).

5.5 Discussion

In this study, we investigated healing of adult human skin maintained ex vivo with various wound sizes and shapes in different culture medium and support conditions. Following optimization of a WHOC model of adult human skin, the effects of PDT treatment were subsequently evaluated in an objective manner. We present an optimized wound size and culture conditions including support system and growth media with respect to cellular, interstitial and extrafibrillar components, for studying wound repair in human skin maintained ex vivo.

Three growth mediums previously used for skin organ cultures including DMEM, WE and MED3 were compared. We found that structure and barrier function of the skin was well preserved until day 14 in WHOC models fed with DMEM or WE. MED3, was unable to maintain tissue viability, although we found limited re-epithelialization in 1 mm partial thickness wounds. This indicated that feeding the dermal layer was sufficient to preserve epidermal viability and differentiation in agreement with previous reports (Moll, et al., 1998; Steinstraesser, et al., 2009; Tavakkol, et al., 1999; Xu, et al., 2012).

Well chamber inserts allowed an increase in excess fluid retention by WHOC, which could cause peri-wound tissue maceration (Okan, et al., 2007). WHOC embedded in collagen showed no increase in cellularity or swelling as had been previously reported, although wound healing closure rates were less compared to well chamber inserts (Bagabir, et al., 2012; Balaji, et al., 2014; Figure 5.19).

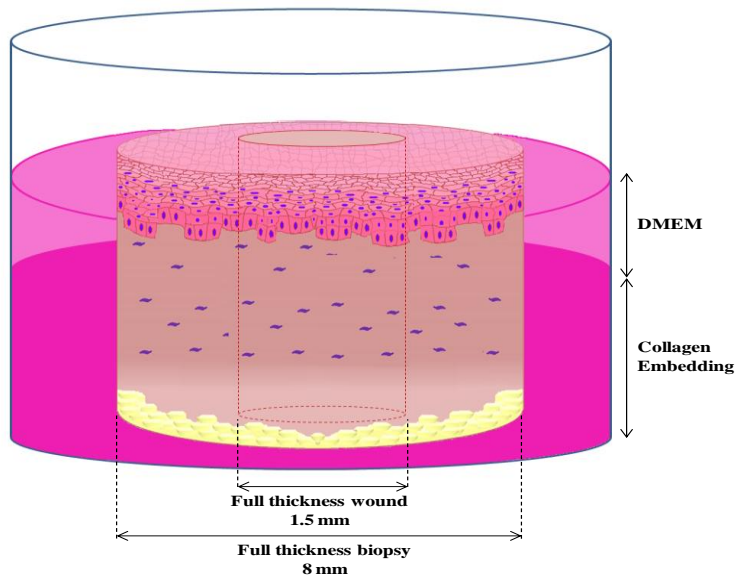


Figure 5.19 Schematic representation of optimal WHOC model. WHOC model with a full thickness wound of 1.5 mm and a fat scaffold in the wound. The dermal layer was embedded in rat tail collagen type one gel (2 mg/ml) and the epidermis was left exposed to air-liquid interface. WHOC was maintained with DMEM growth media in 24 well-cell culture plate.

Our observations suggest that skin “tensegrity” (Pacini, et al., 2012), which is a concept to explain the equilibrium between elements that supports tension and compression, so upon disturbance, this equilibrium will be lost causing either compression or extension. Skin tensegrity appears to be involved in healing of 1mm full-thickness wounds, as re-epithelialization occurred with an increased amount of immature collagen in the wound area. Although, we found that the wound edges in the well chambers appeared to be closer as well as showing an increased proximity with the swollen condition of the tissue biopsy edge, this also has been observed in vivo (Bush, et al., 2005). However, collagen embedded WHOCs did not exhibit these characteristics, which makes it superior to well inserts in long term preservation of WHOCs

Full thickness wounds greater than 1 mm did not close completely, however we observed an advancing re-epithelialization tongue. Morphological characteristics of re-epithelialized WHOCs with a partial wound bed (partial thickness) were found similar to previous ex vivo studies (Coolen, et al., 2010; Moll, et al., 1998). Following the establishing of the optimal WHOC model, we chose to evaluate the WHOC model functionally with PDT.

Previously we had reported that low doses of PDT increases proliferation in fibroblasts derived from normal skin (Mendoza, et al., 2012). Here, we identified an advancing epithelial tongue post-PDT compared to the untreated controls. However, these tongues did not join up due to the lack of a dermal support. Taking into account these findings, we chose to optimize the model further by inserting a scaffold of hypodermal fat, where we observed full re-epithelialization post-PDT.

Others have shown hypodermal fat tissue as a source of adult stem cells and paracrine messengers which can contribute to tissue repair and regeneration (Fu, et al., 2007; Klein, et al., 2007). We showed that 33% of wounds post-PDT treatment were closed compared to untreated wounds. This finding showed that PDT played an important role in initiating and maintaining the process of epidermal regeneration in WHOC models.

Elastic fibres responsible for skin resilience were found to be altered post-PDT, therefore it is possible that PDT may induce elastogenesis in vivo, as found by Sanclemente, et al., (2012). Collagen fibres were also found damaged but later on its density increases, particularly those at the papillary dermis. COLI and III gene and

protein expression were found to be significantly increased post-PDT, with dermal remodelling also reported previously by others including Riekki, et al., (2002).

PCNA levels, related to cell proliferation, prior to PDT and in untreated cultures were similar to that found by Kawahira, et al., (1999) However, PCNA significantly increased at the advancing epithelial tongue and in the dermis post-PDT. In contrast with peripheral and neo-epidermis, PCNA levels were found to be similar on day 14 post-PDT suggesting a decrease in the proliferative potential of the epidermis.

Basal keratinocytes are known to express CK14, affecting cell shape and motility leading to migration and differentiation. High levels of CK14 are known to lead to proliferation *in vivo*, and found closely related with skin tensegrity (Seltmanna, 2013). Here, we found that CK14 increased in keeping with increased cellular proliferation and migration on post-PDT but limited to one week as CK14 expression decreased thereafter. However despite this finding, the neo-epidermis was found to be fully re-epithelialized and differentiated at this time point in the post-PDT treated samples.

p16 regulates protective responses of the cell cycle and apoptosis, allowing DNA to repair itself after damage caused by ageing, oncogene activation and oxidative stress (Elmageed, et al., 2009). Any potential induction of senescence, proliferation or pathways leading to apoptosis by the differential expression of p16 is thought to be dependent on the Rb-signaling pathway and a number of proteins including p53 (Elmageed, et al., 2009; Paunesku, et al., 2001).

When we previously investigated the role of ROS and senescence in vitro, we found that a low dose of PDT increased ROS and induced senescence and cell proliferation (Mendoza, et al., 2012). Similar results had been shown by Blazquez-Castro, et al (2012) but only in human immortalized keratinocytes (HaCaT). Here, we show an increased p16 expression in the advancing tongue which may indicate keratinocyte proliferation post-PDT triggered by ROS. In addition, we found a significant increase in epidermal apoptosis on day 14, which coincides with the end of the re-epithelialization stage (Blázquez-Castro, et al., 2012).

Keratinocytes can influence dermal cells through paracrine mechanisms. In vitro studies had observed that PDT initiated a cascade of signals through ROS generation (Castano, et al., 2005). ROS induced HIF-1 α , and other cytokines such as tumour necrosis factor- α (TNF- α), vascular endothelial growth factor (VEGF), interleukin (IL) as IL-1 and IL-6, which in turn regulates the induction of several MMPs (Almeida-Issa, et al., 2009; Mendoza, et al., 2012).

MMPs are secreted as inactive zymogens, upon the action of other MMPs becomes active. The active forms can degrade several components of the ECM (Alameida-Issa, et al., 2009; Ogata, et al., 1991). MMP3 is a key factor involved in the disorganization of collagen fibrils and in the remodelling of dermal connective tissue after injury. MMP3 cleaves E-cadherin, laminin 5, COLIII, fibronectin, elastin and release active heparin-binding EGF-like factor and angiostatin, degrade insulin-like growth factor binding proteins and also activates MMP1, MMP7 and MMP9 influx (Sternlicht, et al., 2001). We found a significant increase in MMP3 post-PDT, thus promoting keratinocyte and fibroblast migration, also potentially implying the

increased availability of Insulin-like growth factor (IGF) and other growth factors, which can regulate neutrophils (Garg, et al., 2010).

Another MMP related to wound healing is MMP19, which cleaves laminins, tenascin-C, fibronectin and activates other inactive MMPs. We found an increased expression of MMP19 post-PDT, especially at the wound edges, which may suggest its active involvement in the wound repair process post-PDT. Our results suggested that PDT induced dermal remodelling and likely mediated through paracrine pathways inducing MMPs, as had been suggested by Alameida-Issa, et al. (2009).

CD31, expressed in endothelial cells can be indicative of cell diversity, capillary and vessels density. We found a significant decrease in CD31 positive cells post-PDT, although with no apparent impact on the number of capillaries and vessel density. This finding may be explained by increased ROS levels post-PDT application acting on the endothelial cells in addition to other mechanisms. α -SMA is a cellular marker of myofibroblasts, wound contraction and ECM deposition during wound healing. We found an increase in α -SMA gene expression post-PDT. These levels are in keeping with increased rate of wound contraction post-PDT (Hinz, 2007; Sternlicht, et al., 2001).

PDT is known to release damage-associated molecular patterns (DAMPs), which can trigger immunological alerts in order to induce repair as has been previously observed. Li et al., (2010) also has suggested that damage may induce and enhance tissue repair. Here, we have demonstrated that PDT accelerated re-epithelialization

and ECM remodelling by causing enhancing re-epithelialization as well as structural changes in the ECM (Figure 5.20; Garg, et al., 2010; Li, et al., 2010).

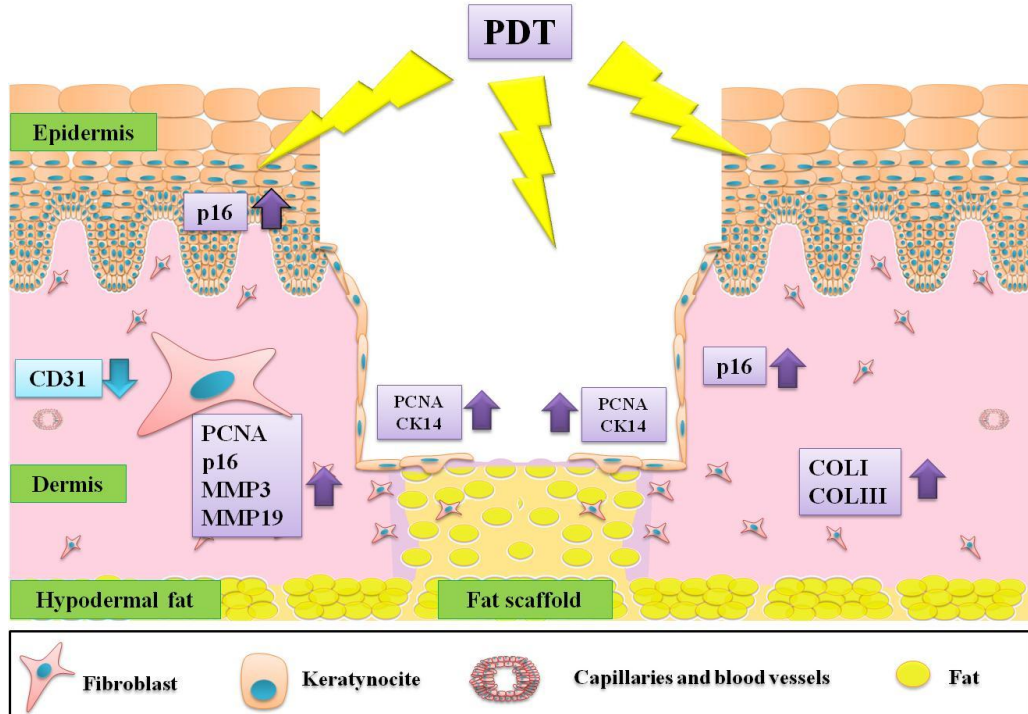


Figure 5.20 Schematic representation of the effect of PDT in WHOCS on day 7.
 We observed an increase in p16, PCNA and CK14 in the epidermis of WHOCS treated with PDT. Also, we observed an increase in p16 and PCNA in the dermis. Additionally we observed an increase in COLI, COLIII, MMP3 and MMP19 and a decrease in CD31 biomarker expressed in capillaries. In conclusion, these results suggested an enhanced of re-epithelialization and ECM remodelling by PDT treatment.

CHAPTER SIX: PHOTODYNAMIC THERAPY AND SKIN SCARRING

6.1 Introduction

Skin scarring *ex vivo* provides the most complete system for studying tissue morphology and structure, since it preserves structure and most of the cellular characteristics of the original tissue, which makes possible the study of the biology and evaluation of novel therapies (Brohem, et al., 2010; Gurtner, et al., 2011; Ramos, et al., 2008; Ud-Din, et al., 2014; Wong, et al., 2011; Yang, et al., 2007).

Photodynamic therapy (PDT) has shown promising results in *vitro* and *in vivo* in the treatment of hypertrophic and keloid scars. Organotypic cultures of keloid fibroblast have also found decreases in collagen synthesis. Limited therapeutic studies have found an improvement in hypertrophic, keloids, and scars where PDT was used as adjuvant after excisional surgery. However only scar appearance, volume, angiogenesis and effectiveness were evaluated. For this reason further investigations are required in order to understand the mechanism of PDT in human skin scarring (Basdew, et al., 2013; Bruscino, et al., 2011; Calzavara-Pinton, et al., 2013; Campbell, et al., 2010; Chiu, et al., 2005; Li, et al., 2014; Mendoza, et al., 2012; Nie, et al., 2010; Sakamoto, et al., 2012; Ud-Din, et al., 2013).

This chapter describes the effects of PDT in phenotypically different scars compared to striae distensae and normal skin ex vivo. Scars vary from fine line scars which are the least fibrotic and the least severe scar form, through hypertrophic scars, an intermediate form of dermal fibrosis, to keloid scars, which are the most severe fibrotic condition of skin scarring. PDT was given after incubation with pro-photosensitisers MALA/5ALA (4hrs) and followed by a fluence of 40 J/cm^2 . Pro-photosensitiser were selected from a literature review, while incubation time was selected according to the results of the investigation described in chapter four, similarly 40 J/cm^2 was chosen, according to the results presented in chapter four. Tissue morphology, apoptosis, proliferation, ECM remodelling and relative gene expression were determined post-PDT.

6.2 Experimental set up

Striae Alba, fine line scars, hypertrophic scars and normal skin were maintained ex vivo for seven days, after PDT treatment. MALA-PDT was compared to 5ALA-PDT, post illumination with 40J/cm^2 . Then histology, immunohistochemical and differential gene expression analysis were performed on the organ cultures. The outline of the experimental methodology is depicted on figure 6.1.

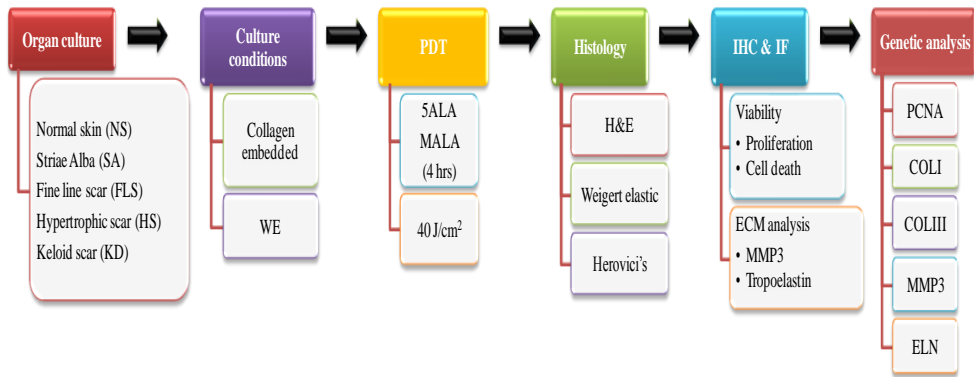


Figure 6.1 Flow chart of the methodology used to investigate the effect of PDT in scars ex vivo.

6.3 Material and methods

6.3.1 Study subject selection and recruitment

Striae distensae (SD) in the form of striae alba (as opposed to striae rubra), fine line scars (FLS), and normal skin (NS) explants were obtained from healthy patients undergoing routine aesthetic surgery. Hypertrophic scars (HS) and keloid scars (KD) were harvested from patients undergoing surgical excision of their lesion as part of their clinical management. In terms of clinical scar severity, which will be referred to later in the text as degree of dermal fibrotic severity, clearly FLS is the least severe and KD is the most severe form with HS as an intermediate form of a dermal fibrotic scar. All samples were diagnosed both clinically and histological to ensure accurate diagnosis. Scar classification and demographic clinical data is shown in Table 6.1. Ethical approval for this study was provided by the North West of England, research

ethics committee (11/NW/0683). Tissue samples were collected following fully informed verbal and written consent.

Table 6.1 Clinical data and source of scar/skin explants

Patient	Gender	Age	Anatomical source of scar/skin explants	Scar classification
1	Female	80	Abdomen	Striae Alba
2	Female	42	Abdomen	Striae Alba
3	Female	31	Abdomen	Striae Alba
4	Female	28	Abdomen	Striae Alba
5	Female	28	Abdomen	Striae Alba
6	Female	50	Arm	Striae Alba
7	Female	57	Abdomen	Fine Line Scar
8	Female	65	Breast	Fine Line Scar
9	Female	30	Abdomen	Fine Line Scar
10	Female	42	Abdomen	Fine Line Scar
11	Female	22	Abdomen	Fine Line Scar
12	Female	42	Abdomen	Fine Line Scar
13	Female	58	Abdomen	Hypertrophic Scar
14	Female	80	Abdomen	Hypertrophic Scar
15	Female	42	Abdomen	Hypertrophic Scar
16	Male	26	Sternum	Keloid Scar
17	Male	24	Shoulder	Keloid Scar
18	Male	52	Ear	Keloid Scar
19	Female	42	Abdomen	Normal Skin
20	Male	71	Abdomen	Normal Skin
21	Female	42	Abdomen	Normal Skin
22	Male	28	Abdomen	Normal Skin

6.3.2 Skin explant preparation

In order to prepare the explants for organ culture the hypodermal fat was surgically excised, the explants were washed several times in phosphate buffer solution (PBS, Sigma-Aldrich, Dorset, UK) and soaked in Dulbecco's modified Eagle's medium

(DMEM; Sigma-Aldrich, Dorset, UK) supplemented with Primocin (InvivoGen, Nottingham, UK) for 30 min and rinsed several times with PBS. Organ cultures (OC) explants were surgically prepared with a 6 mm punch biopsy kit. The full thickness dermal tissue biopsy was subsequently embedded in rat-tail collagen type I gel (2 mg/ml; BD Biosciences, Oxford, UK) and the epidermis was left exposed to the air-liquid interface. Bagabir et al (2011) show that William's medium (WE) preserves better the features of keloid scars in organ culture compare to DMEM, for such a reason the scar organ cultures were maintained with WE supplemented with 100 IU/ml penicillin, 10 µ/ml streptomycin, 10 µg/ml of insulin, 10 ng/ml of hydrocortisone and 2 mM of L-glutamine and cultured in standard conditions (37°C; 5% CO₂/16% O₂ in humidified cell culture incubator). All reagents were from Sigma-Aldrich (Dorset, UK; Figure 6.2A-B).

6.3.3 Photodynamic therapy treatment

Scars, striae alba and normal skin OC explants were exposed to PDT treatment using 2 protoporphyrin IX precursors, 5-aminolevulonic acid (5ALA; Mandeville Medicines, UK) or methyl-aminolevulinate (MALA; Galderma, Watford, UK) and illuminated with a PDT machine (Omnilux PDT™, Photo Therapeutics, Pennsylvania, USA) with an arrangement of red light-emitting diodes (LEDs) of wavelength 633±3 nm and an air cooling system. The PDT machine was adjusted to 40 J/cm² of power intensity and calibrated with an IL1700 radiometer (International Light Technologies Inc, Massachusetts, USA; 13; Figure 6.2C; Mendoza, et al., 2012).

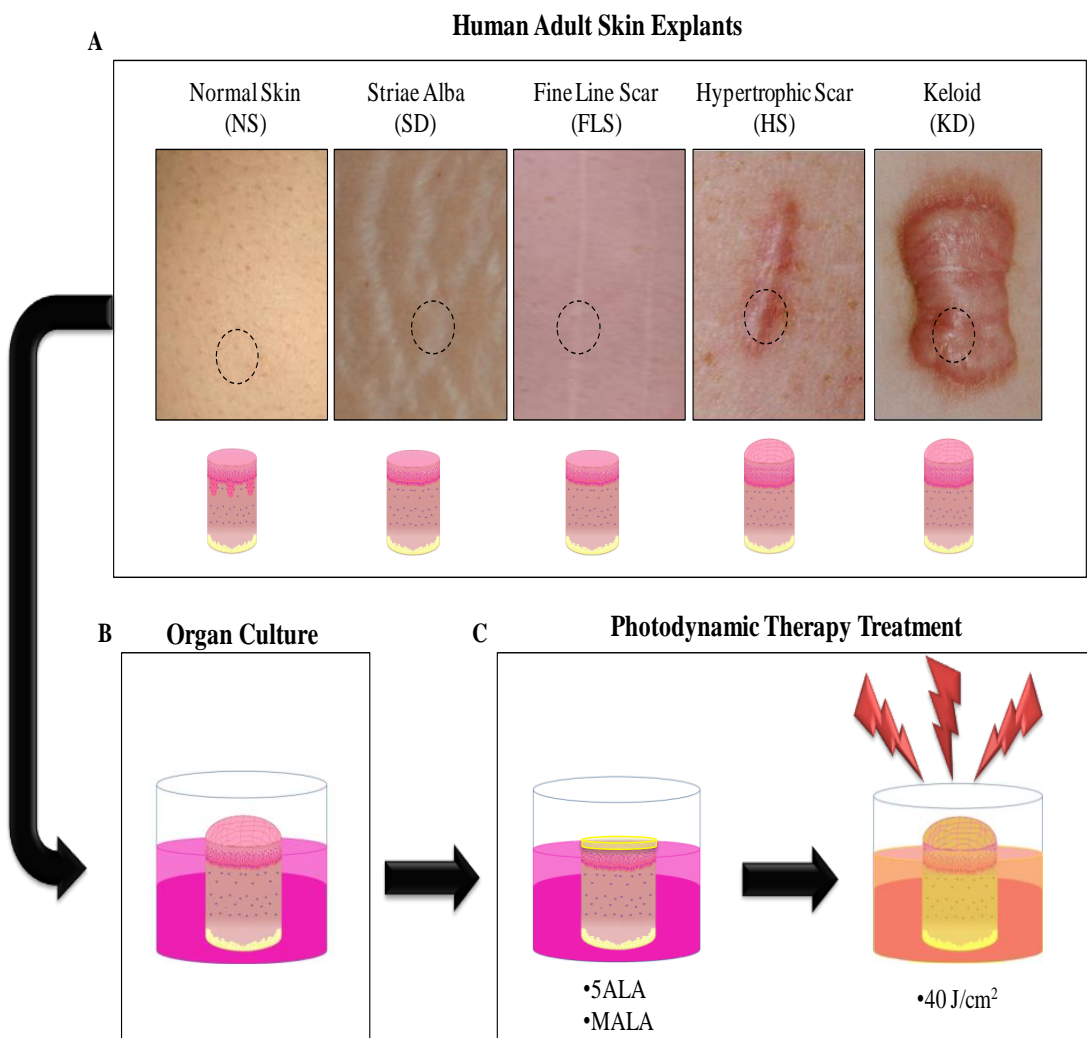


Figure 6.2 Schematic representation of normal skin, striae distensae and scar explants. Full thickness punch biopsies measuring 6mm (A) were embedded in collagen and maintained with supplemented William's E (WE) medium and air-liquid interface (B). Organ cultures were incubated with the pro-drugs aminolevulinic-acid methyl-ester (MALA) or aminolevulinic-acid (5ALA) later illuminated with red led light and maintained 7 day ex vivo post-photodynamic therapy (C). Full-thickness biopsies of 6mm (A) were embedded in collagen and maintained with supplemented WE medium and air-liquid interface (B). Organ cultures were incubated with the pro-drugs 5ALA or MALA, later illuminated with red led light and maintained 7 days ex vivo post-PDT (C).

PDT treatment was given on the day of collection (Day 0). A thin layer (1 mm) of photosensitiser precursors was applied on the epidermis and incubated for 4 hrs under standard conditions and darkness. Organ cultures were washed twice with PBS before illumination and soon after re-embedded in collagen and cultured for 7 days

ex vivo. Collected OCs were fixed, paraffin embedded, sectioned and deparaffinised following standard procedures (Bagabir, et al., 2012). Histology, Immunofluorescence/Immunohistochemistry experiments were done in all patients.

6.3.4 Histology

Representative sections of 5 µm were morphologically studied after H&E, HV and Weigert's elastic differential staining and scanned as previously describe in chapter five.

6.3.5 Immunofluorescence/Immunohistochemistry

3'-OH DNA immunofluorescence (IF; Tunel; FragEL™, Calbiochem-Merck, Darmstadt,GER) was used to assessed apoptosis. Additionally, proliferating nuclear antigen (PCNA), tropoelastin (ELN) and matrix remodelling metalloproteinase 3 (MMP3) were immunostaining (IHC; Table 6.2; Abcam®, Cambridge, UK) and detected with Novocastra Peroxidase Detection Systems (Leica, Milton Keynes, UK). IHC and peroxidase detection were made according to manufacturer's instructions. Stained sections were scanned in a Hamamatsu NanoZoomer 2.0-HT and analysed with NDP.view2 image software (Hamamatsu, Hertfordshire, UK). An objective quantification of cellular markers was made using Definiens Tissue Studio 3.5 Software (Definiens, Munich, GER; Samaroo, et al., 2012).

Table 6.2 List of antibodies

Primary antibody	Dilution	Incubation time
Anti-PCNA antibody (ab18197); Rabbit polyclonal; IgG.	1:200	1 hr
Anti-Elastin antibody [BA-4] (ab9519); Mouse monoclonal; IgG1	1:150	1hr
Anti-MMP3 antibody [EP1186Y] (ab52915); Rabbit monoclonal; IgG.	1:1000	1 hr

PCNA, proliferating cell nuclear antigen; MMP3, metalloproteinase 3

6.3.6 mRNA isolation, cDNA synthesis and qRT-PCR

The gene expression levels were obtained as previously described in chapter five.

The primers used in the study are detailed in Table 6.3.

Table 6.3 Gene and primer sequences for qRT-PCR

Primers	Gene ID	Sequence 5'-3'	Primer position	Amplicon size (bp)
RPL32-L	NM_000994.3	gaagttcctggtccacaacg	319-338	77
RPL32-R	NM_000994.3	gagcgatctcgacacagta	377-395	77
PCNA -L	NM_002592.2	tggagaactggaaatggaaa	755-775	20
PCNA-R	NM_002592.2	gaactggtcattcatcttatgg	826-849	20
Elastin-L	NM_000501.3	cagctaaatacggtgctgctg	2420-2440	21
Elastin-R	NM_000501.3	aatccgaagccaggcttg	2495-2513	19
Collagen I-L	NM_000088.3	gggattccctggacctaag	1866-1885	63
Collagen I-R	NM_000088.3	ggaacacctcgctctcca	1911-1928	63
Collagen III -L	NM_000090.3	ctggaccccagggttcc	3101-3118	75
Collagen III-R	NM_000090.3	catctgatccagggttcca	3156-3175	75
MMP3 -L	NM_002422.3	caaacatattcttttagaggacaa	1259-1285	91
MMP3 -R	NM_002422.3	ttcagctattgtggaaaa	1329-1349	91

RPL32, 60S ribosomal protein L32; PCNA, proliferating cell nuclear antigen; MMP3, metalloproteinase 3.

6.3.7 Statistical analysis

The results are presented as the mean values \pm standard deviation. Statistical significance was calculated with One-way ANOVA and Bonferroni comparison test. Graphics and statistics were generated with GraphPad Prism 5 (GraphPad Software, La Jolla, CA, USA). The differences were considered statistically significant if $p<0.05$.

6.4 Results

6.4.1 Histological evaluation post-5ALA/MALA-PDT

PDT application with either 5ALA or MALA caused fibrotic tissue degradation

Morphological analysis by H&E staining at day 0 (Control) shows typical differences of various scars, striae alba and normal skin (Figure 6.3A-E). All histological characteristics were present after 7 days of being cultured ex vivo (Figure 6.3F-J). Photodynamic therapy treatment was given on day 0 and tissues were maintained 7 days ex vivo (Figure 6.3K-T), and compared to normal skin on day 0 and untreated controls on day 7.

Histological appearance of normal skin shows a minimal effect. However, epidermal rete ridges were no longer preserved in full, epidermal stratification decreased and collagen bundles appeared less dense. PDT effects on scars and striae were more aggressive compared to normal skin; in striae some small areas of epidermal

detachment were found and keratinocytes with pyknotic nucleus were found in all epidermal layers. The collagen bundles in the ECM appeared to have been re-organised an almost unravelled. While in FLS and HS larger areas of epidermal detachment were found. The whole epidermis contained pyknotic cells and the ECM was found to have changed and degraded. However the highest percentage of change was seen in KD, where the epidermis was found to be totally detached (almost dislocated) and there was a ECM complete loss of its typical appearance. However, similar characteristic changes were observed in all tissues following either 5ALA or MALA, PDT treatment.

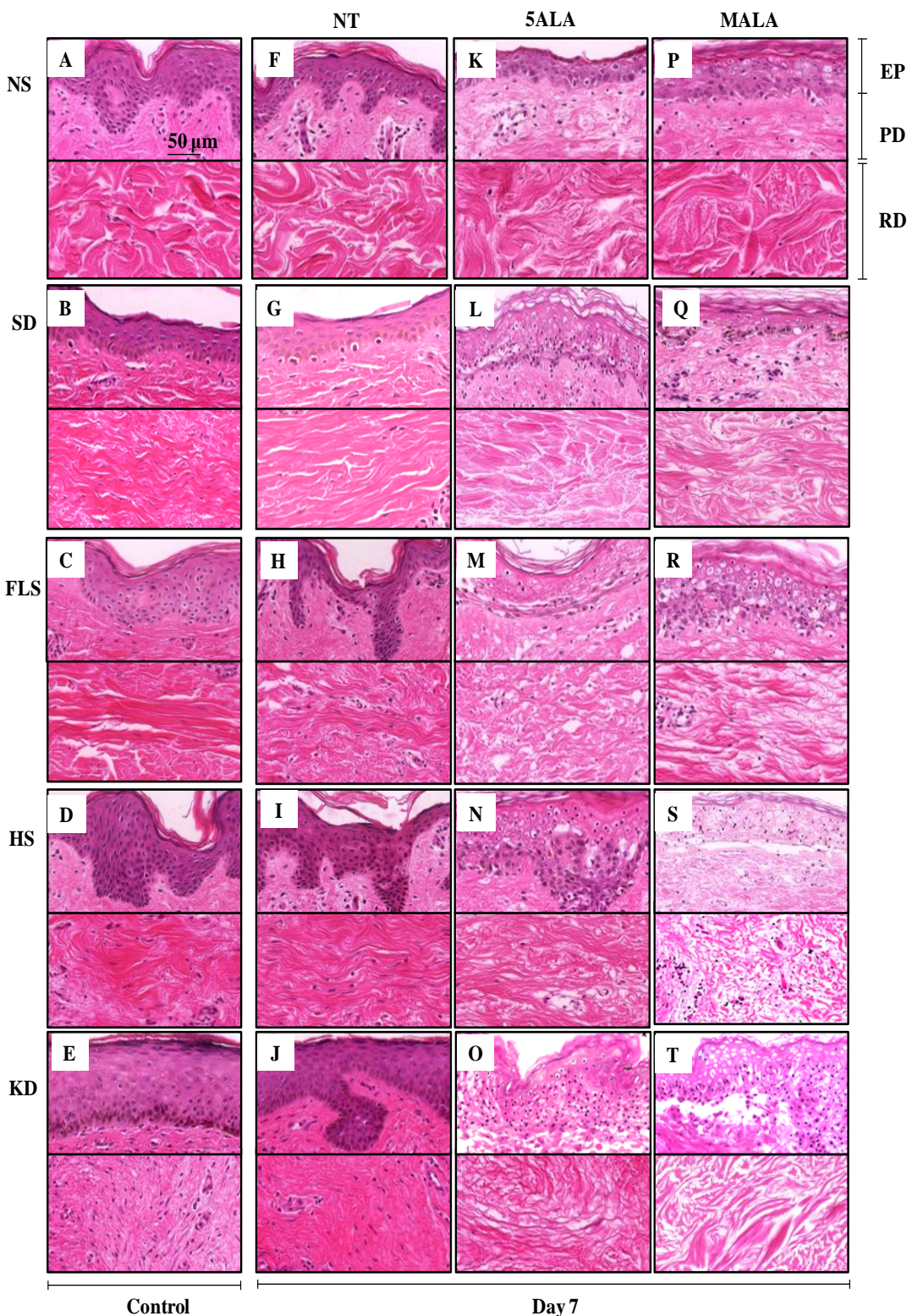


Figure 6.3 Morphological analysis by H&E stain staining. Normal skin (NS; A,F,K&P; $n=4$), striae alba (SD; B,G,L&Q), fine line scar (FLS; C,H,M&R; $n=6$), hypertrophic scar (HS; D,I,N&S; $n=3$) and keloid disease (KD; E,J,O&T; $n=3$) were treated with aminolevulinic-acid methyl-ester (MALA) or aminolevulinic-acid (5ALA) photodynamic therapy. NT denotes Untreated controls, EP denotes Epidermis, PD denotes papillary dermis and RD denotes reticular dermis.

6.4.2 Epidermal apoptosis and proliferation analysis after 5ALA/MALA-PDT

1. Apoptosis was shown to have increased post-PDT

Apoptosis was determined by Tunel assay and was quantified in the basal layer of the epidermis. Apoptosis was found to be increased in relation to the scar severity and phenotype. Normal skin showed apoptotic cells at the stratum spinosum after 5ALA-PDT whilst an even distribution in all epidermal layers was found with MALA-PDT. An average of 15% of apoptotic cells were found with both treatments in normal skin. Epidermal layer of scar lesions were found to be highly apoptotic. SD and FLS staining showed that up to 50% were of apoptotic cells and in HS apoptotic cells increased up to 80%, whilst the epidermis of KD was found to be detached with a few apoptotic cells in the entire basal layer (Fig 6.4A-S).

2. PDT application with either 5ALA or MALA decreased the total number of proliferating cells

Cell proliferation was quantified with PCNA-IHC in the basal layer of the epidermis. Biopsies on day 0 showed typical proliferative characteristics of the normal skin and scars. NS, SD and FLS showed no significant differences between the percentage of proliferative cells at the epidermis which were approximately 25%. HS proliferative cells (39%) were found to be significantly more than NS, SD and FLS, however the vast majority were found to be restricted to the basal layer. In KD, 90% of the cells were found to be proliferative and distributed across the entire tissue. Post-PDT either with 5ALA or MALA, proliferative cells were found to be significantly lower compared to day 0 and compared with untreated controls on 7 day (Figure 6.5A-E).

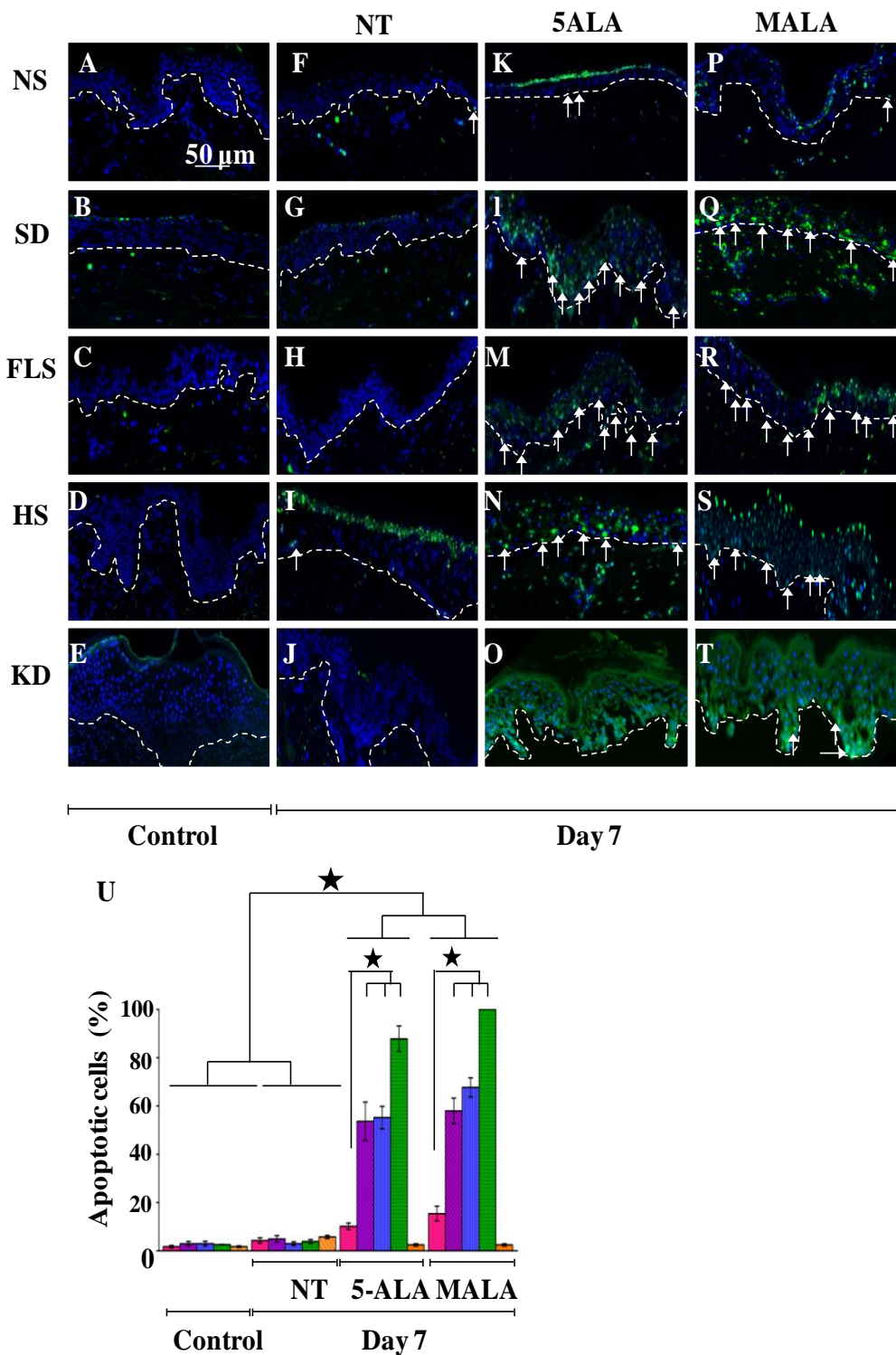


Figure 6.4 Epidermal apoptosis analysis. Normal skin (NS; $n=4$), striae alba (SD; $n=6$), fine line scar (FLS; $n=6$), hypertrophic scar (HS; $n=3$) and keloid disease (KD; $n=3$) were stained with apoptosis-tunnel assay (A-T) at day 0 (control), untreated (NT) and with 5ALA or MALA-PDT. Graphs represent normal skin (pink), striae alba (purple), fine line scar (blue), hypertrophic scar (green) and keloid scar (orange) quantification of apoptotic cells (U). Epidermis (EP) and papillary dermis (PD). ★ Denotes statistically significant difference ($p<0.05$). Mean and standard deviation between patients are represented.

In KD, there were a few proliferative cells across the tissue. Here, PCNA gene expression decreased significantly in both SD and dermal scar lesions (Figure 6.5K-T). PCNA expression was reduced by 2 fold on day 7 in untreated skin compared with treated skin, while the maximum change of 10 fold was observed in KD tissue. Cell proliferation was quantified after through PCNA-IHC in the basal layer of the epidermis. Biopsies on day 0 showed typical proliferative characteristics of the normal skin and scars. NS, SD and FLS show no significant differences between them and the percentage of proliferative cells at the epidermis in averaged was 25%. HS proliferative cells (39%) were found to be significantly more than NS, SD and FLS, however the vast majority were found to be restricted to the basal layer. In KD 90% of the cells were found to be proliferative and distributed across all tissue.

Post-PDT either with MALA or 5ALA, proliferative cells were found to be significantly lower compared to day 0 and compared with untreated controls on 7 day (Figure 6.5F-J). In KD was a no longer detected proliferative cells in all tissue. Here, PCNA genetic expression consistently decreased significantly in striae and scars also (Figure 6.5V). PCNA expression reduced by 2 folds on day 7 between untreated skin and treated skin, while the maximum change of 10 fold was observed in KD tissue.

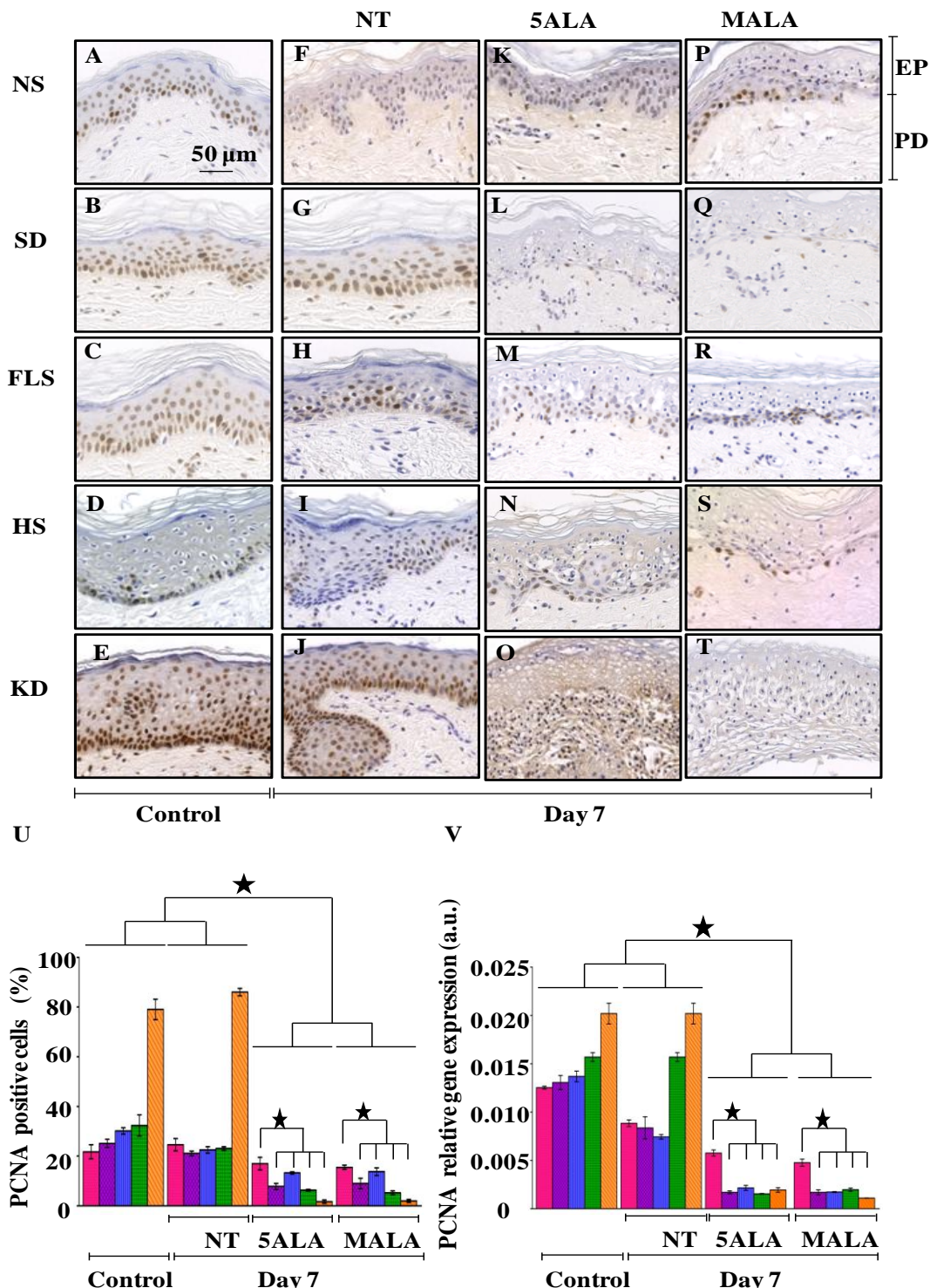


Figure 6.5 Epidermal proliferation analysis. Normal skin (NS; $n=4$), striae alba (SD; $n=6$), fine line scar (FLS; $n=6$), hypertrophic scar (HS; $n=3$) and keloid disease (KD; $n=3$) were stained with proliferating cell nuclear antigen Immunohistochemistry (A-T) at day 0 (control), untreated (NT) and with 5ALA or MALA-PDT. Graphs represent normal skin (■), striae alba (□), fine line scar (■), hypertrophic scar (■) and keloid scar (□) quantification of PCNA positive cells (U); PCNA (V) gene expression. Epidermis (EP) and papillary dermis (PD). ★ Denotes statistically significant difference ($p < 0.05$). Mean and standard deviation between patients are represented.

6.4.3 Extracellular matrix analysis after 5ALA/MALA-PDT

1. Elastic fibres were altered post-PDT

Weigert's elastic stain revealed striking differences in the elastic fibre arrangement prior and post-PDT (Figure 6.6A; differences were subjectively studied by three blind independent evaluators). Post-PDT elastic fibres in normal skin were found to be different compared to SD, FLS, HS and KD, where the change increased accordingly. Elastic fibres rearrangement ranged from broken and untangled fibres in the papillary layer of the dermis of SD and FLS while the highest percentage of change was found in HS. However, elastic fibre change in KD showed an inconsistent pattern, as there was variation in fibres size and organisation across the samples (Figure 6.6A). Further analysis of tropoelastin IHC (Figure 6.6B-D), which is the soluble precursor of elastic fibres, showed significant differences between NS and SD, HS and KD on day 0 (Figure 6.6B). Normal skin showed few positively stained fibres were present at the basal layer which was similar to what was seen in FLS. Although HS showed positive staining in the basal layer and close proximity to the area of the scar, while keloid scars also showed a high percentage of positive staining at the basal layer. However it was no assessed other components as fibrillin, which work as an scaffold for the latter formation of elastic fibres in the wound healing.

Post-PDT ELN positive cells increased in NS, SD, FLS and HS (Figure 6.7A-U). In normal skin positive cells increased especially after they were treated with 5ALA-PDT. As shown previously, KD tissue was found to be affected most, demonstrating no evidence of tropoelastin expression. ELN gene expression in dermal lesions

compared to untreated tissue increased by a maximum of 2.5 fold in HS post-PDT compared to day 7 untreated tissues (Figure 6.7U).

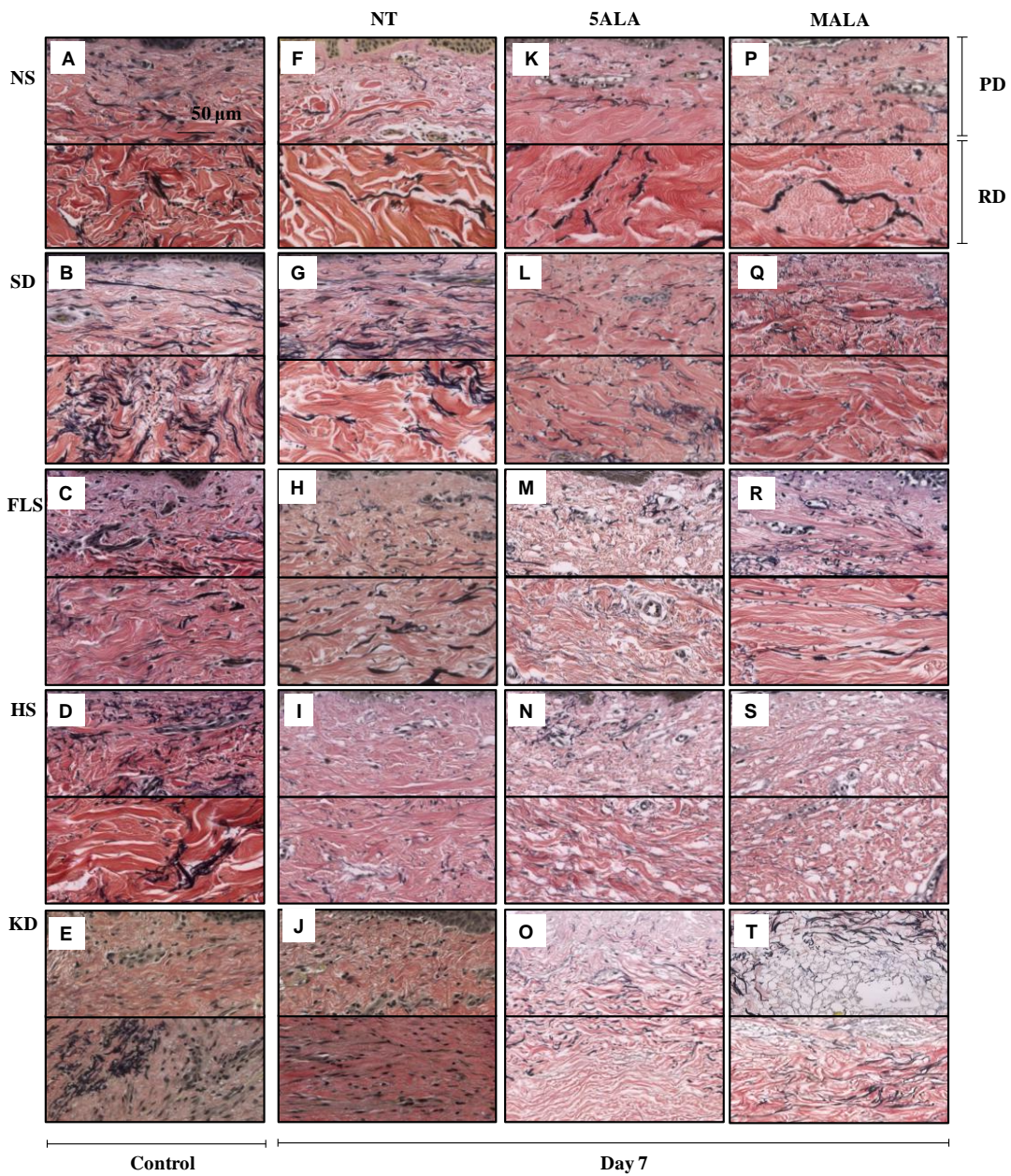


Figure 6.6 Elastic fibre arrangement analysis. Elastic morphological analysis by Weigert's staining were performed in Normal skin (NS; A,F,K&P; $n=4$), striae alba (SD; B,G,L&Q; $n=6$), fine line scar (FLS; C,H,M&N; $n=6$), hypertrophic scar (HS;D,I,N&S; $n=3$) and keloid disease (KD; E,J,O&T; $n=3$) on control (A-E) and compared to untreated controls (F-J; NT) after aminolevulinic-acid (5ALA) or its methyl-ester (MALA) photodynamic therapy. Papillary dermis (PD) and reticular dermis (RD).

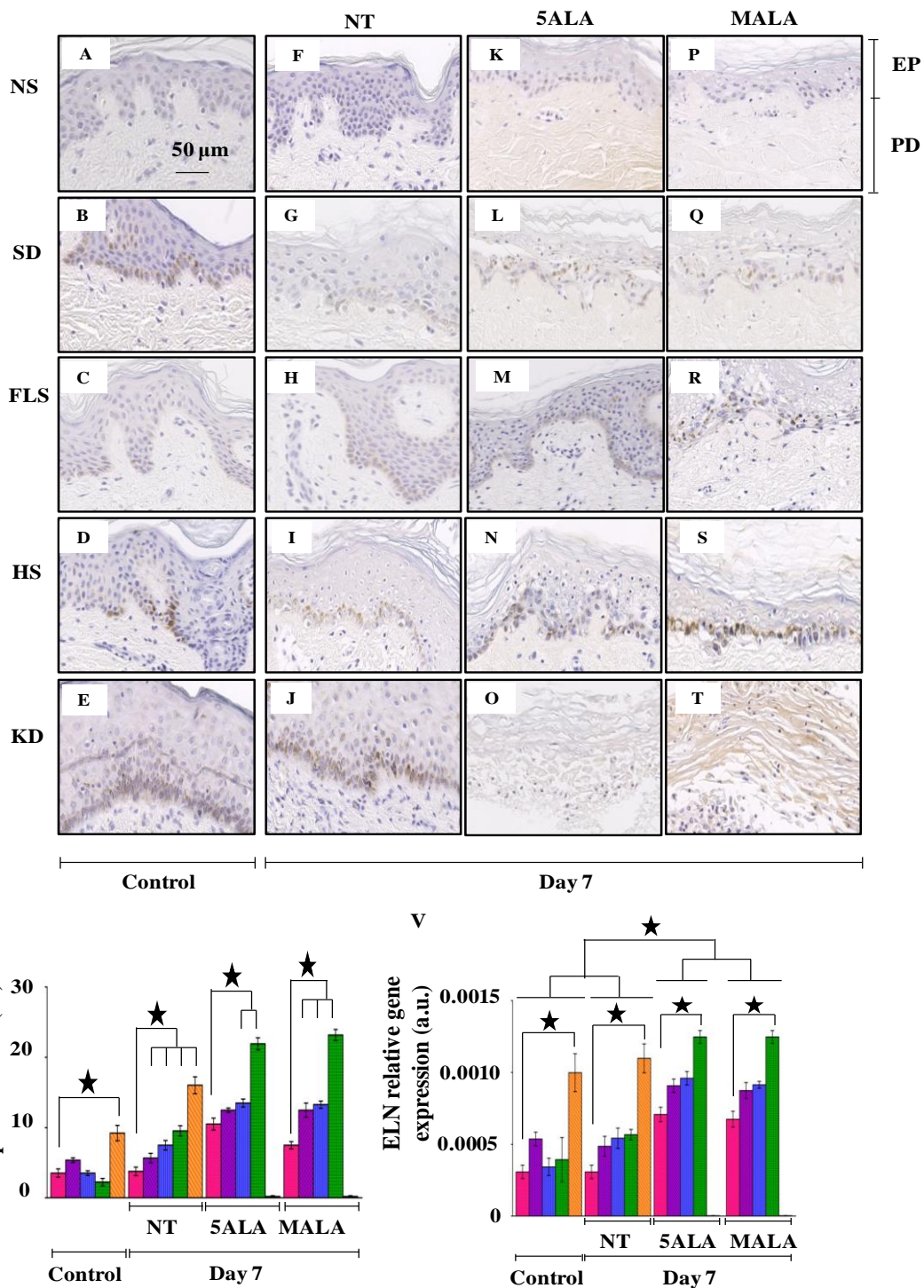


Figure 6.7 Tropoelastin analysis. Tropoelastin Immunohistochemistry (ELN-IHC) analysis were performed in Normal skin (NS; A,F,K&P; $n=4$), striae alba (SD; B,G,L&Q; $n=6$), fine line scar (FLS; C,H,M&R; $n=6$), hypertrophic scar (HS; D,I,N&S; $n=3$) and keloid disease (KD; E,J,O&P; $n=3$) on control (A-E) and compared to untreated controls (NT;F-J) after aminolevulinic-acid (5ALA) or its methyl-ester (MALA) photodynamic therapy. Papillary dermis (PD) and reticular dermis (RD). Graphs show Tropoelastin Immunohistochemistry positive cells quantification (C) and ELN genetic expression (D) of normal skin (■), striae alba (■), fine line scar (■), hypertrophic scar (■) and keloid scar (■). ★ Denotes statistically significant difference ($p < 0.05$). Mean and standar deviation between patients are represented.

2. Collagen fibre arrangement was affected post-PDT, in all dermal lesions with the highest effect seen in keloid tissue

Collagen arrangement varied when comparing normal skin to different scar phenotypes (Figure 6.8A-E). Dermal scars showed collagen fibres with thick bundles parallel to the dermis that became thicker in the reticular dermis of SM, HS and KD. Regardless of the scar phenotype, all collagen fibres were found to be affected by PDT, however this effect increased with the severity of the scar type (Figure 6.8K-T).

Normal skin and SD, showed relaxed collagen fibres and increased expression of COLIII in the papillary dermis compared to day 0 (Figure 6.8K-Q), while in FLS and HS fibres were found degraded, shortened and untangled post-PDT (Figure 6.8M-S). However, the highest effect was observed in KD where the papillary dermis was found most affected and the reticular dermis showed collagen fibres that had become thinner and with increased spaces between them (Figure 6.8O&T).

Further analysis of COLI and COLIII gene expression found both to be decreased in FLS, HS and KD compared to normal skin by day 0 and untreated tissues on day 7 (Figure 6.8U-V).

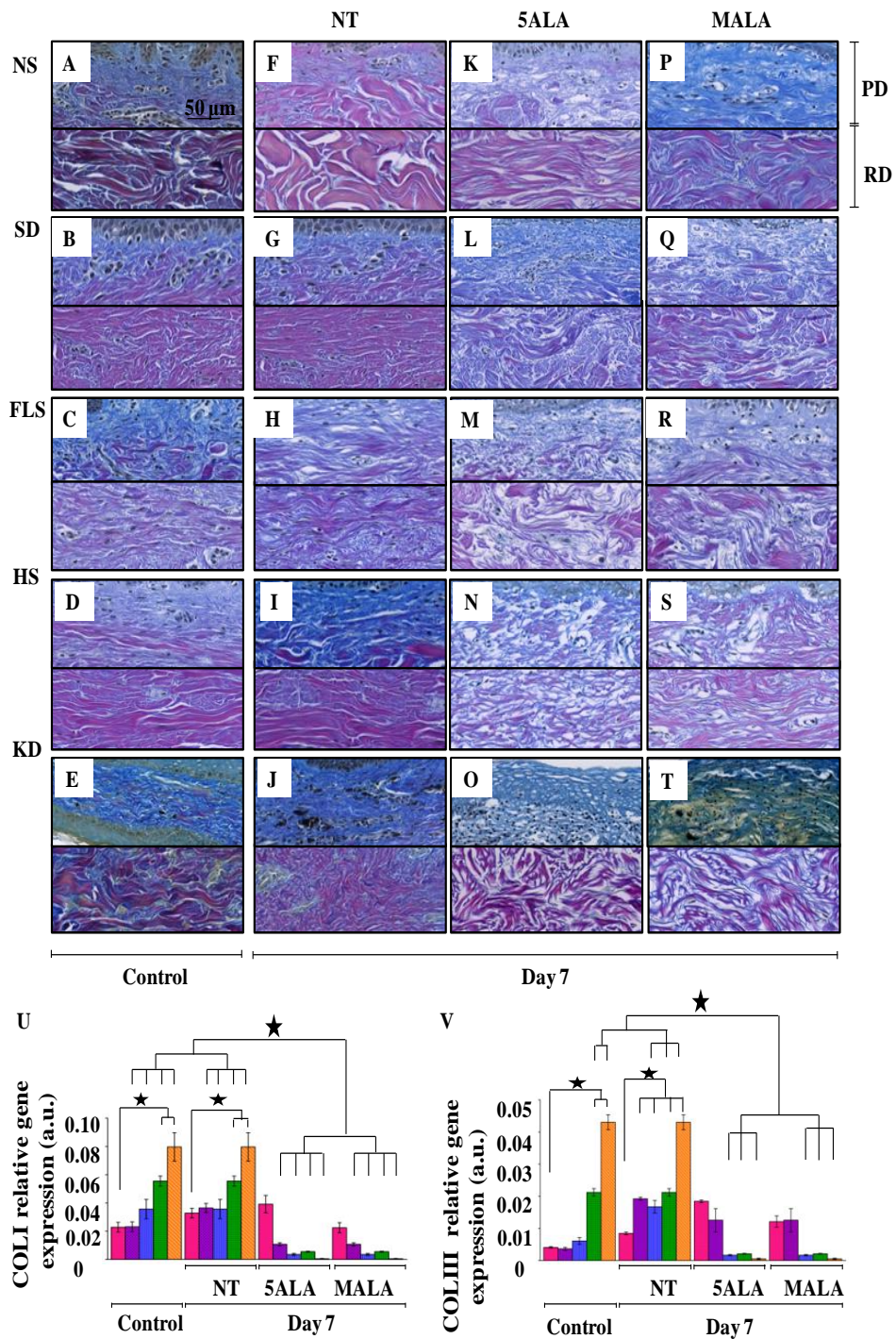


Figure 6.8 Collagen type I and collagen type III analysis. Morphological analysis by Herovici's differential staining of controls (day 0; A-E) compared to untreated controls (NT; F-J) and after aminolevulinic-acid (5ALA; K-O) aminolevulinic-acid methyl-ester (MALA; P-T) photodynamic therapy treatment. NS denotes normal skin ($n=4$), SD denotes striae alba ($n=6$), FLS denotes fine line scar, ($n=6$), HS denotes hypertrophic scar ($n=6$) and KD denotes keloid scar ($n=3$). PD represents papillary dermis and RD represents reticular dermis. Graphs represent genetic expression of normal skin ■, striae alba □, fine line scar ▲, hypertrophic scar ▢ and keloid scar ▣ of COLI (U) and COLIII (V). ★ Denotes statistically significant difference ($p < 0.05$). Mean and standar deviation between patients are represented.

3. MMP3 dermal expression significantly increased post-PDT

MMP3 histological expression was found to be significantly higher post-PDT in all samples, except in KD (Figure 6.9W). MMP3 gene expression showed significant differences between normal skin and dermal scars, the highest expression was found in hypertrophic scars post-PDT, however MMP3 gene expression was found to be similar after application of 5ALA compared with MALA-PDT treatment. The maximum MMP3 gene expression observed was found in HS, which increased approximately 4 fold compared to untreated control tissue on day 7 (Figure 6.9V).

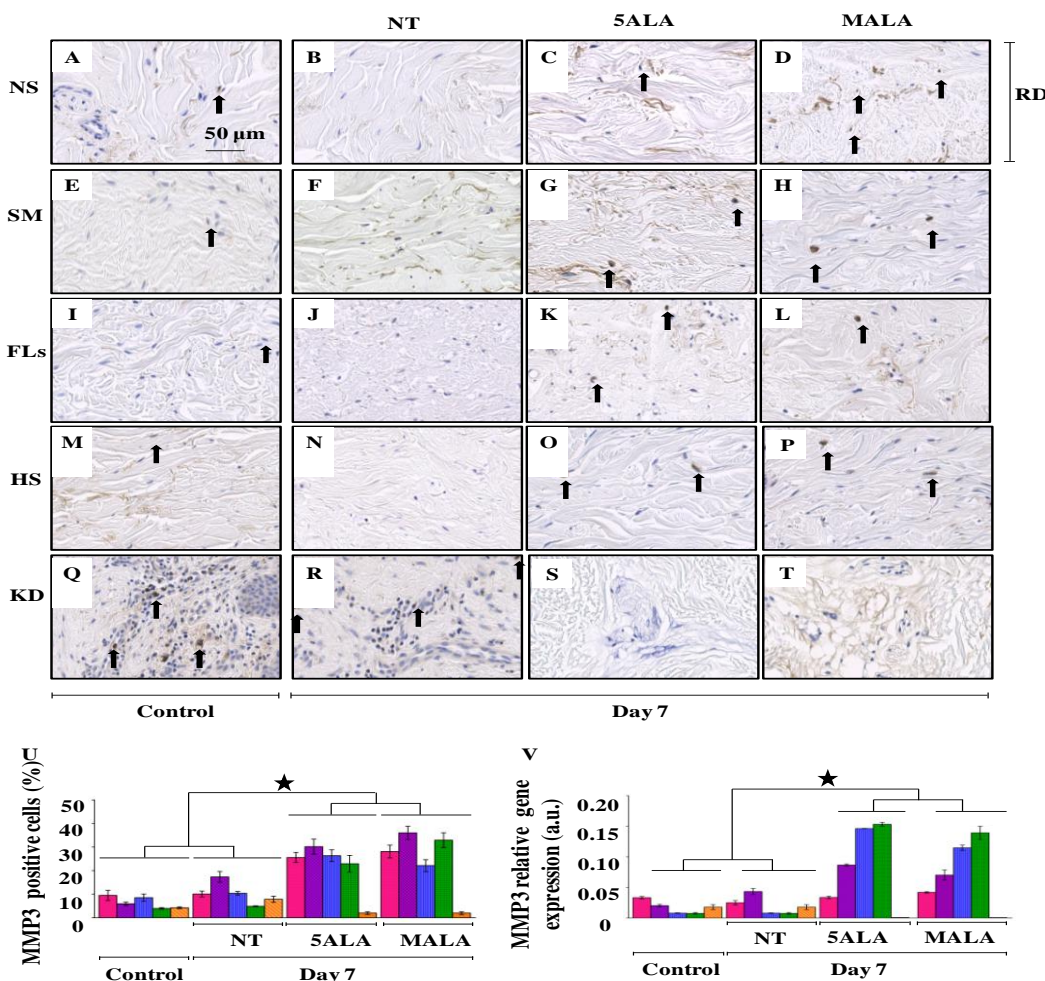


Figure 6.9 MMP3 analysis. MMP3-IHC (A-T). Graphs represent MMP3 positive cells quantification (U) and MMP3 genetic expression (W) of normal skin (■) ($n=4$), striae alba (■) ($n=6$), fine line scar (■) ($n=6$), hypertrophic scar (■) ($n=3$) and keloid scar (■) ($n=3$). ★ Denotes statistically significant difference ($p < 0.05$). Mean and standard deviation between patients are represented.

6.5 Discussion

In this study, we present for the first time, morphological and cellular effect of PDT in dermal fibrosis using our unique ex vivo scar model. This study provides evidence of effects of PDT in different phenotypical dermal scars and striae distensae. All dermal lesions were compared to normal skin and untreated controls. We also compared the effect of 5ALA compared with MALA-PDT.

We demonstrate that PDT affects both the epidermis and the dermis of skin scarring, however, the degree of damage to morphology and cellular content varied according to the exact type of dermal lesion. It became apparent that dermal lesions with higher or more severe degree of dermal fibrosis were affected most. Thus, least effect was observed in fine line scars and the most impact was visible in keloid scars. Additionally, apoptosis increased with increasing severity of dermal fibrosis. Moreover, proliferation decreased and correlated with severity of dermal fibrosis.

There was also a decrease in levels of PCNA gene expression, which matched the PCNA protein levels. ECM fibres, elastin and collagen were found degraded, especially in hypertrophic and keloid scars, while MMP3 expression was shown to be increased, except in KD where KD tissue was found to be extensively damaged. Overall, there was no significant difference between 5ALA and MALA-PDT application to all dermal lesions compared to control (Figure 6.10).

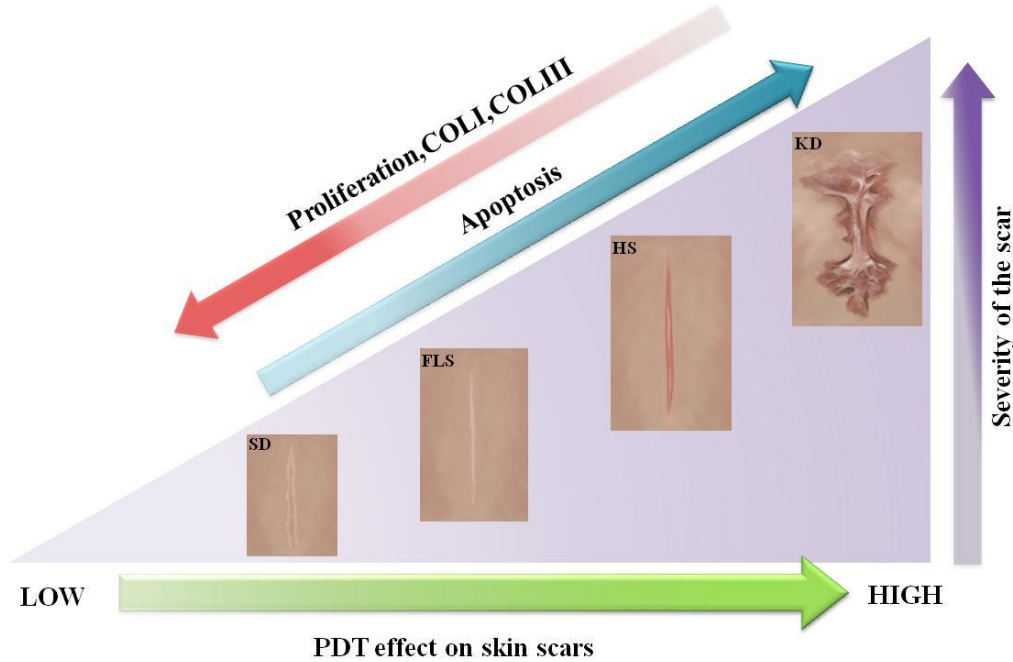


Figure 6.10 Schematic representation of the effects of PDT in phenotypically different skin scars. The lowest effect was observed in striae alba (SD), however the effect increased with increasing severity of the scar type from fine line (FLS), hypertrophic (HS) to keloid (KD). Keloid scar was affected most post-PDT. PDT effects on scars were compared with increased levels of apoptosis and decreased levels in proliferation.

In vitro oncological studies have shown that the effects of PDT varies according to cell type, inducing the most aggressive response according to the degree of cellular differentiation (Pahernik, et al., 1998). This means that from a spectrum of healthy cells to dysplastic and neoplastic cells, the latter would have the highest capacity to synthesize PpIX, from 5ALA or MALA (Wyld, et al., 2001). Here, we have identified increasing levels of PDT effect according to the severity of scar type. Keloid scars were the most affected dermal fibrotic scar. This would make sense as KD is considered to be the most aggressive type of raised dermal fibrotic scar, and considered to have quasi-neoplastic tendencies with keloid cells displaying cancer bioenergetics. This is also evident in the clinical behaviour of KD as it invades

healthy surrounding skin and is characterised by exuberant and proliferative production of distorted ECM (Shih, et al., 2010; Vincent, et al., 2008;).

Thus, keloid fibroblasts are likely to lead to higher ROS generation leading to a greater degree of effect being observed in keloid tissue post-PDT application. We previously demonstrated the effect of PDT in keloid fibroblasts in vitro and showed this to be site specific within the lesion, which correlated with the PpIX accumulation and ROS generation leading to decreased cytoproliferation and increased cell death (Mendoza, et al., 2012). A case report and a subsequent case series by our group also showed similar findings for the effect of PDT on KD (Nie, et al., 2010; Ud-Din, et al., 2013).

MMP3 levels had increased while COLI, COLIII levels decreased post-PDT in scar tissue. Similar results were found by Campbell et al. and Kerrer et al., whilst elastic fibres had been found to have a significant increase after 6-month post-PDT (Sakamoto, et al., 2012; Seo, et al., 2001). This suggested that the photodamage caused by PDT treatment may trigger elastic fibres neo-formation and remodelling of the ECM matrix, also previously suggested by Sanclement, et al., (2012). MMP3 participates actively in ECM remodelling throughout the wound healing process. MMP3 activates MMP1 and degrades fibronectin laminin and collagens III, IV, IX and X and is down-regulated in keloid tissue, suggesting dysregulated degradation of ECM at the remodelling stage (Seifert, et al., 2008; Seo, et al., 2001).

Here, we found compelling evidence of tissue degradation in dermal fibrosis caused by application of PDT. Application of PDT, can cause release of DAMPs, matrikines

and elastokins, which through paracrine communication trigger immunological alerts and MMPs activation, which in turn can induce tissue repair (Li, et al., 2010; Mills, et al., 2014; Volk, et al., 2013). Recently Mills et al. showed that MALA-PDT increases TGF- β 3, MMP1 and MMP9 leading to an improvement of ECM in human wound healing *in vivo*. Additionally a limited number of animal studies and routine dermatological practices have shown evidence of improvement in the cosmetic outcome and faster wound healing post-PDT, but precise molecular mechanisms still unknown (Mills, et al., 2014; Peplow, et al., 2012).

Therefore, the overall effect of PDT on tissue repair and remodelling, may be a combination of elimination of fibrosis and induction of tissue repair as had been demonstrated previously *in vivo* (Campbell, et al., 2010; Nie, et al., 2010; Sakamoto, et al., 2012).

In *vivo*, there is likely to be direct photodamage affecting keloid fibroblasts, in addition to activation of an immune response leading to elimination of fibrotic tissue. The limitations of this study include the total number of patients available to us to investigate, and the number of experimental parameters that were studied in relation to effect of PDT in dermal fibrosis. Certainly, further number of samples in a more comprehensive range of dermal scars including depressed scars, and striae rubra as well as more experimental options looking at the effect of PDT in fibrosis would be ideal in any future study. Similarly, further *in vivo* studies evaluating the optimal dosage, timing and frequency of PDT in different type of dermal scars with diligent follow up to ensure effective long term benefits with a lack of recurrence in the case of more severe dermal fibrosis, is recommended.

CHAPTER SEVEN: CONCLUSIONS AND SUGGESTIONS FOR FUTURE WORK

7.1 Conclusions

7.1.1 Conclusions for the effect of PDT in keloid fibroblasts.

Intracellular accumulation increases after two hours of exposure either with MALA or 5ALA, phototoxicity was found site-specific and dose-dependant, the most affected was the keloid fibroblast from the top however after illumination with 100 J/cm reach up to a maximum of 10% and significant different to normal fibroblasts. Post-PDT cytotoxicity was found dose-dependant and site-specific, margin-specific cells were the most cytotoxic following 10 J/cm² of MALA incubation, while they were less cytotoxic after 5ALA incubation under the same conditions. Cytoproliferation significantly decreases after 40 J/cm², either with MALA or 5ALA as precursor. Apoptosis and necrosis were present post-PDT, but at higher fluence increases necrosis. Senescence was found only after low dose of PDT (10 J/cm²) and increases significantly in keloid fibroblasts from the middle. Generation of ROS correlates with the increases in accumulation of PpIX and increase of cytotoxicity and decreases of Cytoproliferation. Genes related with keloid pathogenesis as COLI, COLIII were found down-regulated. Since the efficacy of PDT depends on intracellular PpIX localisation and accumulation leading to ROS generation, fluence should be customised in accordance with the precursor of photosensitiser for KD

treatment. For example, 40 J/cm² post 5ALA treatment is more effective for middle-specific keloid cells while 20 J/cm² post MALA treatment is more effective for other sites. Since cytotoxicity has only been determined in the cell monolayer culture, an extrapolation of fluence to an ex vivo tissue microenvironment is necessary to optimise the parameters. This study has demonstrated, for the first time, that cytotoxicity post-PDT in keloid fibroblasts can vary depending on the site in a keloid lesion, the precursors of intracellular photosensitiser, accumulation of PpIX and the light energy delivered per unit area. These findings demonstrate a potential future application for site-targeted therapy in the treatment of KD. Based on the fluorometric cytotoxicity and proliferation results, esterified forms of 5ALA would be more efficacious than 5ALA and may induce higher cytotoxicity in margin-specific keloid cells.

7.1.2 Conclusions for the effect of PDT in an optimized ex vivo adult human wound healing model

This study presents an optimised organ culture of human skin wounded ex vivo, which offers a useful model for investigating the process of cutaneous repair and enables evaluation of candidate therapeutic agents. Wound closure was significantly higher in wounds of 1 mm regardless of geometry; however partial thickness wounds were closed taking into account the system of support and growth media, showing that skin ex vivo retains its elastic properties to some extent.

The system of support shows the impact on ECM arrangement, so further investigation regarding physical support is required in order to preserve skin tensegrity and without disruption of nutrients and oxygen distribution. WHOCs of partial thickness embedded in collagen and supplemented DMEM were better organized, showing stratified epidermis and compact dermis with developing neo-epidermis; this suggested the need of a dermal template in ex vivo wound healing in full thickness wound above 1mm. Feeding the dermal layer maintains epidermal viability and stratification better than feeding both dermis and epidermis.

WHOC treated with PDT shows increased re-epithelialization and ECM reconstruction and remodelling. The advancing re-epithelialization tongue was 3.5 folds longer and highly proliferative, with CK14 and p16 increased ($p<0.05$) compared to controls. The neo-epidermis was fully differentiated and neo-collagen formed. PCNA, p16, COLI, COLIII, MMP3, MMP19 and α -SMA were significantly more expressed ($p<0.05$) in dermis surrounding the healing wound than control WHOCs. These findings suggest that PDT improves wound healing in adult human skin, for the first time, demonstrating that PDT increases re-epithelialization and ECM reconstruction and remodelling in this unique wound model.

7.1.3 Conclusions for the effect of PDT in skin scarring

The effects of PDT on skin scars and striae distensae were studied in an ex vivo model. MALA-PDT as compared to 5ALA-PDT shows no statistically significant

difference. Epidermal apoptotic cells consistently increased while proliferation and PCNA expression decreased. ECM fibres were found degraded, especially in hypertrophic and keloid scars. COLI and COLIII gene expression decreased while MMP3 and ELN increased post-PDT significantly, compared to normal skin and untreated controls ($p<0.05$). It was shown for the first time, using the unique ex vivo organ culture model of human skin scarring developed that morphological and cellular effects of PDT correlate with the degree and severity of dermal fibrosis. In view of this, PDT may be ideal in targeted treatment of abnormal skin scarring. Nevertheless,

7.2 Suggestions for future work

7.2.1 Role of PDT in keloid diseases

Keloid disease is a heterogeneous condition; for this reason should be investigated if photodynamic therapy effects vary in relation with the size, deepness and age of the scar. Likewise sex, race and age of the affected patient should be considered in future studies. PDT induces apoptotic cell death in keloid fibroblasts, however if mitochondrial damage is involved still unknown. Similar appearance of necrotic death suggests the affection of membranes, but the precise mechanism still unknown. Additionally apoptotic and necrotic death, still unknown in autophagy also appears post-PDT in keloid fibroblasts. The current investigation was limited by the number of patients and molecules of interest studied, so increasing these numbers will provide a better understanding of the mechanisms affected by PDT, with the ultimate

impact being the development of an efficient treatment for people suffering from keloids.

7.2.2 Role of PDT in wound healing using ex vivo models

WHOC has a limited lifespan, so it is needed to improve the maintenance methods as physical support, growth media and culture conditions. Wound healing response varies according to the characteristics of the initial injury, so the effect of PDT in injuries with different characteristics should be studied. Wound healing involves the differential expression of several biomolecules as growth factor, still unknown its expression post-PDT ex vivo. Increasing the molecules studied related to wound healing ex vivo and post-PDT is needed, in order to increase understanding of both. Further work is required to determine the best point in the wound healing process to apply PDT, in order to improve and speed the process and avoid any contrary effects, as well further validation in vivo.

7.2.3 Role of PDT in skin scars and striae distensae using ex vivo models

Application of PDT requires further validation in vivo in order to determine its dosage, frequency and timing as well as whether it's most effective in isolation or in combination with other treatment modalities such as pre- or post-surgical excision of dermal fibrotic scars. This study has focused on a limited number of scar types and one type of striae, but there are still others, such as intermediate scars and striae rubra, where the use of PDT has not yet been investigated.

PUBLICATIONS

PUBLISHED

“Differential cytotoxic response in keloid fibroblasts exposed to photodynamic therapy is dependent on photosensitiser precursor, fluence and location of fibroblasts within the lesion”. Mendoza J, Sebastian A, Allan E, Allan D, Mandal P, Alonso-Rasgado T, Bayat A. Archives of Dermatological Research. 2012; 304(7): 549-562.

“Optimization of an ex vivo wound healing model in the adult human skin: functional evaluation using photodynamic therapy”. Mendoza J, Sebastian A, Alonso-Rasgado T, Bayat A. Wound repair and Regeneration. 2015; Jun 10. doi: 10.1111/wrr.12325

“Ex vivo evaluation of the effect of photodynamic therapy on skin scars and striae distensae”. Mendoza J, Sebastian A, Alonso-Rasgado T, Bayat A. Photodermatology, Photoimmunology & Photomedicine. 2015; Sep;31(5):239-51. doi: 10.1111/phpp.12180. Epub 2015 Jun 1

POSTER PRESENTATIONS

“Photodynamic therapy increases cytotoxicity in site-specific keloid fibroblasts”. Mendoza J, Sebastian A, Allan E, Allan D, Mandal P, Alonso-Rasgado T, Bayat A. 22nd Annual Meeting of the Wound Healing Society. Atlanta, United States of America 2012.

“Enhanced re-epithelialisation and cell proliferation in a novel ex vivo donut model skin wound by photodynamic therapy”. Mendoza J, Sebastian A, Alonso-Rasgado T, Bayat A. 22nd European Tissue Repair Society Meeting (ETRS). Athens, Greece 2012.

“Ex-vivo verification with histology of the effect of photodynamic therapy in reduction of keloid scar”. Mendoza J, Sebastian A, Alonso-Rasgado T, Bayat A. 22nd European Tissue Repair Society Meeting (ETRS). 23rd Wound Healing Society. Denver, United States of America 2013.

“Low energy dose photodynamic therapy alters skin architecture of striae distensae”. Mendoza J, Sebastian A, Alonso-Rasgado T, Bayat A. 23rd Wound Healing Society Annual Meeting. Denver, United States of America 2013.

“Development and optimisation of ex-vivo human skin organ cultures for long-term wound healing studies”. Mendoza J, Sebastian A, Alonso-Rasgado T, Bayat A. Mendoza J, Sebastian A, Alonso-Rasgado T, Bayat A. 23rd Wound Healing Society Annual Meeting. Denver, United States of America 2013.

REFERENCES

- Aalders MC, van de Vange N, Star WM, Sterenborg HJ. (2001). A Mathematical evaluation of dose-dependent PpIX fluorescence kinetics In vivo. *Photochem Photobiol* 74(2): 311-317.
- Agren MS, Danielsen PL. (2014). Antiscarring pharmaceuticals: lost in translation? *Wound Repair Regen* 22(3): 293-294.
- Akaishi S, Akimoto M, Ogawa R, Hyakusoku H. (2008). The relationship between keloid growth pattern and stretching tension: visual analysis using the finite element method. *Ann Plast Surg* 60(4): 445-451.
- Akasaka Y, Ishikawa Y, Ono I, Fujita K, Masuda T, Asuwa N, et al. (2000). Enhanced expression of caspase-3 in hypertrophic scars and keloid: induction of caspase-3 and apoptosis in keloid fibroblasts in vitro. *Lab Invest* 80(3): 345-357.
- Al-Himdani S, Ud-Din S, Gilmore S, Bayat A. (2014). Striae distensae: a comprehensive review and evidence-based evaluation of prophylaxis and treatment. *Br J Dermatol* 170(3): 527-547.
- Alberts B, Johnson A, Lewis J, Raff M, Roberts K, Walter P. (2002). Molecular biology of the cell. New York, Garland Science
- Alfaro MP, Deskins DL, Wallus M, DasGupta J, Davidson JM, Nanney LB, et al. (2013). A physiological role for connective tissue growth factor in early wound healing. *Lab Invest* 93(1):81-95.
- Allison RR, Sibata CH. (2010). Photodynamic therapy: mechanism of action and role in the treatment of skin disease. *G Ital Dermatol Venereol* 145(4): 491-507.
- Almeida-Issa MC, Piñeiro-Maceira J, Farias RE, Pureza M, Luiz R, Manela-Azulay M. (2009). Immunohistochemical expression of matrix metalloproteinases in photodamaged skin by photodynamic therapy. *Br J Dermatol* 161(3): 647-653.
- ALTEX (2013). EU: final ban on animal experiments for cosmetic ingredients implemented. *ALTEX* 30(2): 268-269.
- Ben Amar M, Wu M. (2014). Re-epithelialization: advancing epithelium frontier during wound healing. *J R Soc Interface* 11(93): doi: 10.1098/rsif.2013.1038.
- Andreadis ST. (2007). Gene-modified tissue-engineered skin: the next generation of skin substitutes *Adv Biochem Eng Biotechnol* 103: 241-274.
- Angell-Petersen E, Sørensen R, Warloe T, Soler AM, Moan J, Peng Q, et al. (2006). Porphyrin formation in actinic keratosis and basal cell carcinoma after topical application of methyl 5-aminolevulinate. *J Invest Dermatol* 126(2): 265-271.
- Antony AK, Kong W, Lorenz HP. (2010). Upregulation of Neurodevelopmental genes during scarless healing. *Ann Plast Surg* 64(2):247-250.

- Arany PR, Flanders KC, Kobayashi T, Kuo CK, Stuelten C, Desai KV, et al. (2006). Smad3 deficiency alters key structural elements of the extracellular matrix and mechanotransduction of wound closure. *Proc Natl Acad Sci USA* 103(24): 9250-9255.
- Atif M, Firdous S, Khurshid A, Noreen L, Zaidi SSZ, and Ikram M. (2009). In vitro study of 5-aminolevulinic acid-based photodynamic therapy for apoptosis in human cervical HeLa. Cell line. *Laser Phys Lett* 12: 886-891.
- Bagabir R, Syed F, Paus R, Bayat A. (2012). Long-term organ culture of keloid disease tissue. *Exp Dermatol* 21(5): 376-381.
- Bagabir R, Syed F, Rautemaa R, McGrouther DA, Pas R, Bayat A. (2011). Up-regulation of Toll-like receptors (TLRs) 6, 7, and 8 in keloid scars. *J Invest Dermatol* 131(10): 2128-2130.
- Bainchi ME. (2007). DAMPs, PAMPs and alarmins: all we need to know about danger. *J Leukic Biol* 81(1): 1-5.
- Baker H. (1989). Clinical dermatology. London, Bailliere London.
- Baker M. (2011). Tissue models: a living system on a chip. *Nature* 471(7340): 661-665.
- Balaji S, Moles CM, Bhattacharya SS, LeSaint M, Dhamija Y, Le L, et al. (2014). Comparison of interleukin 10 homologous on dermal wound healing using a novel human skin ex vivo organ culture model. *J Surg Res* 90(1): 358-366.
- Basdew H, Mehilal R, Al-Mamgani A, van Rooij P, Bhawanie A, Sterenborg HJCM, et al. (2013). Adjunctive treatment of keloids: comparison of photodynamic therapy with brachytherapy. *Eur J Plast Surg* 36(289-294).
- Bayat A, McGrouther DA, Ferguson MW. (2003). Skin scarring *BMJ* 326(7380): 88-92.
- Beanes SR, Dang C, Soo C, Ting K. (2003). Skin repair and scar formation: the central role of TGF-beta. *Expert Rev Mol Med* 5(8): 1-22.
- Berking C, Hegyi J, Arenberger P, Ruzicka T, Jemec GB. (2009). Photodynamic therapy of necrobiosis lipoidica--a multicenter study of 18 patients. *Dermatology* 218(2): 136-139.
- Bjerring P, Christiansen K. (2011). Photodynamic Therapy in Dermatology. Fluorescence-Guided Photodynamic Therapy. M. Gold. New York, Springer.
- Blanpain C, Fuchs E. (2009). Epidermal homeostasis: a balancing act of stem cells in the skin. *Nat Rev Moll Cell Biol* 10(3): 207-217.
- Blazić TM, Brajac I. (2006). Defective induction of senescence during wound healing is a possible mechanism of keloid formation. *Med Hypotheses* 3(649-652).

Blázquez-Castro A, Carrasco E, Calvo MI, Jaénc P, Stockert JC, Juarranza A, et al. (2012). Protoporphyrin IX-dependent photodynamic production of endogenous ROS stimulates cell proliferation. *Eur J Cell Biol* 91(3): 216-223.

Blumenberg M. (2006). DNA microarrays in dermatology and skin biology. *OMICS* 10(3): 243-260.

Böttcher-Haberzeth S, Biedermann T, Reichmann E. (2010). Tissue engineering of skin. *Burns* 36(4): 450-460.

Bouzari N, Davis SC, Nouri K. (2007). Laser treatment of keloids and hypertrophic scars. *Int J Dermatol* 46(1):80-8.

van de Broek LJ, Limandjaja GC, Niessen FB, Gibbs S. (2014). Human hypertrophic and keloid scar models: principles, limitations and future challenges from a tissue engineering perspective. *Exp Dermatol* 23(6): 382-386.

Brohem CA, Cardeal LB, Tiago M, Soengas MS, Barros SB, Maria-Engler SS. (2010). Artificial skin in perspective: concepts and applications. *Pigment Cell Melanoma Res* 24(1): 35-50.

Brooker C (1998) Human Structure and Function: Nursing Applications in Clinical Practice. Second edition. Mosby Elsevier, London.

Brown BC, Moss MT, McGrouther DA, Bayat A. (2010). Skin scar preconceptions must be challenged: importance of self-perception in skin scarring. *J Plast Reconstr Aesthet Surg* 63(6): 1022-1029.

Bruscino N, Lotti T, Rossi R. (2011). Photodynamic therapy for a hypertrophic scarring: a promising choice. *Photodermatol Photoimmunol Photomed* 27(6): 334-335.

Bryan N, Ahswin H, Smart N, Bayon Y, Wohlert S, Hunt JA. (2012). Reactive oxygen species (ROS)--a family of fate deciding molecules pivotal in constructive inflammation and wound healing. *Eur Cell Mater* 24(24): 249-265.

Buffoli B, Rinaldi F, Labanca M, Sorbellini E, Trink A, Guanziroli E, et al. (2014). The human hair: from anatomy to physiology. *Int J Dermatol* 53(3): 331-341.

Bush JA, Ferguson MW, Mason T, McGrouther DA. (2005). Skin tension or skin compression? Small circular wounds are likely to shrink, not gape. *J Plast Reconstr Aesthet Surg* 61(5): 529-534.

Butler PD, Longaker MT, Yang GP. (2008). Current progress in Keloid research and treatment. *J Am Coll Surg* 206(4): 731-742.

Butler PD, Ly DP, Longaker MT, Yang GP. (2008). Use of organotypic coculture to study keloid biology. *Am J Surg* 195(2): 144-148.

Cai H, Gu Y, Sun Q, Zeng J, Dong N, Zhao G. (2011). Effect of hematoporphyrin monomethyl ether-mediated photodynamic therapy on hypertrophic scar fibroblasts. *Photodermatol Photoimmunol Photomed* 27(2): 90-96.

Calzavara-Pinton PG, Rossi MT, Aronson E, Sala R, Italian Group for Photodynamic Therapy. (2013). Retrospective analysis of real-life practice of off-label photodynamic therapy using methyl aminolevulinate (MAL-PDT) in 20 Italian dermatology departments. Part 1: inflammatory and aesthetic indications. *Photochem Photobiol* 12(1): 148-157.

Campbell SM, Tyrrell J, Marshall R, Curnow A. (2010). Effect of MAL-photodynamic therapy on hypertrophic scarring. *Photodiagnosis Photodyn Ther* 7(3): 183-188.

Campisi J, Robert L. (2014). Cell senescence: role in aging and age-related diseases. *Interdiscip Top Gerontol* 39:45-61.

Carmichael SW. (2014), The tangled web of Langer's lines. *Clin Anat* 27(2):162-8.

Casas A, Fukuda H, Di Venosa G, Battle A. (2001) Photosensitization and mechanism of cytotoxicity induced by the use of ALA derivates in photodynamic therapy. *Br J Cancer* 85(2):279–284.

Castano AP, Demidova TN, Hamblin MR. (2004). Mechanisms in photodynamic therapy: part one-photosensitizers, photochemistry and cellular localization. *Photodiagnosis Photodyn Ther* 1(4): 279-293.

Castano AP, Demidova TN, Hamblin MR. (2005). Mechanisms in photodynamic therapy: part two-cellular signalling, cell metabolism and modes of cell death. *Photodiagnosis Photodyn Ther* 2(1): 1-23.

Chakraborti S, Mandal M, Das S, Mandal A, Chakraborti T. (2003). Regulation of matrix metalloproteinases: an overview. *Mol Cell Biochem* 253(1-2): 269-285.

Chaudhuri V, Karasek M. (2006). Mechanisms of microvascular wound repair II. Injury induces transformation of endothelial cells into myofibroblasts and the synthesis of matrix proteins. *In vitro Cell Dev Biol Anim* 42(10): 314-319.

Chiu LL, Sun CH, Yeh AT, Torkian B, Karamzadeh A, Tromberg B, et al. (2005). Photodynamic therapy on keloid fibroblasts in tissue-engineered keratinocyte-fibroblast co-culture. *Lasers Surg Med* 37(3): 231-244.

Choi Y, Hong H, Kim B, Kim M, Park H. (2008). Development of non-invasive measurement system to the thickness of the subcutaneous adipose tissue layer. *Exp Dermatol* 17: 537-541.

Christensen E, Warloe T, Kroon S, Funk J, Helsing P, Soler AM, et al. (2010). Guidelines for practical use of MAL-PDT in non-melanoma skin cancer. *J Eur Acad Dermatol Venereol* 24(5): 505-501.

Companjen AR, van der Wel LI, Wei L, Laman JD, Prens EP. (2001). A modified ex vivo skin organ culture system for functional studies. *Arch Dermatol Res* 293(4): 184-190.

Coolen NA, Schouten KC, Boekema BK, Middelkoop E, Ulrich MM. (2010). Wound healing in a fetal, adult, and scar tissue model: A comparative study. *Wound Rep Reg* 18(3): 294-301.

Definiens Documentation: Tissue Studio® 3.5, © 2012 Definiens AG. München, Germany.

Dewaele M, Martinet W, Rubio N, Verfaillie T, de Witte PA, Piette J., et al. (2011). Autophagy pathways activated in response to PDT contribute to cell resistance against ROS damage. *J Cell Mol Med* 15(6): 1402-1414.

Dunkin CS, Pleat JM, Gillespie PH, Tyler MP, Roberts AH, McGrouther DA. (2007). Scarring occurs at a critical depth of skin injury: precise measurement in a graduated dermal scratch in human volunteers. *Plast Reconstr Surg* 119(6): 1722-1732.

Duong HS, Zhang Q, Kobi A, Le A, Messadi DV. (2005). Assessment of morphological and immunohistological alterations in long-term keloid skin explants. *Cells Tissues Organs* 181(2): 89-102.

Eckes B, Nischt R, Krieg T. (2010). Cell-matrix interactions in dermal repair and scarring. *Fibrogenesis Tissue Repair* 11(3): 4.

Ehrlich HP, Buttle DJ. (1984). Epidermis promotion of collagenase in hypertrophic scar organ culture. *Exp Mol Pathol* 40(2): 223-234.

Adb Elmageed ZY, Gaur RL, Williams M, Abdraboh ME, Rao PN, Raj MH, et al. (2009). Characterization of Coordinated Immediate Responses by p16INK4A and p53 Pathways in UVB-Irradiated Human Skin Cells. *J Invest Dermatol* 129(1): 175-183.

Fearmonti R, Bonde J, Erdmann D, Levinson H. (2010). A Review of scar scales and scar measuring devices. *eplasty* 10: e43.

Ferreira LM, Gragnani A, Furtado F, Hochman B. (2009). Control of the skin scarring response. *An Acad Bras Cienc* 81(3): 623-629.

Fu X, Fang L, Li H, Li X, Cheng B, Sheng Z. (2007). Adipose tissue extract enhances skin wound healing. *Wound Repair Regen* 15(4): 540-548.

Fritsch C, Verwohlt B, Bolsen K, Ruzicka T, Goerz G. (1996). Influence of topical photodynamic therapy with 5-aminolevulinic acid on porphyrin metabolism. *Arch Dermatol Res* 288(9): 517-521.

Garg AD, Nowis D, Golab J, Agostinis P. (2010). Photodynamic therapy: illuminating the road from cell death towards anti-tumour immunity. *Apoptosis* 15(9): 1050-1071.

Garrier J, Bezdetnaya L, Barlier C, Gräfe S, Guillemin F, D'Hallewin MA. (2011). Foslip®-based photodynamic therapy as a means to improve wound healing. *Photodiagnosis Photodyn Ther* 8(4): 321-327.

Gattazzo F, Urciuolo A, Bonaldo P. (2014). Extracellular matrix: a dynamic microenvironment for stem cell niche. *Biochim Biophys Acta* 1840(8): 2506-2519.

Ghahary A, Ghaffari A. (2007). Role of keratinocyte-fibroblast cross-talk in development of hypertrophic scar. *Wound Repair Regen* 15(Suppl 1): S46-S53.

Ghazizadeh S, Taichman LB. (2005). Organization of stem cells and their progeny in human epidermis. *J Invest Dermatol* 124(2): 367-372.

Gold MH, McGuire M, Mustoe TA, Pusic A, Sachdev M, Waibel J, et al. (2014) Updated international clinical recommendations on scar management: part 2--algorithms for scar prevention and treatment. *Dermatol Surg* 40(8):825-831.

Goodman GJ, Baron JA. (2006). Postacne scarring: a qualitative global scarring grading system. *Dermatol Surg* 32(12): 1458-1466.

Groeber F, Holeiter M, Hampel M, Hinderer S, Schenke-Layland K. (2012). Skin tissue engineering- In vivo and in vitro applications. *Clin Plast Surg* 39(1): 33-58.

Gröne A. (2002). Keratinocytes and cytokines. *Vet Immunol Immunopathol* 88(1-2): 1-12.

Gurtner GC, Dauskardt RH, Wong VW, Bhatt KA, Wu K, Vial IN, et al. (2011). Improving Cutaneous Scar Formation by Controlling the Mechanical Environment. *Ann Surg* 254(2): 217-225.

Hadjipanayi E, Mudera V, Brown RA. (2009). Close dependence of fibroblast proliferation on collagen scaffold matrix stiffness. *J Tissue Eng Regen Med* 3(2): 77-84.

Hance MW, Nolan KD, Isaacs JS. (2014). The double-edged sword: conserved functions of extracellular hsp90 in wound healing and cancer. *Cancer (Basel)* 6(2): 1065-1097.

Harris KL, Bainbridge NL, Jordan NR, Sharpe JR. (2009). The effect of topical analgesics on ex vivo skin growth and human keratinocyte and fibroblast behaviour. *Wound Repair Regen* 17(3): 340-346.

He J, Whitacre CM, Xue LY, Berger NA, Oleinick NL. (1998). Protease activation and cleavage of poly (ADP-ribose) polymerase: an integral part of apoptosis response to photodynamic therapy. *Cancer Res* 58(5); 940-946.

- Heng MC. (2011). Wound healing in adult skin: aiming for perfect regeneration. *Int J Dermatol* 50(9):1058-66.
- Hinz B. (2007). Formation and function of the myofibroblast during tissue repair. *J Invest Dermatol* 127(3): 526-537.
- Holick M. (1998). Vitamin D Requirements for Humans of All Ages: New Increased Requirements for Women and Men 50 years and Older. *Osteoporos Int* 2(Suppl 2): S24-29.
- Hollywood KA, Maatje M, Shadi IT, Henderson A, McGrouther DA, Goodacre R, et al. (2010). Phenotypic profiling of keloid scars using FT-IR microspectroscopy reveals a unique spectral signature. *Arch Dermatol Res* 302(10): 705-715.
- Huang C, Ogawa R. (2012). Fibroproliferative disorders and their mechanobiology. *Connect Tissue Res* 53(3): 187-196.
- Hussain SH, Limthongkul B, Humphreys TR. (2013). The biomechanical properties of the skin. *Dermatol Surg* 39(2): 193-203.
- Hwa C, Bauer EA, Cohen DE. (2011). Skin biology. *Dermatol Ther* 24(5): 464-470.
- Inoue K, Aoi N, Sato T, Yamauchi Y, Suga H, Eto H, et al. (2009). Differential expression of stem-cell-associated markers in human hair follicle epithelial cells. *Lab Invest* 89(8): 844-856.
- Jablonski NG. (2004). The evolution of human skin and skin colour *Annu Rev Anthropol* 33: 585-623.
- Javad F, Day PJ. (2012). Protein profiling of keloid scar tissue. *Arch Dermatol Res* 304(7): 533-540.
- Jayasree RS, Gupta AK, Rathinam K, Mohanan PV, Mohanty M. (2001). The influence of photodynamic therapy on the wound healing process in rats. *J Biomater Appl* 15(3): 176-186.
- Ji HT, Chien LT, Lin YH, Chien HF, Chen CT. (2010). 5-ALA mediated photodynamic therapy induces autophagic cell death via AMP-activated protein kinase. *Mol Cancer* 28(9): 91.
- Ji Z, Yang G, Vasovic V, Cunderlikova B, Suo Z., Nesland JM, et al. (2006). Subcellular localization pattern of protoporphyrin IX is an important determinant for its photodynamic efficiency of human carcinoma and normal cell lines. *J Photochem. Photobiol B* 84(3): 213-220.
- Junker JP, Philip J, Kiwanuka E, Hackl F, Caterson EJ, Eriksson E. (2014). Assessing quality of healing in skin: review of available methods and devices. *Wound Repair Regen Suppl* 1: 2-10.
- Kajiya H, Tanaka N, Inazumi T, Seyama Y, Tajima S, Ishibashi A. (1997). Cultured human keratinocytes express tropoelastin. *J Invest Dermatol* 109(5): 641-644.

Katnitakis J. (2002). Anatomy, histology and immunohistochemistry of normal human skin. *Eur J Dermatol* 12(4): 390-399.

Kawahira K. (1999). Immunohistochemical staining of proliferating cell nuclear antigen (PCNA) in malignant and nonmalignant skin diseases. *Arch of Dermatol Res* 291(7-8): 413-418.

Kerrer S, Bosserhoff AK, Weiderer P, Landthaler M, Szeimies RM. (2004). Keratinocyte-derived cytokines after photodynamic therapy and their paracrine induction of matrix metalloproteinases in fibroblasts. *Br J Dermatol* 151(4): 776-783.

Kessel D, Luo Y, Deng Y, Chang CK. (1997). The role of subcellular localization in initiation of apoptosis by photodynamic therapy. *Photochem Photobiol* 65(3): 422-426.

van Kilsdonk JW, van den Bogaard EH, Jansen PA, Bos C, Bergers M, Schalkwijk J. (2013). An in vitro wound healing model for evaluation of dermal substitutes. *Wound Repair Regen* 21(6): 890-896.

Kim CH, Chung CW, Choi KH, Yoo JJ, Kim do H, Jeong YI, et al. (2011). Effect of 5-aminolevulinic acid-based photodynamic therapy via reactive oxygen species in human cholangiocarcinoma cells. *Int J Nanomedicine* 6: 1357-1363.

Klein J, Permana PA, Owecki M, Chaldakov GN, Böhm M, Hausman G, et al. (2007). What are subcutaneous adipocytes really good for? *Exp Dermatol* 16(1): 45-70.

Koskela A, Engström K, Hakelius M, Nowinski D, Ivarsson M. (2010). Regulation of fibroblast gene expression by keratinocytes in organotypic skin culture provides possible mechanisms for the antifibrotic effect of reepithelialization. *Wound Repair Regen* 18(5): 452-459.

Kowal-Vern A, Criswell B. (2005). Burn scar neoplasms: a literature review and statistical analysis. *Burns* 31(4): 403-413.

Kratz G. (1998). Modeling of Wound Healing Processes in Human Skin Using Tissue Culture. *Microsc Res Tech* 1(42): 345-344.

Lam M, Oleinick NL, Nieminen AL (2001). Photodynamic therapy-induced apoptosis in epidermoid carcinoma cells. Reactive oxygen species and mitochondrial inner membrane permeabilization. *J Biol Chem* 276(50): 47379-47386.

LeBleu VS, Macdonald B, Kalluri R. (2007). Structure and function of basement membranes. *Exp Biol Med (Maywood)* 232(9): 1121-1129.

Lebonvallet N, Jeanmaire C, Danoux L, Siblette P, Pauly G, Misery L. (2010). The evolution and use of skin explants: Potential and limitations for dermatological research. *Eur J Dermatol* 20(6): 671-684.

Lee JB, Choi JY, Chun JS, Yun SJ, Lee SC, Oh J, Park HR (2008). Relationship of protoporphyrin IX synthesis to photodynamic effects by 5-aminolaevulinic acid and its esters on various cell lines derived from the skin. *Br J Dermatol* 159(1): 61-67.

Levame M, Meyer F. (1986). The picropolyochrome of Herovici: application in the identification of collagen types I and III. *Pathol Biol* 35:1183-8.

Li F, Huang Q, Chen J, Peng Y, Roop DR, Bedford JS, et al. (2010). Apoptotic cells activate the "phoenix rising" pathway to promote wound healing and tissue regeneration. *Sci Signal* 23(3): 110-113.

Li X, Zhou ZP, Hu L, Zhang WL, Li W. (2014). Apoptotic cell death induced by 5-aminolaevulinic acid-mediated photodynamic therapy of hypertrophic scar-derived fibroblasts. *J Dermatolog Treat* 25(5): 428-433.

Lin JY, Fisher DE. (2007). Melanocyte biology and skin pigmentation. *Nature* 445(7130): 843-850.

Lopes LB, Furnish EJ, Komalavilas P, Flynn CR, Ashby P, Hansen A, et al. (2009). Cell Permanent Peptide Analogues of the Small Heat Shock Protein, HSP20, Reduce TGF-b1-Induced CTGF Expression in Keloid Fibroblasts. *J Invest Dermatol* 129(3): 590-598.

Luo S, Benathan M, Raffoul W, Panizzon RG, Egloff DV. (2001). Abnormal balance between proliferation and apoptotic cell death in fibroblasts derived from keloid lesions. *Plast Reconstr Surg* 107(1): 87-96.

Macdonald I, Dougherty T. (2001). Basic principles of photodynamic therapy. *J Porphyr Phthalocyanines* 5(105): 3228.

MacNeil S. (2007). Progress and opportunities for tissue-engineered skin. *Nature* 445(7130): 874-880.

Maquart FX, Monboisse JC (2014). Extracellular matrix and wound healing. *Pathol Biol (Paris)* 62(2):91-5.

Martins VL, Caley M, O'Toole EA. (2013). Matrix metalloproteinases and epidermal wound repair. *Cell Tissue Res* 351(2): 255-268.

Materazzi S, Pellerito S, Di Serio C, Paglierani M, Naldini A, Ardinghi C, et al. (2007). Analysis of protease-activated receptor-1 and -2 in human scar formation. *J Pathol* 212(4): 440-449.

Mathes SH, Ruffner H, Graf-Hausner U. (2014). The use of skin models in drug development. *Adv Drug Deliv Rev* 69-70: 81-102.

McCarty SM, Cochrane CA, Clegg PD, Percival SL. (2012). The role of endogenous and exogenous enzymes in chronic wounds: A focus on the implications of aberrant

levels of both host and bacterial proteases in wound healing. *Wound Repair Regen* 20(2): 125-136.

McKee P. (1999). Essential skin Pathology. London, Mosby.

McLafferty E, Hendry C, Alistair F. (2012). The integumentary system: anatomy, physiology and function of skin. *Nurs Stand* 19-25(3): 35-42.

Medrado AP, Soares AP, Santos ET, Reis SR, Andrade ZA. (2008). Influence of laser photobiomodulation upon connective tissue remodelling during wound healing. *J Photochem Photobiol B* 29(3): 144-152.

Mendoza J, Sebastian A, Allan E, Allan D, Mandal P, Alonso-Rasgado T, et al. (2012). Differential cytotoxic response in keloid fibroblasts exposed to photodynamic therapy is dependent on photosensitizer precursor, fluence and location of fibroblasts within the lesion. *Arch Dermatol Res* 304(7): 549-562.

Menke NB, Cain JW, Reynolds A, Chan DM, Segal RA, Witten T, et al. (2010). An in silico approach to the analysis of acute wound healing. *Wound Repair Regen* 18(1): 105-103.

Menon GK, Kligman AM. (2009). Barrier funtions of human skin: a holistic view. *Skin Pharmacol Physiol* 22(4): 178-189.

Menon SN, Flegg JA, McCue SW, Schugart RC, Dawson RA, McElwain DL. (2012). Modelling the interaction of keratinocytes and fibroblasts during normal and abnormal wound healing processes. *Proc Biol Sci* 279(1741): 3329-33238.

Mills S, Farrar M, Ashcroft G, Griffiths C, Hardman M, Rhodes L. (2014). Topical photodynamic therapy following excisional wounding of human skin increases production of transforming growth factor- β 3 and matrix metalloproteinases 1 and 9, with associated improvement in dermal matrix organization. *Br J Dermatol* 171(1): 55-62.

Mitts TF, Bunda S, Wang Y, Hinek A. (2010). Aldosterone and mineralocorticoid receptor antagonists modulate elastin and collagen deposition in human skin. *J Invest Dermatol* 130(10): 2396-2406.

Moll I, Houdek P, Schmidt H, Moll R. (1998). Characterization of epidermal wound healing in a human skin organ culture model: Acceleration by transplanted keratinocytes. *J Invest Dermatol* 111(2): 251-258.

Morton CA, Brown SB, Collins S, Ibbotson S, Jenkinson H, Kurwa H, et al. (2002). Guidelines for topical photodynamic therapy: report of a workshop of the British Photodermatology Group. *Br J Dermatol* 146(4): 552-567.

Morton CA, McKenna K, Rhodes LE, et al. (2008). Guidelines for topical photodynamic therapy: update. *Br J Dermatol* 159(6): 1245-1266.

Muehlich S, Cicha I, Garlichs CD, Krueger B, Posern G, Goppelt-Strube M. (2007). Actin-dependent regulation of connective tissue growth factor. *Am J Physiol Cell Physiol* 292(5): C1732-1738.

Nakanishi J, Yamamoto M, Koyama J, Sato J, Hibino T. (2010). Keratinocytes synthesize enteropeptidase and multiple forms of trypsinogen during terminal differentiation. *J Invest Dermatol* 130(4): 944-952.

Namazi MR, Fallahzadeh MK, Schwartz RA. (2011). Strategies for prevention of scars: what can we learn from fetal skin? *Int J Dermatol* 50(1): 85-93.

Nestle FO, Di Meglio P, Qin JZ, Nickoloff BJ. (2009). Skin immune sentinels in health and disease. *Nat Rev Immunol* 9(10): 679-691.

Negre-Salvayre A, Coatrieux C, Ingueneau C, Salvayre R (2007). Advanced lipid peroxidation end products in oxidative damage to proteins. Potential role in diseases and therapeutic prospects for the inhibitors. *Br J Pharmacol* 153(1):6-20.

Nie Z, Bayat A, Behzad F, Rhodes LE. (2010). Positive response of a recurrent keloid scar to topical methyl aminolevulinate-photodynamic therapy. *Photodermatol Photoimmunol Photomed* 26(6): 330-332.

Noodt BB, Berg K, Stokke T, Peng Q, Nesland JM. (1996). Apoptosis and necrosis induced with light and 5-aminolevulonic acid-derived protoporphyrin IX. *Br J Cancer* 74(1): 22-29.

O'Toole EA. (2001). Extracellular matrix and keratinocyte migration. *Clin Exp Dermatol* 26(6): 525-530.

Occlleston NL, Laverty HG, O'Kane S, Ferguson MW. (2008). Prevention and reduction of scarring in the skin by Transforming Growth Factor beta 3 (TGF β 3): from laboratory discovery to clinical pharmaceutical. *J Biomater Sci Polymer Ed* 19(8): 1047-1063.

Ogata Y, Enghild JJ, Nagase H. (1992). Matrix metalloproteinase 3 (stromelysin) activates the precursor for the human matrix metalloproteinase 9. *J Biol Chem* 267(6):3581-4.

Ogawa R, Okai K, Tokumura F, Mori K, Ohmori Y, Huang C, et al. (2012). The relationship between skin stretching/contraction and pathologic scarring: The important role of mechanical forces in keloid generation. *Wound Repair Regen* 20(2): 149-157.

Ohno S, Hirano S, Kanemaru S, Tateya I, Kitani Y, Kojima T, et al. (2011). Prevention of buccal mucosa scarring with transforming growth factor β 3. *Laryngoscope* 121(7): 1404-1409.

Okan D, Woo K, Ayello Ea, Sibbald G. (2007). The role of moisture balance in wound healing. *Adv Skin Wound Care* 20(1): 39-53.

Pacini S, Morucci G, Ruggiero M, Gulisano M, Punzi T. (2012). Tensegrity and plasma for skin regeneration. *Skin Res Technol* 18(3): 356-363.

Pahernik SA, Botzlar A, Hillemanns P, Dellian M, Kirschstein M, Abels C, et al. (1998). Pharmacokinetics and selectivity of aminolevulinic acid-induced porphyrin synthesis in patients with cervical intra-epithelial neoplasia. *Int J Cancer* 73(3): 310-314.

Panzarini E, Inguscio V, Dini L. (2011). Timing the multiple cell death pathways initiated by Rose Bengal acetate photodynamic therapy. *Cell Death Dis* 9: 2e169.

Pajoum SR, Shokrgozar MA, Vossoughi M, Eslamifar A. (2009). In vitro co-culture of human skin keratinocytes and fibroblasts on a biocompatible and biodegradable scaffold. *Iran Biomed J* 13(3): 169-177.

Paunesku T, Mittal S, Protic M, Oryhon J, Korolev S, Joachimiak A, et al. (2001). Proliferating cell nuclear antigen (PCNA): ringmaster of the genome. *Int J Radiat Biol* 77(10): 1007-1021.

Peng Q, Warloe T, Berg K, Moan J, Kongshaug M, Giercksky KE, et al. (1997). 5-Aminolevulinic acid-based photodynamic therapy. Clinical research and future challenges. *Cancer* 79(12): 2282-2308.

Peplow PV, Chung TY, Baxter GD. (2012). Photodynamic modulation of wound healing: A review of human and animal studies. *Photomed Laser Surg* 30(3): 118-148.

Peramo A, Marcel CL, Goldstein SA, Martin DC. (2010). Improved Preservation of the Tissue Surrounding Percutaneous Devices by Hyaluronic Acid and Dermatan Sulfate in a Human Skin Explant Model. *Ann Biomed Eng* 38(3): 1098-1110.

Perry DM, McGrouther DA, Bayat A. (2010). Current tools for noninvasive objective assessment of skin scars. *Plast Reconstr Surg* 126(3): 912-923.

Phan TT, Lim IJ, Aalami O, Lorget F, Khoo A, Tan EK, et al. (2005). Smad3 signalling plays an important role in keloid pathogenesis via epithelial–mesenchymal interactions. *J Pathol* 207(2): 232-242.

Plaetzer K, Krammer B, Berlanda J, Berr F, Kiesslich T. (2009). Photophysics and photochemistry of photodynamic therapy: fundamental aspects. *Lasers Med Sci* 24(2): 259-268.

Ramirez H, Patel SB, Pastar I. (2014). The Role of TGF β Signalling in wound epithelialization. *Adv Wound Care (New Rochelle)* 3(7): 482-491.

Ramos ML, Gragnani A, Ferreira LM. (2008). Is there an ideal animal model to study hypertrophic scarring? *J Burn Care Res.* 29(2): 363-368.

Reddy KK, Hanke CW, Tierney EP. (2010). Rapid wound re-epithelialization and basal cell carcinoma clearance after Mohs micrographic surgery with postoperative photodynamic therapy. *J Drugs Dermatol* 9(2): 143-148.

Renò F, Sabbatini M, Stella M, Magliacani G, Cannas M. (2005). Effect of in vitro mechanical compression on Epilysin (matrix metalloproteinase-28) expression in hypertrophic scars. *Wound Repair Regen* 13(3): 255-261.

Rhodes LE, de Rie MA, Leifsdottir R, Yu RC, Bachmann I, Goulden V, et al. (2007). Five-year follow-up of a randomized, prospective trial of topical methyl aminolevulinate photodynamic therapy vs. surgery for nodular basal cell carcinoma. *Arch Dermatol Res* 143(9): 1131-1136.

Riekki R, Parikka M, Jukkola A, Salo T, Risteli J, Oikarinen A. (2002). Increased expression of collagen types I and III in human skin as a consequence of radiotherapy. *Arch Dermatol Res* 294(4): 178-184.

Rinn JL, Wang JK, Liu H, Montgomery K, van de Rijn M, Chang HY. (2008). A Systems Biology Approach to Anatomic Diversity of Skin. *J Invest Dermatol* 128(4): 776-782.

Rizzo AE, Beckett LA, Baier BS, Isseroff RR. (2012). The linear excisional wound: an improved model for human ex vivo wound epithelialization studies. *Skin Res Technol* 18(1): 125-132.

Robertson CA, Evans DH, Abrahamse H. (2009). Photodynamic therapy (PDT): a short review on cellular mechanisms and cancer research applications for PDT. *J Photochem Photobiol B* 96(1): 1-8.

Rodriguez L, Batlle A, Di Venosa G, Battah S, Dobbin P, MacRobert AJ, et al. (2006). Mechanisms of 5-aminolevulic acid ester uptake in mammalian cells. *Br J Pharmacol* 147(7): 825-833.

Rud E, Gederaas O, Høgset A, Berg K. (2000). 5-aminolevulinic acid, but not 5-aminolevulinic acid esters, is transported into adenocarcinoma cell by system BETA transporters. *Photochem Photobiol* 71(5): 640-647.

Ryan T. (2004). The ageing of the blood supply and the lymphatic drainage of the skin. *Micron* 35(3): 161-171.

Sailer R, Strauss W, Wagner M, Emmert H, Schneckenburger H. (2007). Relation between intracellular location and photodynamic efficacy of 5-aminolevulonic acid-induced protoporphyrin IX in vitro. Comparision between human glioblastoma cells and other cancer cell lines. *Photochem Photobiol Sci* 6(2): 145-151.

Sakamoto FH, Izikson L, Tannous Z, Zurakowski D, Anderson RR. (2012). Surgical scar remodelling after photodynamic therapy using aminolevulinic acid or its methylester: a retrospective, blinded study of patients with field cancerization. *Br J Dermatol* 166(2): 413-416.

Salgado RM, Alcántara L, Mendoza-Rodríguez CA, Cerbón M, Hidalgo-González C, Mercadillo P, et al. (2012). Post-burn hypertrophic scars are characterized by high levels of IL-1 β mRNA and protein and TNF- α type I receptors. *Burns* 33(5): 669-676.

Samaroo HD, Opsahl AC, Schreiber J, O'Neill SM, Marconi M, Qian J, et al. (2012). High throughput object-based image analysis of -amyloid plaques in human and transgenic mouse brain. *J Neurosci Methods* 204(1): 179-188.

Sanclemente G, Correa LA, Garcia JJ, Barrera M, Villa JF, Garcia HI. (2012). Methyl aminolevulinate plus red light vs. placebo plus red light in the treatment of photodamaged facial skin: histopathological findings. *Exp Dermatol* 37(4): 379-386.

Satish L, Kathju S. (2010). Cellular and Molecular Characteristics of Scarless versus Fibrotic Wound Healing. *Dermatol Res Pract* doi:10.1155/2010/790234.

Sayah DN, Soo C, Shaw WW, Watson J, Messadi D, Longaker MT, et al. (1999). Down-regulation of apoptosis-related genes in keloid tissues. *J Surg Res* 87(2): 209-216.

Schäfer M, Werner S. (2008). Cancer as an overhealing wound: an old hypothesis revisited *Nat Rev Mol Cell Biol* 9(8): 628-638.

Schneider LF, Warren SM. (2008). The relationship between keloid growth pattern and stretching tension-visual analysis using the finite element method: a brief history of keloids. *Ann Plast Surg* 60(4): 452-454.

Schreml S, Szeimies RM, Prantl L, Landthaler M, Babilas P. (2010). Wound healing in the 21st century. *J Am Acad Dermatol* 63(5): 866-881.

Schulz JT 3rd, Tompkins RG, Burke JF. (2000). Artificial skin. *Annu Rev Med* 51: 231-244.

Sebastian A, Allan E, Allan D, Colthurst J, Bayat A. (2011). Addition of novel degenerate electrical waveform stimulation with photodynamic therapy significantly enhances its cytotoxic effect in keloid fibroblasts: First report of a potential combination therapy. *J Dermatol Sci* 64(3): 174-184.

Seifert O, Bayat A, Geffers R, Dienus K, Buer J, Löfgren S, et al. (2008). Identification of unique gene expression patterns within different lesional sites of keloids. *Wound Repair Regen* 16(2): 254-265.

Seifert O, Mrowietz U. (2009). Keloid scarring: bench and bedside. *Arch Dermatol Res* 301(4): 259-272.

Seltmann K, Fritsch AW, Käs JA, Magin TM. (2013). Keratins significantly contribute to cell stiffness and impact invasive behaviour. *Proc Natl Acad Sci USA* 110(46): 18507-18512.

- Seo JY, Lee SH, Youn CS, Choi HR, Rhie GE, Cho KH, et al. (2001) Ultraviolet radiation increases tropoelastin mRNA expression in the epidermis of human skin in vivo. *J Invest Dermatol* 116(6):915-919.
- Suter MM, Schulze K, Bergman W, Welle M, Roosje P, Müller EJ. (2009). The keratinocyte in epidermal renewal and defence. *Vet Dermatol* 20(5-6): 515-532.
- Statius van Eps RG, Adili F, Watkins MT, Anderson RR, LaMuraglia GM. (1997). Photodynamic therapy of extracellular matrix stimulates endothelial cell growth by inactivation of matrix-associated transforming growth factor-beta. *Lab Invest* 76(2): 257-266.
- Shih B, Bayat A. (2010). Genetics of keloid scarring. *Arch Dermatol Res* 302(5): 319-339.
- Shih B, Garside E, McGrouther DA, Bayat A. (2010b). Molecular dissection of abnormal wound healing processes resulting in keloid disease. *Wound Repair Regen* 2010(18): 2.
- Sidgwick GP, Bayat A. (2012). Extracellular matrix molecules implicated in hypertrophic and keloid scarring. *J Eur Acad Dermatol Venereol* 26(2): 141-152.
- Silver FH, Siperko LM, Seehra GP. (2003). Mechanobiology of force transduction in dermal tissue. *Skin Res Technol* 9(1): 3-23.
- Sorrell JM, Caplan AI. (2004). Fibroblast heterogeneity: more than skin deep. *J Cell Sci* 117(5): 667-675.
- Stamenkovic I. (2003). Extracellular matrix remodelling: the role of matrix metalloproteinases. *J Pathol* 200(4): 448-464.
- Stapleton M, Rhodes LE. (2003). Photosensitizers for photodynamic therapy of cutaneous disease. *J Dermatolog Treat* 14(2): 107-112.
- Steinbauer JM, Schreml S, Kohl EA, Karrer S, Landthaler M, Szeimies RM. (2010). Photodynamic therapy in dermatology. *J Dtsch Dermatol Ges* 8(6): 454-464.
- Steinstraesser L, Rittig A, Gevers K, Sorkin M, Hirsch T, Kesting M, et al. (2009). A Human Full-Skin Culture System for Interventional Studies. *Eplasty* 9(e5).
- Sternlicht MD, Werb Z. (2001). How matrix metalloproteinases regulate cell behaviour *Annu Rev Cell Biol* 17: 463-516.
- Stoll SW, Johnson JL, Bhasin A, Johnston A, Gudjonsson JE, Rittié L, et al. (2010). Metalloproteinase-mediated, context-dependent function of amphiregulin and HB-EGF in human keratinocytes and skin. *J Invest Dermatol* 130(1): 295-304.
- Stücker M, Struk A, Altmeyer P, Herde M, Baumgärtl H, Lübbbers D. (2002). The cutaneous uptake of atmospheric oxygen contributes significantly to the oxygen supply of human dermis and epidermis. *J Physiol* 538(3): 985-994.

Sullivan T, Eaglstein WH, Davis SC, Mertz P. (2001). The pig as a model for human wound healing. *Wound Repair Regen* 9(2): 66-76.

Sundberg J, Nanney L, Fleckman P, King LE. (2012). Skin and Adnexa. Comparative Anatomy and Histology. E. Inc: 435-455.

Suter MM, Schulze K, Bergman W, Welle M, Roosje P, Müller E. (2009). The keratinocyte in epidermal renewal and defence. *Vet Dermatol* 20(5-6): 515-532.

Syed F, Ahmadi E, Iqbal SA, Singh S, McGrouther DA, Bayat A. (2011). Fibroblasts from the growing margin of keloid scars produce higher levels of collagen I and III compared with intralesional and extralesional sites: clinical implications for lesional site-directed therapy. *Br J Dermatol* 164(1): 83-96.

Syed F, Bagabir RA, Paus R, Bayat A. (2013). Ex vivo evaluation of antifibrotic compounds in skin scarring: EGCG and silencing of PAI-1 independently inhibit growth and induce keloid shrinkage. *Lab Invest* 93(8): 946-960.

Szeimies RM, Torezan L, Niwa A, Valente N, Unger P, Kohl E, et al. (2012). Clinical, histopathological and immunohistochemical assessment of human skin field cancerization before and after photodynamic therapy. *Br J Dermatol* 167(1): 150-159.

Tandara AA, Mustoe TA. (2011). MMP- and TIMP-secretion by human cutaneous keratinocytes and fibroblasts - impact of coculture and hydration. *J Plast Reconstr Aesthet Surg* 64(1): 108-116.

Tavakkol A, Varani J, Elder JT, Zouboulis CC. (1999). Maintenance of human skin in organ culture: role for insulin-like growth factor-1 receptor and epidermal growth factor receptor. *Arch Dermatol Res* 291(12): 643-651.

Teng M, Huang Y, Zhang H. (2014). Application of stems cells in wound healing- An update. *Wound Rep Reg* 22 151-160.

Thanan R, Oikawa S, Hiraku Y, Ohnishi S, Ma N, Pinlaor S, et al. Oxidative stress and its significant roles in neurodegenerative diseases and cancer. *Int J Mol Sci* 2014 16(1):193-217.

Tobin DJ. (2006). Biochemistry of human skin--our brain on the outside. *Chem Soc Rev* 35(1): 52-67.

Toebak MJ, Gibbs S, Bruynzeel DP, Scheper RJ, Rustemeyer T. (2009). Dendritic cells: biology of the skin. *Contact Dermatitis* 60(1): 2-20.

Tomic-Canic M, Komine M, Freedberg IM, Blumenberg M. (1998). Epidermal signal transduction and transcription factor activation in activated keratinocytes. *J Dermatol Sci* 17(3): 167-181.

Tomic-Canic M, Mamber SW, Stojadinovic O, Lee B, Radoja N, McMichael J. (2007). Streptolysin O enhances keratinocyte migration and proliferation and promotes skin organ culture wound healing in vitro. *Wound Repair Regen* 15(1): 71-79.

Tortora G, Nielsen M. (2013). Principles of human Anatomy New York John Wiley & Sons.

Totan S, Echo A, Yuksel E. (2011). Heat shock proteins modulate keloid formation. *Eplasty* 11: e21.

Tschumperlin DJ. (2013). Fibroblasts and the ground they walk on. *Physiology* 28(6): 380-390.

Tucci-Viegas VM, Hochman B, Franca JP, Ferreira LM. (2010). Keloid explant culture: a model for keloid fibroblasts isolation and cultivation based on the biological differences of its specific regions. *Int Wound J* 7(5): 339-348.

Ud-Din S, Bayat A. (2014). New insights on keloids, hypertrophic scars, and striae. *Dermatol Clin* 32(2): 193-209.

Ud-Din S, Thomas G, Morris J, Bayat A. (2013). Photodynamic therapy: an innovative approach to the treatment of keloid disease evaluated using subjective and objective non-invasive tools. *Arch Dermatol Res* 305(3): 205-214.

Uehlinger P, Zellweger M, Wagnières G, Juillerat-Jeanneret L, van de Bergh H, Lange N. (2000). 5-Aminolevulinic acid and its derivatives: physical chemical properties and protoporphyrin IX formation in cultured cells. *J Photochem Photobiol B* 54(1): 72-80.

Venus M, Wateman J, McNab I. (2011). Basic physiology of the skin. *Surgery* 29: 471-474.

Vermolen FJ, Javierre E. (2010). Computer simulations from a finite-element model for wound contraction and closure. *J Tissue Viability* 19(2): 43-53.

Vietti G, Ibouraadaten S, Palmai-Pallag M, Yakoub Y, Bailly C, Fenoglio I, et al. (2013). Towards predicting the lung fibrogenic activity of nanomaterials: experimental validation of an in vitro fibroblast proliferation assay. *Part Fibre Toxicol.* 10;10:52.

Vincent AS, Phan TT, Mukhopadhyay A, Lim HY, Halliwell B, Wong KP. (2008). Human skin keloid fibroblasts display bioenergetics of cancer cells. *J Invest Dermatol* 128(3): 702-709.

Volk SW, Wang Y, Mauldin EA, Liechty KW, Adams SL. (2011). Diminished Type III Collagen Promotes Myofibroblast Differentiation and Increases Scar Deposition in Cutaneous Wound Healing. *Cell Tissues Organs* 194(1): 25-37.

Volk SW, Iqbal SA, Bayat A. (2013). Interactions of the extracellular matrix and progenitors cells in cutaneous wound healing. *Adv Wound Care (New Rochelle)* 2(6): 261-272.

Wan MT, Lin JY. (2014). Current evidence and applications of photodynamic therapy in dermatology. *Clin Cosmet Investing Dermatol* 21(7): 145-163.

Washbrook R, Riley P. (1997). Comparison of delta-aminolaevulinic acid and its methyl ester as an inducer of porphyrin synthesis in cultured cells. *Br J Cancer* 75(10): 1417-1420.

Wolfram D, Tzankov A, Pütlz P, Piza-Katzer H. (2009). Hypertrophic scars and keloids--a review of their pathophysiology, risk factors, and therapeutic management. *Dermatol Surg* 35(2): 171-181.

Wong VW, Akaishi S, Longaker MT, Gurtner GC. (2011). Pushing back: wound mechanotransduction in repair and regeneration. *J Invest Dermatol* 131(11): 2186-2196.

Wong VW, Sorkin M, Glotzbach JP, Longaker MT, Gutner GC. (2011). Surgical approaches to create murine models of human wound healing. *J Biomed Biotechnol* doi: 10.1155/2011/969618.

Wyld L, Reed MW, Brown NJ. (2001). Differential cell death response to photodynamic therapy is dependent on dose and cell type. *Br J Cancer* 84(10): 1384-1386.

Xu W, Jong Hong S, Jia S, Zhao Y, Galiano RD, Mustoe TA. (2012). Application of a partial-thickness human ex vivo skin culture model in cutaneous wound healing study. *Lab Invest* 92(4): 584-599.

Yang DY, Li SR, Wu JL, Chen YQ, Li G, Bi S, et al. (2007). Establishment of a Hypertrophic Scar Model by Transplanting Full-Thickness Human Skin Grafts onto the Backs of Nude Mice. *Plast Reconstr Surg* 119(1): 104-109.

Yang L, Hashimoto K, Shirakata Y. (2012). Epidermogenesis in a skin wound deep through the basement membrane contributes to scar formation. *J Dermatol Sci* 65(3): 224-226.

Yu BD, Mukhopadhyay A, Wong C. (2008). Skin an hair: models for exploring organ regeneration. *Hum Mol Genet* 17(R1):R54-9.

Zhang G. (2009). Activation of peroxisome proliferator-activated receptor-gamma inhibits transforming growth factor-1 induction of connective tissue growth factor and extracellular matrix in hypertrophic scar and fibroblasts in vitro. *Arch Dermatol Res* 301: 515-522.

Zhang Q, Wu Y, Ann DK, Messadi DV, Tuan TL, Kelly AP, et al. (2003). Mechanisms of hypoxic regulation of plasminogen activator inhibitor-1 gene expression in keloid fibroblasts. *J Invest Dermatol* 121(5): 1005-1012.

Zhao H, Xing D, Chen Q. (2011). New insights of mitochondria reactive oxygen species generation and cell apoptosis induced by low dose photodynamic therapy. *Eur J Cancer* 47(8): 2750-2761.

ANNEX 1

Arch Dermatol Res (2012) 304:549–562
DOI 10.1007/s00403-012-1264-y

ORIGINAL PAPER

Differential cytotoxic response in keloid fibroblasts exposed to photodynamic therapy is dependent on photosensitiser precursor, fluence and location of fibroblasts within the lesion

Jenifer Mendoza · Anil Sebastian · Ernest Allan ·
Donald Allan · Parthasarathi Mandal ·
Teresa Alonso-Rasgado · Ardeshir Bayat

Received: 4 April 2012 / Revised: 25 June 2012 / Accepted: 5 July 2012 / Published online: 4 August 2012
© Springer-Verlag 2012

Abstract Treatment of keloid disease (KD) is ill-defined and remains challenging. We previously reported successful clinical application of photodynamic therapy (PDT) in KD. The aim here was to evaluate cytotoxic effect of PDT using methyl aminolevulinate (M-ALA) and 5-aminolevulinic acid (5-ALA) on keloid fibroblasts (KF) ($n = 8$) from different lesional sites (top, middle and margin) as compared to normal skin fibroblasts ($n = 3$).

Electronic supplementary material The online version of this article (doi:10.1007/s00403-012-1264-y) contains supplementary material, which is available to authorized users.

J. Mendoza · A. Sebastian · A. Bayat (✉)
Plastic and Reconstructive Surgery Research, School of
Translational Medicine, Manchester Institute of Biotechnology
(MIB), The University of Manchester, 131 Princess Street,
Manchester M1 7DN, UK
e-mail: Ardeshir.Bayat@manchester.ac.uk

J. Mendoza
e-mail: jengmg@hotmail.com

J. Mendoza · P. Mandal · T. Alonso-Rasgado
Bioengineering Group, School of Mechanical,
Aerospace and Civil Engineering,
The University of Manchester, Manchester, UK

E. Allan
Department of Clinical Oncology,
The Christie NHS Foundation Trust, Manchester, UK

D. Allan
North Western Medical Physics,
The Christie NHS Foundation Trust, Manchester, UK

D. Allan · A. Bayat
Plastic and Reconstructive Surgery Research, Manchester
Academic Health Science Centre (MAHSC), Wythenshawe
Hospital, University Hospital of South Manchester NHS
Foundation Trust, The University of Manchester, Southmoor
Road, Manchester, UK

The effect of protoporphyrin IX (PpIX) precursors was evaluated by fluorescence emission, LDH and WST-1 assay, reactive oxygen species (ROS) generation and qRT-PCR analysis. Apoptosis/necrosis differentiation and senescence were studied by fluorometric staining with Hoechst 33258/propidium iodide and β -galactosidase activity, respectively. Three hours post incubation with 4 mM precursors of photosensitisers, PpIX accumulation was site specific and higher with M-ALA. Cytotoxicity was also site specific (higher in fibroblasts from middle of the keloid as compared to cells from other sites) and increased proportionately to fluence rates post-PDT. Additionally, cytoproliferation was significantly decreased post-PDT depending on the light energy. Fluorescence analysis revealed that M-ALA instigated higher KF cytotoxicity at lower fluence ($\leq 20 \text{ J/cm}^2$) while 5-ALA instigated higher KF cytotoxicity at higher fluence, except in cells derived from middle of the keloid. ROS-mediated cytotoxicity was light energy dependent. Senescence was not observed at higher light energies ($> 10 \text{ J/cm}^2$). Compared to other sites, fibroblasts from the middle were more prone to cell death post 5-ALA treatment. We conclude that cytotoxicity post-PDT in KD fibroblasts is dependent on the lesional site, precursor of intracellular photosensitiser and fluence. Thus, PDT may be used for site-targeted therapy of KD.

Keywords Photodynamic therapy · Keloid fibroblasts · Protoporphyrin IX · ROS generation · Cell death mechanism · Cytotoxicity

Introduction

Keloid disease (KD) is a relatively common fibroproliferative disorder of unknown aetio-pathogenesis [39, 40].

Keloids are defined as benign tumours that grow beyond their border thereby invading into healthy tissue [39, 40]. They are characterized by excessive disorganized production of extracellular matrix (ECM) [39, 40], where apoptosis is down-regulated as compared to normal scars [26, 37, 39]. Keloids also exhibit regions with different genotypic and phenotypic features [6, 16, 17, 42, 44]. Management of KD is a clinical challenge as existing treatment modalities result in limited response coupled with a high recurrence rate [7, 39, 46].

Photodynamic therapy (PDT) is an accepted therapeutic modality for treatment of non-melanoma skin cancer and other pre-malignant skin conditions [3, 33]. It has also shown promise in the rejuvenation of skin and improving scar appearance [2, 9, 41]. PDT uses a specific light source and a precursor drug for an intracellular photosensitiser (PS) which when combined produces cytotoxic agents depending upon the concentration and time of exposure to PS, light dose, light source and exposure site [13, 19, 24, 25, 32, 48]. The most widely used precursors of PS are 5-aminolevulinic acid (5-ALA) and its esterified derivative methyl aminolevulinate (M-ALA) [10, 24, 34]. After 5-ALA/M-ALA administration, cells generate and accumulate PpIX as the PS through the haem biosynthetic pathway [4, 10]. The subcellular damage in PDT is mainly caused by the generation of singlet oxygen and other reactive oxygen species (ROS) according to the site and concentration of the PS within the tissue or the cells [22]. The effects of PDT are initiated with immunosuppression in tissues [13, 27] which further induces apoptosis, necrosis and autophagy [18, 20, 29, 30].

Clinical application of PDT in KD was recently reported by Nie et al. [28], who showed an effective reduction in the keloid tissue volume without secondary side effects or recurrence at 1-year follow up [28]. In addition, PDT given to keloid organotypic co-cultures was shown to induce rearrangement of collagen fibres [12]. In a recent in vitro study, the combined application of PDT and electrical stimulation was shown to be cytotoxic in keloid fibroblasts when compared with normal skin fibroblasts [38]. Cytotoxicity in keloid fibroblasts differs in relation to the lesional sites of the cells [42].

In view of the above findings, the aim of the present study was to investigate the cytotoxic effects of M-ALA-PDT as compared to 5-ALA-PDT in keloid fibroblasts both compared to normal skin fibroblasts. To achieve this aim, surgically removed keloid scar tissue was divided into the following sections (a) top, which included epidermis and papillary dermis; (b) middle, which comprised of reticular dermis only; and (c) margin, otherwise known as the peripheral active margin of the scar (Fig. 1). Our objective was to analyse the effect of PDT on cells isolated from these different anatomical sections of the keloid tissue.

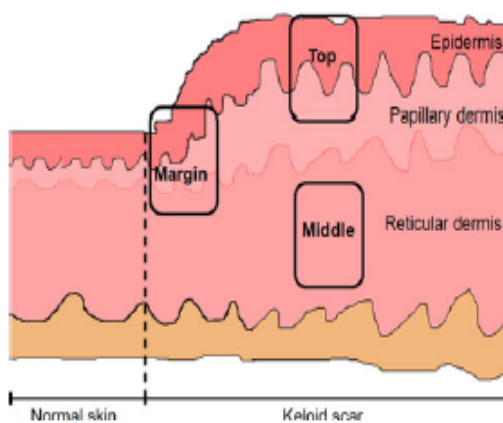


Fig. 1 A diagram of the cross section of a typical keloid scar showing different site-specific lesional sites. *Top* denotes the upper part of the keloid scar (includes epidermis and papillary dermis); *middle* denotes the centre part of the keloid scar (reticular dermis only). Both *top* and *middle* are intralesional samples. *Margin* denotes the peri-lesional or peripheral margin of the keloid scar

Therefore, we applied light energies from 10 to 40 J/cm² after incubation with different concentrations of M-ALA/5-ALA on a monolayer of cells. In the initial part of this study, we quantified PpIX in different cell types and examined the cytotoxicity mechanisms in the absence of precursors for PS, but with light only. Subsequently, PDT was applied and cytoproliferation, apoptosis, necrosis, senescence were investigated and ROS generation was measured.

Materials and methods

Cell culture

Keloid biopsies were obtained from patients after surgical removal of the keloid scar following written consent (Table 1). This study had received ethical approval. Normal skin biopsies were obtained from healthy skin of non-keloid patients. The senior author has clinically diagnosed the scars as keloids by typical phenotypic characteristics and differentiated from hypertrophic scars. Isolation of cells from tissue (KF = keloid fibroblast and NF = normal skin fibroblast) was performed as described by Syed et al. [42]. 1×10^4 cells/well were seeded in 96-well plates or 1.5×10^5 cells were seeded in 8 cm² culture dishes (35 mm diameter, Corning, Sigma-Aldrich, UK) and incubated at 37 °C with 5 % CO₂ before being harvested (6 days) with trypsin and passaged. Cell passages used in the experiments were restricted between 2 and 4. Complete cell growth DMEM medium (with 10 % fetal bovine serum) was replaced with serum-free DMEM medium before the start of any experiment. The outline of the

Table 1 Clinical data of patients. The size of keloid lesions range between 3 and 5 cm in width and 0.5–1 cm in height

Sample	Sex	Age (years)	Biopsy site	Age of scar (years)	Ethnicity	Treatment
Ks1	M	36	Scalp	5	Black	Recurrence post surgery
Ks2	F	35	Sternum	13	Black	None
Ks3	F	26	Earlobe	7	Black	Recurrence post surgery
Ks4	F	54	Sternum	12	Black	Recurrence post surgery
Ks5	F	66	Ear	23	White	None
Ks6	F	28	Chest	7	Black	Recurrence post surgery
Ks7	M	26	Chest	15	Black	Recurrence post surgery
Ks8	M	26	Sternum	13	White	Recurrence post surgery
Ns1	F	39	Abdomen	–	White	–
Ns2	F	25	Breast	–	White	–
Ns3	F	47	Abdomen	–	White	–

Ks denotes keloid scar,
Ns denotes normal skin

experimental methodology is depicted on the online resource (Supplementary material, Fig. 1).

Drugs

5-aminolevulinic acid (5-ALA; Mandeville Medicines, UK) and methyl aminolevulinic acid (M-ALA; Galderma, UK) were dissolved in serum-free DMEM medium at different concentrations of 0.5, 1, 2, 4, 10, and 50.0 mM. We have used similar concentrations of these drugs which are now in clinical practice.

PDT apparatus

This study used PDT machine (Omnilux PDT™, Photo Therapeutics, PA, USA) with a light-emitting diode (LED) and air cooling system which emitted red light of wavelength 633 ± 3 nm. It was adjusted to 35 mW/cm^2 of power intensity, which was configured and calibrated with an IL1700 radiometer (International Light Technologies Inc, MA, USA).

Fluorescence measurement of PpIX after incubation with different concentrations of M-ALA/5-ALA

In order to determine the time taken for intracellular accumulation of PpIX, the fluorescence intensity of PpIX was measured at 400/620 nm in a fluorometric microplate reader (Fluostar optima, BMG Labtech, UK). The different cell types were incubated for different time periods (0, 1, 2, 3, 4, 6, 8, and 10 h) post M-ALA or 5-ALA treatment at different concentrations (0, 0.5, 1, 2, 4, 10 and 50 mM) and the values were normalised with cells without any treatment.

Cell proliferation assay (WST-1)

Cell proliferation was determined by WST-1 assay (WST-1 cell proliferation kit, Roche-Diagnostics, Mannheim,

Germany). WST-1 reagent was added to cells cultured in 96-well plates and treated according to the manufacturer's instructions. The end point absorbance was measured at 450 and 650 nm with a microplate reader (Fluostar optima, BMG Labtech, UK) [38].

Phototoxic analysis

In order to study the phototoxic effect of the light alone, keloid and normal skin fibroblasts were grown in 8 cm^2 cell culture dishes. Here, cells were not incubated with photosensitising precursors. However, cells were exposed to light energies of 5, 10, 20, 40, 60, 80, and 100 J/cm^2 at a power intensity of 35 mW/cm^2 . Subsequently after light exposure, lactate dehydrogenase (LDH) release into the medium (LDH Cytotoxicity Detection kit, Roche Diagnostics, Roche Mannheim, Germany) was measured at 490 and 600 nm with a microplate reader [38].

Cytotoxic analysis of PDT on normal skin and keloid-derived fibroblasts

After incubation with M-ALA or 5-ALA, the cells were treated with 10, 20, and 40 J/cm^2 of light energy. The serum-free cell medium was replaced with complete DMEM medium for further incubation at 37°C and 5 % CO_2 post light exposure. Cytoproliferation (WST-1 assay) was analysed immediately after treatment while cytotoxicity (LDH assay) was assessed at 0, 24 and 72 h after treatment.

Apoptosis, necrosis, and senescence analysis post PDT in normal skin and keloid fibroblasts

Apoptosis and necrosis were analyzed by fluorescence microscopy with Hoechst 33258 (Invitrogen Ltd, USA) and propidium iodide (PI; Sigma-Aldrich company Ltd, UK), respectively. They were analysed 24 h post treatment.

Senescence was assessed by measuring the intracellular activity of β -galactosidase at pH 6 according to manufacturer's instructions (Senescence β -galactosidase Staining Kit, Cell Biolabs, Cambridge, UK).

ROS generation analysis

Reactive oxygen species generation was measured by the intracellular accumulation of the fluorescent probe 2',7'-Dichlorodihydrofluorescin (DCF; OxiSelect ROS Assay kit, Cell Biolabs, CA, USA). The assay was performed according to manufacturer's instructions and fluorescence was measured at 480/530 nm.

RNA isolation, cDNA synthesis and qRT-PCR

Cells were incubated with 4 mM M-ALA/5-ALA and exposed to 10 and 40 J/cm². The cell lysates were collected in TRIzol reagent (Invitrogen, Abingdon, UK) and were processed for RNA isolation, cDNA synthesis and qRT-PCR as described previously [42]. The gene expression levels were normalized with an internal reference gene, RPL32. The primers used in the study are detailed on the online resource (Supplementary material, Table 1).

Statistical analysis

The results are presented as the mean values \pm standard deviation. Statistical significance was calculated with non-parametric ANOVA and Bonferroni post test and graphics were generated with GraphPad Prism 5 (GraphPad Software, La Jolla, CA, USA). Differences between different data sets were compared with the control (cells without any treatment) or within each set (normal skin vs. keloid scar fibroblasts) and were considered significant if $P < 0.05$.

Results

The rate of intracellular accumulation of PpIX with M-ALA in keloid fibroblasts varies compared to 5-ALA

The intracellular accumulation of PpIX in fibroblasts with M-ALA followed a bell-shaped pattern as it reached a maximum within 3–8 h depending on the concentration and site-specificity of fibroblasts (Fig. 2a–d), while 5-ALA followed a different “growth curve” pattern (Fig. 2e–h). This shows an increased retention of 5-ALA compared to M-ALA in fibroblasts. The difference between PpIX accumulation in KF and NF was highest at 4 mM as compared to other precursor concentrations. Moreover, solutions with 4 mM of M-ALA or 5-ALA had better uptake of drugs by keloid fibroblasts without affecting their

viability, when compared with other precursor concentrations. However, there was no significant difference in PpIX generation between different keloid cell types after 5-ALA/M-ALA treatment (Fig. 3). Exposure to 10 and 50 mM of M-ALA/5-ALA increased cytotoxicity significantly (See Online Resource; Supplementary material, Figs. 2, 3, 4 and 5).

Phototoxicity in keloid fibroblasts increased proportionately with fluence

Phototoxicity of KF was significantly higher after light treatment alone as compared to NF (Fig. 4). Cell death was higher for fibroblasts from the top and middle of the keloid at fluence <20 J/cm², whilst fibroblasts from the top and margin were more cytotoxic at 100 J/cm². However, cell death was less than 12 %, even at 100 J/cm².

Cytotoxicity post-PDT followed fluence in a dose-dependent manner

LDH cytotoxicity increased with higher light energies and this increase was proportionate to the fluence (Fig. 5). There was significant increase in cytotoxicity after 72 h as compared to 24 h after PDT. 20 J/cm² had better cytotoxic differentiation between KF and NF than any other energy level at 72 h. Cytotoxicity post treatment with 5-ALA and M-ALA was higher for middle-specific keloid fibroblasts as compared to cells derived from other keloid lesional sites ($P < 0.05$ and $P > 0.05$, respectively).

Cytoproliferation decreased with PDT in an energy-dependent manner

Cytoproliferation of keloid and normal skin fibroblasts decreased significantly after PDT in an energy-dependent manner (Fig. 6). Cytoproliferation decreased by eightfold in KF post 5-ALA/M-ALA treatment at 40 J/cm² and sixfold in NF both compared to cells without any treatment. However, there was significant difference only between cells derived from middle of the keloid as compared to NF post 5-ALA treatment at energies ≤ 20 J/cm².

Apoptosis and necrosis were dependent on keloid lesional site and fluence

Cytotoxicity post PDT in KF was lesion site-specific with more cells prone to necrosis with higher fluence. From Hoechst 33258/PI fluorescence analysis for apoptosis/necrosis, margin-specific keloid fibroblasts were more prone to cell death post M-ALA treatment at low fluence (≤ 10 J/cm²) whilst the same effect was found with middle-specific keloid fibroblasts post 5-ALA treatment at low fluence (≤ 10 J/cm²) (Fig. 7). Interestingly, higher number

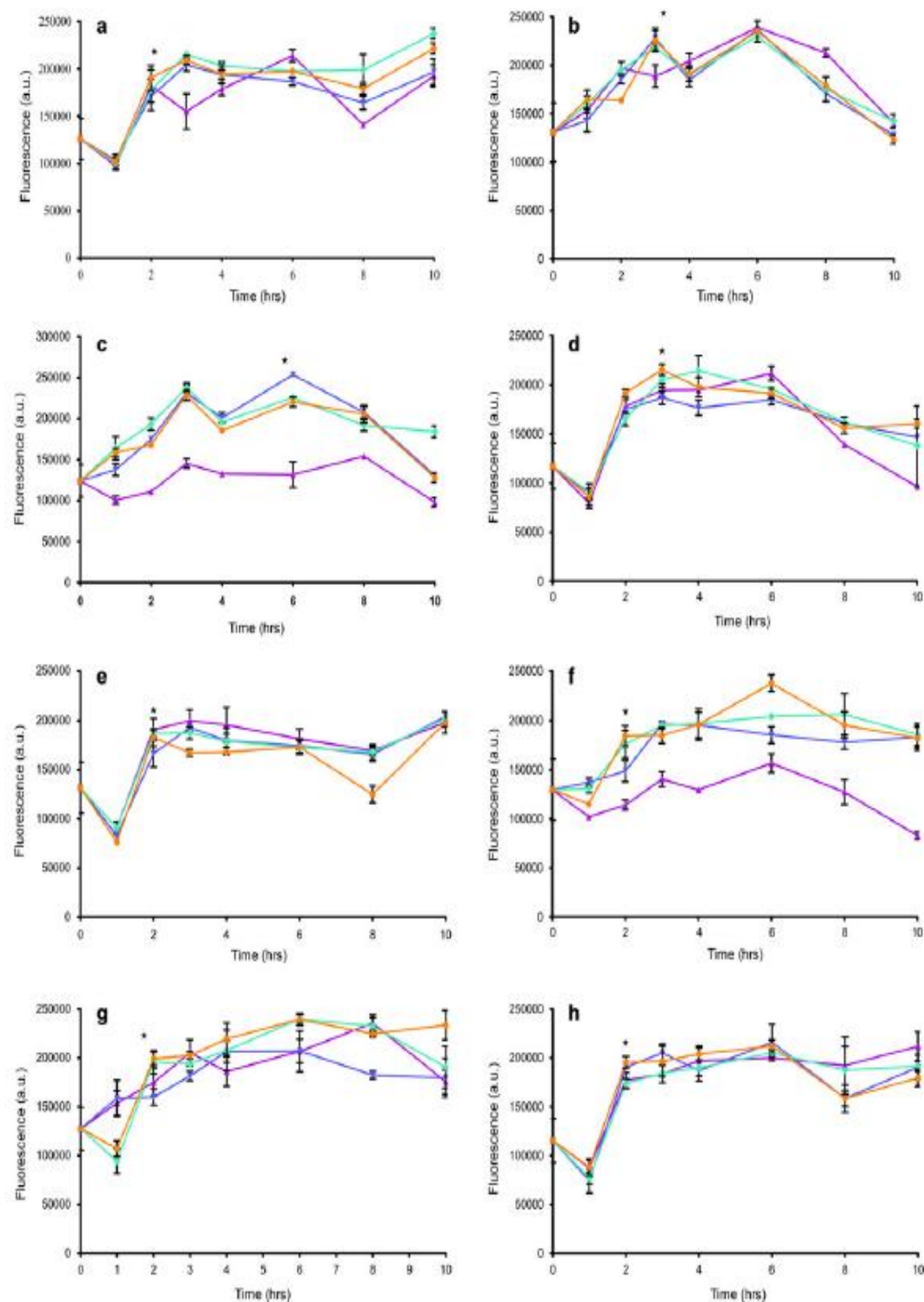


Fig. 2 Kinetics of PpIX accumulation in normal skin (a, e) and keloid fibroblasts from the margin (b, f), top (c, g) and middle (d, h) of the scar post-incubation with different concentrations (0.5, 1.0, 2.0, and 4.0 mM) of M-ALA (a-d) or 5-ALA (e-h). Filled star

denotes significant difference in comparison with cells not exposed to exogenous M-ALA or 5-ALA ($P < 0.05$). Filled triangles, 0.5 mM; inverted triangles 1.0 mM, filled diamonds 2.0 mM, filled circles 4.0 mM

of normal skin fibroblasts were prone to apoptosis ($\sim 55\%$) following M-ALA treatment at 20 J/cm^2 whilst they were better prone to necrosis ($\sim 65\%$) post M-ALA treatment at 20 J/cm^2 . M-ALA instigated higher KF cytotoxicity at lower fluence ($\leq 20 \text{ J/cm}^2$) while 5-ALA instigated higher KF cytotoxicity at higher fluence, with the exception of middle-specific keloid cells.

Senescence increased up to 10 J/cm^2 and completely disappeared at higher energies

β -galactosidase activity increased in KF and NF after exposure to lower light energies (Fig. 8). However at 10 J/cm^2 , M-ALA induced least activity of β -galactosidase in middle-specific keloid fibroblasts while 5-ALA had the maximum for middle-specific cells. Senescence was not present at higher energies. Therefore, induction of senescence was precursor of PS and lesion site-specific. Quantitative data for senescence positive cells are shown in on the online resource (Supplementary material, Fig. 6).

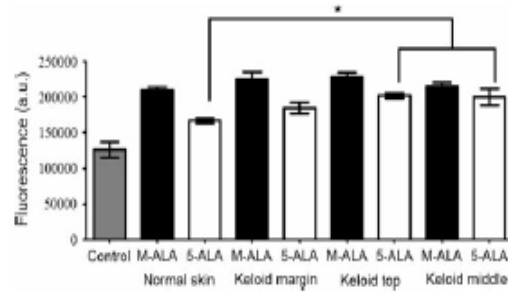
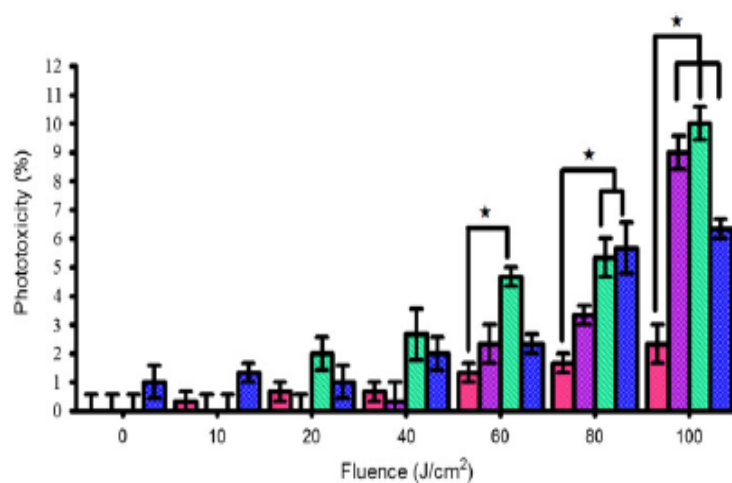


Fig. 3 Fluorescence intensity of PpIX accumulated in normal skin and keloid fibroblasts after 3 h of incubation with 4 mM of M-ALA or 5-ALA. 5-ALA showed significant increase in PpIX accumulation in keloid top and middle fibroblasts compared to normal skin fibroblasts. Filled star denotes statistical significance ($P < 0.05$)

Fig. 4 Percentage of phototoxicity in site-specific keloid fibroblasts compared to normal skin fibroblasts at increasing fluence rates (without any addition of precursors of photosensitiser). Phototoxicity analysis was measured upon fluence rate from a light-emitting diode (LED) arrangement ($633 \pm 3 \text{ nm}$ of wavelength and at 35 mW/cm^2 power intensity) by LDH assay. Filled stars denote statistical significance ($P < 0.05$). Normal skin (pink bars), keloid margin (violet bars), keloid top (green bars) and keloid middle (blue bars)



ROS generation increased with the amount of energy delivered

Reactive oxygen species generation could be correlated to necrosis in any of the cell types and was precursor of PS and lesion site-specific (Fig. 9). ROS generation increased with every site-specific keloid cell following fluence. However, KF from the middle of the keloid scar generated the highest amount of ROS after 5-ALA/M-ALA treatment (at any fluence) compared to any other cell types ($P < 0.05$ and $P > 0.05$, respectively).

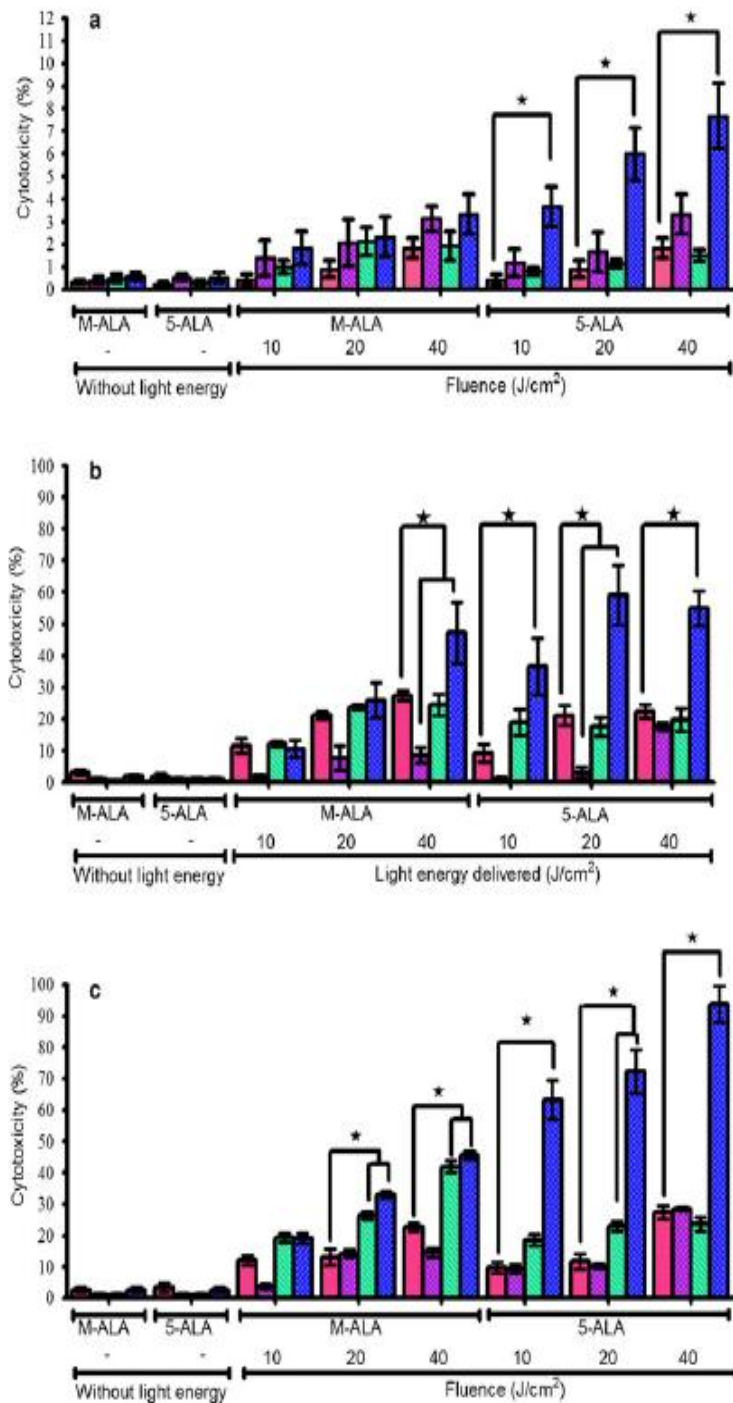
Keloid pathogenesis and apoptosis related genes were down-regulated post-PDT

The selected genes for qRT-PCR studies were markers for apoptosis, keloid pathogenesis and tumour growth. Collagen I, HIF-1, HSP70, Caspase-3 and 9, BCL-2 and Collagen III were down-regulated after PDT (Fig. 10a–h). There was higher down-regulation of cell survival gene B cell lymphoma 2 (BCL-2) in KF by 5-ALA compared to M-ALA while hypoxia-inducible factor (HIF-1) was down-regulated by 5-ALA compared to M-ALA in both KF and NF. Caspase-3 and 9 were up regulated in both NF and KF post 5-ALA as compared to M-ALA treatment. Quantitative data for untreated cells are shown in the online resource (Supplementary material Figs. 7, 8).

Discussion

This study has demonstrated the cytotoxicity levels of normal skin and keloid lesion site-specific fibroblasts following the application of PDT. We compared two precursors of intracellular photosensitiser, investigated the accumulation and degradation profile of intracellular photosensitiser, and

Fig. 5 Percentage of cytotoxicity post PDT in site-specific keloid fibroblasts compared to normal skin fibroblasts with increasing fluence rates. Cytotoxicity analysis at **a** 0 h, **b** 24 h and **c** 72 h by LDH assay. Cytotoxicity increased with higher fluence rates and this increase was proportionate to the energy delivered. Filled stars denote statistical significance ($P < 0.05$). Normal skin (pink bars), keloid margin (violet bars), keloid top (green bars) and keloid middle (blue bars)



measured cytoproliferation, apoptosis and necrosis rate, and senescence, in correlation to PpIX accumulation and ROS generation. Our results show that ROS generation and intracellular PpIX localisation are more critical in determining cytotoxicity than intracellular PpIX accumulation. In addition, ROS generation, cytotoxicity, cytoproliferation and senescence had fluence-dependent profiles. Fluorescence

analysis revealed that M-ALA instigated higher KF cytotoxicity at lower fluence ($\leq 20 \text{ J/cm}^2$) while 5-ALA instigated higher KF cytotoxicity at higher fluence, except in middle-specific keloid cells. Middle specific keloid cells were more prone to cell death post 5-ALA treatment while inconsistencies were observed with other site-specific keloid cells and M-ALA. A summary of results is given in Table 2.

Fig. 6 Percentage of cell proliferation in site-specific keloid fibroblasts compared to normal skin fibroblasts at increasing fluence rates with precursors of photosensitiser. Cytoproliferation of normal skin and keloid fibroblasts significantly decreased after PDT in an energy-dependent manner as measured by mitochondrial WST-1 enzyme assay. Filled stars denote statistical significance ($P < 0.05$). Normal skin (pink bars), keloid margin (violet bars), keloid top (green bars) and keloid middle (blue bars)

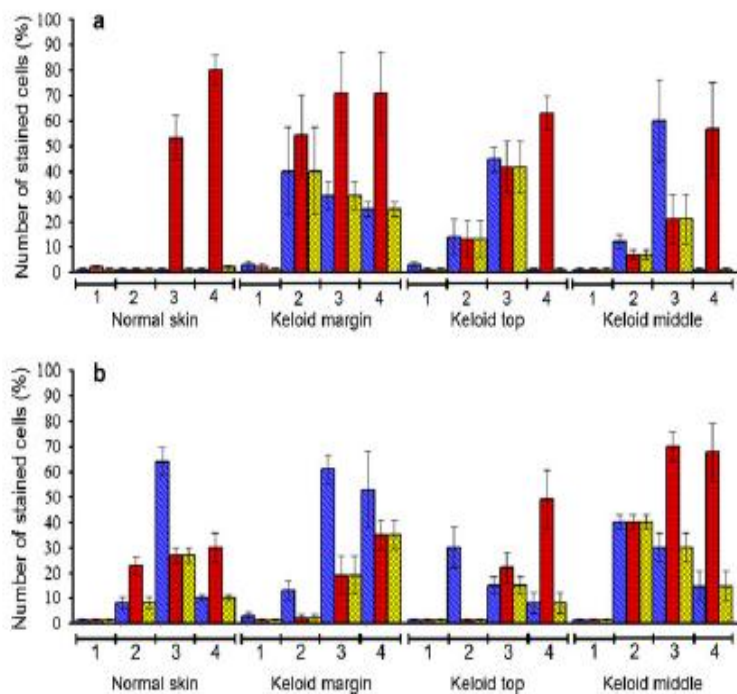
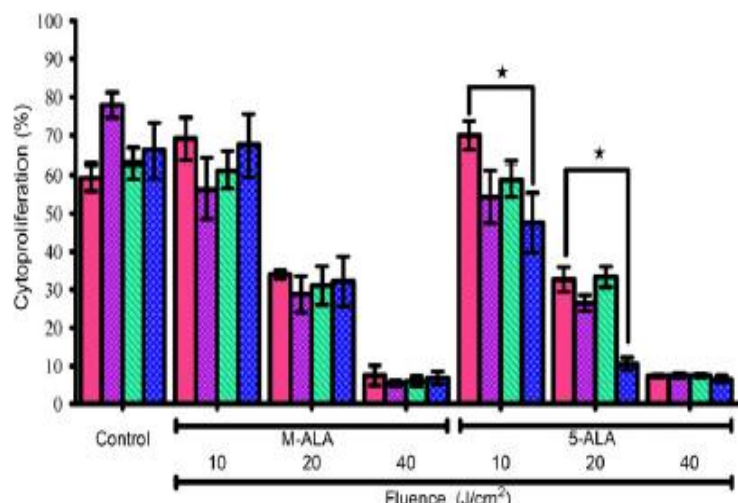


Fig. 7 Hoechst 33258/PI staining in normal skin compared to site-specific keloid fibroblasts 24 h after a M-ALA or b 5-ALA PDT treatment. M-ALA instigated higher cell death at a lower fluence rate ($<20 \text{ J/cm}^2$) whilst 5-ALA instigated higher cell death at a higher rate, except middle-specific keloid cells. The "PpIX intracellular localisation effects" which subsequently initiated different cytotoxic pathways after ROS generation (Fig. 9) could be an explanation for

higher cell death in middle-specific keloid cells compared to margin and top-specific cells. Even though unstained cells were observed post 40 J/cm^2 , the morphology of the cells revealed total cell lysis and indicated 100 % cell death after treatment. Hoechst 33258 (blue bars), Propidium iodide (red bars) and co-localization (yellow bars). 1 Control, 2 treatment with 10 J/cm^2 , 3 Treatment with 20 J/cm^2 , and 4 treatment with 40 J/cm^2

Aminolevulinic acid is an endogenous amino acid and has been promoted as a precursor for the photosensitising agent (PpIX) in PDT [4, 29, 32, 36]. In ALA-based PDT, intracellular PpIX accumulation has proved to be higher in tumour cells [19, 33] and could be detected through the typical red fluorescence under illumination with blue light.

Our results coincided with Sebastian et al. [38], illustrating the higher accumulation of PpIX in KF as compared to NF (Fig. 3). However, there was no significant difference in PpIX accumulation between different lesional sites in the keloid scar itself. Higher degree of PpIX generation in KF was observed after incubation with M-ALA compared to

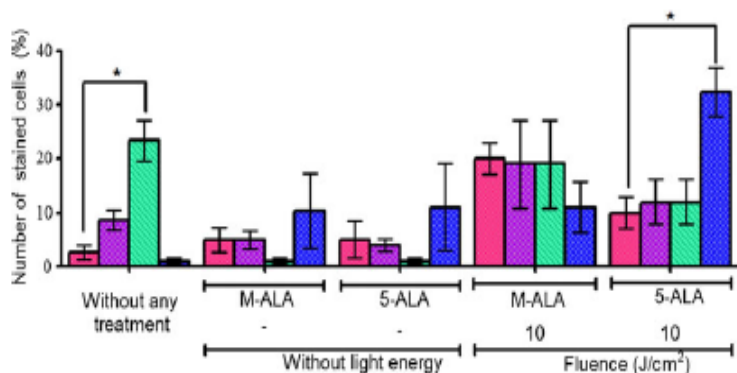
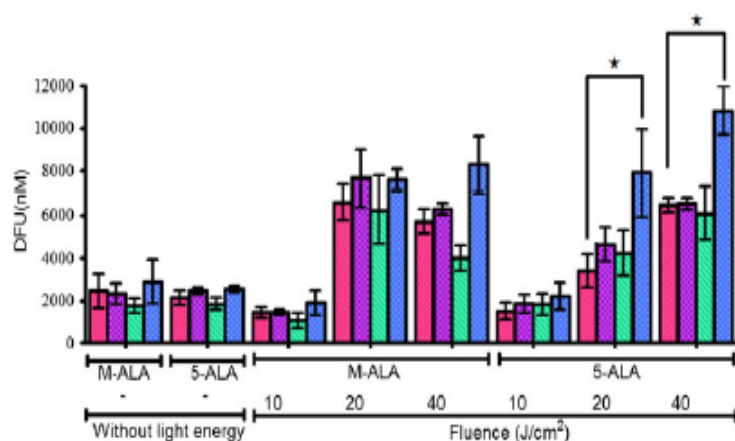


Fig. 8 β -galactosidase staining at pH 6 in normal skin compared to site-specific keloid fibroblasts after M-ALA and 5-ALA PDT treatment. Senescence was not observed at higher energies either due to cell death or incapability of the cell to break down the

chromogenic substrate X-gal. *denotes statistical significance ($P < 0.05$). Normal skin (pink bars), keloid margin (violet bars), keloid top (green bars) and keloid middle (blue bars)

Fig. 9 ROS generation post M-ALA/5-ALA-PDT treatment in normal skin as compared to site-specific keloid fibroblasts. Keloid fibroblasts from the middle of the scar generated more ROS after either M-ALA or 5-ALA PDT as compared to all other cell types. Filled stars denote statistical significance ($P < 0.05$). Normal skin (pink bars), keloid margin (violet bars), keloid top (green bars) and keloid middle (blue bars)



5-ALA ($P > 0.05$). This is because M-ALA penetrates into the cell by different mechanisms which include the facilitation by active transporters of non-polar amino acids or by diffusion, while 5-ALA is taken up by β -amino acids and γ -aminobutyric acid (GABA) [1, 34, 35].

Phototoxicity of cells increased in a dose-dependent manner with the amount of light energy delivered (Fig. 4). Phototoxicity of NF was only 2 % when compared with 10 % of KF even at the highest energy delivered (100 J/cm^2). However, the reduced innate apoptotic activity of KF as compared to normal scar fibroblasts was shown by Sayah et al. [38]. It is possible that external stimuli may accelerate the cytotoxic mechanism in KF more than NF [12]. Interestingly, following 72 h of PDT treatment, cytotoxicity of KF reached 90 % at 40 J/cm^2 , whilst NF was only 30 % under the same conditions (Fig. 5).

It has been reported that top and middle regions in keloid scars are generally quiescent while the margin is highly proliferative [42]. This is in agreement with our results showing higher cell death in keloid middle-specific

cells (Fig. 7) whilst least proliferative (Fig. 6) compared to fibroblasts from other sites. However, selective cell death mechanisms through apoptosis, autophagy and necrosis post PDT are suggested to be based on the cell type, the quantity of PpIX and intracellular PpIX localisation [5, 8, 14, 24, 29, 31]. Intracellular localisation of PpIX occurs in lysosomes, mitochondria, plasma membrane, golgi apparatus and endoplasmic reticulum [11], however the precise cellular localisation of PpIX in keloid fibroblasts have not been studied to date. Additionally, it has already been shown that PpIX accumulation in mitochondria results in higher cell death [21], which may explain our findings with the middle-specific keloid cells. Indeed, this was verified with higher generation of Caspases-3 and 9 seen in middle-specific keloid cells (Fig. 10f, g; qRT-PCR experiments) compared to cells from other sites.

Furthermore, middle-specific keloid cells treated with 5-ALA showed higher senescence, higher cytotoxicity and least proliferation compared to M-ALA treatment. There was a difference in cytotoxic mechanism induction post

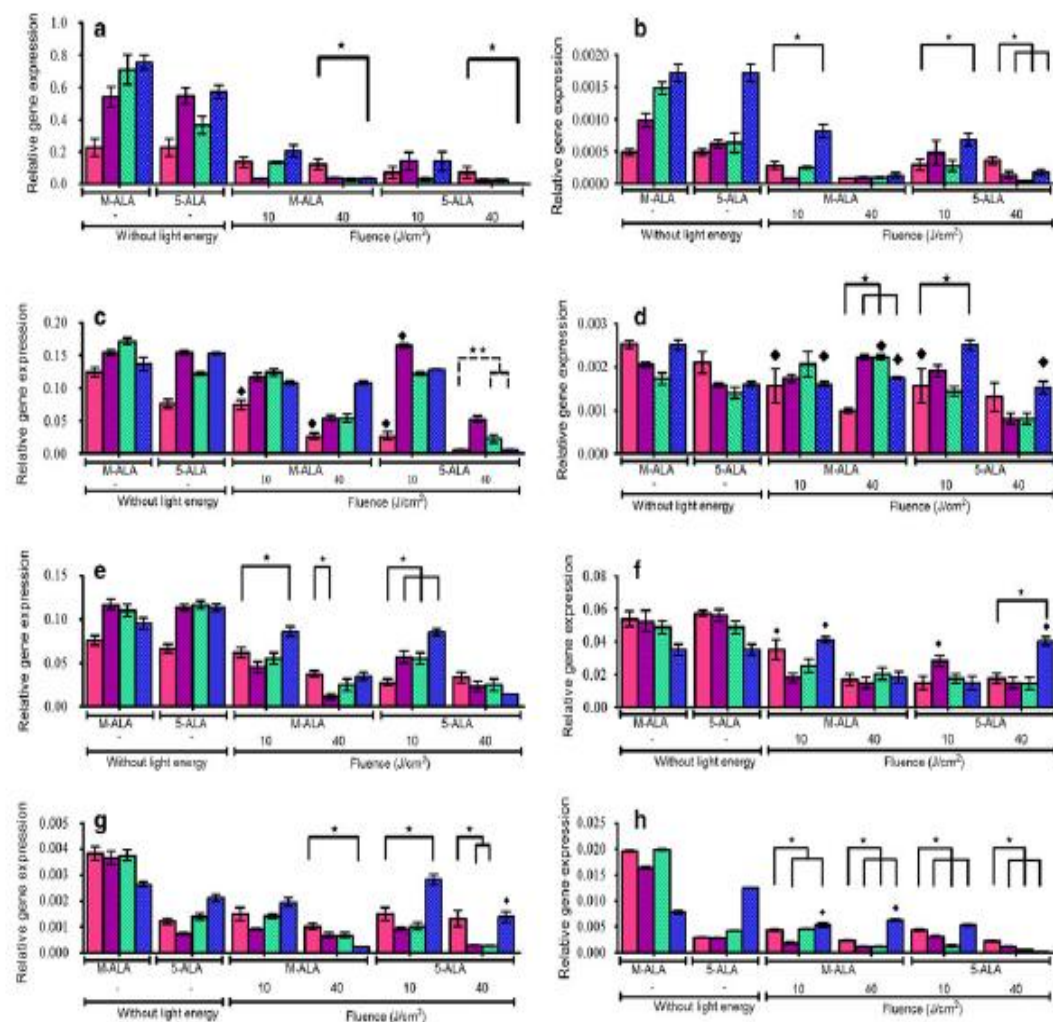


Fig. 10 Relative gene expression levels of keloid-associated genes in site-specific keloid fibroblasts compared to normal skin fibroblasts at increasing fluence rates with and without precursors of photosensitiser. **a** Collagen I, **b** Collagen III, **c** HIF-1, **d** HSP90, **e** HSP70, **f** Caspase-3, **g** Caspase-9, **h** BCL-2. qRT-PCR analysis shows Collagen I, HIF-1, HSP 70, Caspases 3 and 9 were down-regulated as compared to untreated cells (Supplementary Figs. 7, 8) and HSP90 retained similar expression levels post both M-ALA or 5-ALA PDT

treatment. In the graphs, comparisons are made between PDT-treated NF and PDT-treated KF. Filled stars denote statistical significance ($P < 0.05$); double star denotes statistical non-significance ($P > 0.05$); Diamonds denote statistical non-significance compared to cells without any treatment ($P > 0.05$). Normal skin (Pink bars), keloid margin (violet bars), keloid top (green bars) and keloid middle (blue bars)

PpIX accumulation and ROS generation after incubation with 5-ALA/M-ALA as indicated previously by Castano et al. [11]. Moreover, faster elimination of M-ALA than 5-ALA was observed in cultured epithelial cells [47], which could further generate PpIX, post irradiation.

Apoptosis is more preferable to necrosis in clinical situations as it leads to reduced tissue reactions. However, higher concentration of PpIX and light dosage will direct apoptosis towards necrosis as the principal cell death mechanism [45]. We observed the same result beyond 20 J/cm² where the major cellular apoptotic pathway was switched to necrosis (Fig. 7).

In the present study, we observed that the generation of ROS was mostly in accordance with fluence but not with PpIX accumulation. Eventhough PpIX formation was higher in human epidermoid carcinoma cells, any blockade in cellular mechanism inhibited the generation of ROS and subsequent cell death [23]. This was in agreement with PpIX accumulation (Fig. 3) and ROS generation (Fig. 9) where middle-specific keloid cells generated more ROS in spite of lower PpIX accumulation compared to other cell sites. The pattern of ROS generation could be correlated with apoptosis/necrosis mechanisms, with the ratio of necrosis increasing with ROS generation (>10 J/cm²). This

Table 2 Summary of results

Treatment modalities	Cell type	LDH cytotoxicity analysis (%)			WST-1 cell viability analysis (%)	Mechanism of cell death (%)		Positive senescence (%)	ROS generation (nM for 10^3 cells)
		0 h	24 h	72 h		A	N		
M-ALA + 10 J/cm ²	NF	0.5	12	12	70	2	2	20	1,600
	KMr	1.5	5	2	55	40	55	18	1,600
	KT	1	12	20	62	15	12	10	1,500
	KMi	2	11	20	68	12	10	10	2,000
M-ALA + 20 J/cm ²	NF	1	22	12	35	2	52	–	6,200
	KMr	2	10	12	30	30	70	–	6,600
	KT	2	23	28	32	45	42	–	6,200
	KMi	2	25	32	32	60	20	–	7,800
M-ALA + 40 J/cm ²	NF	2	28	22	9	2	80	–	5,800
	KMr	3	10	15	8	25	70	–	6,200
	KT	2	325	42	8	2	62	–	4,000
	KMi	3	48	45	9	2	60	–	8,200
5-ALA + 10 J/cm ²	NF	0.5	10	10	70	8	22	8	1,800
	KMr	1.5	2	10	55	12	2	10	1,900
	KT	1	19	12	60	30	2	10	1,900
	KMi	4	38	62	49	40	40	30	2,000
5-ALA + 20 J/cm ²	NF	1	22	10	32	65	28	–	2,800
	KMr	2	5	10	28	60	20	–	4,500
	KT	1	20	22	32	15	22	–	4,200
	KMi	6	58	72	10	30	70	–	8,000
5-ALA + 40 J/cm ²	NF	2	22	28	8	10	30	–	6,200
	KMr	3.5	20	28	8	55	35	–	6,200
	KT	1.5	21	22	8	10	50	–	6,000
	KMi	8	55	95	8	15	68	–	11,000

NF normal skin fibroblasts, KMr Keloid margin fibroblasts, KT Keloid top fibroblasts, KMi Keloid middle fibroblasts, A apoptosis, N necrosis, nM nanomolar

– denotes absence of positive data

also demonstrated ROS as the principal effector of cell damage post PDT that is demonstrated in Fig. 11. Here, the subcellular target in PDT was mainly affected by ROS, which could potentially lead to lipid peroxidation, cytoskeleton, biological membrane and DNA damage [22].

Reactive oxygen species generation in mitochondria can lead to apoptosis/necrosis through Caspase-dependant pathway, which was evident from the differential expression of Caspases-3 and 9 post-PDT. Generally, Cytochrome c is released from the mitochondria as a pro-signal for apoptosis leading to a reduction in mitochondrial membrane potential, which is followed by the activation of Caspase-3-like proteases [15, 22, 49]. This could be an early indication of apoptosis, post-PDT. However, the dependence of apoptosis/necrosis on Caspases-3 and 9 activation has not been verified in this study. The decreased expression of BCL-2 (marker for mitochondrial cell viability) with increased light energy also supports decreased cell viability.

HSP70 has been shown to be expressed at lower levels in normal skin as compared to keloid fibroblasts and is up-regulated during wound healing process and keloid formation [43]. We observed down-regulation of HSP70 post-PDT, which is another indication of increased cell death. HSP90, which acts as a molecular chaperone to prevent protein unfolding and aggregation, was expressed to similar levels in keloid and normal skin fibroblasts. Our results indicate the minor role of HSP90 in cell death post-PDT. A consistent up-regulation of HIF-1 α was observed in keloids compared to normal skin [50]. However, HIF-1 α was down-regulated in both KF and NF at higher fluence. This could be another indication of the cytotoxic conditions prevailing after PDT as indicated in Fig. 11. Further decrease of HIF-1 α in middle-specific keloid cells following 5-ALA incubation and 40 J/cm² indicate higher cell death, compared to other treatments.

In conclusion, this study for the first time, has demonstrated that cytotoxicity post-PDT in keloid fibroblasts are

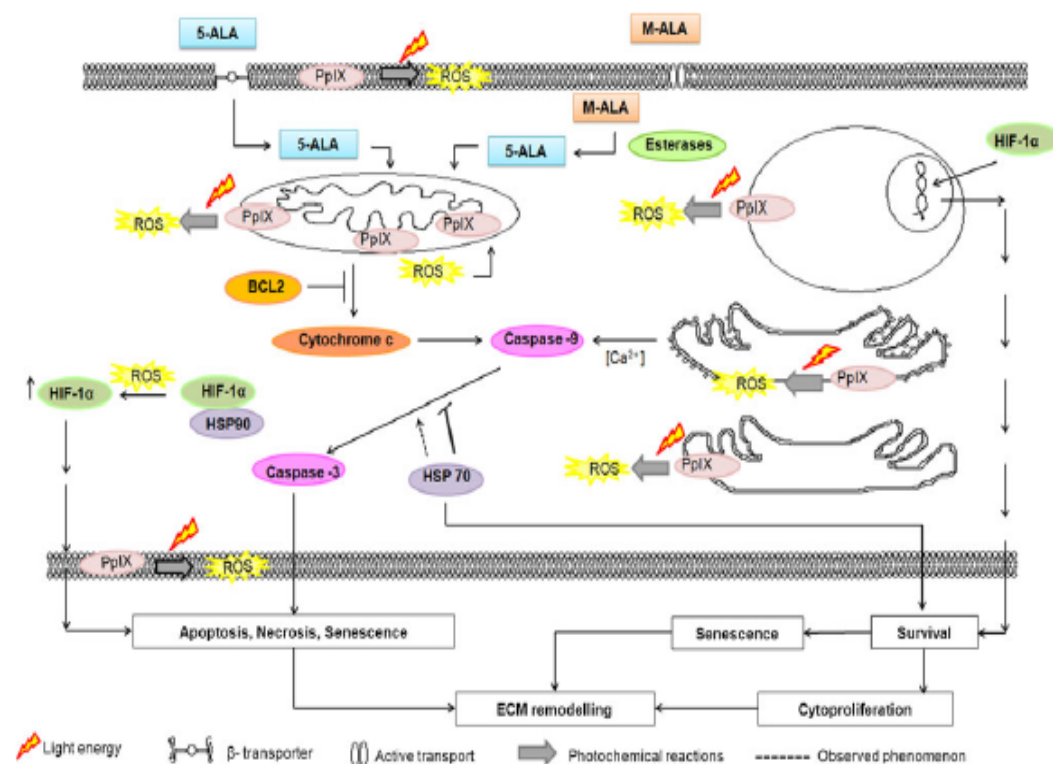


Fig. 11 A diagrammatic representation of the proposed mechanism of cell death/cell survival of fibroblasts by PDT. M-ALA penetrates into the cell by different mechanisms, which include the facilitation by active transporters of non-polar amino acids or by diffusion, while 5-ALA is taken up by β -amino acids and γ -aminobutyric acid (GABA). Esterases cut M-ALA into 5-ALA, which is converted into PpIX in the inner membrane of the mitochondria. The photosensitive properties of PpIX generate intracellular ROS after photochemical reactions. ROS leads to organelle damage, which initiates several

mechanisms which are pro-apoptosis or pro-survival. Caspase-9 and subsequently Caspase-3 are activated by cytochrome *c* released from mitochondria, which leads to apoptosis. HIF-1 binds to nuclear DNA, thereby translating proteins, which can enhance cell survival. HSP70 has been observed to be up-regulated during wound healing process and also in keloid tissue. The combined activity of HSP70 and Caspase-9 may enhance Caspase-3 activity, which may further guide keloid fibroblasts to a preferred cell death mechanism

highly dependent on the lesional site in a keloid lesion, precursors of intracellular photosensitiser, localisation of PpIX and the light energy delivered per unit area. Since the efficacy of PDT depends on intracellular PpIX localisation and ROS generation, fluence should be customised in accordance with the precursor of photosensitiser for KD treatment. For example 40 J/cm² post 5-ALA treatment is more effective for middle-specific keloid cells while 20 J/cm² post M-ALA treatment is more effective for other sites. Again from our fluorometric analysis, margin-specific cells were the most cytotoxic following 10 J/cm² of M-ALA incubation, while they were less cytotoxic after 5-ALA incubation under same conditions. Since cytotoxicity has only been determined in cell monolayer culture, an extrapolation of fluence to ex vivo tissue microenvironment is necessary to optimise the parameters. These findings demonstrate a potential future application for site-targeted therapy in the treatment of KD. Based on our fluorometric cytotoxicity and proliferation results, esterified

forms of 5-ALA would be more efficacious than 5-ALA, and may induce higher cytotoxicity in margin-specific keloid cells.

Acknowledgments Senior author (AB) is in receipt of a personal award from The National Institute for Health Research (United Kingdom). Jenifer Mendoza is receipt of award from the Mexican Government Organization for a full PhD scholarship. The senior author (AB) has received a personal award from The National Institute for Health Research (UK). No industry funding was received for this project.

Conflict of interest The authors declare that they have no conflict of interest.

References

1. Alders MC, van der Vange N, Star WM, Sterenborg HJ (2001) A mathematical evaluation of dose-dependent PpIX fluorescence kinetics in vivo. Photochem Photobiol 74(2):311–317

2. Almeida Issa MC, Pifcero-Maceira J, Farias RE, Pureza M, Raggio Luiz R, Manela-Azulay M (2009) Immunohistochemical expression of matrix metalloproteinases in photodamaged skin by photodynamic therapy. *Br J Dermatol* 161(3):647–653
3. Allison RR, Sibata CH (2010) Oncologic photodynamic therapy photosensitisers: a clinical review. *Photodiagnosis Photodyn Ther* 7(2):61–75
4. Angell-Petersen E, Sørensen R, Warloe R, Soler AM, Moan J, Peng Q, Giercksky KE (2006) Porphyrin formation in actinic keratosis and basal cell carcinoma after topical application of methyl 5-aminolevulinate. *J Invest Dermatol* 126(2):265–271
5. Atif M, Firdous S, Khurshid A et al (2009) In vitro study of 5-aminolevulinic acid-based photodynamic therapy for apoptosis in human cervical HeLa Cell line. *Laser Phys Lett* 12: 886–891
6. Bagadir RA, Syed F, Rautemaa R, McGrouther DA, Pas R, Bayat A (2011) Up-regulation of Toll-like receptors (TLRs) 6, 7, and 8 in keloid scars. *J Invest Dermatol* 131(10):2128–2130
7. Butler PD, Longaker MT, Yang GP (2008) Current progress in Keloid research and treatment. *J Am Coll Surg* 206(4):731–742
8. Cai H, Gu Y, Sun Q, Zeng J, Dong N, Zhao G (2011) Effect of hematoporphyrin monomethyl ether-mediated photodynamic therapy on hypertrophic scar fibroblasts. *Photodermatol Photoimmunol Photomed* 27(2):90–96
9. Bruscino N, Lotti T, Rossi R (2011) Photodynamic therapy for hypertrophic scarring: a promising choice. *Photodermatol Photoimmunol Photomed* 27(6):334–335
10. Casas A, Fukuda H, Di Venosa G, Battle A (2001) Photosensitization and mechanism of cytotoxicity induced by the use of ALA derivates in photodynamic therapy. *Br J Cancer* 85(2): 279–284
11. Castano A, Demidova T, Hamblin M (2004) Mechanisms in photodynamic therapy: part one-photosensitisers, photochemistry and cellular localization. *Photodiagnosis Photodyn Ther* 1(4):279–293
12. Chiu LL, Sun CH, Yeh AT, Torkian B, Karamzadeh A, Tromberg B, Wong BJ (2005) Photodynamic therapy on keloid fibroblasts in tissue-engineered keratinocyte-fibroblast co-culture. *Lasers Surg Med* 37(3):231–244
13. Frost GA, Halliday GM, Damian DL (2011) Photodynamic therapy-induced immunosuppression in humans is prevented by reducing the rate of light delivery. *J Invest Dermatol* 131(4): 962–968
14. Garg AD, Nowis D, Golab J, Agostinis P (2010) Photodynamic therapy: illuminating the road from cell death towards anti-tumour immunity. *Apoptosis* 15(9):1050–1071
15. He J, Whitacre CM, Xue LY, Berger NA, Oleinick NL (1998) Protease activation and cleavage of poly (ADP-ribose) polymerase: an integral part of apoptosis response to photodynamic therapy. *Cancer Res* 58(5):940–946
16. Hollywood KA, Maatje M, Shadi IT, Henderson A, McGrouther DA, Goodacre R, Bayat A (2010) Phenotypic profiling of keloid scars using FT-IR microspectroscopy reveals a unique spectral signature. *Arch Dermatol Res* 302:705–715
17. Javad F, Day PJR (2012) Protein profiling of keloid scar tissue. *Arch Dermatol Res*. doi:10.1007/s00403-012-1224-6
18. Ji HT, Chien LT, Lin YH, Chien HF, Chen CT (2010) 5-ALA mediated photodynamic therapy induces autophagic cell death via AMP-activated protein kinase. *Mol Cancer* 28:91
19. Ji Z, Yang G, Vasovic V, Cunderlikova B, Suo Z, Nesland JM, Peng Q (2006) Subcellular localization pattern of protoporphyrin IX is an important determinant for its photodynamic efficiency of human carcinoma and normal cell lines. *J Photochem Photobiol B* 84(3):213–220
20. Kawaguchi T, Yamamoto S, Naka N, Okishio K, Atagi S, Ogawa M et al (2000) Immunohistochemical analysis of Bcl-2 protein in early squamous cell carcinoma of the bronchus treated with photodynamic therapy. *Br J Cancer* 82(2):418–423
21. Kessel D, Luo Y, Deng Y, Chang CK (1997) The role of sub-cellular localization in initiation of apoptosis by photodynamic therapy. *Photochem Photobiol* 65(3):422–426
22. Kim CH, Chung CW, Choi KH, Yoo JJ, Kim do H, Jeong Yi, Kang DH (2011) Effect of 5-aminolevulinic acid-based photodynamic therapy via reactive oxygen species in human cholangiocarcinoma cells. *Int J Nanomed* 6:1357–1363
23. Lam M, Oleinick NL, Nieminen AL (2001) Photodynamic therapy-induced apoptosis in epidermoid carcinoma cells. Reactive oxygen species and mitochondrial inner membrane permeabilization. *J Biol Chem* 276(50):47379–47386
24. Lee JB, Choi JY, Chun JS, Yun SJ, Lee SC, Oh J, Park HR (2008) Relationship of protoporphyrin IX synthesis to photodynamic effects by 5-aminolevulanic acid and its esters on various cell lines derived from the skin. *Br J Dermatol* 159(1):61–67
25. Lesar A, Ferguson J, Moseley H (2011) An investigation of the fluorescence induced by topical application of 5-aminolevulinic acid and methyl aminolevulinate at different body sites on normal human skin. *Photodiagnosis Photodyn Ther* 8(2):97–103
26. Luo S, Benathan M, Raffoul W, Panizzon RG, Egloff DV (2001) Abnormal balance between proliferation and apoptotic cell death in fibroblasts derived from keloid lesions. *Plast Reconstr Surg* 107(1):87–96
27. Matthews YJ, Damian DL (2010) Topical photodynamic therapy is immunosuppressive in humans. *Br J Dermatol* 162(3):637–642
28. Nie Z, Bayat A, Behzad F, Rhodes LE (2010) Positive response of a recurrent keloid scar to topical methyl aminolevulinate-photodynamic therapy. *Photodermatol Photoimmunol Photomed* 26(6):330–332
29. Noodt BB, Berg K, Stokke T, Peng Q, Nesland JM (1996) Apoptosis and necrosis induced with light and 5-aminolevulonic acid-derived protoporphyrin IX. *Br J Cancer* 74(1):22–29
30. Oleinick NL, Morris R, Belichenko I (2002) The role of apoptosis in response to photodynamic therapy: what, where, why, and how. *Photochem Photobiol Sci* 1(1):1–21
31. Panzarini E, Inguscio V, Dini L (2011) Timing the multiple cell death pathways initiated by rose bengal acetate photodynamic therapy. *Cell Death Dis* 2:e169
32. Peng Q, Warloe T, Berg K, Moan J, Kongshaug M, Giercksky KE, Nesland JM (1997) 5-aminolevulonic acid-based photodynamic therapy. Clinical research and future challenges. *Cancer* 79(12):2282–2308
33. Robertson CA, Evans DH, Abrahamse H (2009) Photodynamic therapy (PDT): A short review on cellular mechanisms and cancer research applications for PDT. *J Photochem Photobiol B* 96(1):1–8
34. Rodriguez L, Battle A, Di Venosa G, Battah S, Dobbin P, MacRobert AJ, Casas A (2006) Mechanisms of 5-aminolevulinic acid ester uptake in mammalian cells. *Br J Pharmacol* 147(7):825–833
35. Rud E, Gederup O, Høgset A, Berg K (2000) 5-aminolevulinic acid, but not 5-aminolevulinic acid esters, is transported into adenocarcinoma cell by system BETA transporters. *Photochem Photobiol* 71(5):640–647
36. Sailer R, Strauss WSL, Wagner M, Emmert H, Schneckenburger H (2007) Relation between intracellular location and photodynamic efficacy of 5-aminolevulonic acid-induced protoporphyrin IX in vitro. Comparison between human glioblastoma cells and other cancer cell lines. *Photochem Photobiol Sci* 6(2):145–151
37. Sayah DN, Soo C, Shaw WW, Watson J, Messadi D, Longaker MT et al (1999) Down-regulation of apoptosis-related genes in keloid tissues. *J Surg Res* 87:209–216
38. Sebastian A, Allan E, Allan D, Colthurst J, Bayat A (2011) Addition of novel degenerate electrical waveform stimulation

- with photodynamic therapy significantly enhances its cytotoxic effect in keloid fibroblasts: first report of a potential combination therapy. *J Dermatol Sci* 64(3):174–184
39. Seifert O, Mrowietz U (2009) Keloid scarring: bench and bedside. *Arch Dermatol Res* 301:259–272
 40. Shih B, Bayat A (2010) Genetics of keloid scarring. *Arch Dermatol Res* 302(5):319–339
 41. Steinbauer JM, Schreml S, Kohl EA, Karrer S, Landthaler M, Szeimies RM (2010) Photodynamic therapy in dermatology. *J Dtsch Dermatol Ges* 8(6):454–464
 42. Syed F, Ahmadi E, Iqbal SA, Singh S, McGrouther DA, Bayat A (2011) Fibroblasts from the growing margin of keloid scars produce higher levels of collagen I and III compared with intralesional and extralesional sites: clinical implications for lesional site-directed therapy. *Br J Dermatol* 164(1):83–96
 43. Totan S, Echo A, Yuksel E (2011) Heat shock proteins modulate keloid formation. *Eplasty* 11:e21
 44. Tucci-Viegas VM, Hochman B, Franca JP, Ferreira LM (2010) Keloid explant culture: a model for keloid fibroblasts isolation and cultivation based on the biological differences of its specific regions. *Int Wound J* 7(5):339–348
 45. Uehlinger P, Zellweger M, Wagni'eres G, Juillerat-Jeanneret L, van den Bergh, Lange N (2000) 5-aminolevulinic acid and its derivates: physical chemical properties and protoporphyrin IX formation in cultured cells. *J Photochem Photobiol B* 54(1):72–80
 46. Urioste SS, Amdit KA, Dover JS (1999) Keloids and hypertrophic scars: review and treatment strategies. *Semin Cutan Med Surg* 18(2):159–171
 47. Washbrook R, Riley PA (1997) Comparison of delta-aminolevulinic acid and its methyl ester as an inducer of porphyrin synthesis in cultured cells. *Br J Cancer* 75(10):1417–1420
 48. Wyld L, Reed MW, Brown NJ (2001) Differential cell death response to photodynamic therapy is dependent on dose and cell type. *Br J Cancer* 84(10):1384–1386
 49. Zhao H, Xing D, Chen Q (2011) New insights of mitochondria reactive oxygen species generation and cell apoptosis induced by low dose photodynamic therapy. *Eur J Cancer* 47(8):2750–2761
 50. Zhang Q, Wu Y, Ann DK, Messadi DV, Tuan TL, Kelly AP et al (2003) Mechanisms of hypoxic regulation of plasminogen activator inhibitor-1 gene expression in keloid fibroblasts. *J Invest Dermatol* 121(5):1005–1012

Optimization of an ex vivo wound healing model in the adult human skin: Functional evaluation using photodynamic therapy

Jenifer Mendoza-Garcia, MSc^{1,2}; Anil Sebastian, PhD²; Teresa Alonso-Rasgado, PhD¹; Ardesir Bayat, BSc (Hons), MBBS, PhD^{1,2,3}

1. Bioengineering Group, School of Materials,

2. Plastic Reconstructive Surgery Research Group, Manchester Institute of Biotechnology (MIB),

3. Center for Dermatology, Institute of Inflammation and Repair, Faculty of Medical and Human Sciences, Manchester Academic Health Science Centre, The University of Manchester, Manchester, United Kingdom

Reprint requests:

Dr. Ardesir Bayat, Plastic & Reconstructive Surgery Research, Institute of Inflammation & Repair, Manchester Institute of Biotechnology, The University of Manchester, 131 Princess Street, Manchester, M1 7DN, United Kingdom.
Tel: 0044 161 306 5177;
Fax: 0044 161 306 5177;
Email: ardesir.bayat@manchester.ac.uk

Manuscript received: October 3, 2014

Accepted in final form: June 1, 2015

DOI:10.1111/wrr.12325

ABSTRACT

Limited utility of in vitro tests and animal models of human repair, create a demand for alternative models of cutaneous healing capable of functional testing. The adult human skin Wound Healing Organ Culture (WHOC) provides a useful model, to study repair and enable evaluation of therapies such as the photodynamic therapy (PDT). Thus, the aim here was to identify the optimal WHOC model and to evaluate the role of PDT in repair. Wound geometry, system of support, and growth media, cellular and matrix biomarkers were investigated in WHOC models. Subsequently, cellular activity, extracellular matrix remodeling, and oxidative stress plus gene and protein levels of makers of wound repair measured the effect of PDT on the optimized WHOC. WHOCs embedded in collagen and supplemented DMEM were better organized showing stratified epidermis and compact dermis with developing neo-epidermis. Post-PDT, the advancing reepithelialization tongue was 3.5 folds longer, and was highly proliferative with CK-14 plus p16 increased ($p < 0.05$) compared to controls. The neo-epidermis was fully differentiated forming neo-collagen. Proliferating nuclear antigen, p16, COL1, COLIII, MMP3, MMP19, and α -SMA were significantly more expressed ($p < 0.05$) in dermis surrounding the healing wound. In conclusion, an optimal model of WHOC treated with PDT shows increased reepithelialization and extracellular matrix reconstruction and remodeling, supporting evidence toward development of an optimal ex vivo wound healing model.

An ideal wound healing model of adult human skin should not only resemble a wound made and evaluated within a system that resembles and incorporates all adult human skin components, processes, and functions but also allow for functional testing of therapies ex vivo and enable evaluation of the effect of these processes in cutaneous repair.^{1,2}

However, some of the existing wound models fall short of this ideal scenario. Monolayer and organotypic cultures provide valuable information about one or few components of the skin at a time, but do not correlate with their in vivo counterparts due to their lack of complexity.¹ In silico or in virtuo models may be useful theoretically but are devoid of the physical characteristics of the native human skin. Finally, animal models although informative, can present with major structural and biological differences notwithstanding the potential cost, ethical, and moral issues associated with their use.¹⁻³

Human skin organ culture is comprised of all skin components and importantly includes the complex interactions between these components, which are, however, maintained

ex vivo. Full thickness skin organ culture is already an established and valuable tool used for understanding human skin pathophysiology, evaluation of novel treatments, and effect of xenobiotics.⁴⁻⁷

A number of such wound healing organ culture models (WHOCs) have been previously reported to be relevant in studying cutaneous wound healing processes.⁴⁻¹⁰ Possible new therapies including anti-inflammatory interleukin 10, anti-fibrotic streptolysin O and demal substitutes have been evaluated using WHOCs.^{4,5,10} However, it is apparent that despite these previously reported approaches, there is a lack of standardization and conformity in testing of WHOCs. The variations in these methodologies include the use of the following; a partial or full thickness wound, different culture conditions, and a range of support and growth mediums.^{6,11} Thus, in the absence of a standardized protocol, the most optimal setup in relation to growth media, physical support systems such as collagen embedding or well chamber inserts and type of wound to study the wound healing process and functional testing of products remains unclear.

Wound Rep Reg (2015) 00:00-00 © 2015 by the Wound Healing Society
This is an open access article under the terms of the Creative Commons Attribution-NonCommercial-NoDerivs License, which permits use and distribution in any medium, provided the original work is properly cited, the use is non-commercial and no modifications or adaptations are made.

1

Although a number of candidate therapies for enhancing skin repair have been evaluated using WHOCs, there has not been any previous report of the role of Photodynamic Therapy (PDT) in cutaneous wound healing using the WHOC model. Recent anti-aging studies in human skin and animal studies have suggested that PDT may have an important role in extracellular matrix (ECM) remodeling and wound healing.^{12–15} PDT works by energy transfer from illumination to molecular oxygen through the action of a photosensitizer, 5-aminolevulonic acid (5-ALA), as precursor of protoporphyrin IX. Cellular effects of PDT depend on tissue type, oxygen tension and dosage, resulting in necrosis, apoptosis, and autophagy.^{16,17}

Thus, the aim of this study was to develop and optimize a WHOC model of human adult skin and to evaluate this functionally with PDT. Histological, immunohistochemical (IHC), and differential gene expression analyses were performed pre- and post-PDT, to increase our understanding of the effects of PDT applied to wound healing in the adult human skin.

METHODS

Skin explants

Skin explants were obtained from 11 healthy patients undergoing routine elective cosmetic surgery (Table 1). Ethical approval for this work was granted by the North West (England, UK) Research Ethics Committee (Ethics Code - 11/NW/0683). Tissue samples were collected following informed consent. Explants were washed several times in phosphate buffer solution (PBS, Sigma-Aldrich, Dorset, UK) and soaked in Dulbecco's modified Eagle's medium (DMEM; Sigma-Aldrich, Dorset, UK) supplemented with Primocin (InvivoGen, Nottingham, UK) for 30 minutes. Skin explants were cut with a full thickness punch biopsy of 8 mm. Two different wounds were then created within the punch biopsy (either partial or full thickness wound). The punch biopsies were placed in two different support systems and maintained with three different commercial media. WHOCs were maintained at 37°C and 5% CO₂/95% O₂ tension (Figure 1A–F; n = 6; WHOCs/donor = 78).

Wounding procedure

WHOC were made with two different wounds. (I) A partial thickness incisional wound, comprising the epidermis and upper part of the dermis, was made with two parallel cuts using a scalpel. The width of each cut was either 1 mm, 2 mm, or 3 mm (Figure 1A). (II) A full thickness excisional wound (donut-shaped model) comprising the epidermis and dermis was made using a punch biopsy kit with a 1 mm, 2 mm, or 3 mm punch in the center of the 8 mm diameter full thickness biopsy (Figure 1B). In WHOCs used for PDT testing (n = 6), the inner wound were filled in with either subcutaneous fat (excised from the harvested tissue) or BD Matrigel (BD Biosciences, Oxford, UK) inside the wound as a fill-in scaffold. The autologous hypodermal fat used to make a scaffold was washed several times with PBS and vortex for 5 minutes at room temperature. The suspension was put in a centrifuge at 1,800 × for 5 minutes. The upper oil-layer was

discarded. The viscous suspension was rinsed three times with PBS and placed into the wound.¹⁸

Tissue support systems and growth media

Two different systems of tissue biopsy support were used: (I) the WHOCs were placed in the middle of a well chamber insert (5 µm; Millipore, Darmstadt, Germany), with a 6 mm diameter perforation. The dermal part was submerged in the liquid medium and the epidermis was left exposed to air–liquid interface⁷ (Figure 1D and F); (II) the WHOCs dermal part was embedded in rat tail collagen type one gel (2 mg/mL; BD Biosciences, Oxford, UK)¹⁹ and the epidermis was left exposed to the air–liquid interface.⁷ Collagen gels were made with the same growth media used in the liquid–air interface (Figure 1C and E).

WHOC models were maintained with three different media, (I) DMEM, (II) William's E medium (WE), and (III) a mixture of DMEM/Ham's F12/EpiLife (MED3; 1: 3). DMEM and WE were supplemented with 100 IU/mL penicillin, 10 µg/mL streptomycin, 10% Foetal Bovine Serum (FBS), 10 µg/mL of insulin, 10 ng/mL of hydrocortisone, and 2 mM of L-glutamine. MED3 was supplemented with EpiLife Define Growth Supplement. The media was changed every other day. All reagents were from Sigma-Aldrich, except EpiLife medium (Cascade Biologics, Portland, OR). WHOCs were harvested on the 14th day and histologically processed under standard protocols.

PDT treatment

WHOCs of 8 mm with 2 mm full thickness excisional biopsy wound were filled (donut like) with either fat or Matrigel scaffold inside the wound and were exposed to PDT and compared to nontreated controls (n = 6; WHOCs/donor = 7). Additionally, WHOCs of 8 mm with 1.5 mm full thickness excisional biopsy wounds were filled with fat scaffold inside the wound and were exposed to PDT and compared to nontreated WHOCs (n = 6; WHOCs/donor = 9). 5-aminolevulonic acid (5-ALA; 20% v/v; Mandeville Medicines, Aylesbury, UK) was consistently applied onto the WHOCs surface and incubated for 3 hours. This was subsequently illuminated with a PDT machine (Omnilux PDT, Photo Therapeutics, PA), with an arrangement of red light-emitting diodes (LEDs) of 633 ± 3 nm wavelength. The power intensity of the PDT machine was adjusted to 20 J/cm² and calibrated with an IL1700 radiometer (International Light Technologies Inc, Peabody, MA).¹⁷ PDT treatment was given once on the third day after collection. The WHOCs were harvested on day 0 (control), the 7th and 14th day post-PDT application and without any treatment. WHOCs were washed twice with PBS before illumination. After illumination, WHOCs were reembedded in collagen. All procedures were undertaken under darkness and sterile conditions. The WHOCs were fixed, paraffin embedded, sectioned, and deparaffinized using standard procedures.¹⁹

Histology

Representative sections of 5 µm, cut nearest to the center of the biopsies were stained. Controls WHOCs on day 0 were compared with WHOCs maintained in the conditions

Table 1. Demographic data and source of skin explants

Patient number	Gender	Age (years)	Anatomical source of skin explants
1	Male	71	Abdomen
2	Female	42	Abdomen
3	Female	38	Abdomen
4	Male	28	Abdomen
5	Female	42	Abdomen
6	Male	42	Breast
7	Female	60	Breast
8	Female	61	Breast
9	Female	51	Breast
10	Female	37	Breast
11	Female	31	Breast

described above. Additionally, in the PDT treated sample analysis, WHOCs treated with PDT were compared with WHOCs without treatment. Tissue morphology and analysis of the advancing epithelial tongue was examined using haematoxylin & eosin (H&E, Sigma-Aldrich), Herovici's (HV), and Weigert's elastic differential staining (WELA; Sigma-Aldrich). H&E and WELA staining were done according to the manufacturer's instructions. HV staining was carried out as described by Bagabir et al.¹⁹ Stained sections were scanned in a Hamamatsu NanoZoomer 2.0-HT and analyzed with NDP.view2 image software (Hamamatsu, Hertfordshire, UK).

Immunohistochemistry/immunofluorescence

Cell death and proliferation were assessed by the 3'-OH DNA end-labeling method (Tunel; FragEL, Calbiochem-Merck, Darmstadt, Germany) and with Proliferating Nuclear Antigen (PCNA) IHC staining, respectively. Additionally selected markers for epidermal differentiation-cytokeratin 14 (CK-14), ECM remodeling-metalloproteinase 3 (MMP3), and metalloproteinase 19 (MMP19), senescence oxidative stress-induction-cyclin-dependent kinase inhibitor 2A (p16), a wound contraction marker α -smooth muscle actin (α -SMA) and vessels marker-platelet endothelial cell adhesion molecule marker CD31 were immunostained with panel of antibodies as shown in Table 2 (Abcam, Cambridge, UK). IHC were detected with Novocastra Peroxidase Detection Systems (Leica, Milton Keynes, UK). IHC and peroxidase detection were performed according to the manufacturer's instructions. Stained sections were scanned in a Hamamatsu NanoZoomer 2.0-HT and analyzed with NDP.view2 image software (Hamamatsu, Hertfordshire, UK). Objective quantification of cellular markers was performed using Definiens Tissue Studio 3.5 Software (Definiens, Munich, Germany).²⁰

RNA isolation, cDNA synthesis and qRT-PCR

Complete WHOCs were collected in TRIzol reagent (Invitrogen, Abingdon, UK) and processed for RNA isolation, cDNA synthesis and qRT-PCR (Qiagen, Manchester, UK) according to the manufacturer's instructions. The gene

expression levels were normalized with an internal reference gene, RPL32. The primers used in the study are detailed in Table 3. A detailed flow chart of the methodology is shown in the Supporting Information figures (please see Figure S1).

Statistical analysis

The results of the study are presented as the mean values \pm standard deviation. Statistical significance was calculated with One-way ANOVA and Bonferroni's comparison test. Graphics and statistics were generated with GraphPad Prism 5 (GraphPad Software, La Jolla, CA). The differences were considered statistically significant if $p < 0.05$.

RESULTS

Ex vivo WHOCs embedded in collagen and supplemented DMEM preserved epidermal and dermal architecture and characteristics

To understand the optimal ex vivo conditions for long-term maintenance of WHOC models, we evaluated the growth medium, the physical WHOC support system in relation to wound size and shape. From H&E analysis, neither epidermolysis nor necrosis was observed after 14 days (D14) ex vivo, indicating the maintenance of intact functional skin.

a. Epidermal analysis (D14)

WHOCs embedded in collagen and well chamber inserts, maintained in DMEM and WE preserved epidermal stratification with presence of melanocytes in the basal layer, intact dermal-epidermal junctions, and rete ridges with peaks and valleys (Figure S2C–F). Additionally, WHOCs fed with only DMEM maintained cuboidal basal keratinocytes as observed on day 0. WHOCs maintained in MED3 showed loss of stratification in both support systems (Figure S2G and H). Epidermal thickness of WHOCs maintained in both support systems was not significantly different from each other. However, epidermal thickness was more dependent on growth media rather than on support systems. Better maintenance of rete ridges was observed in tissues maintained in collagen matrix and cultured in DMEM when compared to all other growth conditions. As assessed with the height of peaks and valleys of rete ridges, WHOCs cultured in collagen matrix and maintained in DMEM and WE were significantly thicker and closer to normal skin than those cultured in MED3 (Figure 1G). Collectively, the epidermal morphology of WHOCs on day 14 was better when collagen embedding and DMEM medium were used. WHOCs fed with MED3 showed nuclear dissolution, epidermal-dermal junction degradation and dislocation as well as inconsistencies in epidermal thickness when compared to those cultured in DMEM and WE (Figure S2B–H).

b. Dermal analysis (D14)

ECM components, capillaries, and cellular components in the dermis of WHOC models embedded in collagen and well chamber inserts maintained in DMEM and WE were morphologically similar to day 0 biopsies.

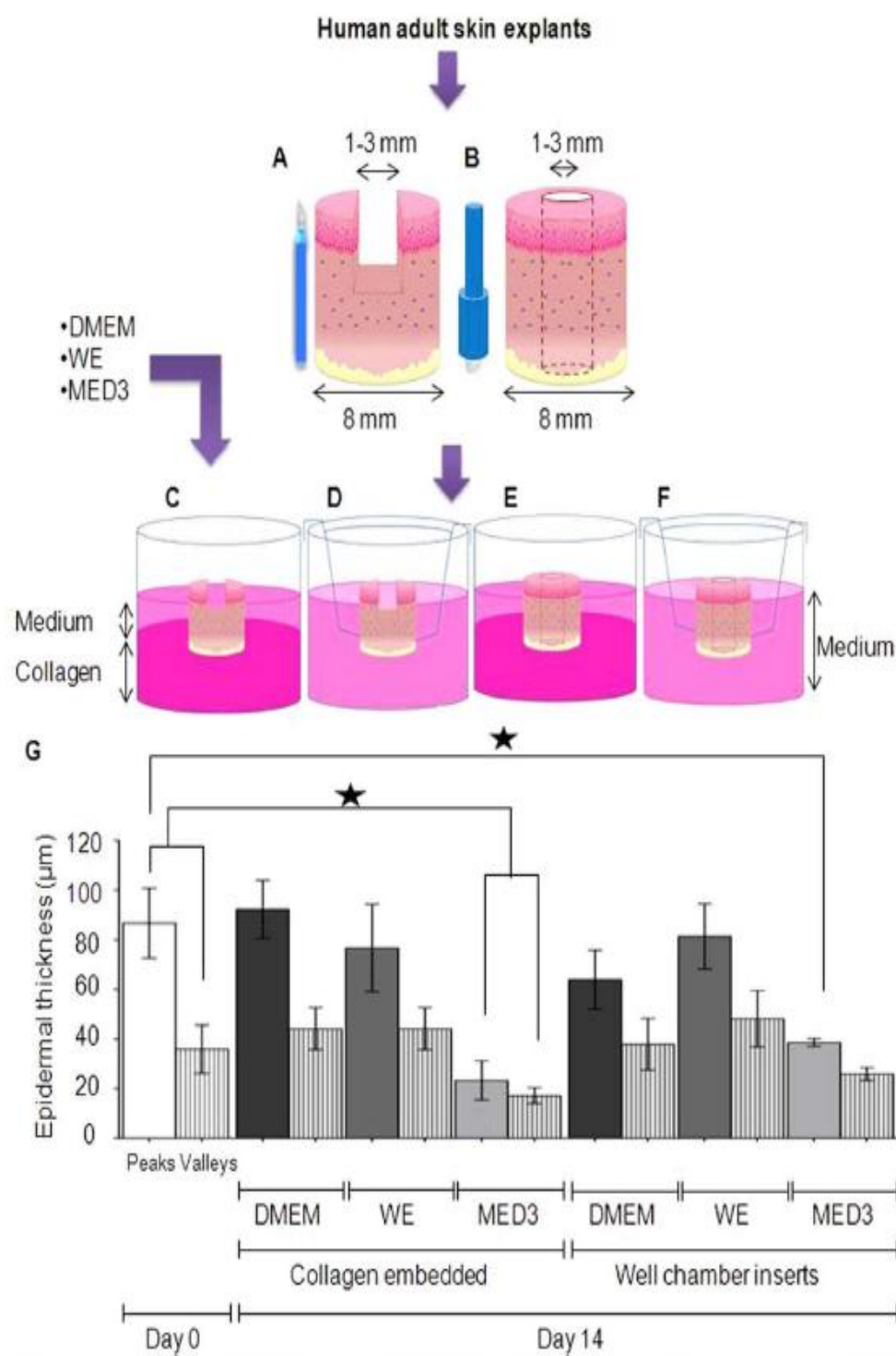


Figure 1. Schematic representation of WHOCS models. Partial (A) or full thickness (B) wounds of 1, 2, or 3 mm in the center of an 8 mm punch biopsy. WHOCS were supported in collagen embedded matrix (C and E) or introduced in well chamber inserts (D and F) and maintained with different supplemented growth media such as DMEM, WE, or MED3. All WHOCS models were exposed to air-liquid interface and collected on day 14. Epidermal thickness of WHOCS maintained in different media and supported with collagen embedded matrix or well chamber inserts and compared to human normal skin processed on day 0 are shown in graph G. □ Denotes peaks and ▨ denotes valleys in the epidermis of skin biopsies on day 0. ■ Denotes peaks and ▨ denotes valleys in the epidermis of skin biopsies on day 14. ★ Denotes significant difference ($p < 0.05$; $n = 6$).

Table 2. List of antibodies

Primary antibody	Dilution	Incubation time
Anti-PCNA antibody (ab18197); rabbit polyclonal; IgG.	1: 200	1 hour
Anti-Cytokeratin 14 antibody [EPR1612] (ab108417); rabbit monoclonal; IgG.	1: 400	30 minutes
Anti-CDKN2A/p16INK4a [2D9A12] antibody (ab54210); mouse monoclonal; IgG2b.	1: 1,000	30 minutes
Anti-MMP3 antibody [EP1186Y] (ab52915); rabbit monoclonal; IgG.	1: 1,000	1 hour
Anti-MMP19 antibody (ab53146); rabbit polyclonal; IgG.	1:1,000	1 hour
Anti-alpha smooth muscle actin antibody (ab5694); rabbit polyclonal; IgG.	1: 400	1 hour
Anti-CD31 antibody (ab32457); rabbit polyclonal; IgG.	1: 200	30 minutes

PCNA, proliferating cell nuclear antigen; MMP3, metalloproteinase 3; CDKN2A/p16INK, cyclin-dependent kinase inhibitor 2A; CD31, platelet endothelial cell adhesion molecule marker.

However, those cultured in MED3 appeared to be degraded. WHOCs maintained in well chamber inserts showed an increase in cellularity and fibroblasts exhibited an altered phenotypic morphology with slight elongation. However, the appearance of swollen tissue and degradation of interstitial and extrafibrillar components in the dermis were distinct from WHOCs maintained in collagen matrix.

Furthermore, the morphology of elastic fibers was evaluated with Weigert's staining. On day 0, elastic fibers in the papillary dermis were thin and elongated, while those in the reticular dermis were aggregated into thick compartments (Supporting Information Figure S21). WHOCs main-

tained for 14 days in collagen matrix were similar to day 0 tissues (Supporting Information Figure S2J, L, and N). However, those cultured in well chambers appeared loose and degraded (Supporting Information Figure S2K, M, and O). Therefore, better preservation of elastic fibers was achieved with collagen matrix compared to using a well chamber support system.

Ex vivo wounds reepithelialization varied according to wound type and tissue support system

To identify the optimal wound dimensions that heal ex vivo, we performed partial and full thickness wounds with the following dimensions: 1, 2, and 3 mm wide. Partial

Table 3. Gene and primer sequences for qRT-PCR

Primers	Gene ID	Sequence 5'-3'	Primer position	Amplicon size (bp)
RPL32-L	NM_000994.3	gaagttctgtccacaacg	319-338	77
RPL32-R	NM_000994.3	ggcgatctggcacagta	377-395	77
PCNA-L	NM_002592.2	tggagaactggaaatggaaa	755-775	95
PCNA-R	NM_002592.2	gaactgggtcaattctctatgg	826-849	95
Keratin 14 -L	NM_000526.4	ccattggggacgtggggac	564-583	69
Keratin 14 -R	NM_000526.4	caatdtcgagaaaggaccttg	612-632	69
p16 -L	NM_000077.4	gtggaccctggctgaggag	649-666	132
p16 -R	NM_000077.4	cttcaatggggatgtctg	761-780	132
Collagen I-L	NM_000088.3	gggattccctggacctaagg	1,866-1,885	63
Collagen I-R	NM_000088.3	ggAACACCCGCTCTCCA	1,911-1,928	63
Collagen III -L	NM_000090.3	ctggacccccagggtcttc	3,101-3,118	75
Collagen III -R	NM_000090.3	catactgtatccgggttcca	3,156-3,175	75
MMP3 -L	NM_002422.3	caaaatcatattcttttagaggacaa	1,259-1,285	91
MMP3 -R	NM_002422.3	ttcagctattttgtttggaaa	1,329-1,349	91
MMP19-L	NM_002429.5	atgcctggacccctgtggatgt	1,006-1,025	76
MMP19-R	NM_002429.5	cccccttggaaaggcatatgtc	1,062-1,081	76
α -SMA-L	NM_001141945.1	ctgttccggccatcttcat	1,262-1,281	70
α -SMA-R	NM_001141945.1	tcatgtatgttgttaggtgt	1,310-1,331	70

RPL32, 60S ribosomal protein L32; PCNA, proliferating cell nuclear antigen; p16, cyclin-dependent kinase inhibitor 2A; MMP3, metalloproteinase 3; α -SMA, α -smooth muscle actin.

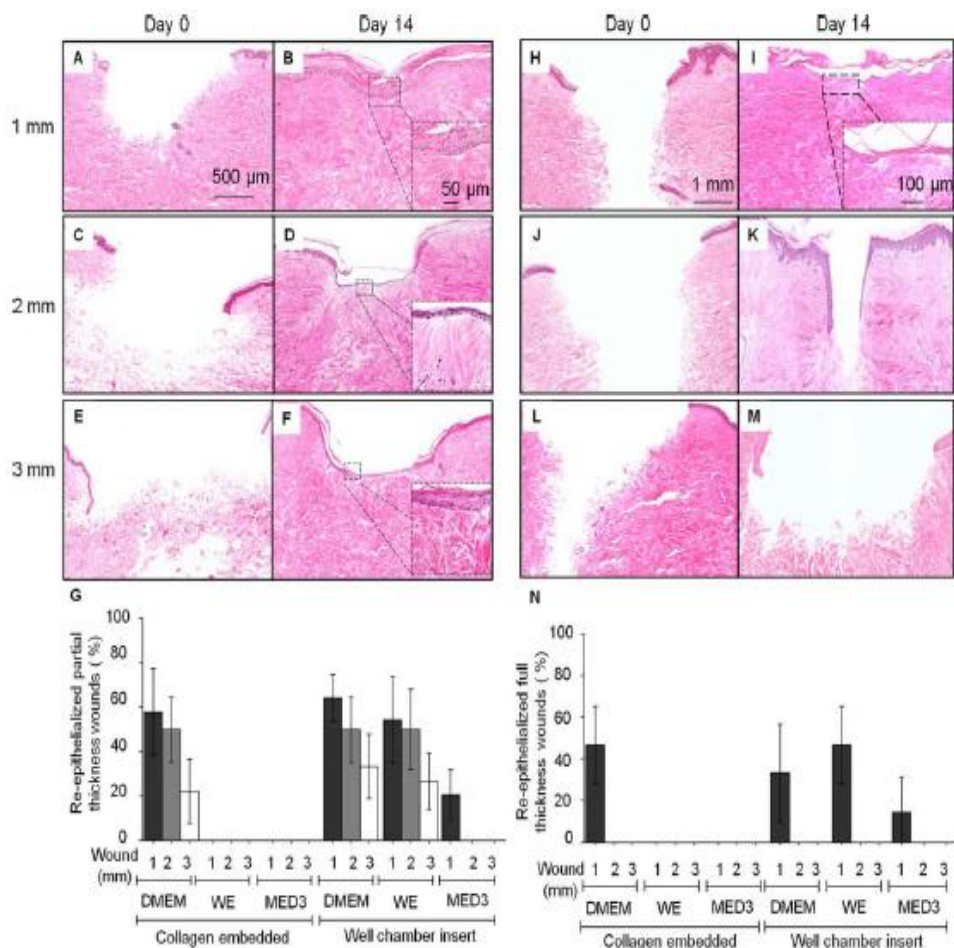


Figure 2. Representative pictures of WHOCs. WHOCs with partial thickness wound (A–F) and full thickness wounds (H–M) cultured ex vivo in collagen embedded matrix. These WHOCs were maintained in DMEM and stained with H&E (original magnification 2.5X and 40X, respectively). The wounds measure 1 mm (A, B, H, and I), 2 mm (C, D, J, and K), and 3 mm (E, F, L, and M; $n=6$). Dotted square shows detail of the reepithelialized area. Graph represents statistical analysis of reepithelialized WHOCs according to the system of support, growth medium and wound size of partial thickness (G) or full thickness wounds (N). ■ Denotes 1 mm, ■■ 2 mm, and □ 3 mm reepithelialized wounds.

thickness wounds were reepithelialized by day 14 compared to full thickness wounds, however, depending on the support system (Figure 2). Keratinocytes in the neo-epidermis of all healed WHOCs appeared to be flat with spindle-shape nuclei, with the absence of any rete ridges in the epidermis (Figure 2A–F).

Reepithelialization was observed only in all partial wound and full thickness wounds of 1 mm thickness. Well chamber inserts had a higher rate of reepithelialization compared to collagen matrix embedding. However, on day 14, degradation of ECM fibers and liquid retention was more noticeable in well chamber inserts compared to collagen embedded WHOCs. DMEM supported re-

epithelialization in WHOCs cultured in both collagen matrix and well chamber inserts. MED3 growth media did not support healing in partial and full thickness (Figure 2G and N). Morphology of the healed wounds in DMEM or WE were found to be better than those cultured in MED3 media.

Wound closure characteristics of reepithelialization and dermal reconstruction

Analysis of ex vivo healing was performed on 2 mm partial thickness wounds cultured in DMEM and embedded in collagen. Here, cell death was observed with 3'-OH DNA

end-labeling method (Tunel), which increased to 20% in peripheral skin and 32% in the neo-epidermis on day 14, compared to normal skin on day 0. The upper epidermal layers in the peripheral skin appeared to have more apoptotic cells compared to the rest of the epidermal layers. Also, apoptotic cells were mostly observed in the upper layers of the reforming neo-epidermis (Figure 2B–E). Proliferation was decreased in peripheral skin (12%) and in the neo-epidermis (10%), compared to normal skin on day 0 (15%; Figure 3F–I).

Cytokeratin 14 (CK-14) is a marker for undifferentiated keratinocytes and disappears at the onset of differentiation.²¹ CK-14 staining was altered in normal skin on day 14 compared to day 0. CK-14 was expressed in several layers of the (basal and suprabasal layers) epidermis compared to the basal layer expression on day 0 (Figure 3J–M). Laminin 5 (LAMA5), which is a marker of epidermal–dermal junction integrity, was significantly increased in the basement membrane of the reepithelialized wounds when compared to normal skin on days 0 and 14 (Figure 3N–Q). Additionally, Herovici's polychrome staining, showed a significant increase in COLIII synthesis near to the reepithelialized wound compared to normal skin on days 0 and 14 (Figure 3R–T).

WHOC models exposed to PDT showed higher rate of wound closure

Next, we investigated whether the rate of wound healing closure in 1.5 mm full thickness WHOCs would be affected by PDT treatment. Here, the reepithelialization tongue was threefold longer compared with the untreated WHOCs (Supporting Information Figures S3E and B). To provide a dermal template for the keratinocytes tongue during wound healing, we introduced either fat or Matrigel into the wound center. The reepithelialization tongue in WHOCs with Matrigel was separated from the scaffold while those with fat exhibited firm attachment to the scaffold (Figure S3C–G). Therefore, better re-epithelialization was observed with the fat scaffold. Post-PDT, reepithelialization tongue on day 7 was 3.5 folds longer compared to the untreated controls (Figure 4A–C). Additionally, 27±5% of the WHOCs post-PDT were found closed, compared to untreated controls on day 14 (Figure 4D–F). Cellular quantification of neo-epidermis showed a 2.6 fold increase in cell numbers compared to untreated WHOCs (Figure 4G). However, small areas of epidermal detachment were observed in the peripheral skin to the neo-epidermis on day 14 in WHOCs treated with PDT compared to untreated controls.

PDT increased apoptosis plus proliferation and maintained the rate of differentiation in WHOCs

Apoptotic and proliferative effect of PDT in WHOCs, were evaluated using TUNEL and PCNA-IHC, respectively. TUNEL assay on day 7 showed no significant difference in apoptosis between PDT-treated and nontreated WHOCs, both in the peripheral skin and in the advancing tongue (5%). However, on day 14, there was a significant increase in cell death in both peripheral skin (40%) and neo-epidermis (59%) post-PDT. This increase in apoptosis was 19-fold post-PDT treatment in the neo-epidermis and 1.6-fold in the peripheral

skin, compared to the untreated controls (Figure 5). Proliferation assay showed that post-PDT, the reepithelialization tongues on day 7 had significant up-regulation of PCNA compared to the untreated WHOCs (1.8 fold; Figure 6D–E and J). PCNA-stained cells were distributed haphazardly in the reepithelialization tongue of PDT-treated WHOCs. Additionally, there was increase in proliferation in the dermis of PDT-treated WHOCs compared to untreated WHOCs. Although, proliferation decreased significantly on Day 14 in PDT-treated WHOCs compared to the untreated controls in the epidermis, a higher cellular proliferation in dermis was sustained until day 14 in PDT-treated WHOCs (Figure 6A–J). There was a significant increase of PCNA gene expression post-PDT compared to untreated controls (Figure 6K).

Post-PDT, CK-14 increased in both PDT-treated and nontreated controls on day 7 (Figure 7A–E and J). However, in addition to its presence in the basal layer, CK-14 was also distributed in stratum spinosum and stratum granulosum of the epidermis. However, on day 14, CK-14 was decreased and was mainly confined to the basal layer of peripheral skin in PDT-treated samples while the spatial pattern of CK-14 staining in nontreated samples was similar to that on 7 day (Figure 7).

PDT increased ECM remodeling plus P16, MMP3, and MMP19 expression

I. Collagen I and III synthesis increased after PDT treatment

Herovici polychrome staining showed COLI and COL-III synthesis to be higher in PDT-treated WHOCs compared to untreated samples. PDT treatment enhanced COLI and III levels in the dermis on days 7 and 14 (x5 and sevenfold change, respectively, on days 7 and 14 for COLI, x10 and 13.5-fold change, respectively, on days 7 and 14 for COLIII; Figure 8A–J). Small areas of neo-collagen were observed substituting the fat scaffold, only in WHOCs post-PDT.

On day 14, degradation of elastic fibers was observed to be increased in PDT-treated WHOCs compared to day 0 and untreated WHOCs on day 14. A number of shortened bundles of elastic fibers were also observed in the ECM post-PDT samples (Supporting Information figure S4B–F).

II. Enhanced MMP3 and MMP19 in PDT-treated WHOCs

Histochemical expression of MMP3 was found to be higher in WHOCs post-PDT compared to untreated and unwounded controls (Supporting Information Figure S4G–K; Figure 8K). MMP3 gene expression was also found to be 7.5 fold higher until day 14 day (Figure 8L). In addition, histochemical expression of MMP19 was found to be higher post-PDT, however, by day 14, it was similar to untreated controls, although higher than unwounded controls (Supporting Information Figure S5B–F; Figure 8M–N). Similarly, MMP19 gene expression was found to be higher on day 7 (statistically significant) and shown to be similar to untreated controls on day 14, however, it was found to be higher than unwounded controls.

III. Enhanced expression of p16 post-PDT treatment

The expression p16 of been correlated to cellular oxidative stress levels.²² The histological expression of

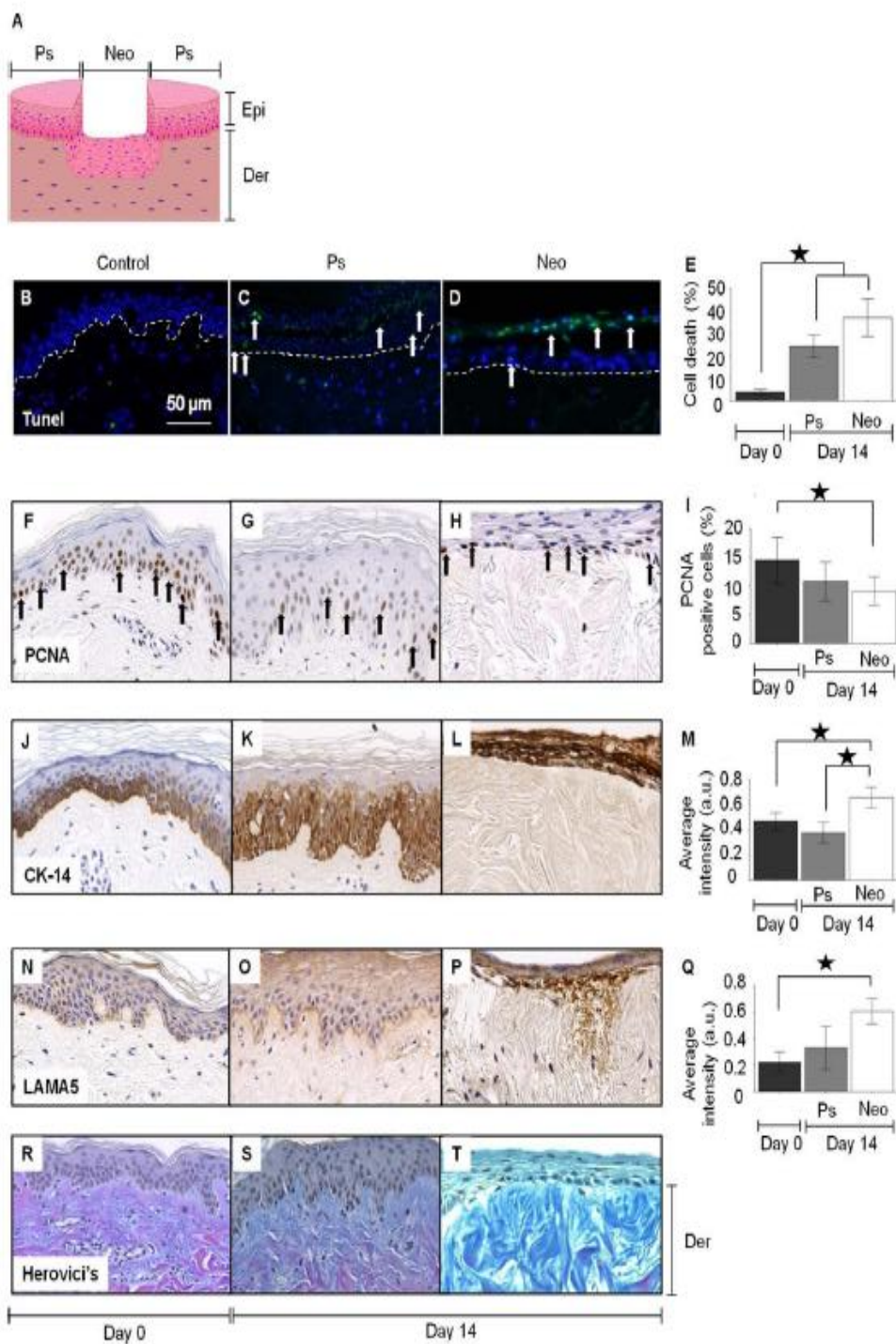


Figure 3. Analysis of normal skin compared to WHOCS after 14 days ex vivo. Schematic representation of analyzed biopsy areas (A). Epi denotes epidermis and Der denotes dermis. WHOCS model with 2 mm partial thickness wound re-epithelialization, cultured in DMEM and collagen embedding (original magnification 40X). Representative pictures are cell death by TUNEL analysis (B-D), PCNA (F-H), CK-14 (J-L), LAMA5 (N-P), and Herovicis differential staining for COL I/COLIII (R-T). Arrows indicate dead cells (B-D) or proliferative cells (F-H). Graphs represent quantitative analysis of cell death (E), PCNA positive cells quantification (I), average intensity of CK-14 (M), and LAMA5 (Q). ■ Denotes unwounded human skin on day 0, □ denotes peripheral skin and ▨ denotes neo-epidermis on day 14. * Denotes significant difference ($p < 0.05$; $n = 6$).

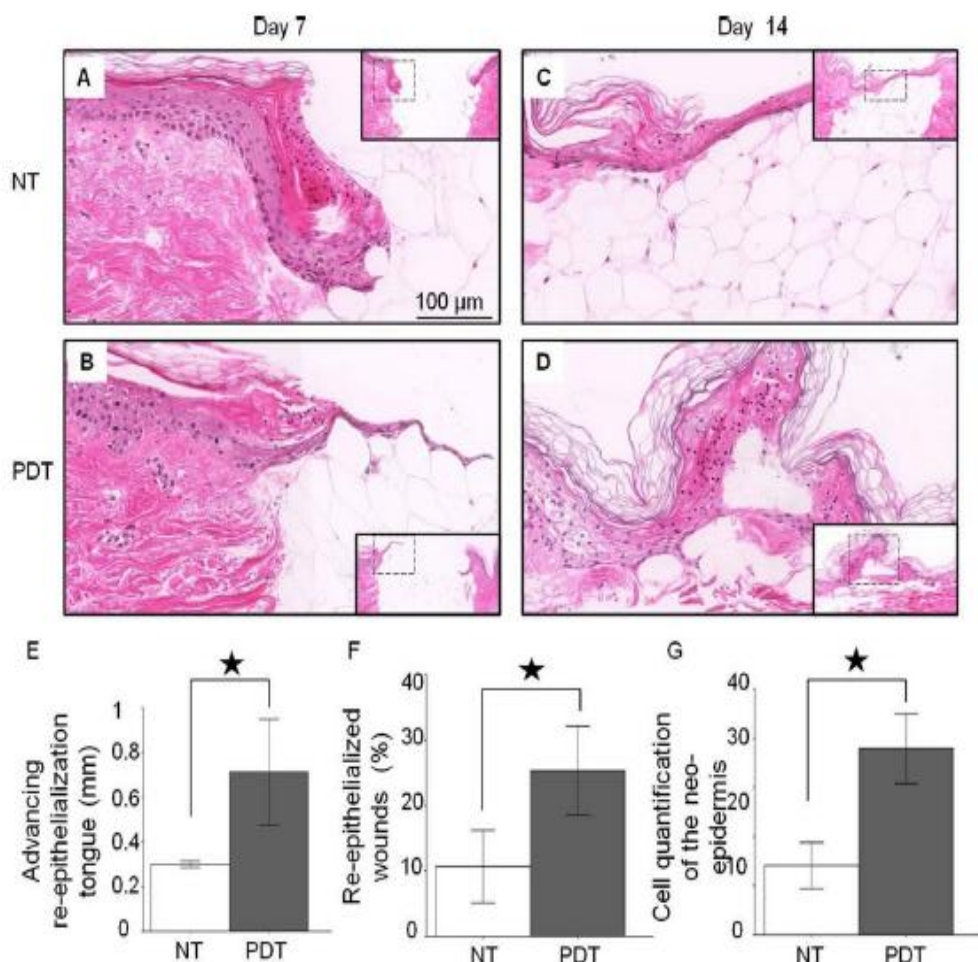


Figure 4. Post-PDT analysis of full thickness WHOCS. Representative images of ex vivo maintained WHOCS which were untreated (NT) or post-PDT (PDT) after 7 (A and B) and 14 days (C and D) maintained ex vivo (original magnification 40X). Graphs represent advancing reepithelialization tongue on day 7 (E), reepithelialized WHOCS on day 14 (F), and cell quantification in the neo-epidermis (G). □ Denotes untreated WHOCS and ■ denotes WHOCS post-PDT. ★ Denotes significant difference ($p < 0.05$; $n = 6$).

p16 was found to be significantly higher at the advancing tongue (30%) compared to day 0, peripheral skin and untreated control (Supporting Information Figure S6E and F). p16 was also found to be increasing in the untreated compared to PDT-treated WHOCS. Although, p16 was found to be significantly higher in the epidermal layer of WHOCS post-PDT, the expression in the dermis was similar in both the untreated and PDT-treated WHOCS on day 14 (Supporting Information Figure S6; Figure 9A and B). p16 gene expression was up-regulated by eightfold on day 14 compared to untreated control on day 0 and was significantly higher compared to the untreated control on day 14 (Figure 9B). Therefore, post-PDT, there was an increase in p16

levels when compared to day 14 controls, which may indicate the ability of PDT to activate stress-related oxidative mechanisms in wound healing.

IV. Increased α -SMA gene expression post-PDT treatment
Histochemical expression of α -SMA was increased minimally but not significantly (Supporting Information figures S7A–E; Figure 9C). However, α -SMA gene expression was found to be up-regulated by 1.5 times higher than the untreated WHOCS (Figure 9D).

V. CD31 intensity decreased post-PDT treatment
On day 14, CD31 staining was significantly decreased in PDT-treated WHOCS compared to the nontreated WHOCS (Figure 9E). This correlates with the increase in MMP3 activation post-PDT.²³

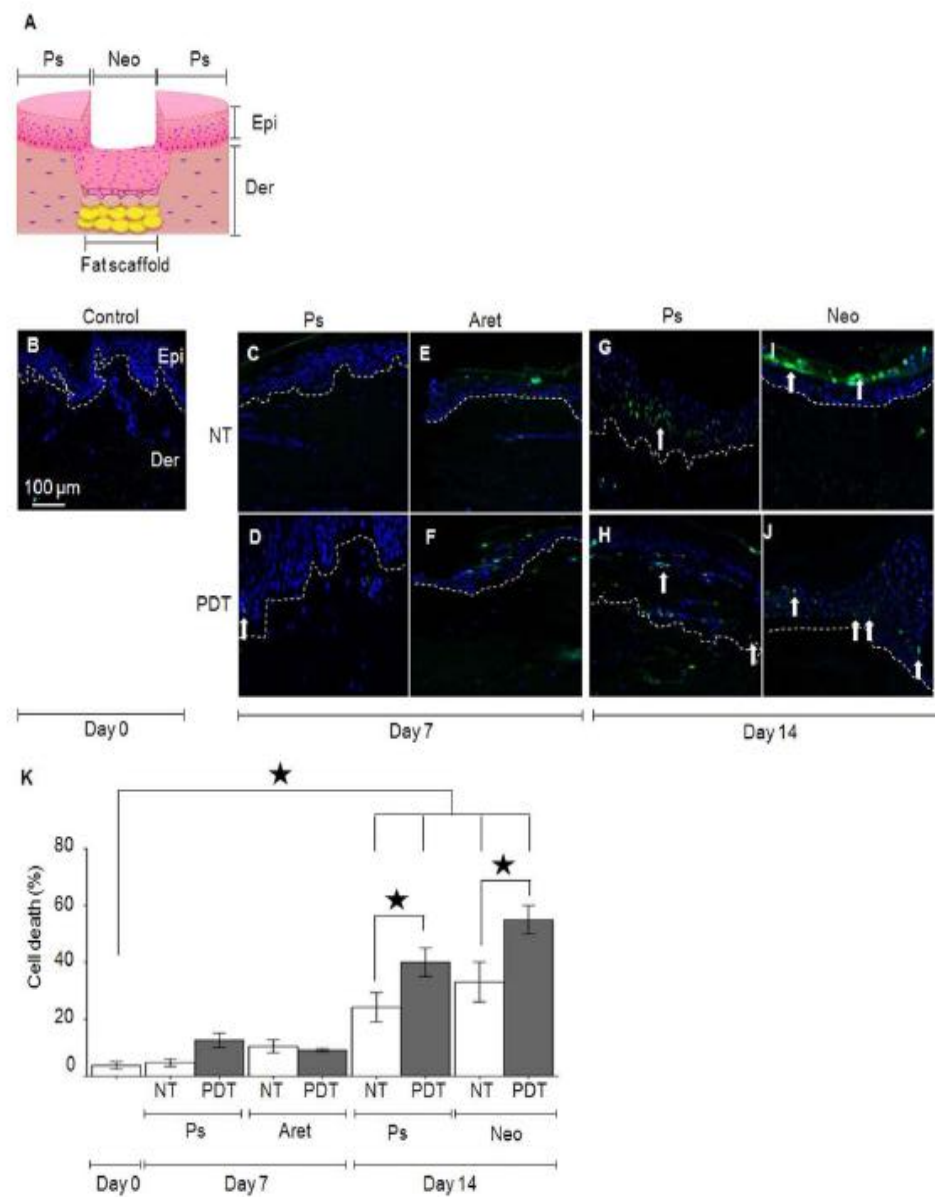


Figure 5. Apoptotic analysis of full thickness WHO Cs post-PDT. Schematic representation of analyzed biopsy areas (A). Epi denotes the epidermis, Der denotes the dermis. Normal human skin processed on day 0 (B) was compared to peripheral skin (Ps) and advancing reepithelialization tongue (Aret) on day 7 and Ps and neo-epidermis (Neo) on 14 day (original magnification 40X). WHO Cs were untreated (NT; C, E, G, and I) or exposed to PDT (D, F, H, and J). Arrows indicate apoptotic cells. Graph represents quantitative analysis of apoptotic cell death (K). □ Denotes control WHO Cs and ■ denotes WHO Cs post-PDT treatment. ★ Denotes significant difference ($p < 0.05$).

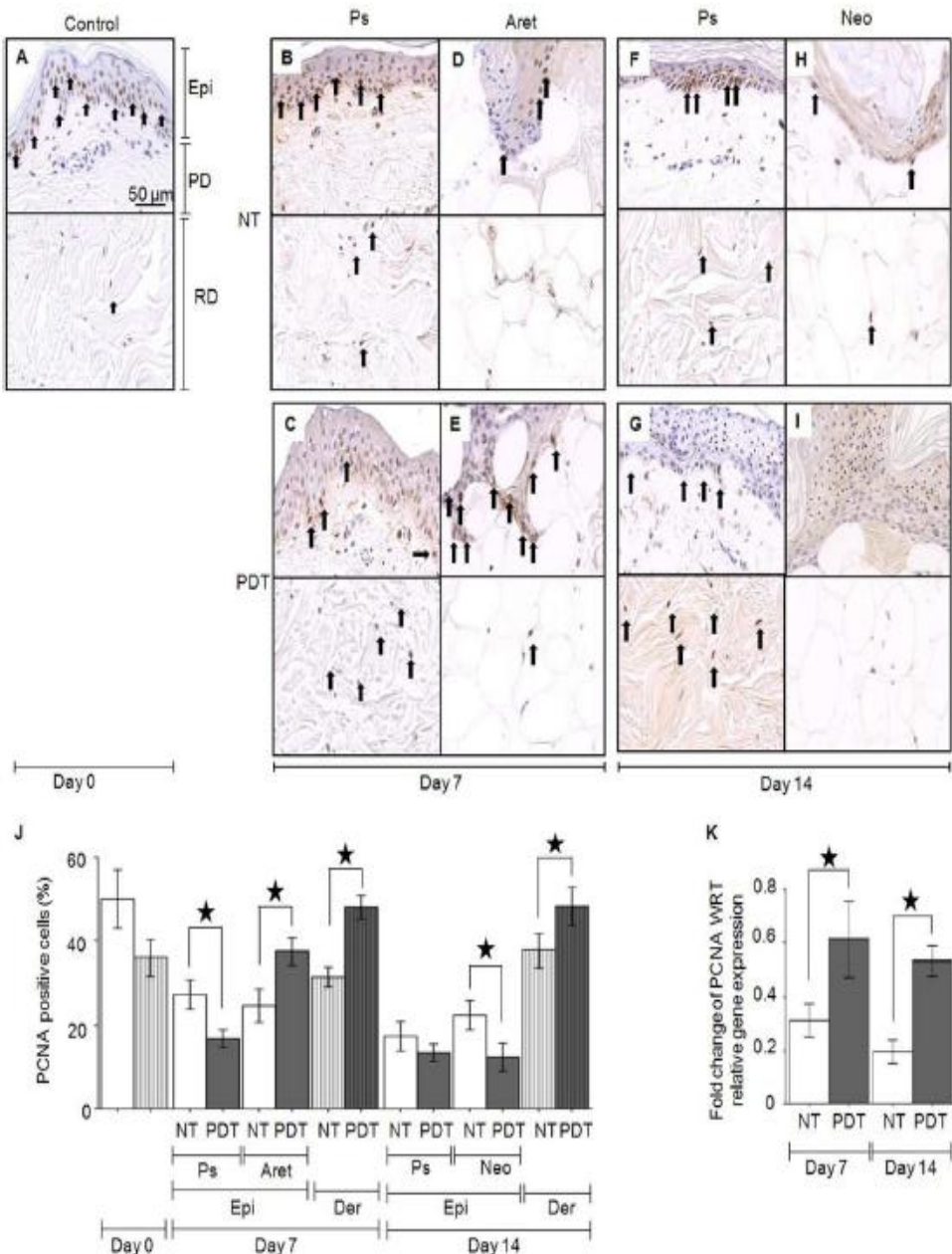


Figure 6. Proliferation analysis post-PDT. Normal human skin processed on day 0 (A) was compared to peripheral skin (Ps) and advancing reepithelialization tongue (Aret) on day 7 and Ps and neo-epidermis (Neo) on day 14 (original magnification 40X). WHOCS were untreated (NT; B, D, F, and H) or exposed to PDT (PDT; C, E, G, and I). Arrows indicate PCNA positive cells in the epidermis (Epi), papillary dermis (PD), and reticular dermis (RD). Graphs represent quantitative analysis of PCNA positive cells (J) and gene expression analysis (K). □ Denotes epidermis and ▨ denoted WHOCS on day 0 or untreated WHOCS on day 14. ■ Denotes epidermis or ▨ denoted WHOCS post-PDT. ★ Denotes significant difference ($p < 0.05$; $n = 6$).

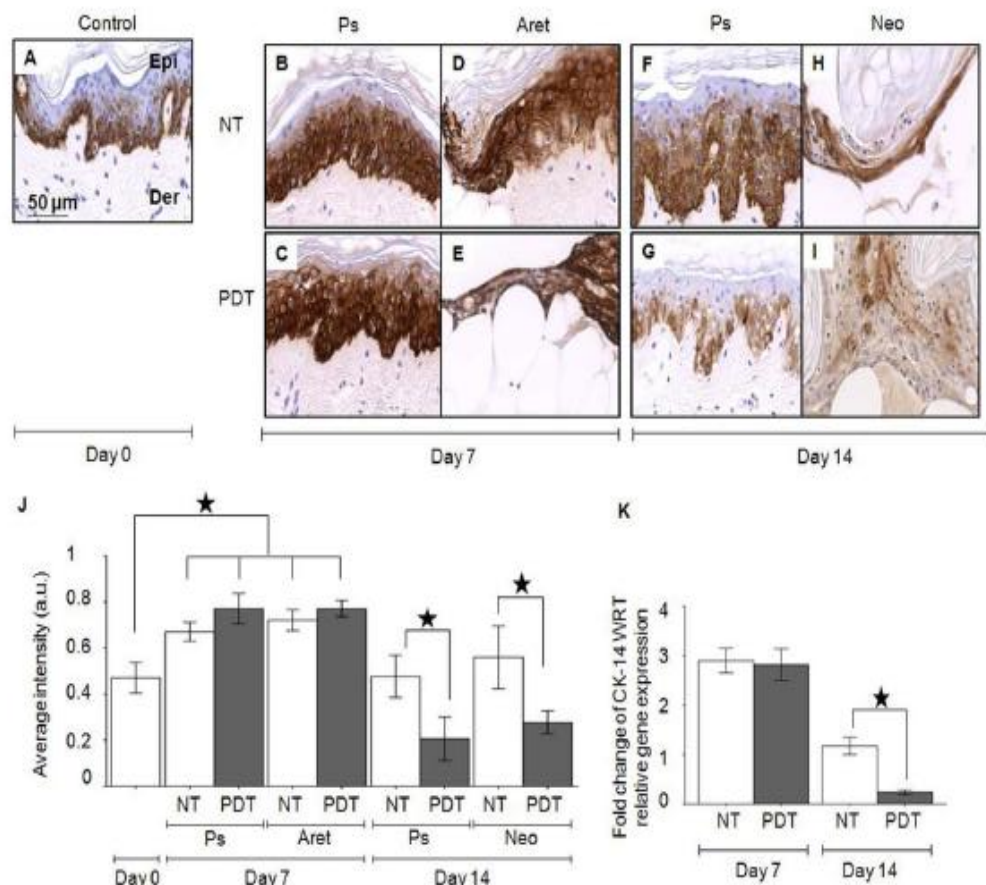


Figure 7. Analysis of CK-14 expression post-PDT. Normal human skin (day 0 control; A) was compared to untreated (NT; B, D, F, and H) controls and post-PDT (C, E, G, and I). CK-14 expression is shown in the peripheral skin (Ps), advancing re-epithelialization tongue (Aret) on day 7 and Ps and Neo-epidermis (Neo) on day 14 (original magnification 40X). Graph represents average intensity of CK-14 IHC (J), and gene expression analysis (K). □ Denotes untreated WHOCs, ■ denotes WHOCs post-PDT. ★ Denotes significant difference ($p < 0.05$; $n = 6$).

DISCUSSION

In this study, we investigated healing of adult human skin maintained ex vivo with various wound sizes and shapes in different culture medium and support conditions. Following optimization of a WHOC model of adult human skin, the effects of PDT treatment were subsequently evaluated in an objective manner. We present an optimized WHOC model based on wound size, culture conditions including support system and growth media with respect to cellular, interstitial, and extrafibrillar components, for studying wound repair in adult human skin maintained ex vivo.

Three growth mediums previously used for skin organ cultures including DMEM, WE, and MED3 were compared. We found that structure and barrier function of the skin was well preserved until day 14 in WHOC models fed with DMEM or WE. MED3 was unable to maintain tissue viability,

although we found limited reepithelialization in 1 mm partial thickness wounds. This indicated that feeding the dermal layer was sufficient to preserve epidermal viability and differentiation in agreement with previous reports.^{6,8,22,24} Well chamber inserts allowed an increase in excess fluid retention by WHOC, which could cause periwound tissue maceration.²⁵ WHOC embedded in collagen showed no increase in cellularity or swelling as had been previously reported, although wound healing closure rates were less compared to well chamber inserts.^{5,19}

Our observations suggest that skin "tensegrity"²⁶ appears to be involved in healing of 1mm full-thickness wounds, as reepithelialization occurred with an increased amount of immature collagen in the wound area. Although, we found that the wound edges in the well chambers appeared to be closer as well as showing an increased proximity with the swollen condition of the tissue biopsy edge. However,

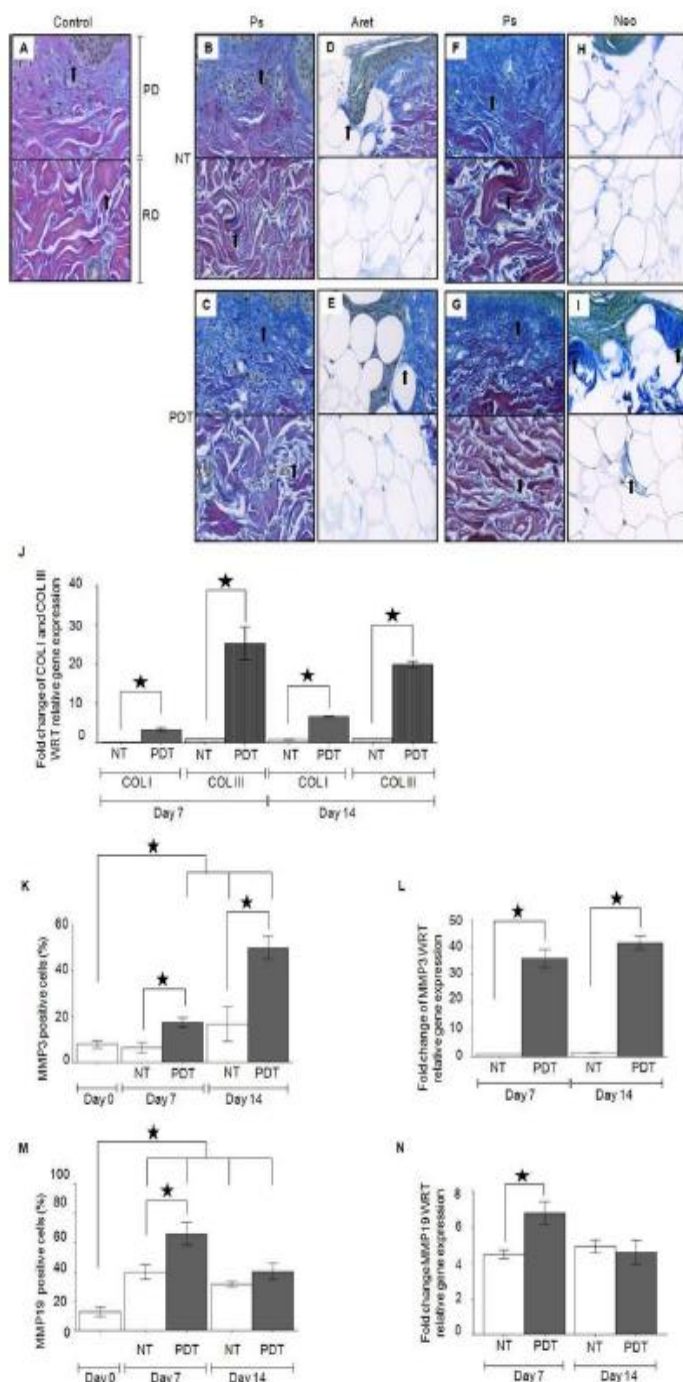


Figure 8. Herovici's differential staining, MMP3 and MMP19 analysis post-PDT. Normal human skin processed on day 0 (A) was compared to peripheral skin (Ps) and advancing re-epithelialization tongue (Aret) on day 7 and Ps and neo-epidermis (Neo) on day 14 (original magnification 40X). Pictures show papillary dermis (PD) and reticular dermis (RD) of WHOCs untreated (NT; B, D, F, and H) and post-PDT (C, E, G, and I). Mature collagen (COLI) was red stain and immature collagen (COLIII) was blue stain, overlapping COLI and COLIII results in a purple stain. Graph represents COLI and COLIII gene expression analysis (J). □ Denotes COLI and ■ denotes COLIII expression in untreated WHOCs, □■ denotes COLI and ■ COLIII in WHOCs post-PDT. MMP3 or MMP19 positive cells quantification (K and M) and gene expression, respectively, (L and N). □ denotes untreated WHOCs and ■ WHOCs post-PDT. ★ Denotes significant difference ($p < 0.05$; $n = 6$).

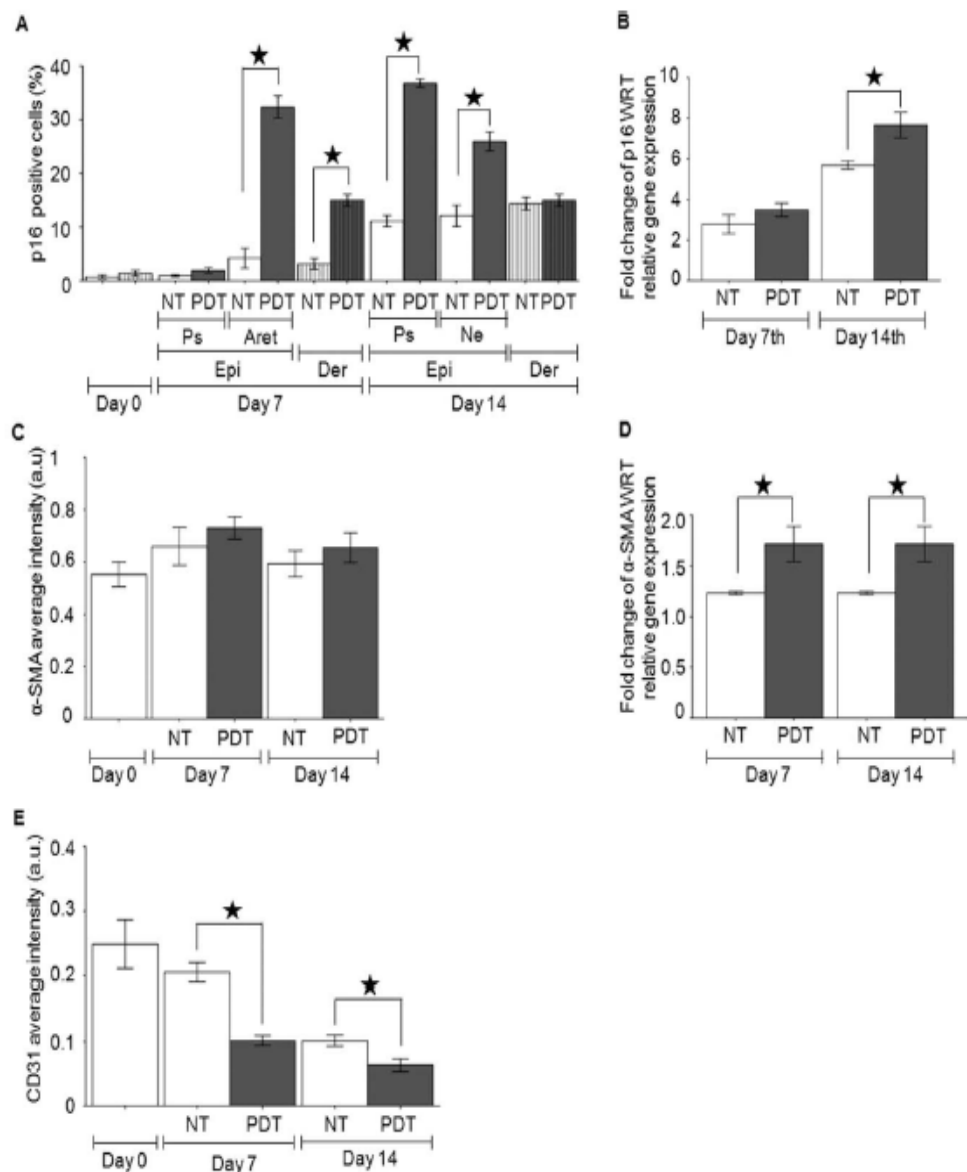


Figure 9. p16, α -SMA and CD31 analysis post-PDT. Graph represents quantification of p16 positive cells (A), p16 gene expression (B), average intensity of α -SMA expression in WHOCS (C), α -SMA gene expression (D), and average intensity of capillaries (E). □ Denotes positive cells in the epidermis of untreated WHOCS or average intensity of untreated WHOCS and ■ Denotes positive cells in the dermis in untreated WHOCS. ■ Denotes positive cells or average intensity of WHOCS post-PDT. ★ Denotes significant difference ($p < 0.05$; $n = 6$).

collagen embedded WHOCS did not exhibit these characteristics, which makes it superior to well inserts in long term preservation of WHOCS.

Full thickness wounds, greater than 1 mm did not close completely; however, we observed an advancing re-

epithelialization tongue. Morphological characteristics of reepithelialized WHOCS with a partial wound bed (partial thickness) were found to be similar to previous ex vivo studies.^{6,27,39} Following establishing an optimal WHOCS model, we chose to evaluate the WHOCS model

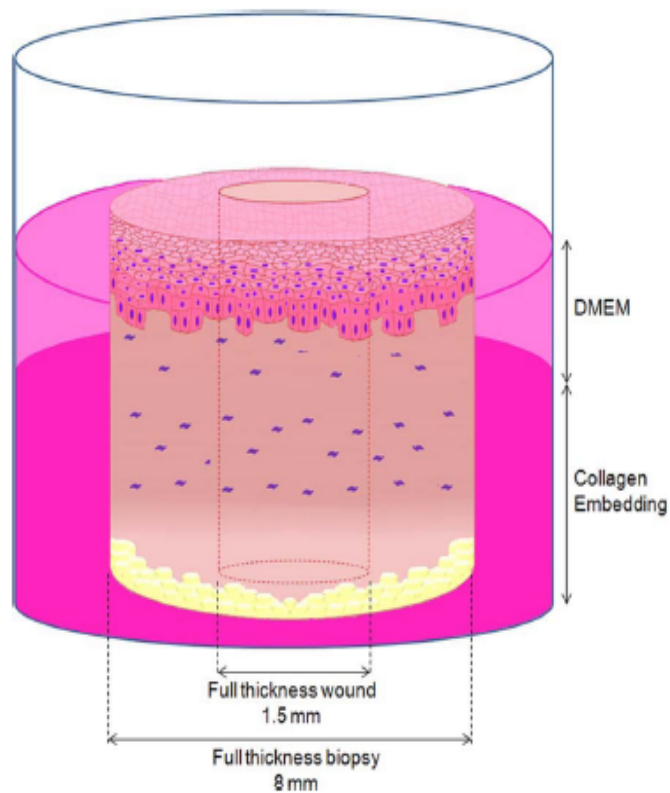


Figure 10. Schematic representation of optimal WHOC model. WHOC model with a full thickness wound of 1.5 mm and a fat scaffold in the wound. The dermal layer was embedded in rat tail collagen type one gel (2 mg/mL) and the epidermis was left exposed to air-liquid interface. WHOC was maintained with DMEM growth media in 24-well cell culture plate.

functionally with PDT. Previously, we had reported that low doses of PDT increases proliferation in fibroblasts derived from normal skin.¹⁷ Here, we identified an advancing epithelial tongue post-PDT compared to the untreated controls. However, these tongues did not join up due to the lack of a dermal support. Taking into account these findings, we chose to optimize the model further by inserting a scaffold of hypodermal fat, where we observed full reepithelialization post-PDT (Figure 10). Others have shown hypodermal fat tissue as a source of adult stem cells and paracrine messengers which can contribute to tissue repair and regeneration.^{28,29} We showed that $27 \pm 5\%$ of wounds post-PDT treatment were closed, compared to untreated wounds. This finding showed that PDT played an important role in initiating and maintaining the process of epidermal regeneration in WHOC models.

Elastic fibers responsible for skin resilience were found to be altered post-PDT, therefore it is possible that PDT may induce elastogenesis, as found by Sanclemente et al.³⁰ Collagen fibers were also found to be affected, particularly those at the papillary dermis. COLI and III gene and protein expression were found to be significantly increased post-PDT, with dermal remodeling also reported previously by others including Riekki et al.³¹

PCNA levels, related to cell proliferation, prior to PDT and in untreated cultures were similar to that found by Kawahira.³² However, PCNA was found to be significantly

increased at the advancing epithelial tongue and in the dermis post-PDT. In contrast with peripheral and neo-epidermis, PCNA levels were found to be similar on day 14 post-PDT suggesting a decrease in the proliferative potential of the epidermis. Basal keratinocytes are known to express CK-14, affecting cell shape and motility leading to migration and differentiation. High levels of CK-14 are known to lead to proliferation in vivo, and found closely related with skin tensile strength.²¹ Here, we found that CK-14 increased in keeping with increased cellular proliferation and migration on post-PDT but limited to one week as CK-14 expression decreased thereafter. However, despite this finding, the neo-epidermis was found to be fully reepithelialized and differentiated at this time point in the post-PDT treated samples. p16 regulates protective responses of the cell cycle and apoptosis, allowing DNA to repair itself after damage caused by ageing, oncogene activation, and oxidative stress.³³ Any potential induction of senescence, proliferation, or pathways leading to apoptosis by the differential expression of p16 is thought to be dependent on the Rb-signaling pathway and a number of proteins including p53.^{33,34} When we previously investigated the role of reactive oxygen species (ROS) and senescence in vitro, we found that a low dose of PDT increased ROS and induced senescence and cell proliferation.¹⁷ Similar results had been shown by Blázquez-Castro et al but only in keratinocytes.³⁵ Here, we show an increased p16

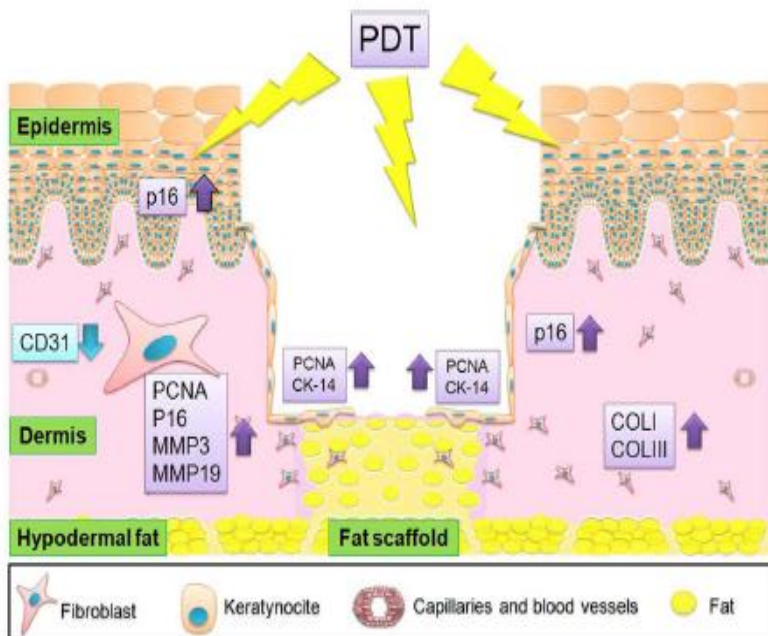


Figure 11. Schematic representation of the effects of PDT in WHOCS on day 7. We observed an increase in p16, PCNA, and CK-14 in the epidermis of WHOCS treated with PDT. In addition, we observed an increase in p16 and PCNA in the dermis. There was also an increase in COLI, COLIII, MMP3, and MMP19 and a decrease in CD31 biomarker expressed in capillaries. In conclusion, these results suggested an increased reepithelialization and ECM remodeling by PDT treatment.

expression in the advancing tongue which may indicate keratinocyte proliferation post-PDT triggered by ROS.³⁵ In addition, we found a significant increase in epidermal apoptosis on day 14, which coincides with the end of the re-epithelialization stage.

Keratinocytes can influence dermal cells through paracrine mechanisms. In vitro studies had observed that PDT initiated a cascade of signals through ROS generation.¹⁷ ROS induced HIF-1 α , and other cytokines such as tumour necrosis factor- α (TNF- α), vascular endothelial growth factor (VEGF), interleukin (IL) as IL-1 and IL-6, which in turn regulates the induction of several MMPs.¹² MMP3 is a key factor involved in the disorganization of collagen fibrils and in the remodeling of dermal connective tissue after injury. MMP3 cleaves E-cadherin, laminin 5, COLIII, fibronectin, elastin and release active heparin-binding EGF-like factor and angiostatin, degrade insulin-like growth factor (IGF) binding proteins and also activates MMP1, MMP7, and MMP9.²³ We found a significant increase in MMP3 post-PDT, thus, promoting keratinocyte and fibroblast migration, also potentially implying the increased availability of IGF and other growth factors, which can regulate neutrophil influx.²³ Another MMP related to wound healing is MMP19, which cleaves laminins, tenascin-C, fibronectin, and activates other inactive MMPs. We found an increased expression of MMP19 post-PDT, especially at the wound edges, which may sug-

gest its active involvement in the wound repair process post-PDT. Our results suggested that PDT induced dermal remodeling and likely mediated through paracrine pathways inducing MMPs, as had been suggested by Almeida et al.¹²

CD31, expressed in endothelial cells can be indicative of cell diversity, capillary, and vessels density.³⁶ We found a significant decrease in CD31 positive cells post-PDT, although with no apparent impact on the number of capillaries and vessel density. This finding may be explained by increased ROS levels post-PDT application acting on the endothelial cells in addition to other mechanisms.²³ α -SMA is a cellular marker of myofibroblasts, wound contraction, and ECM deposition during wound healing.³⁶ We found an increase in α -SMA gene expression post-PDT. These levels are in keeping with increased rate of wound contraction post-PDT.

PDT is known to release damage-associated molecular patterns, which can trigger immunological alerts to induce repair as has been previously observed.³⁷ Li et al also has suggested that damage may induce and enhance tissue repair.³⁸

In summary, we observed an increase in p16, PCNA, CK-14 in the epidermis and an increase in p16 and PCNA in the dermis of WHOCS treated with PDT. Additionally, we observed an increase in COLI, COLIII, MMP3, and MMP19 and a decrease in CD31 in capillaries. Overall,

these results suggested an enhanced reepithelialization and ECM remodeling by PDT treatment (Figure 11).

CONCLUSIONS

In conclusion, this study presents an optimized organ culture of human skin wounded ex vivo, which offers a useful model for investigating the process of cutaneous repair, and enables evaluation of candidate therapeutic agents. The effect of PDT on wound healing in human skin was studied ex vivo for the first time demonstrating that PDT increases reepithelialization and ECM reconstruction and remodeling in this unique wound model.

Acknowledgments

Jenifer Mendoza-Garcia received an award from the Mexican National Council for Science and Technology.

Conflict of Interest

The authors declare that they have no conflict of interest and report no financial interests.

REFERENCES

- Mathes SH, Ruffner H, Graf-Hausner U. The use of skin models in drug development. *Adv Drug Deliv Rev* 2014; 69–70: 81–102.
- Lebonvallet N, Jeanmaire C, Danoux L, Sibille P, Pauly G, Misery L. The evolution and use of skin explants: potential and limitations for dermatological research. *Eur J Dermatol* 2010; 20: 671–84.
- Vermolen FJ, Javierre E. Computer simulations from a finite-element model for wound contraction and closure. *J Tissue Viability* 2010; 19: 43–53.
- van Kilsdonk JW, van den Bogaard EH, Jansen PA, Bos C, Bergers M, Schalkwijk J. An *in vitro* wound healing model for evaluation of dermal substitutes. *Wound Repair Regen* 2013; 21: 890–6.
- Balaji S, Moles CM, Bhattacharya SS, Lesaint M, Dhamija Y, Le LD, et al. Comparison of interleukin 10 homologs on dermal wound healing using a novel human skin *ex vivo* organ culture model. *J Surg Res* 2014; 190: 350–66.
- Moll I, Houdek P, Schmidt H, Moll R. Characterization of epidermal wound healing in a human skin organ culture model: acceleration by transplanted keratinocytes. *J Invest Dermatol* 1998; 111: 251–8.
- Companjen AR, van der Wel LI, Wei L, Laman JD, Prens EP. A modified *ex vivo* skin organ culture system for functional studies. *Arch Dermatol Res* 2001; 293: 184–90.
- Xu W, Jong Hong S, Jia S, Zhao Y, Galiano RD, Mustoe TA. Application of a partial-thickness human *ex vivo* skin culture model in cutaneous wound healing study. *Lab Invest* 2012; 92849: 584–99.
- Peramo A, Marcelo CL, Goldstein SA, Martin DC. Improved preservation of the tissue surrounding percutaneous devices by hyaluronic acid and dermatan sulfate in a human skin explant model. *Ann Biomed Eng* 2010; 38: 1098–110.
- Tomic-Canic M, Mamber SW, Stojadinovic O, Lee B, Radoja N, McMichael J. Streptolysin O enhances keratinocyte migration and proliferation and promotes skin organ culture wound healing *in vitro*. *Wound Repair Regen* 2007; 15: 71–9.
- Kratz G. Modeling of wound healing processes in human skin using tissue culture. *Microsc Res Tech* 1998; 42: 345–50.
- Almeida Issa MC, Piñeiro-Maceira J, Farias RE, Pureza M, Raggio Luiz R, Manela-Azulay M. Immunohistochemical expression of matrix metalloproteinases in photodamaged skin by photodynamic therapy. *Br J Dermatol* 2009; 161: 647–53.
- Garnier J, Bezdetnaya L, Barlier C, Gräfe S, Guillemin F, D'Hallewin MA. Foslip®-based photodynamic therapy as a means to improve wound healing. *Photodiagnosis Photodyn Ther* 2011; 8: 321–7.
- Peplow PV, Chung TY, Baxter GD. Photodynamic modulation of wound healing: a review of human and animal studies. *Photomed Laser Surg* 2012; 30: 118–48.
- Mills SJ, Farmer MD, Ashcroft GS, Griffiths CE, Hardman MJ, Rhodes LE. Topical Photodynamic therapy following excisional wounding of human skin increases production of transforming growth factor- β 3 and matrix metalloproteinases 1 and 9, with associated improvement in dermal matrix organisation. *Br J Dermatol* 2014; 171: 55–62.
- Robertson CA, Evans DH, Abrahamse H. Photodynamic therapy (PDT): a short review on cellular mechanisms and cancer research applications for PDT. *J Photochem Photobiol B* 2009; 96: 1–8.
- Mendoza J, Sebastian A, Allan E, Allan D, Mandal P, Alonso-Rasgado T, et al. Differential cytotoxic response in keloid fibroblasts exposed to photodynamic therapy is dependent on photosensitiser precursor, fluence and location of fibroblasts within the lesion. *Arch Dermatol Res* 2012; 304: 549–62.
- Choi JS, Kim BS, Kim JY, Kim JD, Choi YC, Yang HJ, et al. Decellularized extracellular matrix derived from human adipose tissue as a potential scaffold for allograft tissue engineering. *J Biomed Mater Res A* 2011; 97: 292–9.
- Bagabir R, Syed F, Paus R, Bayat A. Long-term organ culture of keloid disease tissue. *Exp Dermatol* 2012; 21: 376–81.
- Samaroo HD, Opsahl AC, Schreiber J, O'Neill SM, Marconi M, Qian J, et al. High throughput object-based image analysis of β -amyloid plaques in human and transgenic mouse brain. *J Neurosci Methods* 2012; 204: 179–88.
- Seltnarra K, Fritsch AW, Kä JA, Maqin TM. Keratins significantly contribute to cell stiffness and impact invasive behavior. *Proc Natl Acad Sci USA* 2013; 110: 18507–12.
- Tavakkol A, Varani J, Elder JT, Zouboulis CC. Maintenance of human skin in organ culture: role for insulin-like growth factor-1 receptor and epidermal growth factor receptor. *Arch Dermatol Res* 1999; 291: 643–51.
- Stemlicht MD, Werb Z. How matrix metalloproteinases regulate cell behavior. *Annu Rev Cell Dev Biol* 2001; 17: 463–516.
- Steintraesser L, Rittig A, Gevers K, Sorkin M, Hirsch T, Kesting M, et al. A human full-skin culture system for interventional studies. *Eplasty* 2009; 9: e5.
- Okan D, Woo K, Ayello EA, Sibbald G. The role of moisture balance in wound healing. *Adv Skin Wound Care* 2007; 20: 39–53.
- Pacini S, Morucci G, Ruggiero M, Gulisano M, Punzi T. Tensegrity and plasma for skin regeneration. *Skin Res Technol* 2012; 18: 356–63.

27. Coolen NA, Schouten KC, Bockema BK, Middelkoop E, Ulrich MM. Wound healing in a fetal, adult, and scar tissue model: a comparative study. *Wound Rep Reg* 2010; 18: 291–301.
28. Fu X, Fang L, Li H, Li X, Cheng B, Sheng Z. Adipose tissue extract enhances skin wound healing. *Wound Rep Reg* 2007; 15: 540–8.
29. Klein J, Pernama PA, Owecki M, Chaklakov GN, Böhm M, Hausman G, et al. What are subcutaneous adipocytes really good for...? *Exp Dermatol* 2007; 16: 45–70.
30. Sanclemente G, Correa LA, Garcia JJ, Barrera M, Villa JF, Garcia HI. Methyl aminolevulinate plus red light vs placebo plus red light in the treatment of photodamaged facial skin: histopathological findings. *Clin Exp Dermatol* 2012; 37: 379–86.
31. Riekki R, Parikka M, Jukkola A, Salo T, Risteli J, Oikarinen A. Increased expression of collagen types I and III in human skin as a consequence of radiotherapy. *Arch Dermatol Res* 2002; 294: 178–84.
32. Kawahira K. Immunohistochemical staining of proliferating cell nuclear antigen (PCNA) in malignant and nonmalignant skin diseases. *Arch Dermatol Res* 1999; 291: 413–8.
33. Elmageed ZY, Gaur RL, Williams M, Abdraboh ME, Rao PN, Raj MH, et al. Characterization of Coordinated Immediate Responses by p16INK4A and p53 Pathways in UVB-Irradiated Human Skin Cells. *J Invest Dermatol* 2009; 129: 175–83.
34. Paunescu T, Mittal S, Protic M, Oryhon J, Korolev SV, Joachimiak A, et al. Proliferating cell nuclear antigen (PCNA): ringmaster of the genome. *Int J Radat Biol* 2001; 77: 1007–21.
35. Blázquez-Castro A, Carrasco E, Calvo MI, Jaén P, Stockert JC, Juarranza A, et al. Protoporphyrin IX-dependent photodynamic production of endogenous ROS stimulates cell proliferation. *Eur J Cell Biol* 2012; 91: 216–23.
36. Hinz B. Formation and function of the myofibroblast during tissue repair. *J Invest Dermatol* 2007; 127: 526–37.
37. Garg AD, Nowis D, Golab J, Vandenebelle P, Krysco DV, Agostini P. Immunogenic cell death, DAMPs and anticancer therapeutics: an emerging amalgamation. *Biochim Biophys Acta* 2010; 1805: 53–71.
38. Li F, Huang Q, Chen J, Peng Y, Roop DR, Bedford JS, et al. Apoptotic cells activate the "phoenix rising" pathway to promote wound healing and tissue regeneration. *Sci Signal* 2010; 23: 110–3.
39. Lu Z, Hasse S, Bodo E, Rose C, Funk W, Paus R. Towards the development of a simplified long-term organ culture method for human scalp skin and its appendages under serum-free conditions. *Exp Dermatol* 2007; 16: 37–44.

Supporting Information

Additional Supporting Information may be found in the online version of this article at the publisher's web-site:

Figure S1. Flow chart of the methodology adopted in this study. Control used were (A) punch biopsy with external diameter of 8mm and an internal wound of 1, 2, or 3 mm at day 0, (B) punch biopsy with a external

diameter of 8 mm and a wound of 2 mm at day 0, additionally to control WHOCs, which were not treated with PDT and (C) punch biopsy with a external diameter of 8 mm and a wound of 1.5 mm at day 0, additionally to control WHOCs, which were not treated with PDT.

Figure S2. Morphological analysis by H&E and Weigert's differential staining in the healthy peripheral skin adjacent to the wound. Schematic representation of peripheral skin (Ps), neo-epidermis (Neo), epidemis (Epi) and dermis (Der) are shown in (A). WHOC models were maintained in three different media such as DMEM, WE and MED3, and supported in collagen embedded or in well chamber inserts. Human normal skin processed on day 0 stained with H&E (B) or Weigert's elastic staining (I) and WHOC models processed on day 14 (B–O; original magnification 40X). Double arrows show peaks of the rete ridges and single arrows show elastin fibers at the papillary dermis (PD) or reticular dermis (RD).

Figure S3. H&E images of WHOC models with 2 mm wound center, untreated and post-PDT. The initial day is represented in (A). WHOC models with empty wound center (B&E), filled with Matrigel (C&F) and autologous hypodermal fat (D&G) on day 7. Arrows show the advancing reepithelialization tongue.

Figure S4. Representative images of Weigert's elastic stain (B–F) and MMP3-IHC (G–K) analysis. Images show schematic representation of analysed areas (A) in papillary dermis (PD) and reticular dermis (RD). WHOC untreated (NT) and post-PDT (original magnification 40X). Elastic fibers were stained black. Arrows show positively stained MMP3 cells. (Original magnification 40X) treated WHOCs. Arrows show elastic fibers or MMP3 positive cells.

Figure S5. Representative images of MMP19-IHC analysis in the dermis (B–F; 40X). Schematic representation of WHOC model (A). WHOCs were untreated (NT) or post-PDT, as indicated in the figures. Arrows show positively stained cells.

Figure S6. Representative images of p16-IHC. Images show schematic representation of analysed areas (A) in papillary dermis (PD) and reticular dermis (RD), normal human skin processed on day 0 (B) and WHOCs untreated (NT) and post-PDT (PDT) treated WHOCs collected on days 7 and 14 (C–J; Original magnification 40X). Arrows show p16-positive cells in the epidemis (Epi), reticular dermis (RD), advancing reepithelialization tongue (Aret) and neo-epidermis (Neo).

Figure S7. Representative images of α -SMA IHC (A–E) and CD31 endothelial marker-IHC (F–J). Normal human skin processed on day 0 (A&F). WHOCs on day 0 were compared to untreated (NT) and post-PDT treated WHOCs on days 7 and 14, maintained ex vivo (original magnification 5X).

ORIGINAL ARTICLE

Ex vivo evaluation of the effect of photodynamic therapy on skin scars and striae distensaeJenifer Mendoza-Garcia^{1,2}, Anil Sebastian², Teresa Alonso-Rasgado¹ & Ardesir Bayat^{1,2,3}¹Bioengineering Group, School of Materials, The University of Manchester, Manchester, UK.²Plastic & Reconstructive Surgery Research Group, Manchester Institute of Biotechnology (MIB), The University of Manchester, Manchester, UK.³University Hospital of South Manchester NHS Foundation Trust, Centre for Dermatology, Institute of Inflammation and Repair, Faculty of Medical and Human Sciences, University of Manchester, Manchester Academic Health Science Centre, Manchester, UK.**Key words:**

ex vivo; keloid and hypertrophic scar; photodynamic therapy; scar models; striae distensae

Correspondence:

Dr Ardesir Bayat, Manchester Institute of Biotechnology, The University of Manchester, 131 Princess Street, Manchester M1 7DN, UK.
 Tel: +441613065177
 Fax: +441613065177
 e-mail: ardesir.bayat@manchester.ac.uk

Accepted for publication:
 30 March 2015

Conflicts of interest:
 None declared.

SUMMARY**Background**

Skin scars and striae distensae (SD) are common dermal disorders with ill-defined treatment options. There is emerging clinical evidence for use of photodynamic therapy (PDT) in treating skin fibrosis. Therefore, the aim here was to investigate the effect of PDT on skin scars and SD in an ex vivo model of human skin scarring.

Methods

Photodynamic therapy, with 5ALA or MALA in addition to illumination with 40 J/cm² of red light, was applied to striae alba, fine line, hypertrophic and keloid scars ex vivo ($n = 18$). General morphology was assessed by H&E, Herovici's and Weigert's differential staining. Apoptosis, proliferation, metalloproteinase 3 and tropoelastin expression were quantified immunohistochemically, and differential gene expression of proliferating cell nuclear antigen (PCNA), collagen (COL) type I and type III, matrix metalloproteinase 3 (MMP3) and tropoelastin (ELN) was assessed by real-time quantitative reverse transcription polymerase chain reaction.

Results

Apoptosis increased, which correlated with decreased proliferation and PCNA gene expression. Post-PDT, matrix components were found to be re-organised in both hypertrophic and keloid scars. COLI and COLIII genetic expression decreased, whilst MMP3 and ELN increased significantly post-PDT compared to normal skin and untreated controls ($P < 0.05$). However, no significant difference between 5ALA and MALA-PDT treatments was observed.

Conclusion

Using our unique ex vivo model, we show for the first time morphological and cellular effect of application of PDT, which correlates with the degree and severity of dermal fibrosis. In view of this, PDT may be ideal in targeting treatment of abnormal skin scarring.

Photodermatol Photoimmunol Photomed 2015; **: **–**

A dermal scar is the permanent, irreversible and visible endpoint of the wound healing process following penetrative injury to the human skin. Whilst in some individuals, these dermal scars remain flat and linear; in others, they can become raised as hypertrophic scars or spread beyond the boundary of the original wound and become keloid scars. *Striae distensae* (SD) are atrophic dermal scars which arise from mechanical injury to the both the epidermis and dermis as a result of an over stretching or rapidly growing skin (1–4).

Skin scar phenotype can vary from (a) stretched or widespread flat scar, which is histologically characterised by a thin epidermis, fine collagen bundles arranged in straight parallel lines; (b) fine line scars (FLSs), which are commonly seen after first intention healing in normal wound healing where a scar is formed in the absence of mechanical tension; (c) depressed or atrophic scars, which usually appear after specific dermatoses such as acne or herpes and can be tethered to subdermal structures; (d) hypertrophic scars, which are a raised dermal scars that remain within the boundaries of the original wound and are histologically characterised with an increased fibroblast density and distorted collagen bundles; (e) keloid scars, which are also raised dermal scars, but do not remain within the boundary of the original wound and continue to grow beyond into healthy surrounding skin, and histologically show increased fibroblast density and marked proliferation rates and (f) scar contractures can develop in raised dermal lesions in either hypertrophic or keloid types, and can develop across joints or crease lines (1, 2, 5).

Skin scars and SD are common dermal disorders with ill-defined treatment options. Effective management of raised dermal scars and SD continues to remain a clinical challenge for clinicians. Despite a plethora of treatment modalities such as surgery, laser therapy, cryosurgery, steroid injection and topical or intralesional use of anti-fibrotic compounds, there is no clear rationale and importantly no ideal way of eradicating and preventing recurrence of such lesions (1, 5, 6).

There is emerging evidence for the role of photodynamic therapy (PDT) in treating skin fibrosis. PDT has shown promising results in both *in vitro* and *in vivo* case studies in the treatment of acne, hypertrophic and keloid scars (7–11). *In vitro* studies of monolayer cultures of fibroblasts derived from hypertrophic and keloid scars have shown a dose-dependent cytotoxic response to PDT (12–14). In addition, organotypic cultures of keloid fibroblasts were found to show a decrease in collagen synthesis post-PDT (15). PDT has also been dem-

onstrated to be of value in clinical treatment of raised dermal scars such as hypertrophic and keloid scars either alone or as an adjuvant therapy following excisional surgery (16, 17).

Photodynamic therapy uses a photosensitiser, along with energy from illumination with a specific wavelength, resulting in the production of reactive oxygen species (ROS), which are generated in a dose-dependent manner. Depending upon the site of generation and the amount of ROS, the tissue response and ensuing damage can be variable. Responses can vary from proliferation, senescence, autophagy, apoptosis and necrosis at cellular level. Additionally, collagen degradation, damage-associated molecular pattern molecules (DAMPs) release and paracrine stimulation of metalloproteinases and immunological cells had also been observed in a number previous studies (18–20). However, the exact mechanism and mode of delivery of PDT to raised dermal scars and SD remain unclear.

An ideal model to study human dermal fibrosis and its putative treatment candidates has not been developed and optimised as yet. *In vitro* studies are subject to high variability due to the external culture environment experienced by cells grown *in vitro*. Additionally, organotypic cultures lack several key components of the full complement of the entire tissue. There is no ideal animal model as animal skin has significant structural difference compared to human skin, and importantly, none of the lesions such as keloid scars can be replicated in an animal model. Therefore, *ex vivo* organ cultures of dermal fibrosis provide us with a superior model to investigate the effect of candidate therapies in fibrosis (21–24).

Thus, the aim here was to investigate the effect of PDT on skin scars and SD in an *ex vivo* model of human skin scarring. In this study, for the first time, we present our findings following evaluation of the effect of PDT on normal skin (NS) compared to a variety of skin scars including FLSs, hypertrophic and keloid scars, and SD. Histological, immunohistochemical and differential gene expression analyses were performed post-PDT, to evaluate the potential mechanism of action of PDT on dermal fibrosis.

MATERIAL AND METHODS

Study subject selection and recruitment

Striae distensae in the form of *striae alba* as opposed to *striae rubra*, FLSs and NS explants were obtained from healthy patients undergoing routine aesthetic surgery.

Hypertrophic scars (HS) and keloid scars (KD) were harvested from patients undergoing surgical excision of their lesion as part of their clinical management. In terms of clinical scar severity, which will be referred to later in the text as degree of dermal fibrotic severity, clearly FLS is the least severe and KD is the most severe form with HS as an intermediate form of a dermal fibrotic scar. All samples were diagnosed both clinically and histologically to ensure accurate diagnosis. Scar classification and demographic clinical data are shown in Table 1. Ethical approval for this study was provided by the north-west of England, research ethics committee (11/NW/0683). Tissue samples were collected following fully informed verbal and written consent.

Skin explant preparation

To prepare the explants for organ culture (OC), the hypodermal fat was surgically excised, the explants were washed several times in phosphate buffer solution (PBS; Sigma-Aldrich, Dorset, UK) and soaked in Dulbecco's modified Eagle's medium (DMEM; Sigma-Aldrich) supplemented with Primocin (InvivoGen, Nottingham, UK) for 30 min and rinsed several times with PBS. Organ culture explants were surgically prepared with a 6-mm punch biopsy kit. The full-thickness dermal tissue biopsy was subsequently embedded in rat-tail collagen

type I gel (2 mg/ml; BD Biosciences, Oxford, UK), and the epidermis was left exposed to the air–liquid interface (24). Organ cultures were maintained with William's medium (WE), supplemented with 100 IU/ml penicillin, 10 µg/ml streptomycin, 10 µg/ml of insulin, 10 ng/ml of hydrocortisone and 2 mM of L-glutamine and cultured in standard conditions (37°C; 5% CO₂/95% O₂ tension). All reagents were from Sigma-Aldrich (Fig. 1a,b).

Photodynamic therapy treatment

Scars, striae alba and NS OC explants were exposed to PDT treatment using 2 protoporphyrin IX precursors, 5-aminolevulinic acid (5ALA; Mandeville Medicines, UK) or methyl aminolevulinate (MALA; Galderma, Watford, UK) and illuminated with a PDT machine (Omnilux PDT™; Photo Therapeutics, Pennsylvania, PA, USA) with an arrangement of red light-emitting diodes (LEDs) of wavelength 633 ± 3 nm and an air cooling system. The PDT machine was adjusted to 40 J/cm² of power intensity and calibrated with an IL1700 radiometer (International Light Technologies Inc, Massachusetts MA, USA; 12; Fig. 1c).

Photodynamic therapy treatment was given on the day of collection (day 0). A thin layer (1 mm) of photosensitiser precursors was applied on the epidermis and

Table 1. Clinical data and source of scar/skin explants

Patient	Gender	Age	Anatomical source of scar/skin explants	Scar classification	Age of scar (years)
1	Female	80	Abdomen	Striae Alba	55
2	Female	42	Abdomen	Striae Alba	17
3	Female	31	Abdomen	Striae Alba	6
4	Female	28	Abdomen	Striae Alba	3
5	Female	28	Abdomen	Striae Alba	3
6	Female	50	Arm	Striae Alba	25
7	Female	57	Abdomen	Fine Line Scar	—
8	Female	65	Breast	Fine Line Scar	—
9	Female	30	Abdomen	Fine Line Scar	—
10	Female	42	Abdomen	Fine Line Scar	—
11	Female	22	Abdomen	Fine Line Scar	—
12	Female	42	Abdomen	Fine Line Scar	—
13	Female	58	Abdomen	Hypertrophic Scar	1
14	Female	80	Abdomen	Hypertrophic Scar	2
15	Female	42	Abdomen	Hypertrophic Scar	5
16	Male	26	Sternum	Keloid Scar	2
17	Male	24	Shoulder	Keloid Scar	5
18	Male	52	Ear	Keloid Scar	2
19	Female	42	Abdomen	Normal Skin	—
20	Male	71	Abdomen	Normal Skin	—
21	Female	42	Abdomen	Normal Skin	—
22	Male	28	Abdomen	Normal Skin	—

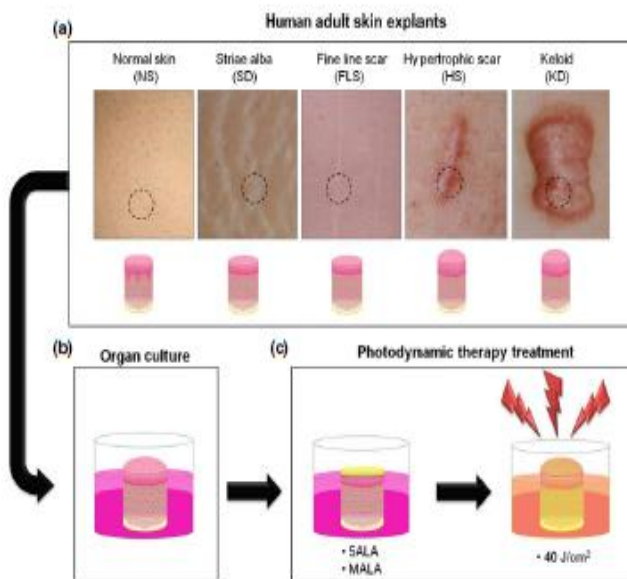


Fig. 1. Schematic representation of normal skin, SD and scar explants. Full-thickness punch biopsies measuring 6 mm (a) were embedded in collagen and maintained with supplemented William's E (WE) medium and air-liquid interface (b). Organ cultures were incubated with the pro-drugs aminolevulinic acid methyl ester (MALA) or 5-aminolevulinic acid (SALA) later illuminated with red LED light and maintained 7 days ex vivo post-photodynamic therapy (c).

incubated for 4 h under standard conditions and darkness. Organ cultures were washed twice with PBS before illumination and soon after re-embedded in collagen and cultured for 7 days ex vivo. Collected OCs were fixed, paraffin-embedded, sectioned and deparaffinised following standard procedures (24).

Histology

Representative sections of 5 µm were morphologically studied after haematoxylin and eosin (H&E; Sigma-Aldrich), Herovici's (HV) and Weigert's elastic differential staining (WELA; Sigma-Aldrich). H&E and WELA staining were performed according to the manufacturer's instructions. HV staining was carried out as described by Bagabir *et al.* (24). Stained sections were scanned with a Hamamatsu NanoZoomer 2.0-HT and analysed with NDP.view2 image software (Hamamatsu, Hertfordshire, UK).

Immunofluorescence/Immunohistochemistry

3'-OH DNA immunofluorescence (IF) TUNEL by FragEL™ (Calbiochem-Merk, Darmstadt, Germany) was used to assess apoptosis. Additionally, proliferating nuclear antigen (PCNA), tropoelastin (ELN) and matrix

Table 2. List of antibodies

Primary antibody	Dilution	Incubation time (h)
Anti-PCNA antibody (ab18197); Rabbit polyclonal; IgG	1: 200	1
Anti-elastin antibody [BA-4] (ab9519); Mouse monoclonal; IgG1	1: 150	1
Anti-MMP3 antibody [EP1186Y] (ab52915); Rabbit monoclonal; IgG	1 : 1000	1

PCNA, proliferating cell nuclear antigen; MMP3, matrix metalloproteinase 3.

remodelling metalloproteinase 3 (MMP3) were immunohistochemically (IHC; Table 2; abcam®, Cambridge, UK) stained and detected with Novocastra Peroxidase Detection Systems (Leica, Milton Keynes, UK). IHC and peroxidase detection were performed according to manufacturer's instructions. Stained sections were scanned in a Hamamatsu NanoZoomer 2.0-HT and analysed with NDP.view2 image software (Hamamatsu). An objective quantification of cellular markers was made using Definiens Tissue Studio 3.5 software (Definiens, Munich, Germany; ref. 25).

Photodermatol Photoimmunol Photomed 2015; **: ***
© 2015 John Wiley & Sons A/S. Published by John Wiley & Sons Ltd

Table 3. Gene and primer sequences for qRT-PCR

Primers	Gene ID	Sequence 5'-3'	Primer position	Amplicon size (bp)
RPL32-L	NM_000994.3	gaagtccctggccacaacg	319–338	77
RPL32-R	NM_000994.3	gagcgatctcgacagta	377–395	77
PCNA -L	NM_002592.2	tggagaactggaaatggaaa	755–775	20
PCNA-R	NM_002592.2	gaactggtcattcatcttatgg	826–849	20
Elastin-L	NM_000501.3	cagctaaatacgggtctgt	2420–2440	21
Elastin-R	NM_000501.3	aatcogaaggcaggcttg	2495–2513	19
Collagen I-L	NM_000088.3	gggatcccctgacctaag	1866–1885	63
Collagen I-R	NM_000088.3	ggaaacactcgcttcca	1911–1928	63
Collagen III -L	NM_000090.3	ctggaccccagggtcttc	3101–3118	75
Collagen III-R	NM_000090.3	catctgatccagggtttca	3156–3175	75
MMP3 -L	NM_002422.3	caaaacatattcttttagaggacaa	1259–1285	91
MMP3 -R	NM_002422.3	ttcagctatggcttggaaa	1329–1349	91

RPL32, 60S ribosomal protein L32; PCNA, proliferating cell nuclear antigen; MMP3, matrix metalloproteinase 3.

RNA isolation, cDNA synthesis and qRT-PCR

Organ cultures were collected in TRIzol reagent (Invitrogen, Abingdon, UK) and processed for RNA isolation, cDNA synthesis and qRT-PCR (Qiagen, Manchester, UK) according to the manufacturer's instructions. The gene expression levels were normalised with an internal reference gene, RPL32. The primers used in the study are detailed in Table 3.

Statistical analysis

The results are presented as the mean values \pm standard deviation. Statistical significance was calculated with one-way ANOVA and Bonferroni's comparison test. Graphics and statistics were generated with GraphPad Prism 5 (GraphPad Software, La Jolla, CA, USA). The differences were considered statistically significant if $P < 0.05$.

RESULTS

PDT application with either 5ALA or MALA caused fibrotic tissue degradation

Morphological analysis by H&E staining at day 0 (Control) shows typical differences of various scars, striae alba and NS (Fig. 2a–e). All histological characteristics were present after 7 days of being cultured *ex vivo* (Fig. 2f–j). Photodynamic therapy treatment was given on day 0 and tissues were maintained 7 days *ex vivo* (Fig. 2k–t) and compared to NS on day 0 and untreated controls on day 7. Histological appearance of NS shows a minimal effect. However, epidermal rete ridges were no longer preserved in full, epidermal stratification decreased

and collagen bundles appeared less dense. PDT effects on scars and striae were more aggressive compared to NS; in striae, some small areas of epidermal detachment were found and keratinocytes with pyknotic nucleus were found in all epidermal layers. The collagen bundles in the ECM appeared to have been re-organised and almost unravelled. Whilst in FLS and HS, larger areas of epidermal detachment were found. The whole epidermis contained pyknotic cells and the ECM was found to have changed and become degraded. However, the highest percentage of change was seen in KD, where the epidermis was found to be totally detached (almost dislocated), and there was a ECM complete loss of ECM's typical appearance. However, similar characteristic changes were observed in all tissues following either 5ALA or MALA PDT treatment, but not in the controls (not-treated with PDT), which maintained the epidermis attached to the basal lamina and dermis. Both controls and PDT-treated OCs had been cultured *ex vivo* for 7 days after treatment in similar conditions.

Apoptosis was shown to have increased post-PDT

Apoptosis was determined by Tunel assay and was quantified in the basal layer of the epidermis. Apoptosis was found to be increased in relation to the scar severity and phenotype. Normal skin showed apoptotic cells at the stratum spinosum after 5ALA-PDT, whilst an even distribution in all epidermal layers was found with MALA-PDT. An average of 15% of apoptotic cells were found with both treatments in NS. Epidermal layer of scar lesions was found to be highly apoptotic. SD and FLS staining showed that up to 50% were of apoptotic cells and in HS apoptotic cells increased up to 80%, whilst the

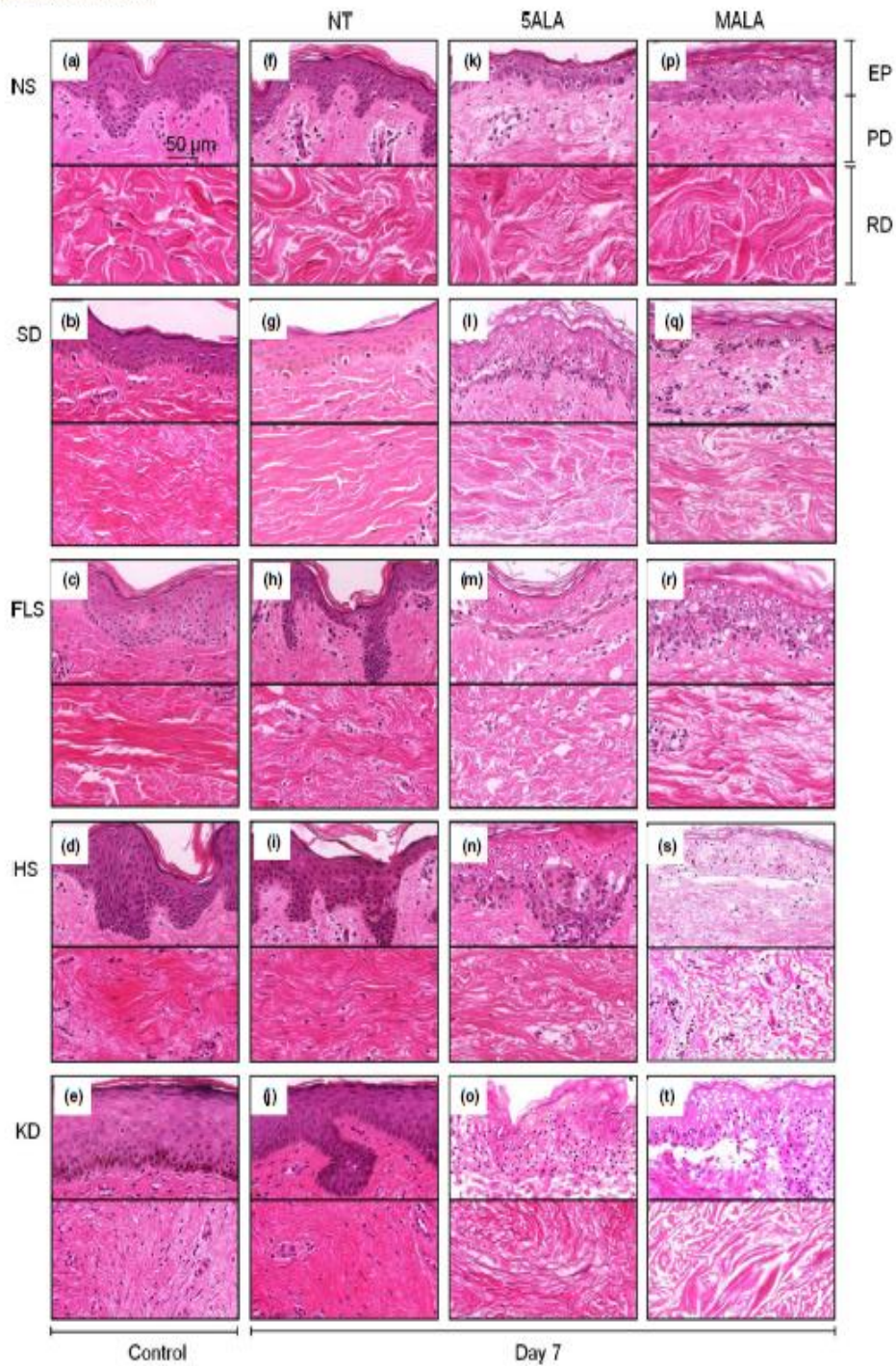


Fig. 2. Morphological analysis by haematoxylin and eosin stain staining of normal skin and fibrotic dermal lesions. Normal skin (NS; a, f, k and p), striae alba (SD; b, g, l and q), fine line scar (FLS; c, h, m and r), hypertrophic scar (HS; d, i, n and s) and keloid disease (KD; e, j, o and t) were treated with amino levulinic acid methyl ester (MALA) or 5-amino levulinic acid (SALA) photodynamic therapy. NT denotes untreated controls, EP denotes epidermis, PD denotes papillary dermis, and RD denotes reticular dermis.

epidermis of KD was found to be detached with a few apoptotic cells in the entire basal layer (Fig. 3a,b).

PDT application with either 5ALA or MALA decreased the total number of proliferating cells

Cell proliferation was quantified with PCNA-IHC in the basal layer of the epidermis. Biopsies on day 0 showed typical proliferative characteristics of the NS and scars. NS, SD and FLS showed no significant differences between the percentages of proliferative

cells at the epidermis which were approximately 25%. HS proliferative cells (39%) were found to be significantly more than NS, SD and FLS; however, the vast majority were found to be restricted to the basal layer. In KD, 90% of the cells were found to be proliferative and distributed across the entire tissue. Post-PDT either with 5ALA or MALA, proliferative cells were found to be significantly lower compared to day 0 and compared with untreated controls on day 7 (Fig. 3d,e). In KD, there were a few proliferative cells across the tissue. Here, PCNA gene expression decreased significantly in both SD and dermal scar lesions

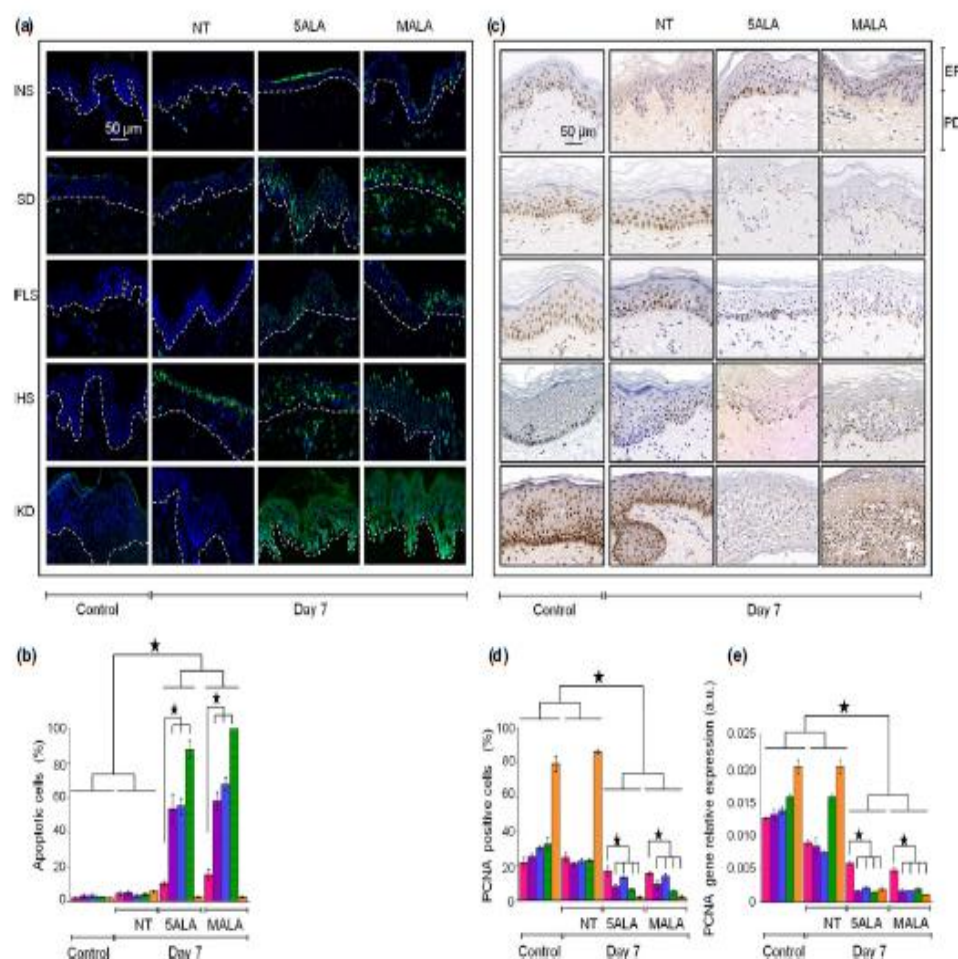


Fig. 3. Epidermal apoptosis and proliferation analysis. Normal skin (NS), striae alba (SD), fine line scar (FLS), hypertrophic scar (HS) and keloid disease (KD) were stained with apoptosis tunnel assay (a) or proliferating cell nuclear antigen (PCNA) immunohistochemistry (c) at day 0 (control), untreated (NT) with 5ALA or MALA-PDT. Graphs represent normal skin (red), striae alba (purple), fine line scar (blue), hypertrophic scar (green) and keloid scar (orange) quantification of apoptotic cells (b), PCNA-positive cells (d) and PCNA (e) gene expression. Epidermis (EP) and papillary dermis (PD). * denotes statistically significant difference ($P < 0.05$).

(Fig. 3f). PCNA expression was reduced by twofold on day 7 in untreated skin compared with treated skin, whilst the maximum change of 10-fold was observed in KD tissue.

Elastic fibres were altered post-PDT

Weigert's elastic stain revealed striking differences in the elastic fibre arrangement prior and post-PDT (Fig. 4a). Post-PDT elastic fibres in NS were found to be different compared to SD, FLS, HS and KD, where the change increased accordingly. Elastic fibre rearrangement ranged from broken and untangled fibres in the papillary layer of the dermis of SD and FLS, whilst the highest percentage

of change was found in HS. However, elastic fibre change in KD showed an inconsistent pattern, as there was variation in fibres size and organisation across the samples (Fig. 4a). Further analysis of tropoelastin IHC (Fig. 4b-d), which is the soluble precursor of elastic fibres, showed significant differences between NS and SD, HS and KD on day 0 (Fig. 4b). Normal skin showed few positively stained fibres were present at the basal layer which was similar to what was seen in FLS. Although HS showed positive staining in the basal layer whilst keloid scars also showed a high percentage of positive staining at the basal layer.

Post-PDT, ELN-positive cells increased in NS, SD, FLS and HS. In NS, positive cell numbers increased

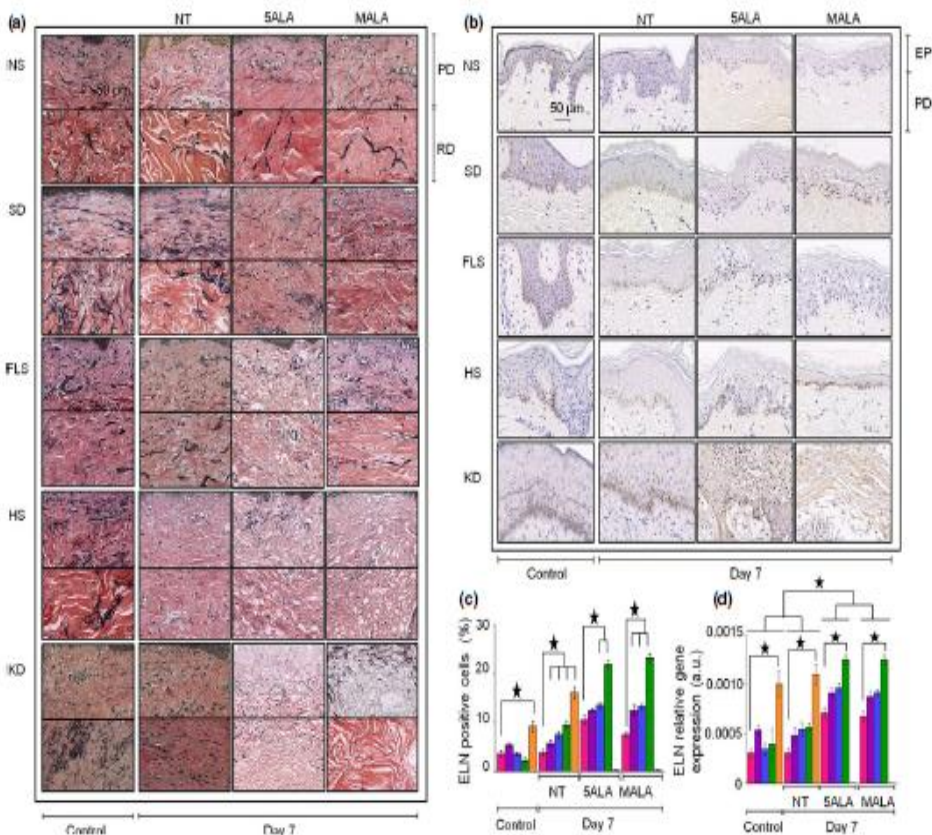


Fig. 4. Elastic fibre analysis. Elastic morphological analysis by Weigert's staining (a) and tropoelastin immunohistochemistry (ELN-IHC) analysis (b) were performed in normal skin (NS), striae alba (SD), fine line scar (FLS), hypertrophic scar (HS) and keloid disease (KD) on control and compared to untreated controls (NT) and aminolevulinic acid methyl ester (MALA) or 5-aminolevulinic acid (SALA) photodynamic therapy. Papillary dermis (PD) and reticular dermis (RD) tissue cross sections for each scar type are presented. Graphs show tropoelastin immunohistochemistry positive cell quantification (c) and ELN gene expression levels of (d) of normal skin (■), striae alba (□), fine line scar (□), hypertrophic scar (■) and keloid scar (□). ★ denotes statistically significant difference ($P < 0.05$).

especially after they were treated with 5ALA-PDT (Fig. 4b,c). As shown previously, KD tissue was found to be affected most, demonstrating no evidence of tropoelastin expression. ELN gene expression in dermal lesions compared to untreated tissue increased by a maximum of 2.5-fold in HS post-PDT compared to day 7 untreated tissues (Fig. 4d).

Collagen fibres arrangement was found to be affected post-PDT, in all dermal lesions but most in keloid tissue

Collagen arrangement varied when comparing NS to different scar phenotypes (Fig. 5a–e). Dermal scars showed collagen fibres with thick bundles parallel to the dermis that became thicker in the reticular dermis of SM, HS and KD. Regardless of the scar phenotype, all collagen fibres were found to be affected by PDT; however, this effect increased with the severity of the scar type (Fig. 5k–t). Normal skin and SD showed relaxed collagen fibres and increased expression of COLIII in the papillary dermis compared to day 0 (Fig. 5k–q), whilst in FLS and HS, fibres were found degraded, shortened and untangled post-PDT (Fig. 5m–s). However, the highest effect was observed in KD where the papillary dermis was found most affected and the reticular dermis showed collagen fibres that had become thinner and with increased spaces between them (Fig. 5o,t). Further analysis of COLI and COLIII gene expression found both to be decreased in FLS, HS and KD compared to NS by day 0 and untreated tissues on day 7 (Figs 5u,v and 6).

MMP3 dermal expression significantly increased post-PDT

Matrix metalloproteinase 3 histological expression was found to be significantly higher post-PDT in all samples, except in KD (Fig. 5w). MMP3 gene expression showed significant differences between NS and dermal scars; the highest expression was found in hypertrophic scars post-PDT; however, MMP3 gene expression was found to be similar after application of 5ALA compared with MALA-PDT treatment. The maximum MMP3 gene expression observed was found in HS, which increased approximately fourfold compared to untreated control tissue on day 7 (Fig. 5x).

DISCUSSION

In this study, we present for the first time morphological and cellular effect of PDT in dermal fibrosis using our

unique *ex vivo* scar model. This study provides evidence of effects of PDT in different phenotypical dermal scars and SD. All dermal lesions were compared to NS and untreated controls. We also compared the effect of 5ALA with MALA-PDT.

We demonstrate that PDT affects both the epidermis and the dermis of skin scarring, however, the degree of damage to morphology and cellular content varied according to the exact type of dermal lesion. It became apparent that dermal lesions with a more severe degree of dermal fibrosis were affected most. Thus, least effect was observed in FLS, and the most impact was visible in keloid scars. Additionally, apoptosis increased with increasing severity of dermal fibrosis. Moreover, proliferation decreased and correlated with severity of dermal fibrosis. There was also a decrease in levels of PCNA gene expression, which matched the PCNA protein levels. ECM fibres, elastin and collagen were found degraded, especially in hypertrophic and keloid scars, whilst MMP3 expression was shown to be increased, except in KD where KD tissue was found to be extensively damaged. Overall, there was no significant difference between 5ALA and MALA-PDT application to all dermal lesions compared to control.

In vitro oncological studies have shown that the effects of PDT vary according to cell type, inducing the most aggressive response according to the degree of cellular differentiation (26). This means that from a spectrum of healthy cells to dysplastic and neoplastic cells, the latter would have the highest capacity to synthesise PpIX, from 5ALA or MALA (27). Similarly oncologic investigations had showed that 5ALA and MALA can show an uptake by almost every cell present in the skin (higher in neoplastic cells) and can penetrate a depth of 2 mm. Additionally, red light (635 nm) has a penetration depth of 3–5 mm without showing any toxic effects (28, 29). Here, we have identified increasing levels of PDT effect according to the severity of scar type. Keloid scars were the most affected dermal fibrotic scar. This would make sense as KD is considered to be the most aggressive type of raised dermal fibrotic scarring and considered to have quasi-neoplastic tendencies with keloid cells displaying cancer bioenergetics (30). This is also evident in the clinical behaviour of KD as it invades healthy surrounding skin and is characterised by exuberant and proliferative production of distorted ECM (31, 32). Thus, keloid fibroblasts are likely to lead to higher ROS generation leading to a greater degree of effect being observed in keloid tissue post-PDT application. We previously demonstrated the effect of PDT in keloid fibroblasts *in vitro* and showed this to be site specific within the lesion, which correlated with the

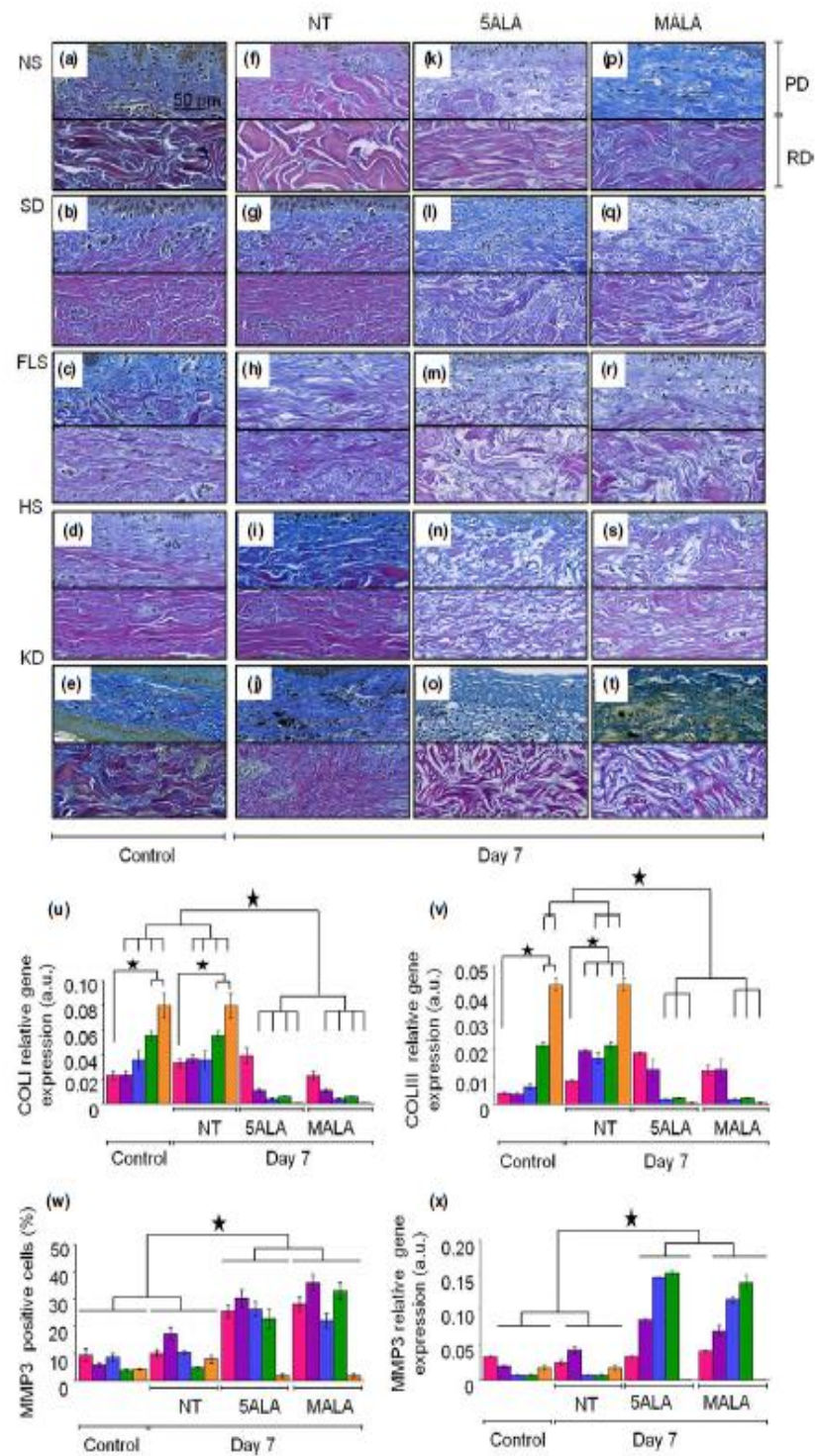


Fig. 5. Collagen type I, collagen type III and matrix metalloproteinase 3 analysis. Morphological analysis by Herovici's differential staining of controls (day 0; a-e) compared to untreated controls (NT; f-j) and after 5-amino levulinic acid (SALA; k-o) aminolevulinic acid methyl ester (MALA; p-t) photodynamic therapy treatment. NS denotes normal skin, SD denotes striae alba, FLS denotes fine line scar, HS denotes hypertrophic scar, and KD denotes keloid scar. PD represents papillary dermis and RD represents reticular dermis. Graphs represent gene expression levels of normal skin (■), striae alba (□), fine line scar (■), hypertrophic scar (■) and keloid scar (■) of COLI (U) and COLIII (V), histological quantification of MMP3 (w) and MMP3 genetic expression (x). * denotes statistically significant difference ($P < 0.05$).

PpIX accumulation and ROS generation leading to decreased cytoproliferation and increased cell death (12). A case report and a subsequent case series by our group also showed similar findings for the effect of PDT on KD (10, 11).

Matrix metalloproteinase 3 levels had increased, whilst COLI and COLIII levels decreased post-PDT in scar tissue. Similar results were found by Campbell *et al.* (8) and Kerrer *et al.* (33), whilst elastic fibres had been found to have a significant increase after 6 months post-PDT (16, 34). This suggested that the photodamage caused by PDT treatment may trigger elastic fibres neof ormation and remodelling of the ECM matrix, also previously suggested by Sanclement *et al.* (35). MMP3 participates actively in ECM remodelling throughout the wound healing process. MMP3 activates MMP1 and degrades fibronectin, laminin and collagens III, IV, IX and X which is downregulated in keloid tissue, suggesting dysregulated degradation of ECM at the remodelling stage (36).

Here, we found compelling evidence of tissue degradation in dermal fibrosis caused by application of PDT. Application of PDT can cause release of DAMPs, matrikines and elastokines, which through paracrine communication trigger immunological alerts and MMPs activation, which in turn can induce tissue repair (21, 37-39). Recently Mills *et al.* showed that MALA-PDT increases TGF- β 3, MMP1 and MMP9 leading to an improvement of ECM in human wound healing *in vivo*. Additionally, a limited number of animal studies and routine dermatological practices have shown evidence of improvement in the cosmetic outcome and faster wound healing post-PDT, but precise molecular mechanisms remain unknown (39, 40).

Therefore, the overall effect of PDT on tissue repair and remodelling may be a combination of elimination of fibrosis and induction of tissue repair as had been demonstrated previously *in vivo* (8, 10, 16). *In vivo*, there is likely to be direct photodamage affecting keloid fibroblasts, in addition to activation of an

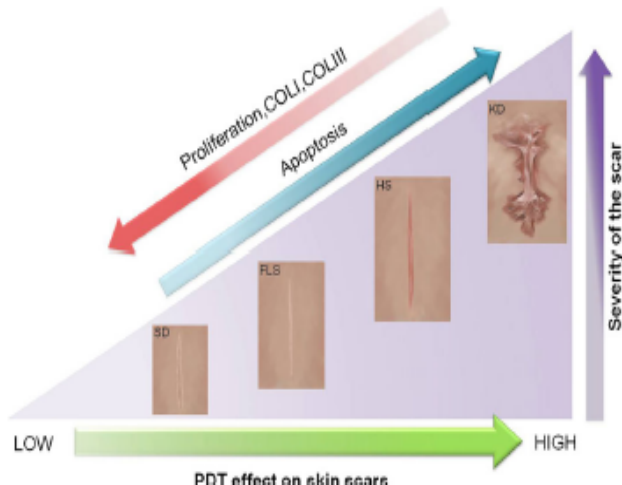


Fig. 6. Schematic representation of the effect of photodynamic therapy in phenotypically different scar types. The lowest effect was observed in striae alba (SD); however, the effect increased with increasing severity of the scar type from fine line (FLS), and hypertrophic scars (HS) to keloid disease (KD). Keloid scars were affected most post-PDT. PDT effects on scars were compared with increased levels of apoptosis and decreased levels in proliferation.

immune response leading to elimination of fibrotic tissue. The limitations of this study include the total number of patients available to us to investigate and the number of experimental parameters that were studied in relation to effect of PDT in dermal fibrosis. Certainly, further number of samples in a more comprehensive range of dermal scars including depressed scars, striae rubra and more experimental options looking at the effect of PDT in fibrosis would be ideal in any future study. In view of the limitations of the *ex vivo* model for evaluating the scar response to PDT, further *in vivo* studies evaluating the optimal dosage, timing and frequency of PDT in different types of dermal scars with diligent follow-up to ensure effective long-term benefits with a lack of recurrence in particular in the case of more severe dermal fibrotic lesions are recommended.

CONCLUSION

We show, for the first time, using our unique *ex vivo* OC model of human skin scarring that morphological and cellular effect of PDT correlates with the degree and severity of dermal fibrosis. In view of this, PDT may be ideal in targeted treatment of abnormal scarring. Additionally, application of PDT requires further validation *in vivo* to determine its dosage, frequency and timing as well as whether it is most effective in isolation or in combination with other treatment modalities such as pre- or post-surgical excision of dermal fibrotic scars.

ACKNOWLEDGEMENTS

Jenifer Mendoza-Garcia received an award from the Mexican National Council for Science and Technology.

REFERENCES

- Ud-Din S, Bayat A. New insights on keloids, hypertrophic scars, and striae. *Dermatol Clin* 2014; 32: 193–209.
- Bayat A, McGrouther DA, Ferguson MW. Skin scarring. *BMJ* 2003; 326: 88–92.
- Ud-Din S, Bayat A. Strategic management of keloid disease in ethnic skin: a structured approach supported by the emerging literature. *Br J Dermatol* 2013; 169(Suppl 3): 71–81.
- Perry DM, McGrouther DA, Bayat A. Current tools for noninvasive objective assessment of skin scars. *Plast Reconstr Surg* 2010; 126: 912–923.
- Mustoe TA. Scars and keloids. *BMJ* 2004; 328: 1329–1330.
- Agren MS, Danielsen PL. Antiscarring pharmaceuticals: lost in translation? *Wound Repair Regen* 2014; 22: 293–294.
- Calzavara-Pinton PG, Rossi Mt, Aronson E, Sala R. A retrospective analysis of real-life practice of off-label photodynamic therapy using methyl aminolevulinate (MAL-PDT) in 20 Italian dermatology departments Part 1: inflammatory and aesthetic indications. *Photochem Photobiol Sci* 2013; 12: 148–157.
- Campbell SM, Tyrell J, Marshall R, Curmow A. Effect of MAL-photodynamic therapy on hypertrophic scarring. *Photodiagnosis Photodyn Ther* 2010; 7: 183–188.
- Brusino N, Loti T, Rossi R. Photodynamic therapy for a hypertrophic scarring: a promising choice. *Photodermatol Photoimmunol Photomed* 2011; 27: 334–335.
- Nie Z, Bayat A, Behzad F, Rhodes LE. Positive response of a recurrent keloid scar to topical methyl aminolevulinate-photodynamic therapy. *Photodermatol Photoimmunol Photomed* 2010; 26: 330–332.
- Ud-Din S, Thomas G, Morris J, Bayat A. Photodynamic therapy: an innovative approach to the treatment of keloid disease evaluated using subjective and objective non-invasive tools. *Arch Dermatol Res* 2013; 305: 205–214.
- Mendoza J, Sebastian A, Allan E et al. Differential cytotoxic response in keloid fibroblasts exposed to photodynamic therapy is dependent on photosensitiser precursor, fluence and location of fibroblasts within the lesion. *Arch Dermatol Res* 2012; 304: 549–562.
- Li X, Zhou ZP, Hu I, Zhang WJ, Li W. Apoptotic cell death induced by 5-aminolevulinic acid-mediated photodynamic therapy of hypertrophic scar-derived fibroblasts. *J Dermatol Treat* 2014; 25: 428–433.
- Cai H, Gu Y, Sun Q, Zeng J, Dong N, Zhao G. Effect of hematoporphyrin monomethyl ether-mediated photodynamic therapy on hypertrophic scar fibroblasts. *Photodermatol Photoimmunol Photomed* 2011; 27: 90–96.
- Chiu LI, Sun CH, Yeh AT et al. Photodynamic therapy on keloid fibroblasts in tissue-engineered keratinocyte-fibroblast co-culture. *Laser Surg Med* 2005; 37: 231–244.
- Sakamoto F, Izikson L, Tannous Z, Zurakowski D, Anderson RR. Surgical scar remodelling after photodynamic therapy using aminolevulinic acid or its methylester: a retrospective, blinded study of patients with field cancerization. *Br J Dermatol* 2012; 166: 413–416.
- Basew H, Mehlal R, Al-Mamgani A et al. Adjunctive treatment of keloids: comparison of photodynamic therapy with brachytherapy. *Eur J Plast Surg* 2013; 36: 289–294.
- Blaquier-Castro A, Carrasco E, Calvo M et al. Protoporphyrin IX-dependent photodynamic production of endogenous ROS stimulates cell proliferation. *Eur J Cell Biol* 2012; 91: 216–223.
- Garg AD, Nowis D, Golab J, Agostinis P. Photodynamic therapy: illuminating the road from cell death towards anti-tumour immunity. *Apoptosis* 2010; 15: 1050–1071.
- Ji HT, Chien LT, Lin YH, Chien HF, Chen CT. 5-ALA mediated photodynamic therapy induces autophagic cell death via AMP-activated protein kinase. *Mol Cancer* 2010; 28: 91.
- Brohem CA, Cardeal IB, Tiago M, Soengas MS, Barros SB, Maria-Engler SS. Artificial skin in perspective: concepts and applications. *Pigment Cell Melanoma Res* 2010; 24: 35–50.
- Yang DY, Li SR, Wu JL et al. Establishment of a hypertrophic scar model by transplanting full-thickness human skin grafts onto the backs of nude mice. *Plast Reconstr Surg* 2007; 119: 104.
- Wong VW, Sorkin M, Glotzbach JP, Longaker MT, Gutner GC. Surgical approaches to create murine models of

- human wound healing. *J Biomed Biotechnol* 2011; 2011: 969618. doi:10.1155/2011/969618.
24. Bagabir R, Syed F, Paus R, Bayat A. Long-term organ culture of keloid disease tissue. *Exp Dermatol* 2012; 21: 376–381.
 25. Samaroo HD, Opsahl AC, Schreiber J et al. High throughput object-based image analysis of β -amyloid plaques in human and transgenic mouse brain. *J Neurosci Methods* 2012; 204: 179–188.
 26. Pahernik SA, Botzlar A, Hillemanns P et al. Pharmacokinetics and selectivity of aminolevulinic acid-induced porphyrin synthesis in patients with cervical intraepithelial neoplasia. *Int J Cancer* 1998; 78: 310–314.
 27. Wyld I, Reed MW, Brown NJ. Differential cell death response to photodynamic therapy is dependent on dose and cell type. *Br J Cancer* 2001; 84: 1384–1386.
 28. Wan MT, Lin JY. Current evidence and applications of photodynamic therapy in dermatology. *Clin Cosmet Investig Dermatol* 2014; 21: 145–163.
 29. Robertson CA, Evans DH, Abrahamse H. Photodynamic therapy (PDT): a short review on cellular mechanisms and cancer research applications for PDT. *J Photochem Photobiol B* 2009; 96: 1–8.
 30. Vincent AS, Phan TT, Mukhopadhyay A, Lim HY, Halliwell B, Wong KP. Human skin keloid fibroblasts display bioenergetics of cancer cells. *J Invest Dermatol* 2008; 128: 702–709.
 31. Shih B, Bayat A. Genetics of keloid scarring. *Arch Dermatol Res* 2010; 302: 319–339.
 32. Shih B, Garside E, McGrouther D, Bayat A. Molecular dissection of abnormal wound healing processes resulting in keloid disease. *Wound Rep Regen* 2010; 18: 139–153.
 33. Kerrer S, Bosserhoff AK, Weiderer P, Landthaler M, Szeimies RM. Keratinocyte-derived cytokines after photodynamic therapy and their paracrine induction of matrix metalloproteinases in fibroblasts. *Br J Dermatol* 2004; 151: 776–783.
 34. Seo JY, Lee SH, Youn CS et al. Ultraviolet radiation increases tropoelastin mRNA expression in the epidermis of human skin in vivo. *J Invest Dermatol* 2001; 116: 915–919.
 35. Sanclemente G, Correa LA, Garcia JJ, Barrera M, Villa JF, Garcia HI. Methyl aminolevulinate plus red light vs. placebo plus red light in the treatment of photodamaged facial skin: histopathological findings. *Clin Exp Dermatol* 2012; 37: 379–386.
 36. Seifert O, Bayat A, Geffers R et al. Identification of unique gene expression patterns within different lesional sites of keloids. *Wound Rep Regen* 2008; 16: 254–265.
 37. Volk SW, Iqbal SA, Bayat A. Interactions of the extracellular matrix and progenitor cells in cutaneous wound healing. *Adv Wound Care (New Rochelle)* 2013; 2: 261–272.
 38. Li F, Huang Q, Roop DR, Bedford JS, Li CY. Apoptotic cells activate the "phoenix rising" pathway to promote wound healing and tissue regeneration. *Sci Signal* 2010; 23: 110–113.
 39. Mills SJ, Farrar MD, Ashcroft GS, Griffiths CE, Hardman MJ, Rhodes LE. Topical PDT following excisional wounding of human skin increases production of TGF- β 3, MMP-1 and MMP-9 with associated improvement in dermal matrix organisation. *Br J Dermatol* 2014; 171: 55–62. doi:10.1111/bjd.12843.
 40. Peplow PV, Chung TY, Baxter GD. Photodynamic modulation of wound healing: a review of human and animal studies. *Photomed Laser Surg* 2012; 30: 118–148.